



National Library  
of Canada

Bibliothèque nationale  
du Canada

Acquisitions and  
Bibliographic Services Branch

Direction des acquisitions et  
des services bibliographiques

395 Wellington Street  
Ottawa, Ontario  
K1A 0N4

395, rue Wellington  
Ottawa (Ontario)  
K1A 0N4

Yours truly / Votre référence

Cheers / Bonne référence

## NOTICE

## AVIS

The quality of this microform is heavily dependent upon the quality of the original thesis submitted for microfilming. Every effort has been made to ensure the highest quality of reproduction possible.

La qualité de cette microforme dépend grandement de la qualité de la thèse soumise au microfilmage. Nous avons tout fait pour assurer une qualité supérieure de reproduction.

If pages are missing, contact the university which granted the degree.

S'il manque des pages, veuillez communiquer avec l'université qui a conféré le grade.

Some pages may have indistinct print especially if the original pages were typed with a poor typewriter ribbon or if the university sent us an inferior photocopy.

La qualité d'impression de certaines pages peut laisser à désirer, surtout si les pages originales ont été dactylographiées à l'aide d'un ruban usé ou si l'université nous a fait parvenir une photocopie de qualité inférieure.

Reproduction in full or in part of this microform is governed by the Canadian Copyright Act, R.S.C. 1970, c. C-30, and subsequent amendments.

La reproduction, même partielle, de cette microforme est soumise à la Loi canadienne sur le droit d'auteur, SRC 1970, c. C-30, et ses amendements subséquents.

Canada

# **Functional Properties of Polyurethane Based Sealants Blended with Polymeric Modifiers**

Michael A. Lacasse

A thesis

in the

Centre for Building Studies

Presented in Partial Fulfillment of the Requirements  
for the Degree of Doctor of Philosophy at  
Concordia University  
Montreal, Quebec, Canada

May, 1991

© Michael A. Lacasse, 1991



National Library  
of Canada

Acquisitions and  
Bibliographic Services Branch

395 Wellington Street  
Ottawa, Ontario  
K1A 0N4

Bibliothèque nationale  
du Canada

Direction des acquisitions et  
des services bibliographiques

395, rue Wellington  
Ottawa (Ontario)  
K1A 0N4

*Your file - Votre référence*

*Our file - Notre référence*

The author has granted an irrevocable non-exclusive licence allowing the National Library of Canada to reproduce, loan, distribute or sell copies of his/her thesis by any means and in any form or format, making this thesis available to interested persons.

L'auteur a accordé une licence irrévocable et non exclusive permettant à la Bibliothèque nationale du Canada de reproduire, prêter, distribuer ou vendre des copies de sa thèse de quelque manière et sous quelque forme que ce soit pour mettre des exemplaires de cette thèse à la disposition des personnes intéressées.

The author retains ownership of the copyright in his/her thesis. Neither the thesis nor substantial extracts from it may be printed or otherwise reproduced without his/her permission.

L'auteur conserve la propriété du droit d'auteur qui protège sa thèse. Ni la thèse ni des extraits substantiels de celle-ci ne doivent être imprimés ou autrement reproduits sans son autorisation.

ISBN 0-315-90875-0

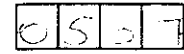
Canada

Name TRICIA L. HARRISON

Dissertation Abstracts International is arranged by broad, general subject categories. Please select the one subject which most nearly describes the content of your dissertation. Enter the corresponding four-digit code in the spaces provided.

Building Engineering

SUBJECT TERM



SUBJECT CODE

Subject Categories

**THE HUMANITIES AND SOCIAL SCIENCES**

**COMMUNICATIONS AND THE ARTS**

Architecture	0729
Art History	0377
Cinema	0900
Dance	0378
Fine Arts	0357
Information Science	0723
Journalism	0391
Library Science	0399
Mass Communications	0708
Music	0413
Speech Communication	0459
Theater	0465

**EDUCATION**

General	0515
Administration	0514
Adult and Continuing	0516
Agricultural	0517
Art	0273
Bilingual and Multicultural	0282
Business	0688
Community College	0275
Curriculum and Instruction	0727
Early Childhood	0518
Elementary	0524
Finance	0277
Guidance and Counseling	0519
Health	0680
Higher	0745
History of	0520
Home Economics	0278
Industrial	0521
Language and Literature	0279
Mathematics	0280
Music	0522
Philosophy of	0998
Physical	0523

Psychology	0525
Reading	0535
Religious	0527
Sciences	0714
Secondary	0533
Social Sciences	0534
Sociology of	0340
Special	0529
Teacher Training	0530
Technology	0710
Tests and Measurements	0288
Vocational	0747

**LANGUAGE, LITERATURE AND LINGUISTICS**

Language	
General	0679
Ancient	0289
Linguistics	0290
Modern	0291
Literature	
General	0401
Classical	0294
Comparative	0295
Medieval	0297
Modern	0298
African	0316
American	0591
Asian	0305
Canadian (English)	0352
Canadian (French)	0355
English	0593
Germanic	0311
Latin American	0312
Middle Eastern	0315
Romance	0313
Slavic and East European	0314

**PHILOSOPHY, RELIGION AND THEOLOGY**

Philosophy	0422
Religion	
General	0318
Biblical Studies	0321
Clergy	0319
History of	0320
Philosophy of	0322
Theology	0469

**SOCIAL SCIENCES**

American Studies	0323
Anthropology	
Archaeology	0324
Cultural	0326
Physical	0327
Business Administration	
General	0310
Accounting	0272
Banking	0770
Management	0454
Marketing	0338
Canadian Studies	0385
Economics	
General	0501
Agricultural	0503
Commerce-Business	0505
Finance	0508
History	0509
Labor	0510
Theory	0511
Folklore	0358
Geography	0366
Gerontology	0351
History	
General	0578

Ancient	0579
Medieval	0581
Modern	0582
Black	0328
African	0331
Asia, Australia and Oceania	0332
Canadian	0334
European	0335
Latin American	0336
Middle Eastern	0333
United States	0337
History of Science	0585
Law	0398
Political Science	
General	0615
International Law and Relations	0616
Public Administration	0617
Recreation	0814
Social Work	0452
Sociology	
General	0626
Criminology and Penology	0627
Demography	0938
Ethnic and Racial Studies	0631
Individual and Family Studies	0628
Industrial and Labor Relations	0629
Public and Social Welfare	0630
Social Structure and Development	0700
Theory and Methods	0344
Transportation	0709
Urban and Regional Planning	0999
Women's Studies	0453

**THE SCIENCES AND ENGINEERING**

**BIOLOGICAL SCIENCES**

Agriculture	
General	0473
Agronomy	0285
Animal Culture and Nutrition	0475
Animal Pathology	0476
Food Science and Technology	0359
Forestry and Wildlife	0478
Plant Culture	0479
Plant Pathology	0480
Plant Physiology	0817
Range Management	0777
Wood Technology	0746
Biology	
General	0306
Anatomy	0287
Biostatistics	0308
Botany	0309
Cell	0379
Ecology	0329
Entomology	0353
Genetics	0369
Immunology	0793
Microbiology	0410
Molecular	0307
Neuroscience	0317
Oceanography	0416
Physiology	0433
Radiation	0821
Veterinary Science	0778
Zoology	0472
Biophysics	
General	0786
Medical	0760

Geodesy	0370
Geology	0372
Geophysics	0373
Hydrology	0388
Mineralogy	0411
Paleobotany	0345
Paleoecology	0426
Paleontology	0418
Paleozoology	0985
Palynology	0427
Physical Geography	0368
Physical Oceanography	0415

**HEALTH AND ENVIRONMENTAL SCIENCES**

Environmental Sciences	0768
Health Sciences	
General	0566
Audiology	0300
Chemotherapy	0992
Dentistry	0567
Education	0350
Hospital Management	0769
Human Development	0758
Immunology	0982
Medicine and Surgery	0564
Mental Health	0347
Nursing	0569
Nutrition	0570
Obstetrics and Gynecology	0380
Occupational Health and Therapy	0354
Ophthalmology	0381
Pathology	0571
Pharmacology	0419
Pharmacy	0572
Physical Therapy	0382
Public Health	0573
Radiology	0574
Recreation	0575

Speech Pathology	0460
Toxicology	0383
Home Economics	0386

**PHYSICAL SCIENCES**

Pure Sciences	
Chemistry	
General	0485
Agricultural	0749
Analytical	0486
Biochemistry	0487
Inorganic	0488
Nuclear	0738
Organic	0490
Pharmaceutical	0491
Physical	0494
Polymer	0495
Radiation	0754
Mathematics	0405
Physics	
General	0605
Acoustics	0986
Astronomy and Astrophysics	0606
Atmospheric Science	0608
Atomic	0748
Electronics and Electricity	0607
Elementary Particles and High Energy	0798
Fluid and Plasma	0759
Molecular	0609
Nuclear	0610
Optics	0752
Radiation	0756
Solid State	0611
Statistics	0463
Applied Sciences	
Applied Mechanics	0346
Computer Science	0984

Engineering	
General	0537
Aerospace	0538
Agricultural	0539
Automotive	0540
Biomedical	0541
Chemical	0542
Civil	0543
Electronics and Electrical	0544
Heat and Thermodynamics	0348
Hydraulic	0545
Industrial	0546
Marine	0547
Materials Science	0794
Mechanical	0548
Metallurgy	0743
Mining	0551
Nuclear	0552
Packaging	0549
Petroleum	0765
Sanitary and Municipal	0554
System Science	0790
Geotechnology	0428
Operations Research	0796
Plastics Technology	0795
Textile Technology	0994

**PSYCHOLOGY**

General	0621
Behavioral	0384
Clinical	0622
Molecular	0622
Developmental	0620
Experimental	0623
Industrial	0624
Personality	0625
Physiological	0989
Psychobiology	0349
Psychometrics	0632
Social	0451



CONCORDIA UNIVERSITY

Division of Graduate Studies

This is to certify that the thesis prepared

By: Michael A. Lacasse


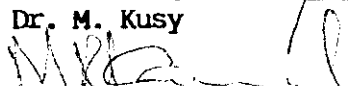

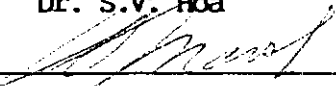
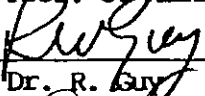
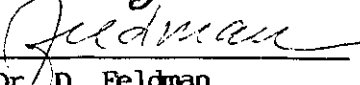
Entitled: **Functional Properties of Polyurethane Based Sealants  
Blended with Polymeric Modifiers**

and submitted in partial fulfillment of the requirements for the degree of

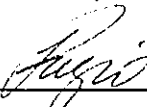
Doctor of Philosophy (BUILDING STUDIES)

complies with the regulations of this University and meets the accepted standards with respect to originality and quality.

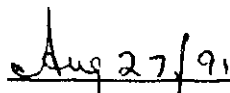
Signed by the final examining committee:

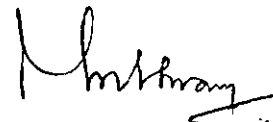
 _____	Chair , Assoc. Dean, Graduate Studies
Dr. M. Kusy	
 _____	External Examiner
Dr. M. Kamal	
 _____	Concordia External to Program
Dr. S.V. Hoa	
 _____	Internal Examiner
Prof. C. Marsh	
 _____	Internal Examiner
Dr. R. Guy	
 _____	Thesis Supervisor
Dr. D. Feldman	

Approved by



Director, Centre for Building Studies

  
Date



Dean of Faculty of Engineering  
and Computer Science

## Abstract

### Functional Properties of Polyurethane Based Sealants Blended with Polymeric Modifiers

Michael A. Lacasse Ph. D. (Building Studies)  
Concordia University, 1991

Novel polyurethane based two-component self-leveling sealant formulations, incorporating various types of kraft processed lignins including softwood, hardwood, and eucalyptus wood lignin, were produced and their performance properties established in a research program which sought to develop more durable cost effective sealants as well as cultivate a market for lignin, a highly underutilized by-product of the pulp and paper industry. The tensile and compressive performance characteristics of lignin and kaolin filled sealant formulations, compounded at different volumetric filler loadings, were compared and the results indicated that both types of filler increase the modulus of the base elastomer in relation to the semi-empirical relation of Nielsen. This suggests that the mechanical properties are dependent on the maximum packing fraction of the respective fillers which in turn, is a function of their particle size and size distribution. The relationship between the modulus and the volumetric filler loading was useful in the preparation of sealant formulations having optimum filler contents. Finally, these optimum formulations were prepared for a subsequent testing program in which the tensile strength and cyclic performance of the sealants was compared to that of existing two-component self-leveling sealant compounds currently available on the market. Results of these performance tests indicate that lignin filled elastomeric sealants, in most instances, have adequate tensile strength and perform adequately if subjected to a moderate cyclic strain program. Further improvements in performance properties may be obtained if adjustments to the particle size are made and this is warranted considering six to ten times cost advantage these fillers possess in relation to conventional fillers.

## Acknowledgements

The author is grateful to Dr. Dorel Feldman, Professor at the Centre for Building Studies, for his supervision, guidance, and encouragement during the course of this work.

The author wishes to thank Mrs. Dorina Banu, research associate, for having assisted in completing both the DSC and DMA analysis and Dr. Christina Luchian, postdoctoral fellow, for the IR analysis. Both co-workers made many helpful suggestions regarding various aspects of this work and their guidance is gratefully acknowledged.

The author is grateful to Dr. Almeria Natansohn, Associate Professor at Queen's University in Kingston, for having completed the NMR portion of this study.

A note of thanks is extended to all the technicians who helped in this endeavour and in particular, Mr. Hans Obermier, Mr. Joseph Hrib, Mr. Wesley Fitch, Mr. Joseph Zilka and Mr. Zak Gohneim. Particular thanks is given to Mr. Derik Hunziker for his assistance in completing contact angle measurements.

The author would also like to express his appreciation to the following agencies or foundations which provided partial funding for this project:

Natural Sciences and Engineering Research Council of Canada

Canadian Mortgage and Housing Corporation

Standards Council of Canada

F.W. McConnel Foundation, Concordia University

Acknowledgement must also be made of the contribution by the Bayer Corporation of Canada for having provided the prepolymers and many of the related sealant products. Thanks is extended to Mr. Yvan Maillet for having coordinated these efforts.

A very special note of thanks is extended to the author's wife, Andrea, and his daughter, Carolynn, for their continued support throughout this endeavour.

## TABLE OF CONTENTS

### 1. INTRODUCTION

1.1	Purpose & Objectives of Research	1
1.2	Use & Significance of Sealants in Construction	3
1.3	Lignin as a Base for Polymeric Products	6

### 2. FUNDAMENTAL & APPLIED RESEARCH RELATED TO LIGNIN-POLYMER SYSTEMS

2.1	Fundamental Studies of Lignin-Polymer Systems	10
2.1.1	Lignin-thermoplastic Polymer Systems	10
2.1.2	Lignin-thermosetting Polymer Systems	11
2.2	Applied Research of Lignin-Polymer Systems	19
2.2.1	Lignin graft Copolymers	19
2.2.2	Lignin-Polymer Adhesive Systems	20
2.2.3	Lignin elastomer Systems	21
2.3	Summary of Research Related to Lignin-Polymer Systems	32



### 3. RESEARCH PROGRAM

3.1	Outline of Research Program	34
3.2	Polyurethane Synthesis, Prepolymer Components & the Formulation of Elastomeric Sealants	39
3.2.1	Synthesis	39
3.2.1.1	Basic Reactions & Reaction Products	39
3.2.1.2	Polyurethane Prepolymers	41
3.2.2	Polyurethane Elastomer Sealant Formulations	41
3.2.3	Compounding Elastomeric Sealant Formulations	50
3.2.3.1	Preparation of Unfilled Elastomers	51
3.2.3.2	Preparation of Filled Elastomers	55
3.3	Physical Characterization of Particulate Fillers	59
3.3.1	Particle Size & Size Distribution	59
3.3.1.1	Estimation of Particle Size Using Light Microscopy	59
3.3.1.2	Particle Size Distribution	59
3.3.2	Maximum Packing Fraction & Oil Absorption	64
3.3.3	Specific Gravity of Particulate Fillers	68
3.4	Characterization of Unfilled & Filled Elastomers	69
3.4.1	Characterization Using the Swelling Method	69
3.4.1.1	Molecular Weight Between Crosslinks of PUR Elastomers	69
3.4.1.2	Swelling Phenomenon in Filled Elastomers	71
3.4.2	Mechanical Properties in Tension & Compression	72
3.4.2.1	Tensile Tests	74
3.4.2.2	Compression Tests	77
3.4.2.3	Compression Set	77
3.4.2.4	Hardness Tests	78
3.4.3	Thermal Behaviour - Glass Transition Temperature	80
3.4.3.1	Differential Scanning Calorimetry	80
3.4.3.2	Dynamic Mechanical Analysis	81

3.4.4	Infrared & Nuclear Magnetic Resonance Spectroscopy	84
3.4.4.1	Infrared Spectroscopy	84
3.4.4.2	Nuclear Magnetic Resonance	84
3.4.5	Surface Analysis Techniques	86
3.4.5.1	Surface Analysis of Elastomer Matrix	89
3.4.5.2	Surface Analysis of Particulate Fillers	92
3.4.6	Performance Testing of Sealants	94
3.4.6.1	Performance Test Methods	94
3.4.6.2	Review of Direct Test Methods	96
3.4.6.3	Description of Sealant Testing Devices	100

#### 4. RESULTS & DISCUSSION

4.1	Introduction	107
4.2	Preliminary Investigations	109
4.2.1	Thermal Analysis of Sealant Formulation Components	109
4.2.2	Particle Size Analysis of Fillers	111
4.2.3	Mechanical Properties of Preliminary Elastomer Formulations	117
4.3	Characterization of Unfilled Elastomers	125
4.3.1	Molecular Weight of PUR by the Swelling Method	125
4.3.2	Mechanical Properties of Unfilled Elastomers	133
4.3.2.1	Curing as Determined Using Hardness Tests	133
4.3.2.2	Tensile Characteristics	137
	a) Introduction	137
	b) Tensile tests on TA type specimens	140
	c) Tensile tests on TB type specimens	146
4.3.2.3	Compression Characteristics	150
	a) Stress-strain Behaviour	150
	b) Compression set	153
4.3.3	Thermal Analysis of Unfilled Elastomers	158

4.4	Characterization of Filled Elastomers	163
4.4.1	Swelling Behaviour	163
4.4.2	Curing of Filled Formulations	168
4.4.3	Mechanical Properties in Tension	173
4.4.4	Mechanical Properties in Compression	182
	4.4.4.1 Stress-strain Behaviour	182
	4.4.4.2 Compression Set	189
4.4.5	Spectroscopic Analysis	190
	4.4.5.1 Infrared Spectroscopy	190
	4.4.5.2 CP-MAS NMR	192
4.4.6	Thermal Analysis of Filled Elastomers	195
4.5	Analysis of the Surface Properties of PUR Elastomers & Particulate Fillers	201
4.5.1	Surface Properties of Elastomer Matrix	201
4.5.2	Surface Properties of Particulate Fillers	206
4.6	Performance Properties	212
4.6.1	Tensile tests	212
4.6.2	Karpati Performance Test	214
4.6.3	Cyclic Performance Test	219
<b>5. <u>CONCLUSIONS &amp; RECOMMENDATIONS</u></b>		
5.1	Conclusions	222
5.2	Recommendations	228
	REFERENCES	234
	APPENDIX	243

## LIST OF FIGURES

Figure No.		Page No.
1.1	Current and suggested uses for lignin [14].	7
1.2	Chemical products derivable from lignin [15].	8
2.1	Reaction product of lignin & HMTA in phenol [19].	11
2.2	Reaction of lignin and phenol [19].	12
2.3	Vulcanizate properties vs lignin loading for natural, SBR, nitrile & neoprene rubbers. Numbers on the tensile curves represent ultimate elongation [50].	23
2.4	Tensile stress-strain curves obtained from acrylic polyblends adhered to aluminum substrates. Curve 1: A-L,100:0 pbw; 2: A-L,100:5; 3: A-L,100:10; 4:100,12.5; 5:100:15 [3].	26
2.5	Tensile stress-strain curves obtained from L-PUR polyblends adhered to aluminum substrates. Curve 1: L-PUR, 0:100 pbw; 2: L-PUR, 5:100; 3: L-PUR, 10:100; 4: L-PUR 12.5:100; 5: L-PUR, 15:100; 6: L-PUR 20:100 [4].	28
2.6	Tangent modulus of L-PUR polyblends as a function of lignin loading in control (C), artificial weathering (AW), and natural weathering (NW) conditions. Substrates : ( ) wood; ( ) mortar; ( ) aluminum [4].	29

2.7	(a) SEM of neat PUR surface (500x). Surface texture of PUR matrix is even. Pits and protuberances can be seen on surface. (b) SEM of L-PUR polyblend surface (20:100;500X). L particles are embedded throughout the PUR matrix [5].	30
2.8	DSC curves of lignin and L-PUR polyblends [5].	31
3.1	Outline of research program.	35
3.2	Basic synthesis reactions for polyurethane products [65].	40
3.3	Polyaddition of polyfunctional PUR reaction components [65].	41
3.4	Idealized structure of crosslinked PUR, based on Desmophen 1920D and Desmodur E14.	46
3.5	Doubled sized glove box.	52
3.6	Dependency of $\psi\phi_i$ on the volume fraction of particulate filler, $\phi_i$ , incorporated in a polymeric matrix [80].	66
3.7	Test set-up for tension & compression testing. 1. Instron Universal Testing Machine; 2. Instron UTM control module; 3. XT based personal computer hosting data acquisition system.	73
3.8	TA type tensile test specimen & test set-up.	75
3.9	TB type tensile specimen and test set-up.	76
3.10	Surface analysis of elastomer matrix using the sessile drop technique: a) photographic set-up; b) video camera set-up.	90
3.11	Apparatus for evaluating the capillary flow rates of various wetting liquids through a column of packed particulate matter.	93

3.12	a) PRL natural exposure test rig; b) Sealant weathering test rack; c) Close-up of centre of test rack [113-115].	98
3.13	Hand operated sealant testing device [119].	99
3.14	Sealant testing vise used in Karpati performance test.	100
3.15	Sealant testing devices shown mounted on a test frame.	102
3.16	Automatic sealant testing set-up.	104
3.17	Detail of sealant testing rig.	105
4.1	Particle size distribution for various particulate fillers used in this study.	113
4.2	Photomicrographs of filler particles: Set #1 (uppermost series of 2): Indulin AT @ 150X (left) and 300X (right); Set #2: Eucalin; Set #3: Tomlinite; Set #4: Sillitin Z86.	115
4.3	Shore "A" indentation hardness of preliminary PUR based sealant formulations in relation to curing time.	123
4.4	Adhesive strength of unfilled elastomer formulations in relation to stoichiometric ratio.	124
4.5	Number average molecular weight of PUR elastomer formulations as a function of SR,BPR & PC.	128
4.6	Comparative analysis of theoretical to experimental number average molecular weights between crosslinks for unfilled PUR elastomer formulations.	132
4.7	Indentation hardness (Shore "A") as a function of time for unfilled elastomers of constant BPR (BPR=1) having different plasticizer contents and stoichiometric ratios. Series A: PC = 30%; B: PC = 34%; C: PC = 40%.	134

4.8	Indentation hardness of unfilled PUR elastomers as a function of (a) Baylith paste ratio & (b) plasticizer content (PC) at constant stoichiometry.	136
4.9	Evaluation of the strain energy density based on the load deformation properties of the test specimen.	138
4.10	Tensile test on unfilled PUR elastomer type TA specimens for formulations having different plasticizer contents.	143
4.11	Tensile tests on unfilled PUR elastomer type TA specimens for formulations having different polyol ratios (Baylith OH/Desmophen OH).	144
4.12	Tensile tests on PUR elastomer type TA specimens for formulations having different stoichiometric ratios (NCO/OH).	145
4.13	Tensile tests on unfilled PUR elastomer type TB specimens for formulations having different plasticizer contents.	147
4.14	Tensile tests on unfilled PUR elastomer type TB specimens for formulations having different polyol ratios (Baylith OH/Desmophen OH).	148
4.15	Tensile tests on unfilled PUR elastomer type TB specimens for formulations having different stoichiometric ratios (NCO/OH).	149
4.16	Supposed secondary (intermolecular, e.g. hydrogen) bond formation in urethane elastomers [64].	155
4.17	Degree (%) of compression set of unfilled PUR elastomers in relation to the Baylith paste & stoichiometric ratios of the formulation.	157

4.18	Glass transition temperature of unfilled elastomers as a function of (a) plasticizer content & (b) Baylith paste ratio at given stoichiometries.	160
4.19	Glass transition temperature of polymeric mixture as a function of diluent concentration.	161
4.20	Swelling of filled PUR elastomer formulations. Dependence of elastomer on the volume loading of particulate fillers.	166
4.21	Curing of (a) Tomlinite & (b) Indulin AT filled elastomers at different filler loadings.	169
4.22	Curing of (a) Eucalin & (b) Sillitin/Titanox filled elastomers at different filler loadings.	170
4.23	Curing of various filled formulations at 15% volume loading in relation to the base unfilled formulation (28C).	172
4.24	Tensile characteristics of TA type PUR based elastomer specimens filled with Indulin AT at different volumetric loadings.	175
4.25	Tensile characteristics of TA type PUR based elastomer specimens filled with Eucalin at different volumetric loadings.	176
4.26	Tensile characteristics of TA type PUR based elastomer specimens filled with Sillitin/Titanox at different volumetric loadings.	177
4.27	Tensile characteristics of TA type PUR based elastomer specimens filled with Tomlinite at different volumetric loadings.	178



4.28	Tensile characteristics of TA type PUR based elastomer specimens having different filler types at 15% volumetric loading.	179
4.29	Elastic modulus ratio ( $E/E_0$ ) of filled PUR based elastomers as a function of volumetric loading (%) for different filler types in comparison to theory of Guth [133] and Nielsen [84].	181
4.30	Compression tests on type C PUR based elastomer specimens filled with Indulin AT at different volumetric loadings.	184
4.31	Compression tests on type C PUR based elastomer specimens filled with Eucalin at different volumetric loadings.	185
4.32	Compression tests on type C PUR based elastomer specimens filled with Sillitin/Titanox at different volumetric loadings.	186
4.33	Compression tests on type C PUR based elastomer specimens filled with Tomlinite at different volumetric loadings.	187
4.34	Elastic modulus ratio in compression for filled PUR based elastomers as a function of volumetric loading for different filler types.	188
4.35	Infrared spectra of (a) lignin (Tomlinite); (b) unfilled PUR elastomer; (c) lignin filled (10 %v) PUR elastomer.	191
4.36	CP-MAS NMR spectra of: (a) lignin (TOMLINITE), 100 scans, 2ms contact time; (b) polyurethane lignin formulation (30% lignin by weight), 200 scans, 10 ms contact time; polyurethane, 1500 scans, 20 ms contact time.	193
4.37	Signal intensity at 76 ppm for the polyurethane as such [ ] and blended with lignin (TOMLINITE) [ ] against contact time.	194

4.38	Dynamic mechanical analysis of unfilled and filled elastomers. Tan $\delta$ as a function of temperature for various PUR filled elastomers.	196
4.39	Shifts in $T_g$ as a function of volumetric filler loading for various fillers.	198
4.40	Swelling coefficient as a function of degree of shift.	199
4.41	Filler characterization: swelling coefficient as a function of maximum packing fraction.	200
4.42	Digitized image (100x) of a sessile drop of water on the surface of a PUR elastomer 10 seconds after contact with the surface.	202
4.43	Contact angle of a wetting liquid on the surface of a PUR based elastomer substrate as a function of the surface tension of the wetting liquid.	205
4.44	Contact angle analysis of lignin fillers. Cosine of the contact angle as a function of the surface energy of the wetting liquid.	207
4.45	Contact angle analysis of selected pigments. Cosine of the contact angle as a function of the surface energy of the wetting liquid [106].	208
4.46	Dependency of the work of adhesion $W_A$ , on the tensile modulus at different volumetric loadings.	211
4.47	Tensile (TB) stress-strain characteristics of commercially based (A1, A2, A3) and filled (ST, TO) PUR based sealants.	213
4.48	Commercially produced PUR sealants (A2, A3) undergoing cyclic movement.	215

4.49	Stages of deformation: $\pm$ width change as a function of the number of cycles to failure.	217
4.50	Stage 3 results for A2 and A3 type PUR sealants: log strain (width change) versus log time.	218
4.51	Strain amplitude as a function of the number of cycles to failure for ST & TO filled PUR based sealants.	221

## LIST OF TABLES

Table No.		Page No.
1.1	Projected average annual growth rates of synthetic sealants in the US market for the period 1985-1990.	5
2.1	Comparison of properties of three types of urethane foams [26].	14
3.1	Physical & chemical properties of isocyanate prepolymers [68].	43
3.2	Physical & chemical properties of polyol prepolymers [68].	44
3.3	Polyurethane formulation components.	48
3.4	Classification of unfilled polyurethane elastomers.	53
3.5a	Physical properties of inorganic particulate fillers.	56
3.5b	Chemical analysis of inorganic fillers.	56
3.5c	Physical characteristics of organic particulate fillers.	57
3.6	Classification of filled PUR elastomers.	58
3.7	Characteristics of wetting liquids used in surface energy evaluations.	91

3.8	Degrading factors used in laboratory tests simulation of aging [112].	95
4.1	Results of thermal analysis of formulation components using the DSC technique.	110
4.2	Particle size of fillers as determined by the sedimentation technique.	112
4.3	Results from microscopic observation of filler particles.	116
4.4	Summary of trail formulations N <sup>o</sup> 1 to N <sup>o</sup> 3.	119
4.5	Summary of trail formulations N <sup>o</sup> 4 & N <sup>o</sup> 6.	120
4.6	Summary of trail formulations N <sup>o</sup> 7,9 & N <sup>o</sup> 10 & preliminary test results.	121
4.7	Calculation of $M_{c,s}$ of unfilled elastomers.	126
4.8	Theoretical molecular weights for PUR elastomers.	131
4.9	Tensile properties of unfilled PUR elastomer type TA specimens as a function of plasticizer content.	141
4.10	Tensile properties of unfilled PUR elastomer type TA specimens a function of baylith paste ratio.	141
4.11	Tensile properties of unfilled PUR elastomer type TA specimens as a function of stoichiometric ratio.	141
4.12	Tensile properties of unfilled PUR elastomer type TB specimens.	146
4.13	Calculation of $M_c$ based on compression tests.	152

4.14	Degree (%) of compression set of unfilled PUR elastomers as a function of baylith paste ratio, stoichiometric ratio & plasticizer content.	153
4.15	$T_g$ of unfilled elastomer formulations.	158
4.16	Swelling results from filled elastomers.	165
4.17	Characteristic particulate filler coefficients based on swelling behaviour.	167
4.18	Mechanical properties of filled PUR based elastomers.	174
4.19	Mechanical properties of filled PUR elastomers in compression.	183
4.20	Compression set of filled PUR elastomers.	189
4.21	Results from contact angle measurements on PUR elastomers using the sessile drop technique.	203
4.22	Results from analysis of contact angle data from PUR elastomers.	204
4.23	Results from analysis of contact angle of particulate fillers.	209
4.24	Degree of interaction between filler and polymeric matrix.	210
4.25	Tensile performance of PUR sealants.	212

## LIST OF EQUATIONS

Equation No.		Page No.
3.1	Equivalent spherical diameter of filler particles according to Stoke's law [77].	61
3.2	Effective depth of hydrometer [78].	62
3.3	Percentage of filler remaining in suspension [78].	63
3.4	Modulus ratio according to Neilsen [84].	64
3.5	Maximum packing fraction according to Patton [85].	66
3.6	Number average molecular weight between crosslinks [88].	70
3.7	Number of effective network chains per unit volume of elastomer [89,90].	70
3.8	Characterization of swelling phenomena in filled elastomers [91].	71
3.9	Dynamic elastic modulus obtained using Dupont 982 DMA [101].	83
3.10	Surface analysis of fillers: cosine of contact angle, $\Theta$ [61].	86
3.11	Rate of capillary rise of a liquid through a porous medium [62,109].	87
3.12	Column packing constant.	87
3.13	Polymer-filler interaction parameter [63].	88

3.14	Matrix bonding coefficient [63].	88
4.1	Specific surface area according to the Gates method [59].	111
4.2	Factor to take into account additives in elastomers [89].	125
4.3	Molecular weight as determined using swelling method.	125
4.4	Theoretical molecular weight of PUR elastomer.	130
4.5	Theoretical molecular weight of PUR elastomer without castor oil.	130
4.6	Theoretical molecular weight of PUR elastomer as a function of stoichiometric ratio.	130
4.7	Strain energy density of elastomer under tensile elongation [125].	138
4.8	Calculation of average strain energy density.	139
4.9	Average strain energy density as a function of average stress-strain curve.	139
4.10	Stress as a function of shear modulus and extension ratio [71].	140
4.11	Calculation of reduced modulus of polymer.	140
4.12	Shear modulus related to molecular parameters of elastomer [71].	150
4.13	Evaluation of $T_g$ of a binary system of polymer and diluent [128].	159
4.14	Swelling behaviour according to Kraus [91].	163



4.15	Volume fraction of elastomer in swollen specimen.	164
4.16	Modulus ratio according to the theory of reinforcement developed by Guth [133].	180
4.17	Solid-vapour surface energy according to Lee [63].	204
4.18	Calculation of the work of adhesion ( $W_A$ ) and cohesion ( $W_C$ ) [61].	209
4.19	Number of cycles to failure of elastomer products [140].	219

## LIST OF ABBREVIATIONS & NOTATIONS

### Abbreviations

A-L	acrylic-lignin (polyblend)
ASTM	American Society of Testing Materials
AT	Indulin AT lignin particulate filler
AW	artificial weathering (test conditions)
BPR	Baylith paste ratio (polyol ratio)
C	control (test conditions)
CBS	Centre for Building Studies
CGSB	Canadian government standards board
CP-MAS	cross polarized-magic angle spin (NMR)
CPU	central processing unit
DMS	dimethylsulphide
DMSO	dimethylsulphoxide
DSC	differential scanning calorimetry
EU	Eucalin lignin particulate filler
EW	equivalent weight
HDPE	high density polyethylene
HMTA	hexamethylene tetramine
HPL	hydroxypropyl-lignin
i.d.	inside diameter
IR	infrared
KPL	kraft lignin polyol
LOI	loss on ignition
L-PUR	lignin-polyurethane (polyblend)
MDI	polymeric methylene diisocyanate
MW	molecular weight
NCO	isocyanate functional group
NMR	nuclear magnetic resonance
NW	natural weathering (test condition)
OA	oil absorption
OH	hydroxyl functional group
pbw	parts by weight

PBDG	polybutadiene glycol
PC	plasticizer content
PEG	poly(ethylene glycol)
PHD	poly Harnstoff dispersion polyether
PP	polypropylene
PRL	Princes Risborough Laboratory
PUR	polyurethane
PVC	polyvinyl chloride
RH	relative humidity
SBR	styrene-butadiene rubber
SEM	scanning electron microscope
SR	stoichiometric ratio
ST	Sillitin Z86/Titanox particulate filler
TA	tensile test configuration type "TA"
TB	tensile test configuration type "TB"
TDI	toluene diisocyanate
TMP	trimethylol propane
TO	Tomlinite lignin particulate filler

## Notations

$a$	cross-section area of sedimentation cylinder
$a_o$	cross-sectional area of disk
$b$	interaction parameter
$b_f$	extent of interaction, filler
$b_p$	extent of interaction, elastomer
$C$	mechanical constant related to shear modulus
$D$	equivalent spherical diameter of particles
$E$	Young's modulus; modulus of filled elastomer
$E_f$	modulus of particulate filler
$E_o$	modulus of unfilled elastomer
$E_p$	modulus of base polymer
$f$	factor related to additives present in the elastomer
$G$	Shear modulus
$h_o$	height of the undeformed, unswollen disk
$k$	column packing constant
$k_E$	Einstein coefficient
$l$	distance of rise of a liquid through a column
$l_o$	gauge length
$L_o$	effective depth of hydrometer
$L_1$	distance along stem of hydrometer
$L_2$	overall length of the hydrometer bulb
$m$	factor related to effective network formation
$M_{c,c}$	Number average MW between crosslinks, compression
$M_{c,s}$	Number average MW between crosslinks, swelling
$M_n$	Number average molecular weight
$M_t$	theoretical molecular weight between crosslinks
$p_i$	load imparted on $i^{\text{th}}$ specimen
$P$	% of particulate matter remaining in suspension
$Q$	proportionality constant
$r$	hydrometer reading
$R$	Universal gas constant (82057 cm <sup>3</sup> -g/K-mole)
$S$	slope of the compression-deflection curve
$SA$	surface area
$SG_f$	specific gravity of particulate filler
$SG_k$	specific gravity of kerosene

$SG_s$	specific gravity of suspending medium
$t$	time which liquid takes to rise a given distance
$t_s$	sedimentation time
$T$	absolute temperature in Kelvin
$T_g$	glass transition temperature
$T_{gd}$	glass transition temperature of diluent
$T_{gp}$	glass transition temperature of polymer
$T_{1\rho H}$	spin-lattice relaxation time in the rotating frame
$U_i$	strain energy density of $i^{\text{th}}$ specimen
$U_n$	average strain energy density
$V_a$	volume of additives
$V_o$	volume of polymer
$V_r$	volume of elastomer
$V_s$	volume of solvent
$V_B$	volume of hydrometer bulb
$W$	oven dry mass of particulate matter
$W_a$	work of adhesion
$W_c$	work of cohesion
$W_f$	weight of filler
$W_{bk}$	weight of pycnometric flask & kerosine
$W_{bkt}$	weight of flask, kerosine and filler
$W_o$	weight of unswollen elastomer
$W_s$	weight of swollen elastomer
$W_{sol}$	weight of solvent
$X_m$	average particle size in weight increment

## Greek Notations

$\alpha$	deformation ratio
$\gamma$	surface tension of wetting liquid
$\gamma_c$	critical surface energy for wetting
$\gamma_{Ls}$	liquid / solid surface energy
$\gamma_{LV}$	liquid / vapour surface energy of the wetting liquid
$\gamma_{sv}$	solid / vapour surface energy
$\Gamma$	function of the filler-elastomer modulus ratio
$\delta$	density
$\delta_e$	density of elastomer
$\delta_f$	density of filler
$\delta_{sol}$	density of solvent
$\epsilon_b$	strain at break
$\epsilon_i$	strain of $i^{\text{th}}$ specimen
$\eta$	viscosity of wetting liquid
$\eta_s$	viscosity of the suspending medium
$\Theta$	contact angle of wetting liquid
$\kappa$	function of the Einstein coefficient, $k_E$
$\lambda$	extension ratio ( $\lambda = 1 + \epsilon$ )
$\xi$	constant, characteristic of filler
$\sigma$	force per unit area (stress)
$\sigma_{av}$	average stress function
$\sigma_b$	stress at break
$\sigma_i$	stress of $i^{\text{th}}$ specimen
$\nu_2$	volume fraction of polymer in elastomer matrix
$\nu_e$	number of effective network chains
$\nu_{r0}$	$\nu_r$ of unfilled elastomer
$\phi_f$	volume fraction of filler in the filled elastomer
$\phi_m$	maximum packing factor
$\phi_{p,s}$	volume fraction of polymer in the swollen sample
$\psi$	reduced concentration scale factor
$\omega_d$	weight concentration of diluent
$\omega_p$	weight concentration of polymer
$\Omega$	polymer-matrix bonding coefficient

## CHAPTER 1

### INTRODUCTION

#### 1.1 PURPOSE & OBJECTIVES OF RESEARCH

The research program has a dual purpose: to help develop more resilient, durable and cost effective sealants; to aid in cultivating a market for lignin, a highly under utilized renewable polymeric material, and readily available byproduct of the pulp and paper industry.

The function of a sealant is to provide an effective seal between adjoining building materials such that the entry of water (liquid or vapour) and air at these joints is prevented, thus ensuring a weather-tight seal of the building envelope. The sealant must be capable of adhering to various building materials, be resistant to exposure in the most severe weather conditions over extended periods of time, yet be flexible enough to accommodate joint movement due to thermal and moisture effects.

Previous work has shown that the addition of lignin to various elastomeric based sealants in certain cases enhanced the tensile properties of these sealants [1-5]. The degree to which the properties were enhanced depended on the type

of sealant being blended and the amount of lignin present in the polymer matrix. In the case of polyurethane based sealants, lignin is considered to act as a reinforcing filler in a two phase polymer-particulate system.

The objective of this program is to establish the variation in the functional properties of polyurethane based sealants blended with various types of lignins including softwood (Indulin AT), hardwood (Tomlinite) and eucalyptus wood (Eucalin) kraft lignins, in comparison to a representative commercially produced sealant product. The functional properties relate to both the physico-chemical and the performance properties of the formulations. Physico-chemical properties consider not only physical and chemical aspects of the components but also the mechanical characteristics of the formulations. The performance properties will aid to evaluate these formulations from a practical standpoint.



## 1.2 USE & SIGNIFICANCE OF SEALANTS IN CONSTRUCTION

The outside envelope of a building undergoes cyclic movements in responding to changing temperature and moisture conditions. It may consist of building elements such as panels or various materials with joints between them, or large wall sections interrupted by expansion joints. These building elements or sections expand and contract as one unit with any change of temperature or moisture content and the resulting movements are accommodated at the joint.

The function of a joint in the external wall of a building is:

1. to prevent or limit contact through the joint between internal and external environments (i.e. to prevent the passage of water, air or dust)
2. to withstand the effects of changing the environmental conditions to which the joint will be exposed through its intended life.

Polymeric materials, called sealants, applied as viscous liquids, have been found to be most suitable for this purpose [6]. The sealant is formulated such that it keeps its shape when applied and hardens through chemical or physical processes to form a viscoelastic rubber-like material that withstands extension and compression. The sealant is extended at low temperatures and compressed at high temperatures because the building elements meeting at the joint contract with decreasing temperature and expand with rising temperature.

The demands on these materials are severe, because of the large temperature changes on the outside of buildings and the subsequent and simultaneous cyclic movement imposed on the sealants. Hence sealant behaviour under cyclical movement and simultaneous temperature changes is of prime importance in determining their performance properties.

The significance of sealants in the building industry may be appreciated by evaluating the extent of the sealant market. According to a market survey conducted in 1985 by market consultants Frost and Sullivan [7], the value of the sealant market in the US construction industry is in the order of 240 million dollars (US) representing 42% of the total market volume. If the consumer retail market is included, assuming that the retail end use is largely for building projects, then the dollar value and market share increase to 435 million (US) and 74% respectively.

The most extensively used sealants in the construction industry in order of market share are shown in Table 1.1, which also lists the respective average annual growth rates forecast for the period between 1985 and 1990.

The group of five synthetic sealants listed are expected to grow at an average annual rate of 6%. Of this group, silicone and polyurethane based products have above average growth rates, with an average annual growth rate of 7 and 6.6% respectively. The decreased market share expected for polysulphide products is a direct result of gains made by both silicone and polyurethane based sealants. The major factors responsible for their increased

Table 1.1 [7]	
AVERAGE ANNUAL GROWTH RATES OF SYNTHETIC SEALANTS IN THE US MARKET FOR THE PERIOD 1985 - 1990	
SEALANT BASE	AVERAGE ANNUAL GROWTH RATE %
Silicone	7.0
Polyurethane	6.6
Polysulphide	-1.0
Butyl	3.0
Acrylic	5.2
Other*	2.8
* e.g. includes among others: polyvinyl acetates, oleoresinous caulks, asphaltic based resins, hot-melts, neoprenes, fluorocarbons, etc.	

market share is reported to be substantial price reductions brought about by improvements in formulation and formulation technology.

Similar results were reported by the Freedonia Group, a business research organization based in Cleveland [8]. The average annual growth rate of sealants in the period between 1986 and 1991 is estimated to be 2.8% whereas the demand for silicone and polyurethane sealants will grow nearly 7% per year through to 1991 due to their decrease in price.

### 1.3 LIGNIN AS A BASE FOR POLYMERIC PRODUCTS

It has long been the object of chemists to extract and commercially utilize the lignin recovered from natural ligno-cellulosic materials such as wood for the production of phenolics, and other raw materials [9-11]. Although lignin is currently highly underutilized (e.g. 2% of 1980 production [12]), it has the potential of becoming a major source of polymer-based products for different industries including the construction industry for such items as building board adhesive binders, coatings, adhesives, foam insulation, and more recently, for reinforcing agents in elastomers.

Most lignin product applications are based on **technical** lignins (i.e. lignosulphonates and kraft lignin), which are separated during pulping processes. The sulphate and soda pulping processes result in spent liquors, called black liquors, from which alkali or kraft lignins may be obtained. Lignosulphonate spent liquors are derived from the sulphite or acid pulping process. The spent liquors are a by-product of these industries and may be used as a source of fuel, as a source of low molecular weight chemicals, or the basic polymer from which may be derived more useful high molecular weight products as depicted in Figure 1.1 [13,14].

Lignin is primarily used as an energy source. The recovery of process chemicals is based on the incineration of the pulping residue in the form of black caustic liquors. The calorific value of this organic material in the spent liquors is

a significant economic factor when considering the comparative cost of oil required to sustain a similar process. The sulphite process does not require the burning of waste liquor to economically sustain the industrial process, however, the residue has often been disposed of by discharge into the sewer system thus becoming a source of pollution. This has prompted in more recent years the intensified use of lignosulphonates as an energy source [13].

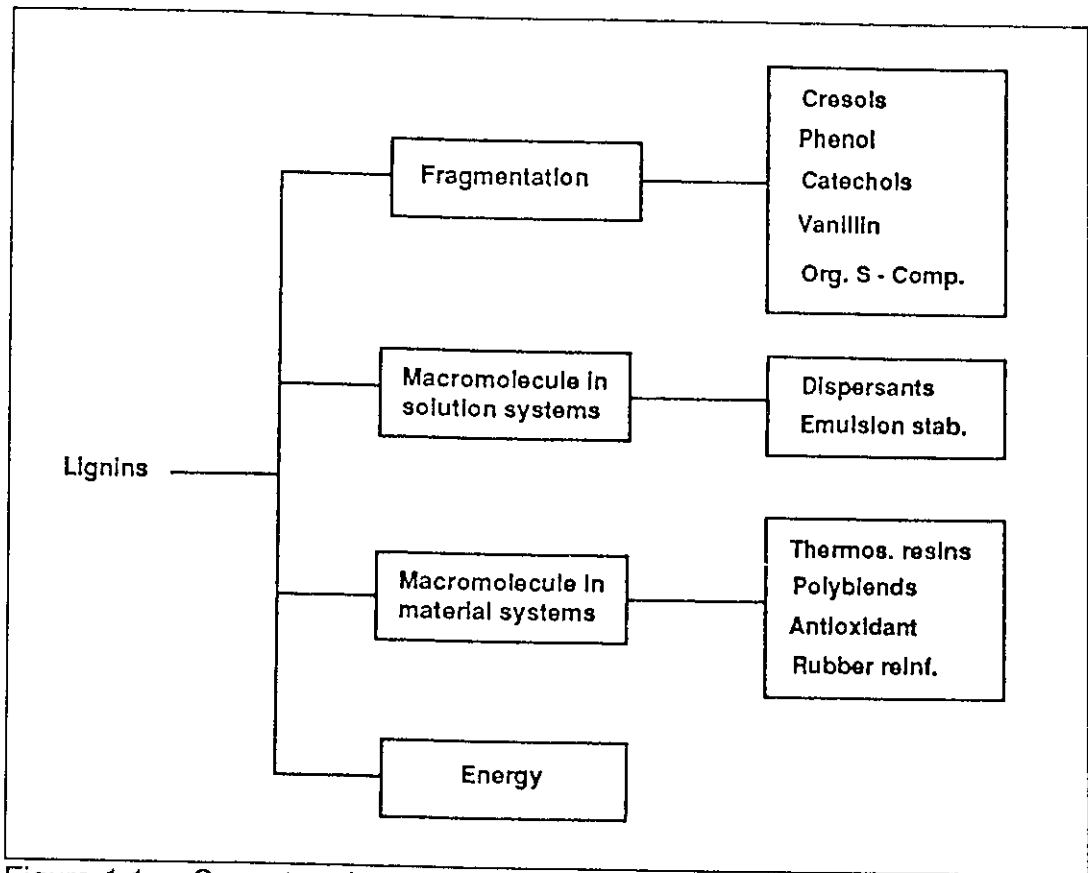


Figure 1.1 Current and suggested uses for lignin [14].

Lignin may serve as a source for a number of chemicals by fragmentation of lignin macromolecules to simple aromatic and aliphatic compounds. The principal chemical products which may be derived from lignin are illustrated in figure 1.2.

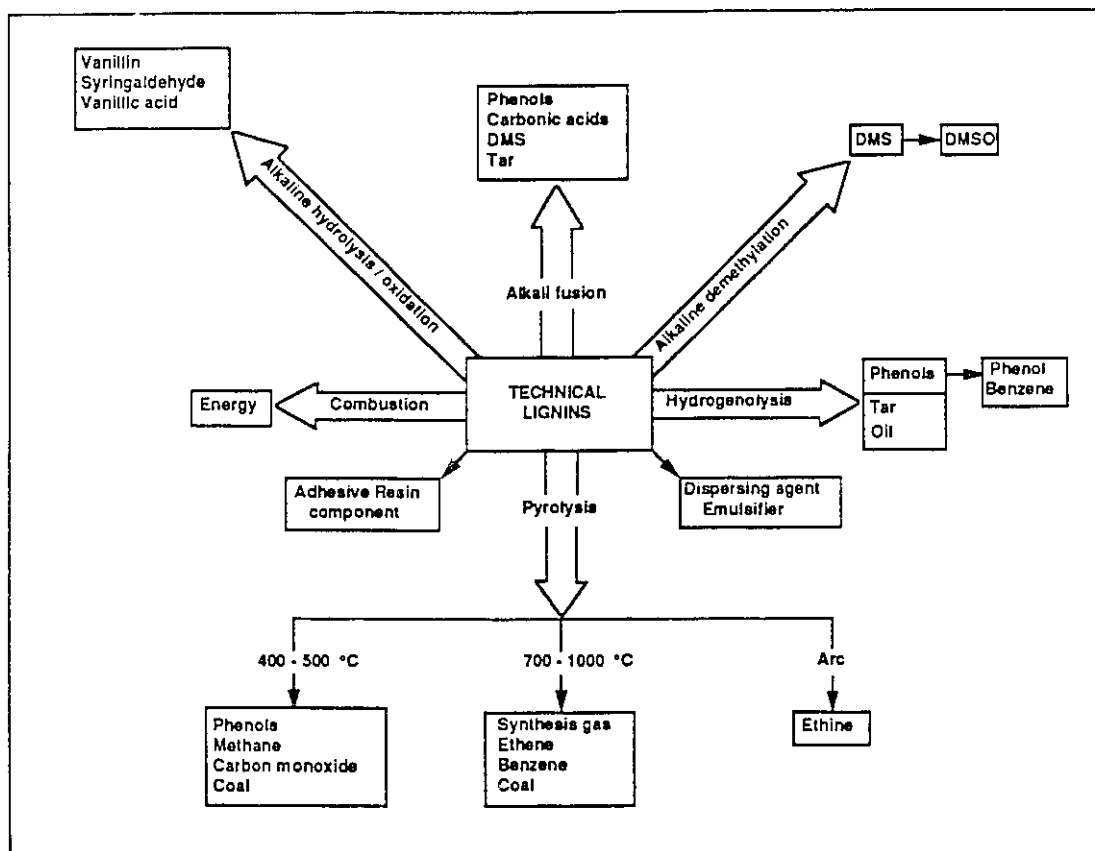


Figure 1.2 Chemical products derivable from Lignin [15].

Vanillin, dimethylsulphide (DMS), and dimethylsulfoxide (DMSO) are produced on an industrial scale, and are obtained from dimethylation of kraft black liquor. Of these chemicals, vanillin (a flavouring additive) is the most important chemical with respect to commercial utilization. DMSO is used as a solvent for biological and pharmaceutical materials, as well as for numerous other medical and chemical

uses. Other chemicals such as ethanol, acetic acid, turpentine and tall oil acids may also be obtained from various pulping processes [16].

## CHAPTER 2

### FUNDAMENTAL & APPLIED RESEARCH RELATED TO LIGNIN-POLYMER SYSTEMS

#### 2.1 FUNDAMENTAL STUDIES OF LIGNIN-POLYMER SYSTEMS

##### 2.1.1 LIGNIN-THERMOPLASTIC POLYMER SYSTEMS

Filler and additives are frequently used for effective modification of the properties of polyolefins. The properties, processability as well as the price of the original polymer can be altered by choosing a proper filler.

Chodak et al. [17] investigated the influence of lignin addition on the crosslinking characteristics of polypropylene (PP). In order to demonstrate the effect of various lignin functional groups on the properties of PP, kraft lignin and several of its derivatives were investigated as potential additives. The results show that polymerization of olefins are influenced mainly by hydroxyl (OH) groups present in the lignin. Unmodified kraft lignin has the greatest effect on the radical transformation reaction, since it contains many more OH groups than the lignin derived additives. It was also observed that the reactivity of aromatic OH groups (i.e. those attached to the aromatic ring in lignin) is greater than that of the aliphatic OH groups.

The use of lignin as a filler in high density polyethylene (HDPE) and PP has been studied by Klason and Kubat [18]. Lignin appears to behave as a reinforcing



filler which, when combined with either HDPE or PP, serves to moderately increase the modulus of these polyolefins. The relatively low increases in modulus are due to the low modulus of lignin (6.6 GPa). The authors state however, that there was no reduction in the stress at rupture in blended specimens.

### 2.1.2 LIGNIN-THERMOSETTING POLYMER SYSTEMS

The potential use of lignin for the production of plastics has been established in past years [19]. It has been shown that alkali lignin is able to react directly with HMTA (hexamethylene tetramine) in the presence of phenol in the same measure as hydrolytic lignin. It is assumed that this process takes place with the formation of the product illustrated in figure. 2.1

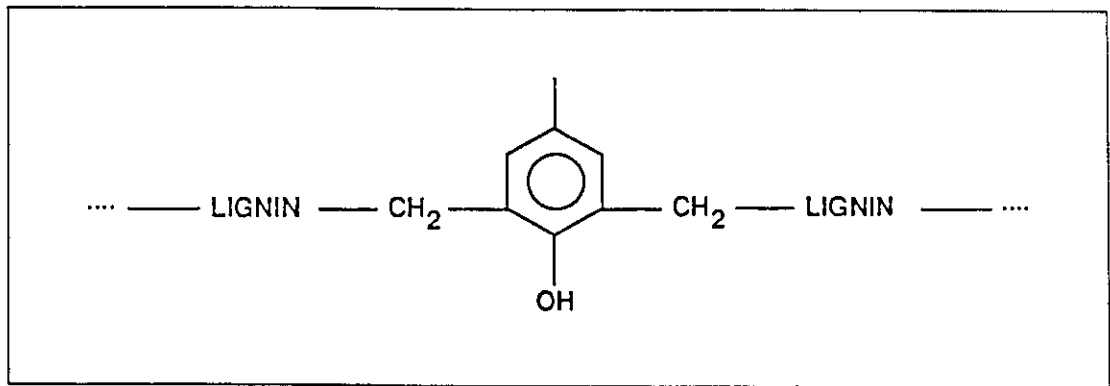


Figure 2.1 Reaction product of lignin & HMTA in phenol [19].

Considering that lignin may be represented by the formula  $C_{47}H_{55}O_{19}$ , and that one mole of lignin may react with four moles of phenol, Barg [20] has put forward the following microstructure for the resulting product, phenol-lignin. Figure 2.2 shows the reaction which leads to this product.

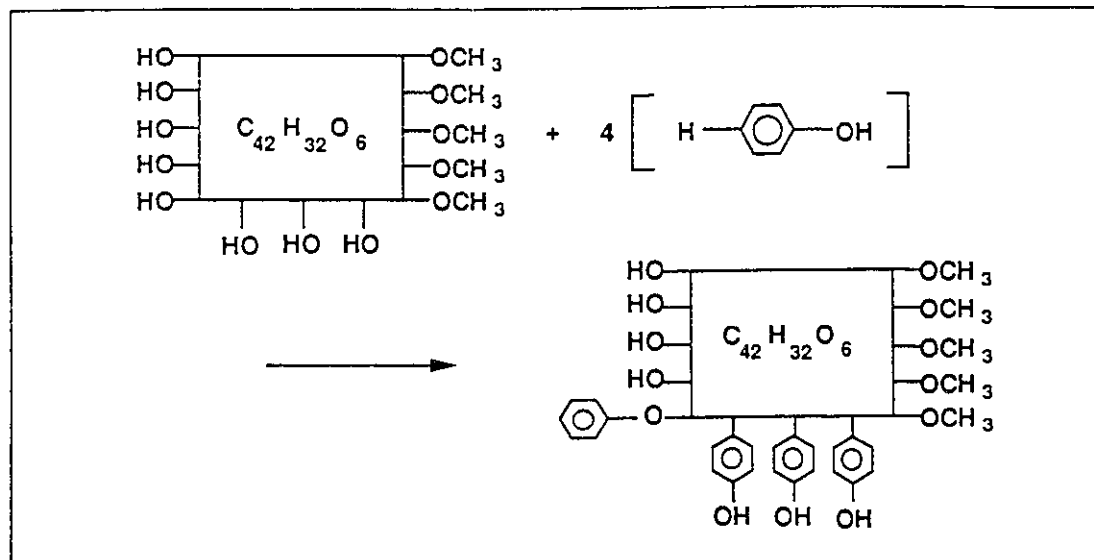


Figure 2.2 Reaction of lignin and phenol [19].

The reaction of lignin with phenol and isocyanates was investigated by Kratzl et al. [21]. These preliminary studies, designed to determine the potential utilization of lignin in the plastics industry, showed that in the case of lignin-isocyanate reactions, few products of technical value could be obtained. This was due to the scarcity of active positions within the lignin macromolecular structure. Much of the work related to polymer-lignin products has since focused on increasing the reactivity of the lignin by modifying specific reactive groups to enhance the polycondensation process.

Moorer et al.[22] employed lignin in the formation of polyurethane foams, by dissolving lignin in glycol and then reacting it with diisocyanate. The reaction was described in terms of the isocyanate acting as a crosslinking agent, linking the two kinds of polyol. The hydroxyl groups in lignin were assumed to be the key to this reaction.

Christian and co-workers [23] sought to increase the number of reactive positions in lignin by condensation with ethylene oxide, propylene oxide, and an alkyl sulphide. The reactions were shown to produce hydroxyl groups suitable for mixing and reacting with diisocyanates in the formation of rigid polyurethane foam.

More recently, studies by Glasser have been conducted to elucidate the mode of formation of new polyurethanes synthesized from lignin isocyanate combinations [24-34].

Hsu and Glasser [24,25] demonstrated that lignin may be carboxylated by reacting it with maleic anhydride to form a non-hydrolysable copolymer. The carboxyl and phenolic groups of this copolymer offer reactive sites for oxyalkylation to a polyol. This may be achieved by reacting the saponified copolymer with propylene oxide in the presence of an alkali catalyst. The carboxyl groups are esterified, and the phenolic and aliphatic hydroxyl groups are etherified to yield a highly viscous, homogeneous active and polyfunctional polyester-polyether polyol suitable for mixing and reaction with diisocyanates.

To further demonstrate the versatility of lignin as a co-reactant in polyurethane formation, Glasser et al. [26] undertook the production of polyurethane foams from carboxylated lignin. Foam properties are summarized in Table 2.1. Both carboxylated and non-carboxylated kraft lignin polyols are compared to commercial polyurethane foam in terms of strength, appearance, and water sorption properties. The non-carboxylated polyol is definitely inferior in

Table 2.1 [26]			
COMPARISON OF PROPERTIES OF THREE TYPES OF URETHANE FOAMS			
PROPERTY	KLP*	Carboxylated KLP	Commercial foam
I. Strength Properties:			
@ density (mg/cc)	94.1	39.2	39.2
Compressive strength (kPa)	77	161	119
Modulus of elasticity (MPa)	3.7	2.7	-
Recovery (%)	0	90	80
II. Water absorption (%) @ 61.7 mg/cc density	18	9	10
* KLP: Kraft Lignin Polyol			

quality to the carboxylated polyol, which itself compares favourably with the commercial product. More significantly, the carboxylated lignin polyol has superior recovery and sorption properties than those of the commercial foams.

It is well known that the structure of any thermosetting resin can be described in terms of a relatively high molecular weight backbone polymer that is tied together by crosslinking segments. The properties of the network are then determined by the nature of the two components (main polymer and crosslinking agent) and the number of crosslinking sites introduced into the system (crosslinking density). By changing any one, or any combination of these structural features, the properties of the network are changed, allowing for the formulation of products with a wide range of properties.

Based on this premise, Glasser et al. conducted a series of tests on hydroxypropyl lignin polyol-isocyanate derivatives [27-33]. In an initial experimental series, the fundamental methods of controlling the lignin-polyurethane network were determined by first establishing the methods of synthesis of these polymers and their characterization in terms of chemical structure, thermal properties, molecular weights, and solubilities in various organic solvents [27-29].

The property relationships of lignin-based polyurethane films were evaluated in a second test series [30-33]. Lignin-based polyurethane films were synthesized from hydroxypropyl lignin derivatives and either an aliphatic or aromatic isocyanate. Saraf and Glasser [30] first examined the effect of lignin type, diisocyanate type, and composition in terms of the stoichiometry, on thermal and mechanical properties. Variation in the stoichiometry had no noticeable effect on the modulus or tensile strength, but did significantly influence the glass transition temperature ( $T_g$ ), swelling and strain at break.

The straight chain characteristics of the particular diisocyanates had a controlling influence on the thermal and mechanical properties of the films. Glass transition temperatures of the polyurethanes increase generally with the stoichiometric ratio (SR).

Rials and Glasser [31,32] established the effect of the crosslinking density on polyurethane films properties by varying both the stoichiometry and the hydroxyl content of the hydroxypropyl-lignin polyol. In the former study [31], the maximum effective crosslinking was found to occur at a SR of 3, after which the density

levelled off. It is suggested that the higher concentration of diisocyanate, in comparison to conventional polyurethane systems (i.e. 3:1 vs 2:1), is due to the high polydispersity of the lignin polyol, which excludes incorporation of lower molecular weight fractions into the network. Thus the influence of the sol fraction on the physical properties of the polymer network was significant, but the manner and the degree to which it affected the overall behaviour of the network could not yet be ascertained.

The latter study by Rials and Glasser [32], refers to the variation of hydroxyl content of the polyol prepolymer. The crosslinking density was found to vary directly with the hydroxyl content of the polyol. The  $T_g$  of the polyurethane films varied linearly with the crosslink density of the network. The dynamic mechanical properties of the films were found to be sensitive to the weight fraction of extractables in the network.

Saraf et al. [33] studied polyurethane synthesized from blends of hydroxypropyl-lignin (HPL) derivatives with poly(ethylene glycol)s (PEG). The effect of soft segment incorporation in relation to content and molecular weight was examined on the basis of thermal and mechanical properties. A steady drop in  $T_g$  was observed, with increasing PEG (soft segment) content and a significant increase in  $T_g$  with rising molecular weights. The tensile behaviour was considerably modified by the addition of even minor percentages of PEG. Both Young's modulus and tensile strength decreased with increased PEG content, whereas the ultimate strain at break increased for similar percentages of PEG in

the blend. Hence the mechanical properties were particularly sensitive to glycol content. Uniformity in structure, reduction in brittleness, and considerable improvement in mechanical properties with the inclusion of minor PEG constituents, indicated that the lignin-based network polyurethane could be synthesized with a wide range of performance characteristics.

In a subsequent experimental program [34], the effect of concentration of polybutadiene glycol (PBDG) in a mixture of HPL was examined in relation to the thermal and mechanical properties. A phase separation between the two polyol components in the polyurethanes was detected by thermal and mechanical analysis. This effect was evident for nearly all degrees of mixing. It was concluded that polyurethane films behaved like rubber-toughened lignin networks when PBDG was the discrete phase, and like lignin-reinforced rubber when the lignin derivative phase was discrete.

Yoshida et al. [35] investigated the synthesis of polyurethanes having various stoichiometric ratios, and kraft lignin (free of low molecular weight fractions) by polyaddition of kraft lignin, a polyether polyol, and polymeric methylene diisocyanate (MDI) in tetrahydrofuran solution. Films, made by solvent casting, were tested with respect to their swelling behaviour and tensile properties. The main findings were: At low stoichiometric ratios, kraft lignin contributed effectively to the formation of three dimensional polymer network. The results further show that when an optimum quantity of kraft lignin (5-20% depending on the SR ratio) is used, the resulting polyurethanes show improved mechanical properties

compared to the polyurethanes synthesized with the polyether polyol as the only polyol component. At high contents of kraft lignin (> 30%) the polyurethanes were hard and brittle regardless of the SR ratio used. This is attributed to the combined effect of increased crosslink density and of an increase in chain stiffness.



## 2.2 APPLIED RESEARCH OF LIGNIN-POLYMER SYSTEMS

Applied research in the area of lignin-polymer systems has been ongoing in essentially three distinct areas: lignin graft copolymers, lignin-polymer adhesive systems, and lignin-elastomer systems. These areas of research will be briefly discussed with special emphasis on lignin-elastomer systems since a knowledge of these types of systems is particularly significant in gaining an understanding of lignin based elastomeric sealants.

### 2.2.1 LIGNIN GRAFT COPOLYMERS

The development of lignin graft copolymers for use as thixotropic agents in drilling mud has been ongoing for a number of years [13], however more recently, attention has been directed towards the synthesis of new lignin-graft copolymers [36-38] where the grafting was done with polyacrylamide.

Meister and Patil [37] have developed a method to chemically initiate polymerization of 2-propenamide on kraft pine lignin. Proof that grafting has occurred was obtained from size exclusion chromatography, solubility, dialysis, and fractionation. The grafted lignin is an amorphous brown solid soluble in most organic solvents but does not dissolve in water or DMSO. The graft copolymer outperforms an equal concentration of chrome lignosulphonate when the compounds are tested as thinners for use in bentonite drilling mud [37,38].

## 2.2.2 LIGNIN-POLYMER ADHESIVE SYSTEMS

An extensive review has been made of the various adhesive systems elsewhere [39] and more recent developments in the utilization of lignin as a wood adhesive has been reviewed by Matte and Doucet [40].

The latter work differentiates between two ways to use lignin as a wood adhesive. The first is through chemical treatment of the wood surface thus enhancing the reactivity of lignin and thereby allowing the formation of chemical bonds between wood particles under appropriate thermodynamic conditions. The second way consists of first extracting lignin from wood as a soluble derivative, such as lignosulphonates, and then adding these derivatives, either in solution or in the unmodified form, to the surfaces of the bonds.

The former review describes the various polymeric based systems used to produce both kraft and lignosulphonate thermosetting adhesive systems for use as wood adhesives. The development of wood adhesives has been considered, in recent years, to be the most promising application for lignin-polymer adhesive systems [40]. The adhesives used in these applications have been formaldehyde based, manufactured from gas and petroleum such as urea-formaldehyde, melamine-formaldehyde and phenol-formaldehyde [41]. More than half of all formaldehyde produced in North America is used for the manufacture of these polymers [42-44]. Their dependence on gas and petroleum prices was of particular concern during the energy crisis of the early 1970's which saw a levelling off of wood board production. Furthermore, the detrimental effects of

formaldehyde gas emitted from formaldehyde foam insulation prompted official banning of these products used in construction, and consequently has focused attention on the use of formaldehyde in the manufacture of building products. Hence, despite continued supply at low cost, there is an ever increasing demand for new adhesive products which are independent of the cost of gas and oil, and are nontoxic. For this reason, research on lignin-polymer systems is of continued importance in the area of lignin phenol-formaldehyde, lignin urea-formaldehyde, lignin polyisocyanate adhesives, as well as other adhesive systems.

In both reviews the development of an adhesive system requires that lignin, in either the kraft or lignosulphonate form, be modified in some way to accommodate the chemical and processing requirements of the different adhesive systems.

### 2.2.3 LIGNIN ELASTOMER SYSTEMS

The use of lignin as a reinforcing filler in natural elastomers such as rubbers has been well documented [45,46]. Lignin filled rubbers can be obtained in three ways:

- i) by dry mill rolling the lignin in powdered form in to the elastomer;
- ii) by introducing hydrated lignin into rubber with the aid of specialized mixing equipment;
- iii) by the coprecipitation of lignin and rubber from a lignin-latex mixture.

In the first instance, the process does not lead to the reinforcement of the rubber because the coalescence of lignin particles, brought about by the milling

process, forms agglomerates which are difficult to disperse and whose size cause a reduction in the reinforcing effect. Hence in this case lignin acts as an extender.

Hydrated lignin, containing approximately 60% moisture, is used to make lignin pastes which are then introduced in to the rubber using normal rubber compounding equipment. The paste is made by dispersing the hydrated lignin in a plasticizer after which the excess moisture is removed by evaporation. The lignin is prevented from forming agglomerations by continuously mixing the paste during the evaporation process.

The third and most widely used process for incorporating lignin into the rubber is by introducing lignin at the latex stage. For example, it has been shown that alkali lignin is an excellent reinforcing agent for styrene-butadiene rubber (SBR) when coprecipitated with rubber from latex. Problems can still occur because low molecular weight lignin or non-lignin constituents of kraft lignin prevent lignin from dispersing in SBR. These constituents act as agglomerating or coupling agents which promote the clustering of lignin particles. The removal of these detrimental materials can raise the softening temperature and reinforcing ability of lignin [47].

Keilen et al. [48-50] have demonstrated that kraft lignin coprecipitated with natural, styrene-butadiene (figure 2.3), nitrile, or neoprene rubbers can yield tensile strengths comparable (at the same volume loadings) to carbon blacks.

Raff and Tomlinson [51] observed that the reinforcing ability of alkali lignin, for GR-S rubber, was greatly enhanced with increasing oxidation of the lignin prior

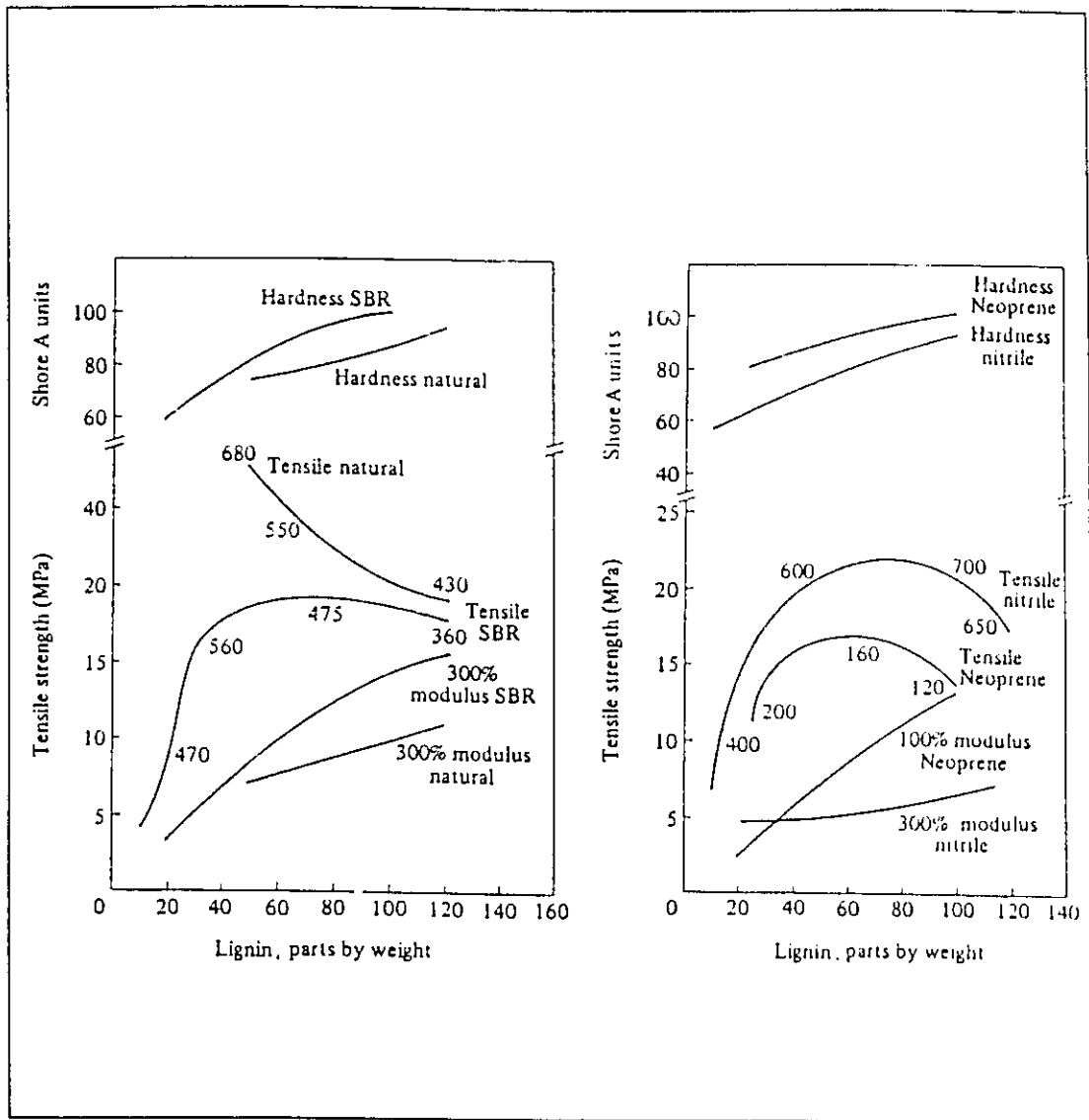


Figure 2.3 Vulcanizate properties vs lignin loading for natural, SBR, nitrile & neoprene rubbers. Numbers on the tensile curves represent ultimate elongation [50].

to co-precipitation with the latex. The oxidation of lignin is performed by bubbling air through an aqueous solution of lignin acid salt or lignin sodium salt; by purposely oxidizing the black liquor prior to or during its precipitation treatment; or by oxidizing the lignin acid salt in dry powdered form in a current of hot air or oxygen with or without the aid of a catalyst [46].

To improve the reinforcing characteristics of lignin, various modifications have been proposed, such as treatment with urea-formaldehyde [52], heat treatment in the presence of an aldehyde [53], combination with phenol-formaldehyde resin [54], treatment with organic polyisocyanate [55], and combination with water [56]. Lignin-rubber masterbatches that are at least partially treated with a diisocyanate can exhibit improved hot tensile strength, abrasion, and reduced torsional hysteresis [57]. Heating of lignin synthetic rubber masterbatches for 5-40 min at 150-175°C tends to improve abrasion resistance and lower torsional hysteresis [58].

These procedures are considered technologically complex and uneconomical and have not therefore found extensive industrial applications [45]. However, there still exists a great potential for the use of lignin as a constituent within polymer-elastomer systems when considering the high cost to volume ratio of certain synthetic elastomers (e.g. silicones, polyurethanes, polysulphides, acrylics). Elastomeric sealants often contain reinforcing fillers, extenders and thixotropic agents and other such additives, which improve the functional properties of the elastomer and reduce the cost of the final product. Cost reductions are obtained because the cost of the elastomer is generally in the order of five times that of the additives [59]. Hence the use of lignin, an abundant and relatively low priced substance, in a system with high-priced elastomers would also serve not only to improve properties, but also to reduce final product costs.

The use of lignin in such a manner has been the basis of a number of investigations undertaken at the CBS [1-5].

Investigations by Beznaczuk [1] utilized the uncured silicone sealant and kraft lignin, polyblended by mechanical mixing only. Specimens of varying formulation were cast between substrates of wood, aluminum and mortar and after a 14-day cure, were exposed to laboratory control (24°C, 35% R.H.), and accelerated weathering (4 cycles daily between -30°C and +30°C for a total of 400 cycles) conditions. In comparison with unfilled sealants, there were only two cases where the strength of the polyblends was higher after tensile testing. Furthermore, all tensile testing failures were adhesive, indicating that lignin may in fact be a suitable reinforcement of silicone sealants if the adhesive bond to the substrate can be made more reliable. This may be achieved through the use of a primer on substrates prior to sealant application.

Lacasse [2] and Feldman et al. [3] have shown that improvements in the mechanical properties of acrylic based sealants are due to the inclusion of lignin. This reinforcing effect is illustrated in figure 2.4 in which the tensile characteristics of lignin filled acrylic sealants adhered to aluminum substrates are given for elastomers having increasing amounts of lignin.

Feldman et al. [4] have shown that polyurethane (PUR) based sealants, when blended with kraft lignin (L), have superior tensile properties than the unblended elastomer. Sealants were tested in a detailed program where lignin-sealant blends, having blend ratios varying between 0 and 20 parts by weight

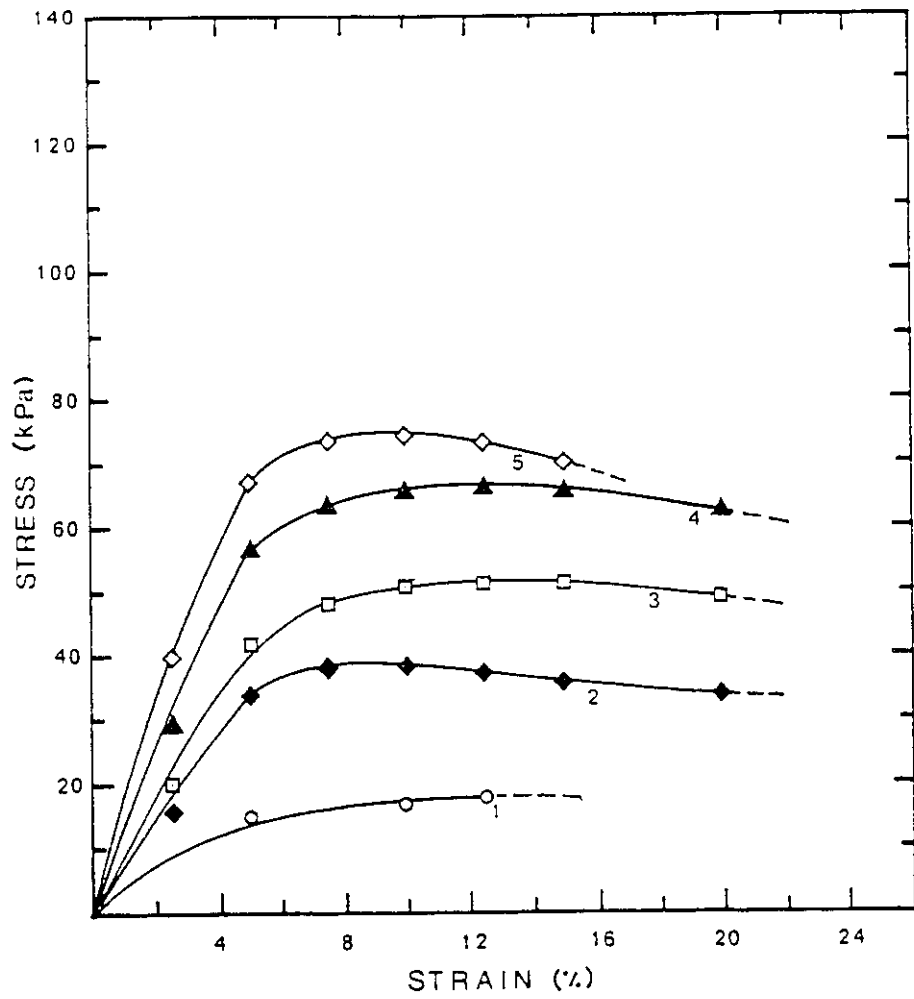


Figure 2.4 Tensile stress-strain curves obtained from acrylic-lignin (A-L) polyblends adhered to aluminum substrates. Curve 1: A-L,100:0 pbw; 2: A-L,100:5; 3: A-L,100:10; 4:A-L, 100:12.5; 5:A-L,100:15 [3].



(pbw) of lignin, were prepared on substrates of aluminum, mortar and wood, and subjected to different weathering conditions. Results of tensile tests showed that generally, lignin acts as a reinforcing agent which adds rigidity to the elastomer matrix, as indicated by the increase in modulus of blended sealants with the addition of lignin. This is illustrated in figure 2.5, which shows the tensile stress-strain curves obtained from unweathered lignin polyurethane blends adhered to an aluminum substrate. The effect on the modulus is equally apparent from figure 2.6 in which the tangent modulus is given as a function of lignin loading for specimens adhered to different substrates and having been subjected to different testing conditions. There is seen to be an increase in modulus with the addition of lignin.

The durability of the blends, as measured by the change in mechanical properties of the specimens subjected to natural and artificial weathering programs in relation to the control conditions, is generally neither hindered nor improved with the addition of lignin.

The results of these studies has also shown that lignin, when incorporated in such type of polymeric systems, is considered to act as a reinforcing filler in a two-phase polymer-particulate system. Evidence of phase separation was obtained through studies undertaken by Feldman and Lacasse [5] in which the morphology of PUR based sealants modified with lignin was investigated using scanning electron microscopy (SEM) and differential scanning calorimetry (DSC).

The SEM photomicrographs, shown in figure 2.7a and 2.7b, clearly emphasize the different morphologies of the constituent phases.

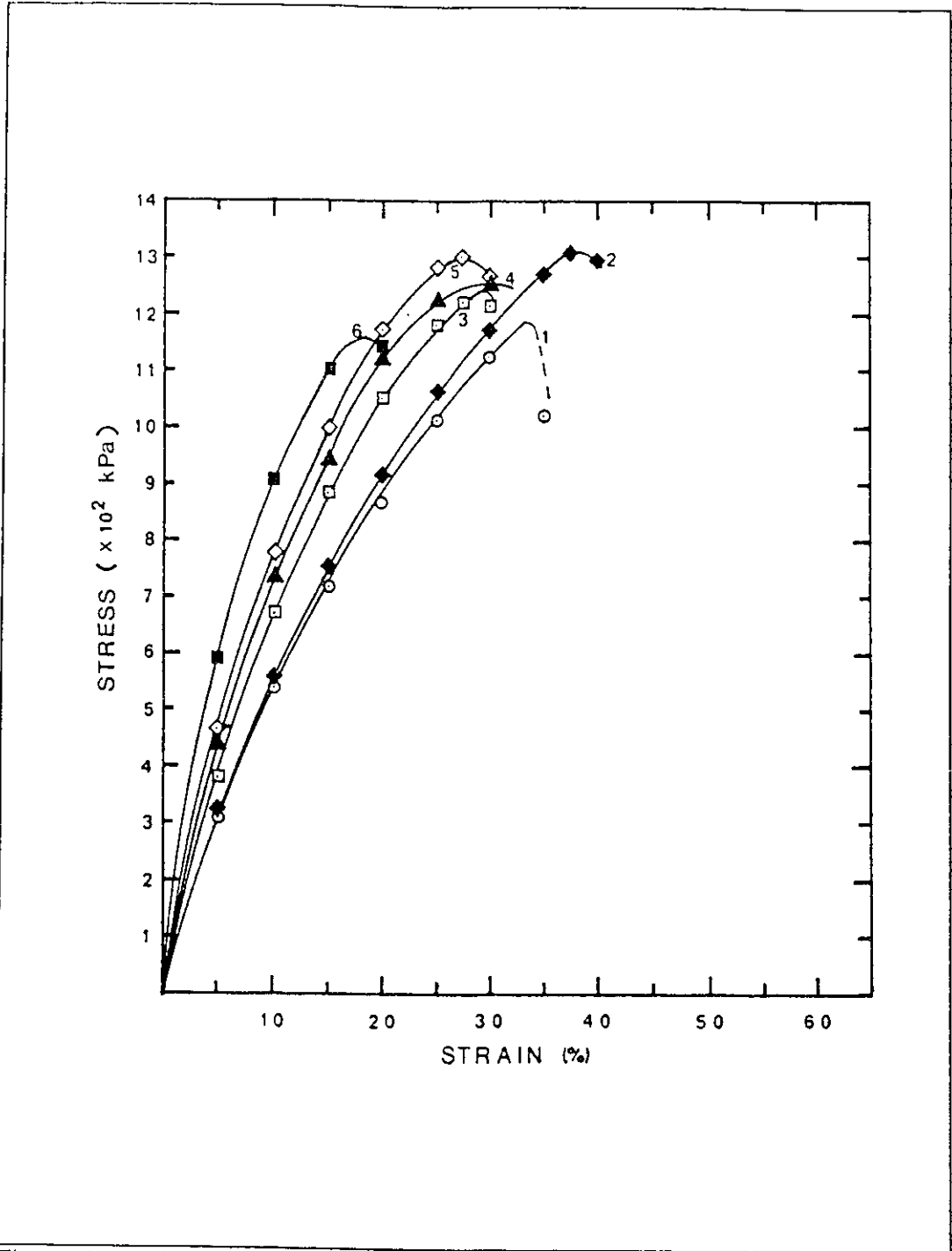


Figure 2.5 Tensile curves obtained from lignin-polyurethane (L-PUR) polyblends adhered to aluminum substrates. Curve 1:L-PUR,0:100 pbw; 2:L-PUR, 5:100; 3:L-PUR, 10:100; 4:L-PUR, 12.5:100; 5:L-PUR, 15:100; 6:L-PUR, 20:100 [4].

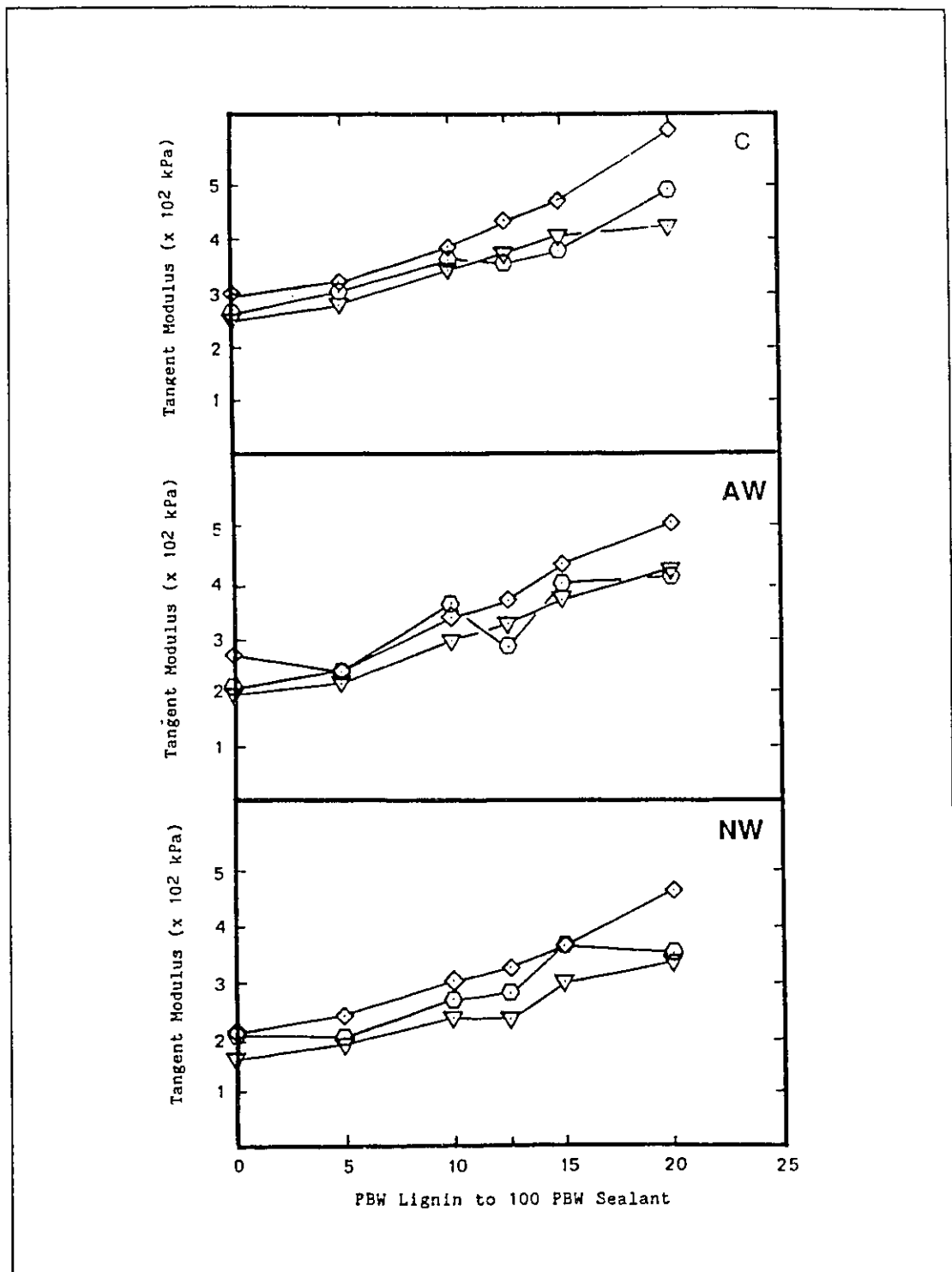


Figure 2.6 Tangent modulus of L-PUR polyblends as a function of lignin loading in control (C), artificial weathering (AW), and natural weathering (NW) conditions. Substrates : (▽) wood; (◻) mortar; (◇) aluminum [4].

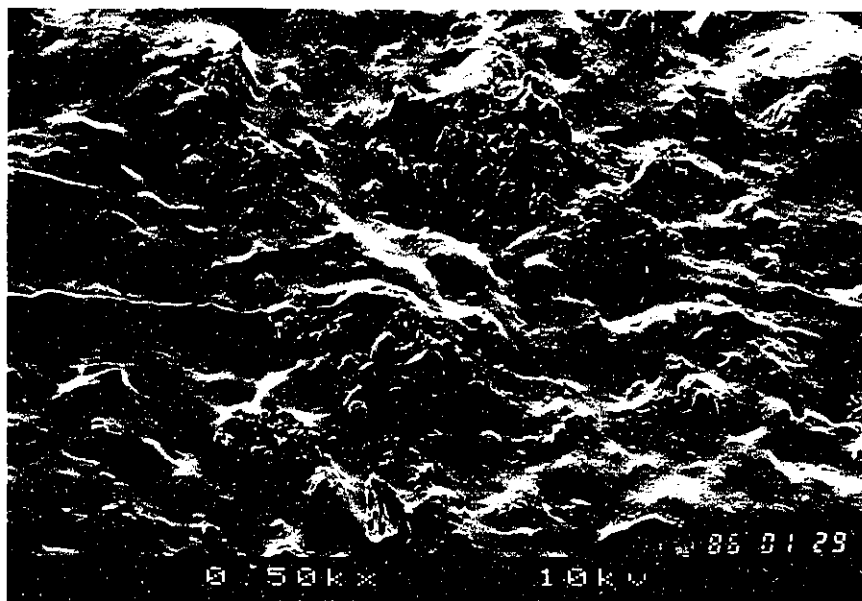
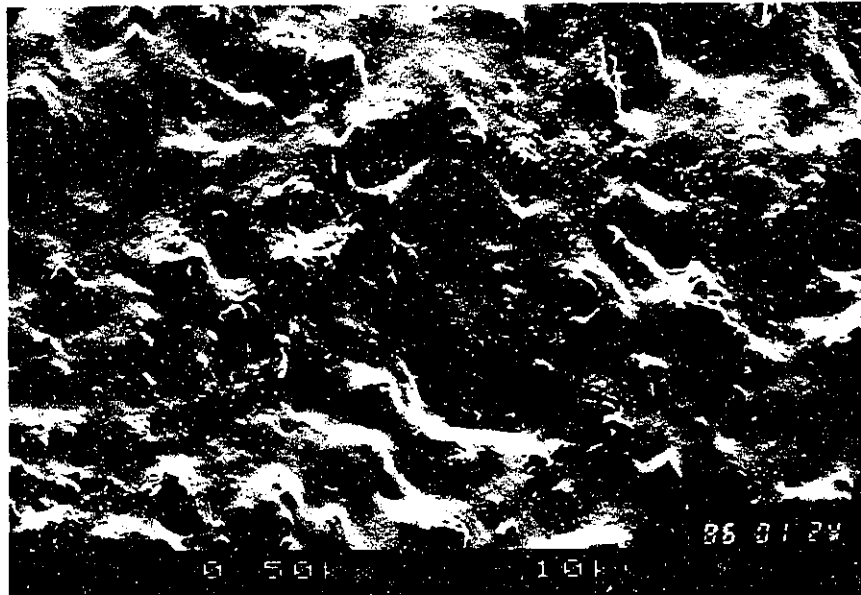


Figure 2.7 (a) SEM of neat PUR surface (500x). Surface texture of PUR matrix is even. Pits and protuberances can be seen on surface. (b) SEM of L-PUR polyblend surface (20:100;500X). Lignin particles are embedded throughout the PUR matrix [5].

This study was also concerned with the compatibility of blend components. It is known that the glass transition temperature ( $T_g$ ) of binary blends whose constituent phases are miscible, is a function of the  $T_g$  of the constituent phases and can be estimated as having a value dependent on the magnitude of the  $T_g$  of each phase and the proportion of each component in the blend [60]. Hence miscible components yield blends having a single  $T_g$ ; conversely the  $T_g$  of blends having immiscible components will show, in the case of a binary mixture, two distinct  $T_g$ 's, each characteristic of the  $T_g$  of the component.

In this study, no shift in the  $T_g$  of the PUR sealant was observed with the addition of lignin as shown in figure 2.8. The differential calorimetric analysis (DSC) indicates that the two phases are immiscible.

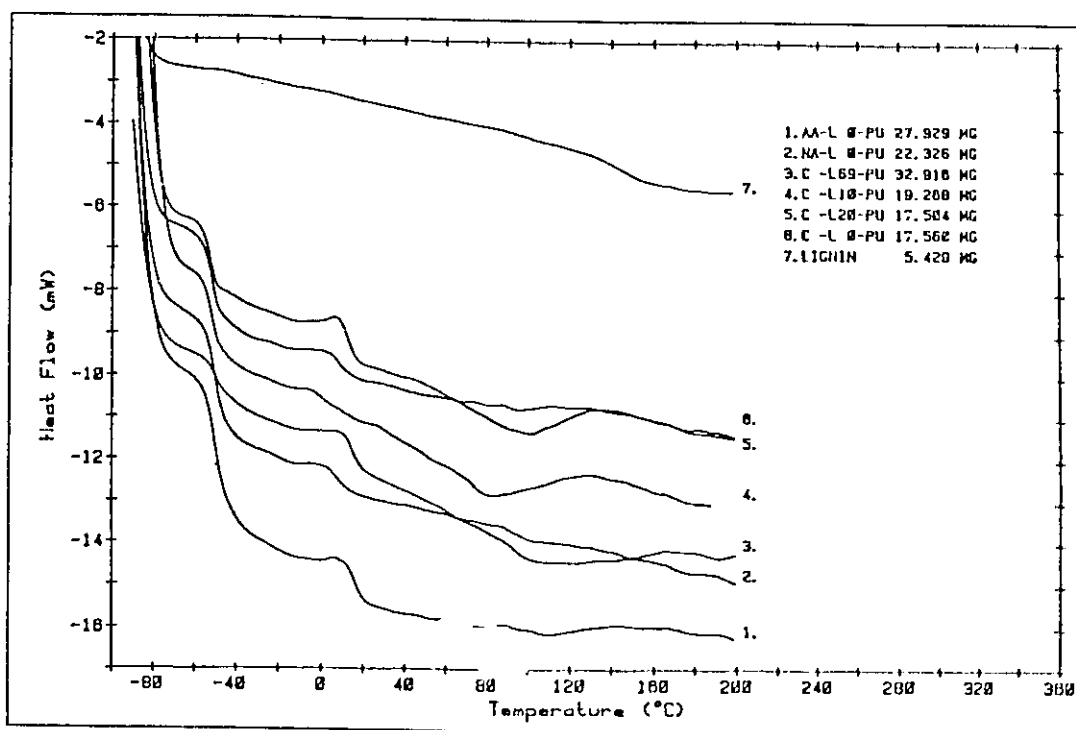


Figure 2.8 DSC curves of lignin and L-PUR polyblends. Analysis conducted at a heating rate of 20°C/min in a nitrogen atmosphere [5].

### 2.3 SUMMARY OF RESEARCH RELATED TO LIGNIN-POLYMER SYSTEMS

A review of current research in the area of lignin-polymer systems has shown that there exist several alternative schemes for the incorporation of lignin in solid materials.

Modification of lignin through hydroxypropylation leads to products having a wide range of physical properties. It has been demonstrated that the modulus, stress and strain at rupture, glass transition temperature and other relevant properties can be adjusted according to the lignin content in the blend.

The method of fractionation of lignin into molecular weight ranges suitable for the synthesis of polyurethane plastics and elastomers has also been successfully developed.

Practical applications derived from the use of either of these techniques would depend on the relative cost of either method.

Lignin-polymer systems have found a number of practical applications as thixotropic agents in drilling muds, as wood adhesives and as reinforcing fillers in various elastomers including natural and synthetic rubbers.

In the case of lignin-elastomer systems the reinforcing effects are well known, however the economic and technological requirements have restrained their extended use despite the development of numerous methods to enhance the properties of lignin in such systems.

The requirement for strength in elastomers used as sealants is not as stringent as for rubber products and the incorporation of lignin in elastomeric based

sealants does not require complex nor costly physical modifications for lignin to be considered a functional filler. Although research has been ongoing in describing the phenomenological characteristics of lignin in various polymeric based elastomer systems, there have been fewer studies undertaken to elucidate the physical characteristics of lignin particles and the possible role they play in the enhancement of the functional properties of elastomers.

Within this context, elastomeric systems such as building sealants, have been used as a vehicle to explore the possible physical or chemical interactions which occur between lignin, a low cost, abundant polymeric filler, and a supporting PUR matrix.

The reinforcing effects of particulate fillers are brought about by the inclusion of the filler within the rubbery matrix and are dependent on the volume fraction of filler in the elastomer formulation. Although research has been conducted with respect to the phenomenon of reinforcement by lignin fillers, the effect of particle size and the contribution of the surface energy of lignin to the extent of reinforcement has yet to be considered. This work is also a contribution to this area of research.

## CHAPTER 3

### RESEARCH PROGRAM

#### 3.1 OUTLINE OF RESEARCH PROGRAM

This research program is a contribution towards establishing the functional properties of PUR based sealants blended with lignin particulate modifiers. An outline of the experimental program is given in figure 3.1, where it is seen that the functional properties relate to both the physico-chemical and the performance properties of the formulations.

For the purposes of more easily reviewing the different experimental aspects of the work, the program has been subdivided into five phases, the first four of which concern elucidating the physico-chemical characteristics of both neat and blended PUR elastomers. The performance properties of specific sealant blends are compared and evaluated to commercially available sealants in the final phase of the program.

A description of the base materials, general principles concerning the synthesis of PUR elastomers and sealant formulation methods as well as detailed descriptions of the test methods and characterization techniques will be given in the following section. This section will be used to briefly describe each phase of the experimental program.



#### PRELIMINARY INVESTIGATIONS

- Established the physical & chemical characteristics of the various formulation components.
- Developed methodology for formulating & testing elastomeric sealants.
- Compared the mechanical properties of different sealant formulations to identify a base elastomer suitable for further study.

#### CHARACTERIZATION OF UNFILLED ELASTOMERS

- Physical phenomena determined as a function of formulation parameters
  - Molecular weight
  - Curing
  - Mechanical properties in tension & compression
- Selected a suitable formulation for use in a filled elastomer system.

#### CHARACTERIZATION OF FILLED ELASTOMERS

- Characterized filled elastomers in terms of:
  - Swelling phenomenon
  - Curing
  - Mechanical properties in tension & compression
  - IR & NMR spectroscopy.

#### INTERACTION ANALYSIS BASED ON SURFACE PROPERTIES OF ELASTOMER MATRIX & FILLERS

- Surface properties of elastomer matrix using sessile drop technique.
- Surface properties of fillers using the column-rise method.
- Analysis of the interaction between elastomer matrix & fillers.

#### PERFORMANCE PROPERTIES

- Performance of elastomers is evaluated in terms of:
  - standard tensile tests.
  - cyclic fatigue tests.

Figure 3.1 Outline of research program

The preliminary investigations undertaken in the initial phase were useful in that they helped determine the most likely combinations of PUR components which could yield a functional sealant (i.e. a low modulus sealant, having a Shore "A" value of < 50, and possessing sufficient adhesion to an aluminum substrate so as to maintain an integral joint at an extension of 25% of the initial joint width). The evaluation of the various formulations was made using tensile and hardness tests in conjunction with DSC analysis. Results from this phase are given in section 4.2. Based on these results, a specific formulation was established (base formulation) from which all subsequent formulations were blended. A description of the base formulation and its components is given in section 3.2.

Also included in this section is a description of the different fillers in terms of their particle size and size distribution, packing fraction and other significant physical and chemical parameters relevant to the formulation of sealants.

In the second phase of the program, a study was conducted to evaluate the change in relevant functional properties (i.e. modulus & adhesion) as a function of various chemical parameters including the stoichiometric ratio (SR) of active blend components, plasticizer content (PC), and polyol ratio (referred to as the Baylith paste ratio, i.e. BPR). A description of these parameters and their expected effect on the mechanical and physico-chemical properties of the sealants is given in section 3.2. An analysis of the results obtained from this phase permitted a more rational choice to be made concerning the specific formulation to use when blending modified, i.e. pigmented or filled sealants. The results of this phase in

the experimental program are given in section 4.3.

Various types of filled elastomers were formulated in the third phase of the program. Four different types of fillers were used (including three kraft lignin based organic modifiers), in varying volumetric proportions such that useful formulations could be made. Mechanical tests similar to those performed to evaluate the properties of the unfilled formulations were used to characterize the filled formulations. In addition to physical testing, infrared and nuclear magnetic resonance spectroscopy was useful in determining if any chemical interactions between the lignin and PUR occurs. These tests were conducted in conjunction with an assessment of the number average molecular weight between crosslinks of the elastomers as determined by swelling. Results of this study are provided section 4.4.

In order to further elucidate the nature of the interaction between the fillers and the PUR elastomer, a basic study related to the surface energy of both these formulation components was initiated in the fourth phase of the program.

Different methods were used to evaluate the critical surface energy of either the filler or the elastomer. In the former case, a "column rise" method was used in which the rate of advance of a series of liquids through a packed column of filler was related to the advancing contact angle of these liquids on the filler.

The critical surface energy of the elastomer was evaluated by measuring the advancing angle of a sessile drop on the surface of the neat polymer. An assessment of the interaction between these two formulation components was

made based on the theory of the equation of state as developed by Lee [61-63]. Results of this phase of the program are given in section 4.5.

The performance properties of specific formulations of modified elastomers are given in the fifth and final phase of the experimental program. Standard mechanical tests are used to evaluate the various formulations and the results are compared with those obtained from three similar commercially available sealant blends. Accelerated aging tests are used to assess the long term durability of these types of new products. Results from this phase are given in section 4.6.

## 3.2 POLYURETHANE SYNTHESIS, PREPOLYMER COMPONENTS & THE FORMULATION OF ELASTOMERIC SEALANTS

### 3.2.1 SYNTHESIS

#### 3.2.1.1 Basic Reactions & Reaction Products

Polyurethanes are made by a polyaddition polymerization process in which bi- or polyfunctional hydroxyl or amino groups containing compounds react with di- or polyisocyanates as shown in figure 3.2 [64-66].

Other reactions which may occur and are also significant from the point of view of sealant formulation are:

- i) the reaction of isocyanates and amines (i.e. ammonia & hydrazines) which are significantly more reactive than hydroxyl containing compounds;
- ii) the reaction of isocyanates and water to form ureas.

Although the reactivity of the urethane and urea groups formed as products of these reactions is considerably lower than that of the primary reactions, under certain conditions these may react with additional isocyanate to form allophanates and biurets. Allophanates are formed from the reaction of urethanes and isocyanates whereas biurets from the reaction of urethanes with ureas.



### 3.2.1.2 Polyurethane (PUR) Prepolymers

Polyisocyanates and polyfunctional reactants undergo polyaddition leading to macromolecules as shown in figure 3.3.

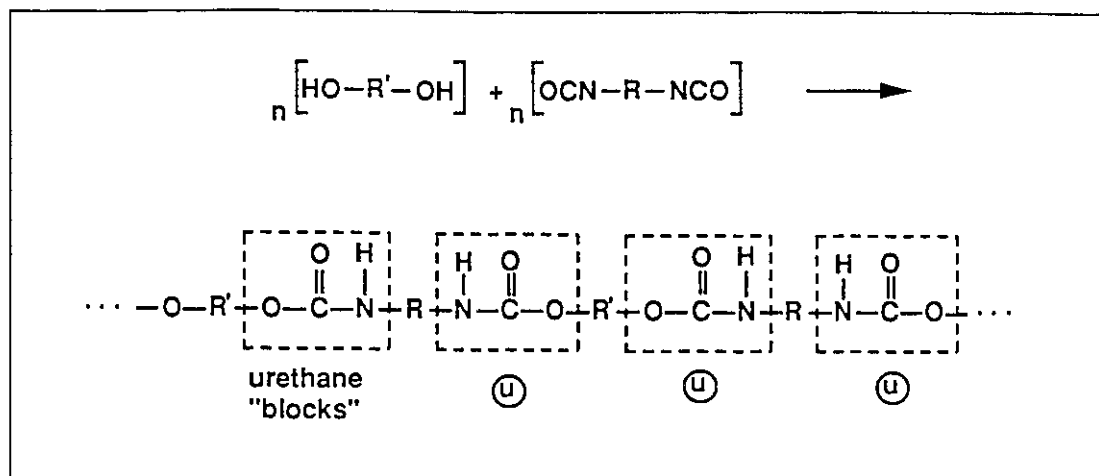


Figure 3.3 Polyaddition of polyfunctional PUR reaction components [65].

Many different types of isocyanates and polyols can be used to form PUR's and in the latter case the choice of compounds is quite extensive. However, the properties of the final product are dependant on the chain length and functionality of the starting components [65,66]. The use of prepolymers makes it possible to overcome problems which have been known to occur in a single step conversion of the basic raw materials. Typical problems are those associated with mixing due to different viscosities or strongly different reaction rates of the components. In an isocyanate prepolymer for instance, the length of the polyol chain determines how far urethane groups in the prepolymer are apart, hence the viscosity and reactivity of such type of product can be controlled by formulating the prepolymer in a narrow molecular weight range as well as through the choice of basic raw materials.

The simplest form of polyisocyanate prepolymer is, for example, the reaction product of difunctional compounds of both isocyanate and a hydroxyl polyester or polyether at a molar ratio of 2:1 yielding a diisocyanatodiurethane.

A special class of polyether polyols exists which contains organic substances dispersed in the polyol in which the dispersoid may in part be chemically bound to the polyether. For example, polyurea polyols are produced by the in situ reaction of isocyanates and amines (e.g. hydrazines) which combine to form urea dispersions in a polyether polyol matrix. To a certain degree it is supposed that hydroxyl groups of the polyether chain take part in the reaction, however this is dependent on the method of preparation and the stoichiometric quantities used in the process. The stable dispersions obtained from this process are called PHD (poly Harnstoff dispersions) polyethers [66,67].

A list of the different isocyanate and polyol prepolymers used in this study are given in Tables 3.1 and 3.2 respectively [68]. Desmodur VL is a low molecular weight MDI based aromatic polyisocyanate prepolymer. Mondur XP 743 is also a MDI based polyisocyanate but of higher molecular weight useful in the formulation of sealants and coatings. This isocyanate prepolymer was used in combination with mixtures of Desmophen based polyols. Desmodur E14 is a TDI based difunctional isocyanate prepolymer of higher molecular weight ( $M_n = 2400$  g/mol) most suited, as was determined from the results of preliminary work, to the formulation of sealants. The molecular weight of the long chain polyether from which this prepolymer is made is estimated to be 2050 g/mol.



Table 3.1 [68]

## PHYSICAL &amp; CHEMICAL PROPERTIES OF ISOCYANATE PREPOLYMERS

NAME	STRUCTURE	NCO Content %	Density (@ 20°C) g/cc	Viscosity (@ 20°C) mPa.s	EW g	f	M <sub>n</sub> g/mol
DESMODUR VL	MDI <sup>**</sup> polyisocyanate prepolymer	30	1.22	130	160	-	-
MONDUR XP 743	MDI <sup>**</sup> polyisocyanate prepolymer	8	1.16	3000	525	2	1050
DESMODUR E14	TDI <sup>***</sup> diisocyanate prepolymer	3.5	1.05	8500	1200	2	2400

EW: Equivalent weight; f: functionality; M<sub>n</sub>: Molecular weight (number average).

\* all products are those produced by the Bayer Corporation, Can.

\*\* MDI: 4-4' diphenyl methane diisocyanate

\*\*\* TDI: toluene diisocyanate

Table 3.2 [68]

**PHYSICAL & CHEMICAL PROPERTIES OF POLYOL PREPOLYMERS**

NAME	STRUCTURE	OH Content %	Density (@ 20°C) g/cc	Viscos. (@ 20°C) mPa.s	EW	f	M <sub>n</sub> g/mol
DESMOPHEN 550U	Branched polyether	11.5	1.01	600	148	-	-
DESMOPHEN 1140	Branched polyglycol having ether & ester groups	8	1.04	1400	215	-	-
DESMOPHEN 1150	Branched polyglycol having ether & ester groups	5	1.01	3500	340	-	-
DESMOPHEN 1920D	Branched dispersoid grade polyether	0.85	1.08	3300	2000	3	6000

EW: Equivalent weight; f: functionality; M<sub>n</sub>: Molecular weight (number average).  
 \* all products are those produced by the Bayer Corporation, Can.

Three different types of polyol prepolymers were used in this study. Desmophen 1140 and 1150 are both branched polyglycols with ether and ester groups and are particularly useful when combined with Mondur XP 743. Desmophen 1920D is a PHD polyether containing 20% by weight of a polyurea dispersion. The dispersion acts as a filler which may strengthen and stiffen the resulting polymeric matrix. This prepolymer is based on a trimethylol propane polypropylene, polyethylene polyol having a molecular weight of 4800 g/mol [67,69]. When this trifunctional polyol is blended in stoichiometric amounts (i.e. NCO/OH = 1) a crosslinkable PUR is formed which has an idealized structure as shown in figure 3.4. The proportion of urethane links estimated from the idealized structure is 2-2.5 wt.%. This implies that the resulting morphological structure is essentially amorphous and hence single phase (i.e. without segmented structure) such that the detection of hard blocks by various analytical means is particularly difficult in light of their low concentration.

This is also typical of the type of structure to be found in elastomeric materials which require little strength but a high degree of elastic recovery [66]. Essentially, in such type of polymers, the intermolecular forces (secondary bonds) acting are those of the polyether segments (soft segments) and these play an increasingly significant role in determining the overall hardness and strength of the polymer [64].



### 3.2.2 POLYURETHANE ELASTOMER SEALANT FORMULATIONS

Polyurethane based sealants are formulated not only from the combination of isocyanate and polyol prepolymers, but also include a number of other components which assure the processing of a useful product. A typical formulation would require a catalyst, plasticizer and antioxidant. The use of moisture absorbing molecular sieves has also been shown to be useful in reducing the amount of surface bubble formation in the elastomer due to the reaction product escaping to the surface [68].

The different components used in the base formulation are given in Table 3.3. A brief description of each of the components follows.

**Catalysts** are used either to initiate a chemical reaction or to advance it to completion [70]. The latter category of catalysts are used in this study in the form of calcium and lead octoate. The amount of catalyst present in a given formulation determines the rate of reaction of the chemical process and this amount has to be adjusted such that the blend is workable for a sufficient amount of time to permit ease of application. The quantity of catalyst needed to advance a chemical reaction is often quite small (e.g. 1% by wt. of formulation). Thus, to ensure an even distribution of catalytic action, the catalyst is mixed with solvent, enabling its thorough dispersion throughout the polymer matrix.

**Plasticizer** is used to augment the low temperature extensibility of polymer blends. The extensibility of elastomers is a function of the glass transition temperature ( $T_g$ ), which is the temperature at which an elastomer changes from

Table 3.3

## POLYURETHANE FORMULATION COMPONENTS

COMPONENT	NAME	DESCRIPTION	Density (20°C) g/cc	Other Information
CATALYST <sup>1</sup>	LEAD 24%	Lead Octoate	1.1-1.2	NIL
	CALCIUM 5%	Calcium Octoate	0.9-0.92	NIL
PLASTICIZERS	MESAMOLL <sup>2</sup>	Alkyl Sulphonic Ester of Phenol	1.03	Vis.:95-125 mPa.s
	SANTICIZER <sup>3</sup>	Butyl Benzyl Phthalate	1.115	Vis.:2.12 mPa.s
MOLECULAR SIEVE <sup>2</sup>	BAYLITH L PASTE	Zeolite in 50% (wt.) Castor oil	1.25	Water absorption capacity 10% (wt.)
ANTIOXIDANT <sup>2</sup>	VULCANOX BKF	2,2'methylene-bis(4-methyl-6tert.butyl phenol)	1.04	NIL
SOLVENT <sup>4</sup>	SOLVESSO 100	Naphtalene		NIL

1. Product of Hüls Canada; 2. Product of Bayer Canada;

3. Product of Monsanto Canada; 4. Product of Esso Canada.

\*Vis.: Absolute viscosity;

the rubbery state to the glassy state as it is cooled. This effect is evident from observation of the change in elastic modulus with temperature, where at  $T_g$ , the modulus of the elastomer changes three orders of magnitude [71]. Sealants are often required to perform at extremely low temperatures and consequently, in order to maintain their rubbery qualities in these conditions, are blended with plasticizers of lower glass transition temperature than the base elastomer. The amount of plasticizer used in this study has been varied such that optimum properties could be obtained.

A molecular sieve acts as a sponge to absorb excess moisture from hydrophilic polyols and from the surface of fillers [68]. Free surface moisture is the cause of bubble formation in elastomers due to the reaction of water with isocyanates which produces carbon dioxide gas. The reaction of isocyanates and water yields urethane products which are different from those obtained from the reaction of isocyanates and polyols and consequently these former reactions may alter the final structure such that a sealant with different physical properties than those required is produced. Bubble formation, although not in itself detrimental to the overall strength of the resulting elastomer, is not considered advantageous from the point of view of forming products with predetermined properties. The molecular sieve used in this study is Baylith L paste, which is an alkali aluminosilicate dispersed in castor oil (50% by weight). Castor oil contains a certain percentage of hydroxyl groups and this must be taken into account when establishing the stoichiometric ratio of components.

### 3.2.3 COMPOUNDING ELASTOMERIC SEALANT FORMULATIONS

Elastomeric sealants may be formulated to be either single or two-component systems, either of which system can be made to be non-sagging or self-levelling. Non-sagging elastomeric sealant compounds are used in vertical joints whereas self-levelling compounds are formulated such that they can easily be applied to a horizontal joint. For the purposes of the study, either system could have been used to demonstrate the viability of mixing lignin fillers in a PUR based elastomer. The choice of system was based on practical considerations related to the type and availability of processing equipment and raw materials required to produce either type of sealant system. The preparation of single-component formulations is complicated by the nature of the raw materials used in their preparation. These materials can release toxic vapours at room temperature and furthermore are extremely hygroscopic. Consequently the blending process would have to had been carried out using specialized equipment.

Two component systems are often formulated using prepolymers. Prepolymers do not require that exceptional care be taken with regards to either potential health hazards or chemical activity of the base materials but special care is nonetheless required. Furthermore, the use of prepolymers permits formulating compounds using readily available and easily maintained mixing equipment.

The hygroscopic nature of the isocyanate and polyol prepolymers necessitated that precautions be taken with respect to the storage of materials and the level of moisture present while blending the components. For this purpose, a



double sized glove box, as shown in figure 3.5, was fabricated in which all moisture sensitive chemicals were stored and final formulations were prepared. Access to the chamber is made through either end via air-tight openings. The chamber is equipped with a nitrogen gas inlet port, gas and vacuum exhaust ports, as well as an electrical outlet. Two methods were used to ensure a dry atmosphere in the chamber: a positive pressure was maintained in the box using dry nitrogen gas (purged of moisture by passage through a packed column of desiccant), such that moisture laden air could not enter; a bed of desiccant was placed in the bottom of the chamber so as to absorb any traces of moisture present in the nitrogen atmosphere.

#### 3.2.3.1 Preparation of Unfilled Elastomer Formulations

Various unfilled formulations were prepared in order to study the change in thermal and mechanical properties as a function of their stoichiometric ratio (SR), plasticizer content (PC) and polyol ratio (BPR). A list of different formulations and the associated chemical parameters is shown in Table 3.4.

Details with regards to calculating the appropriate amounts of each component according to the prescribed formulation parameters are given in appendix A.1. Included in the appendix are actual component weights for each formulation series given in Table 3.4.

---

Figure 3.5 Doubled sized glove box

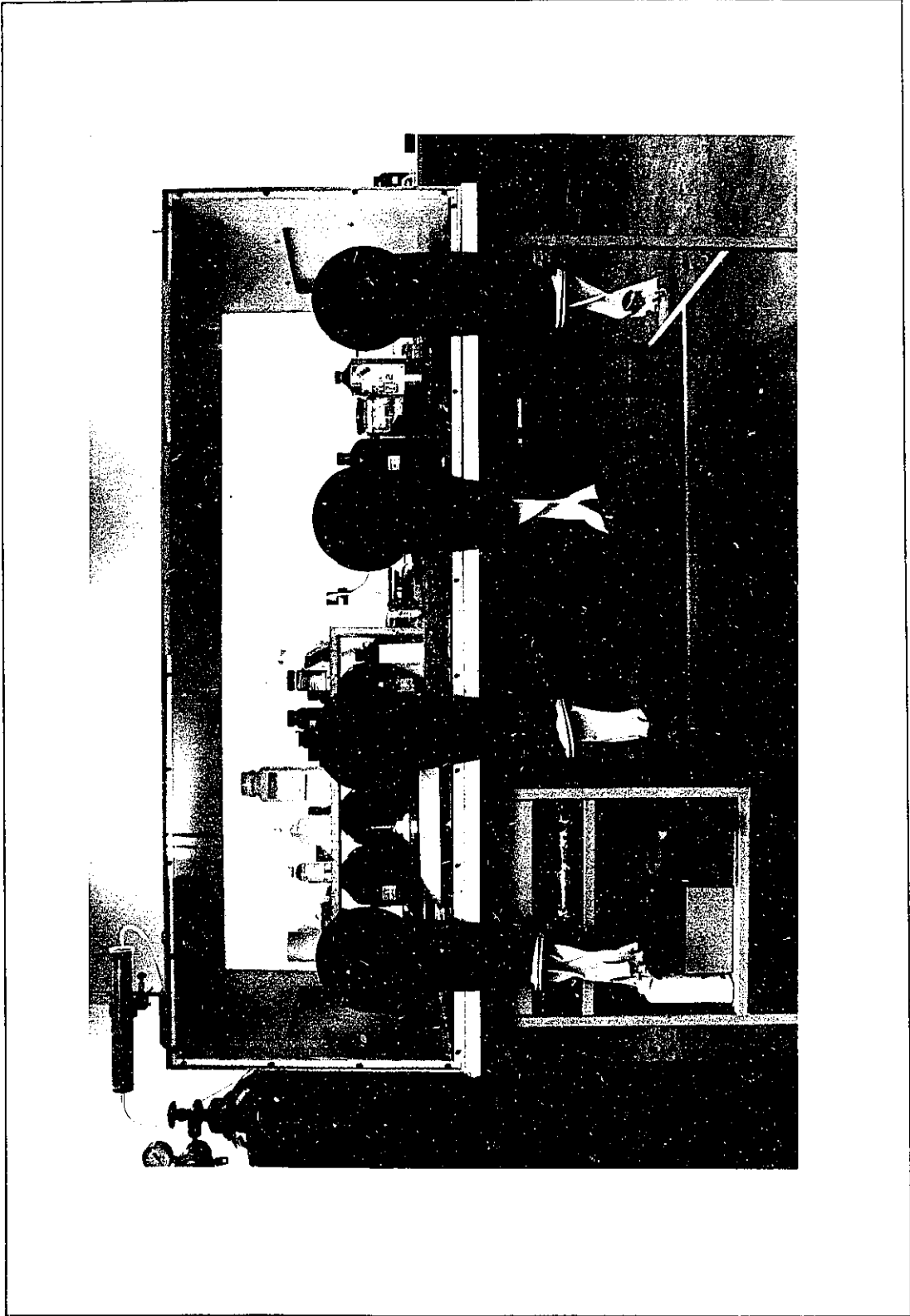


Table 3.4

CLASSIFICATION OF UNFILLED POLYURETHANE ELASTOMERS			
SERIES A			
Plasticizer Content = 30 wt.%			
BAYLITH PASTE RATIO	STOICHIOMETRIC RATIO		
	1.023	1.062	1.1
0.588	15A	18A	20A
0.794	35A	38A	40A
1.0	25A	28A	30A

SERIES B			
Plasticizer Content = 34 wt.%			
BAYLITH PASTE RATIO	STOICHIOMETRIC RATIO		
	1.023	1.062	1.1
0.588	15B	18B	20B
0.794	35B	38B	40B
1.0	25B	28B	30B

SERIES C			
Plasticizer Content = 40 wt.%			
BAYLITH PASTE RATIO	STOICHIOMETRIC RATIO		
	1.023	1.062	1.1
0.588	15C	18C	20C
0.794	35C	38C	40C
1.0	25C	28C	30C

The stoichiometric ratio refers to the molar ratio of active components in the formulations, which in the case of polyurethane based products refers to the ratio of active isocyanate to hydroxyl groups.

The plasticizer content is measured in relation to the quantity of polymer components (Desmophen 1920D, Desmodur E14, & Baylith paste) in the formulation on a weight percent (wt.%) basis. The polyol ratio refers to the molar ratio of hydroxyl groups provided by the Baylith paste (which contains 50 wt.% castor oil) to that provided by the primary polyol.

Formulations were blended by weighing individual components ( $\pm 0.01\text{g}$ ) in a 250 ml glass beaker and stirring these manually for 3 minutes after each component had been added. The order of mixing of these components is given below:

- i) Polyol Prepolymer
- ii) Baylith Paste
- iii) Plasticizer
- iv) Isocyanate Prepolymer
- v) Catalyst & solvent

Blended formulations were then poured in the various moulds, the size and nature of which are given in appendix A.3. The cast elastomers were permitted to cure in the glove box at room temperature for at least 24 hours, depending on the rate of cure of the system, after which they were allowed to complete their curing process in standard laboratory conditions (25°C & 50% RH). The curing process was monitored on a regular basis using hardness tests as described in section 3.4.2.4.

### 3.2.3.2 Preparation of Filled Elastomers

The use of fillers results mainly from the requirement of physical properties: with suitable fillers the modulus of elasticity can be increased over a greater temperature range, stability and heat distortion can be increased, and the thermal expansion coefficient can be decreased [72]. It is also evident that fillers may be classified according to their reinforcing effect, the non-reinforcing ones being referred to as extenders. Extenders may however impart other useful properties to the sealant including protection against ultraviolet radiation (e.g. white-hiding pigments), colour, control of thermal expansion, shrinkage, or other useful properties [59,65]. The various particulate fillers used in this study are given in Tables 3.5a, 3.5b and 3.5c, which also lists their respective properties relevant to the formulation of sealants.

The preparation of filled formulations required two additional steps in comparison with the formulation procedure used for preparing unfilled specimens. The particulate matter was dried in a forced air oven at 105°C for 24 hours and then allowed to cool to room temperature in a desiccator. The dried matter was then dispersed in the plasticizer in appropriate proportions, using a high speed disk dispenser operating at 5000 - 6000 rpm. The disk was fabricated such that optimum dispersion could be obtained given the size of the container and the quantity of plasticizer and particulate matter being dispersed. The dispersion process continued until a uniform paste was obtained.

Table 3.5A

## PHYSICAL PROPERTIES OF INORGANIC PARTICULATE FILLERS

NAME	TYPE	S.G.	Specific Surface Area m <sup>2</sup> /g	Average Particle Size µm	Oil Absorption g/100g	φ <sub>m</sub>
SIL-CO-SIL #400	Ground silica	2.65	0.6	7.4	33	0.52
SILLITIN Z86	Silica/Kaolin	2.60	12	1.35	45-55	0.42
TITANOX 2101	Titanium dioxide	4.00	10	0.3	25	0.48

Table 3.5B

## CHEMICAL ANALYSIS OF INORGANIC FILLERS

NAME	TYPE	SiO <sub>2</sub>	Fe <sub>2</sub> O <sub>3</sub>	Al <sub>2</sub> O <sub>3</sub>	TiO <sub>2</sub>	CaO	MgO	LOI
SIL-CO-SIL #400 <sup>1</sup>	Ground silica	99.8	0.015	0.047	0.013	<0.01	0.01	0.09
SILLITIN Z86 <sup>2</sup>	Aluminum Silicate	80.5	0.7	12.5	0.7	0.5	0.5	3.6
TITANOX 2101 <sup>3</sup>	Titanium dioxide	-	-	-	92	-	-	8

1. Ottawa Industrial Sand Co., Ottawa, Illinois, U.S.A. (Debro Chem);
2. Hoffman Mineral, Franz Hoffman & Sehne KG, Neuburg/Donau, W. Germany;
3. NL Chem Canada Inc., Montreal.

Table 3.5C

## PHYSICAL CHARACTERISTICS OF ORGANIC PARTICULATE FILLERS

NAME	TYPE	S.G.	Specific Surface Area m <sup>2</sup> /g	Average Particle Size µm	pH	Oil Absorption g/100g	φ <sub>m</sub>
EUKALIN <sup>1</sup>	Kraft lignin - Eucalyptus wood	1.379	-	10.5 <sup>*</sup>	9-10	40	0.63
INDULIN AT <sup>2</sup>	Kraft lignin - softwood	1.238	1.5	8	6.5	85	0.471
TOMLINITE <sup>3</sup>	Kraft lignin - hardwood	1.295	0.7	16	6	74	0.49

1. Empresa Nacional de Celulosas, S.Q., Madrid, Spain;

2. Westvaco, Chemical Division, Charleston, S.C., U.S.A.;

3. Domtar Corporation, Cornwall, Ontario.

\* Estimated visually from photomicrographs of EU particles

The mixing order for filled formulations was the same as that for unfilled ones with the exception that the dispersed phase was added where, in the case of unfilled formulations, plasticizer was required. The different elastomer series for filled PUR elastomers is shown in Table 3.6. Actual weights for the various components are given in appendix A.2.

Table 3.6				
CLASSIFICATION OF FILLED PUR ELASTOMERS				
Loading % v/v	PARTICULATE FILLERS			
	TO	AT	EU	ST
5	50TO	50AT	50EU	50ST
7.5	75TO	75AT	75EU	75ST
10	100TO	100AT	100EU	100ST
12.5	125TO	125AT	125EU	125ST
15	150TO	150AT	150EU	150ST
TO: Tomlinite Kraft lignin; AT: Indulin AT Kraft lignin; EU: Eucalin Kraft lignin; ST: Sillitin Z86/Titanox::Kaolin/Titanium dioxide.				



### 3.3 PHYSICAL CHARACTERIZATION OF PARTICULATE FILLERS

#### 3.3.1 PARTICLE SIZE & SIZE DISTRIBUTION

It has been shown that the modulus of filled polymers is dependent not only on the volume fraction of filler in the blend but also on the filler particle size [73]. Generally, non-adhering particles of a particulate filler composite exhibit dewetting (debonding) during a tensile test. It has been shown that the stress at which dewetting occurs depends on the particle size of the filler, as was suggested by Gent [74]. It has been further shown that non-adhering particles which are smaller than 5 $\mu\text{m}$  may not show dewetting at all if stress levels to cause dewetting are larger than the cohesive strength of the polymer. Consequently the particle size and particle size distribution of the particulate modifiers is significant from the point of view of explaining the tensile behavior of the blends.

##### 3.3.1.1 Estimation of Particle Size Using Light Microscopy

Reflected LM is valuable for examining the texture of solid and opaque materials [75,76]. Furthermore, light microscopy requires a minimum of difference in refractive index between phases for contrast and can best be obtained with differences in opacity or color [76].

Evidently the particle size of fillers may easily be ascertained by means of the light microscope. Accordingly, a series of color as well as monochrome photomicrographs were made using an Olympus (model BHM) reflected brightfield incident light microscope. Magnifications of 50X, 100X, 200X and 500X are

possible to view the features of the particles. Photomicrographs were taken of suitably prepared specimens comprised of particulate fillers dispersed on a plane surface. The particle sizes are measured directly from the photomicrograph taking into account the magnification of the particles.

#### 3.3.1.2 Particle Size Distribution

Particle size distribution has significance in the evaluation of rheological properties of pigmented slurries and, more appropriately, to the elucidation of mechanical characteristics of filled elastomers and plastics.

The particle size distribution of particulate fillers used in this study was determined in accordance with ASTM D3360 and ASTM D422 [77,78]. The former standard is used to determine the particle size distribution in the sub-sieve size range ( $<75\mu\text{m}$ ) of common extender pigments such as aluminum silicate (kaolin clay), magnesium silicate (talc), calcium carbonate (calcite, dolomite or precipitated calcium carbonate) and mica pigments. The method may also be extended to the denser pigments such as titanium dioxide.

The latter method is used for analyzing the particle size of soils in the same range of sizes and it was useful in providing details concerning the specifications of certain apparatus used in the particle size analysis.

The method uses the sedimentation technique as a means of obtaining a particle size distribution curve. The technique is based on Stoke's law and is particularly applicable to fillers having a major fraction of particles falling in the

range from 1.5 to 15 $\mu$ m, but having a total particle size range of at least two decades.

The method consists of measuring the density of a suspension of particulate filler by means of a hydrometer, at a defined distance beneath the surface of the suspension and at appropriately selected times such that the sedimentation times can be converted to a particle size distribution according to both Stoke's law and the percentage of filler remaining in the suspension at the time the reading is taken.

Stokes law is given below:

$$D = \sqrt{\frac{30 \eta_s}{980 (SG_f - SG_s)} \cdot \frac{L_o}{t_s}}$$

Equ. 3.1 [77]

where:

- D = equivalent spherical diameter of particles, (mm);
- $\eta_s$  = viscosity of the suspending medium, (Poise);
- $L_o$  = distance from the surface of the suspension to the level at which the density of the suspension is being measured, (cm);
- $t_s$  = time interval from the beginning of sedimentation to the taking of the reading, (min);
- $SG_f$  = specific gravity of particulate filler;
- $SG_s$  = specific gravity of suspending medium.

The viscosity of the suspending medium is dependent on the temperature, hence to insure accurate readings, the test was carried out in controlled conditions.

The distance,  $L_e$ , from the surface of the suspension at a time,  $t_s$ , is the effective depth at which the density of the suspension is measured and is given by the following equation:

$$L_e = L_1 + \frac{1}{2} \left[ L_2 - \frac{V_B}{a} \right]$$

Equ. 3.2 [78]

where:

- $L_e$  = effective depth, (cm);
- $L_1$  = distance along stem of hydrometer from the top of the bulb to the mark for a hydrometer reading, (10.5 cm @ 1.000 & 2.3 cm @ 1.031);
- $L_2$  = overall length of the hydrometer bulb, (14.0 cm);
- $V_B$  = volume of hydrometer bulb, (67.0 cc);
- $a$  = cross-section area of sedimentation cylinder, (27.8 cm<sup>2</sup>).

The values for  $L_1$ ,  $L_2$ ,  $V_B$ , and  $a$ , given above, are for a 151H-62 type hydrometer conforming to ASTM E100 [79].

The particle size distribution is calculated based on the percentage of filler remaining in the suspension in relation to the equivalent spherical diameter. The percentage of soil remaining in the suspension,  $P$ , at the level at which the hydrometer is measuring the density of the suspension is calculated as follows:

$$P = \left[ \frac{100000}{W} \cdot \frac{SG_f}{SG_f - SG_s} \right] \cdot (r - SG_s)$$

Equ. 3.3 [78]

where:

- P = percentage of filler remaining in suspension at time  $t_s$  ;
- W = oven dry mass of particulate matter in a total test sample, (g);
- r = hydrometer reading;
- SG<sub>f</sub>, SG<sub>s</sub> = specific gravities of particulate matter and suspending medium respectively.

The procedure was carried out in separate simultaneous determinations in which 30g samples of particulate filler was dispersed in 1000 ml of suspending medium (distilled water with appropriate dispersing agent added) and placed in a sedimentation flask. The temperature of the tests was maintained at 20°C by placing the flasks in a thermostatically controlled water bath. The bath is capable of holding five sedimentation flasks, hence each test series consisted in determining the particle size distribution of four samples, the fifth flask reserved as a blank solution such that the density of the suspension could be compared to the blank at each determination. Hydrometer readings were taken at prescribed time intervals. Results from these tests are given in section 4.5.2

### 3.3.2 MAXIMUM PACKING FRACTION AND OIL ABSORPTION

Solid fillers, when incorporated in a rubbery matrix, always increase the modulus of the composite and the extent of increase is essentially dependent on the packing characteristics of the filler particles [59].

The Kerner equation [80], as modified by Lewis and Nielsen [81-84], has been successfully used to explain the relative increase in modulus of elastomers filled with solid particulate fillers in relation to the particular physical characteristics of these fillers, and has the form:

$$\frac{E}{E_0} = \frac{1 + \kappa \Gamma \phi_f}{1 - \Gamma \psi \phi_f}$$

$$\kappa = k_E - 1 = 2.5 - 1 = 1.5$$

$$\Gamma = \frac{\frac{E_f}{E_0} - 1}{\frac{E_f}{E_0} - \kappa} \quad \frac{E_f}{E_0} = \frac{6.6 \text{ GPa}}{0.6 \text{ MPa}} = 11000$$

$$\psi = 1 + \left( \frac{1 - \phi_m}{\phi_m^2} \right) \phi_f$$

Equ. 3.4 [84]

The subscripts o and f refer to the elastomer matrix (continuous phase) and the filler (dispersed phase), respectively.

The constant  $\kappa$  is a function of the Einstein coefficient,  $k_E$ , which can be evaluated from measurements of the relative increase in absolute viscosity of a particulate filled liquid medium in relation to the volume fraction of filler added to the suspension [59]. The value of  $k_E$  represents the limiting value of the viscosity ratio (intrinsic viscosity) at zero filler volume.

The value of  $\Gamma$  is dependent on the filler-elastomer ratio and is in the order of  $10^4$  to  $10^5$  for most elastomer filled systems [59]. Hence the value of  $\Gamma$  is close to unity for values of  $\kappa$  less than or equal to 10 and consequently the reinforcing effect is mostly dependent on the value of the product  $\psi\phi_i$ . As shown in figure 3.6, the factor  $\psi$  enables the use of a reduced concentration scale to take into account the existence of the maximum packing fraction,  $\phi_m$ , the volumetric fraction at which filler particles are the most closely packed in a suspending medium. Clearly, for values of  $\phi_m$  which are smaller than the theoretical values, the latter derived from the knowledge of the assumed packing configuration of ideal spherical filler particles, there is a significant increase in the reinforcing effect at volume fractions approaching the value of  $\phi_m$ . Hence an estimate of the maximum packing fraction is useful for determining the extent of reinforcement which may be derived from a particular type of filler.

The maximum packing fraction may be estimated from the amount of liquid which must be added to a filler to convert it from a dry appearance to a wet appearing fluid mass.

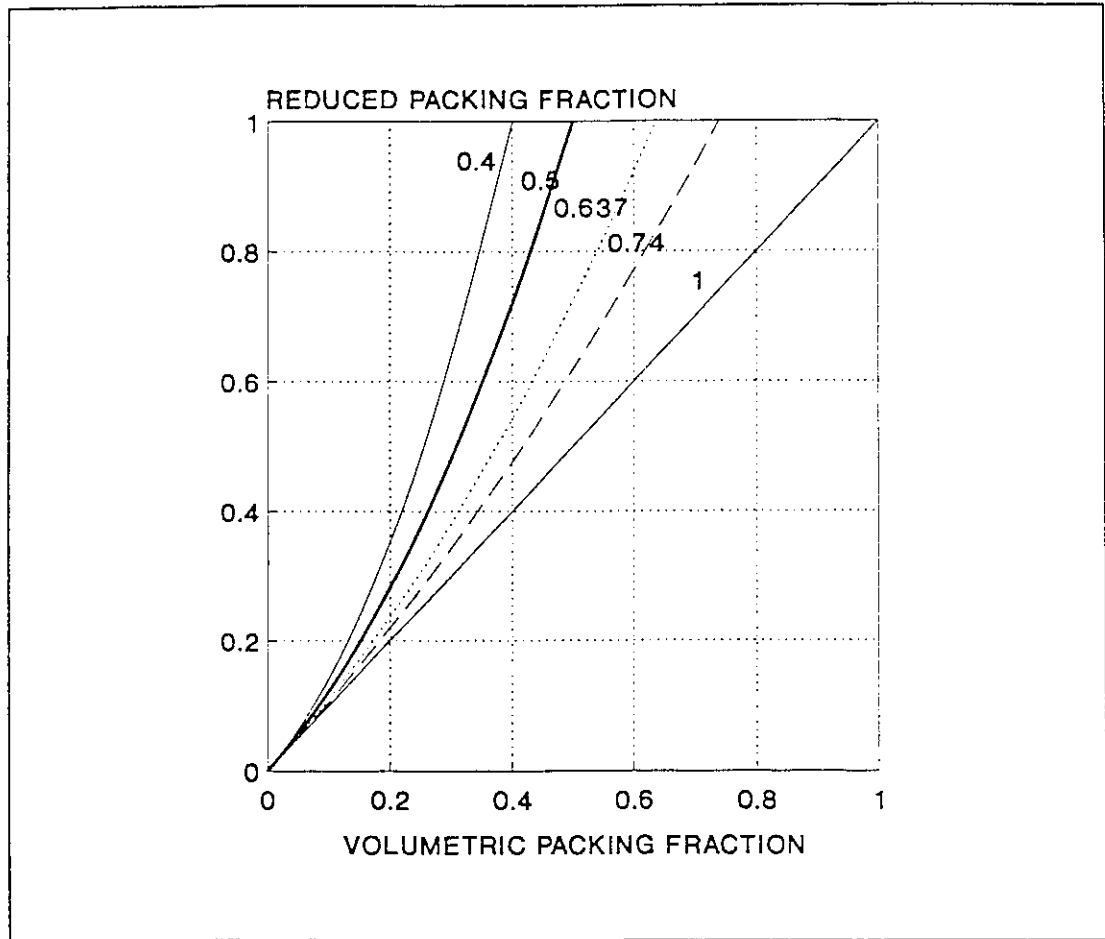


Figure 3.6 Dependency of  $\psi\phi_1$  on the volume fraction of particulate filler  $\phi_1$ , incorporated in a polymer matrix for fillers having different values of  $\phi_m$  [84].

According to Patton [85], the packing factor is related to the absorption of wetting liquid by a filler in the following manner:

$$\phi_m = \frac{\frac{100}{\delta_f}}{\frac{OA}{0.935} + \frac{100}{\delta_f}}$$

Equ. 3.5 [85]



where:

- $\phi_m$  = maximum packing factor;
- OA = oil absorption (g/100g);
- $\delta_f$  = density of filler (g/cc).

The method described in ASTM D281 [86], referred to as the spatula rub-out method, is commonly used to determine the value of OA. The technique is used to evaluate the weight of linseed oil taken up by a given weight of dried filler in sufficient quantity to form the required paste.

Oil absorption values were determined for SIL-CO-SIL (silica), Titanox (titanium dioxide), Tomlinite (hardwood kraft lignin), Indulin AT (softwood kraft lignin) and Eucalin (eucalyptus kraft lignin) fillers. These results, together with the corresponding values for the maximum packing fraction, are given in Table 3.5a and 3.5c. They are based on an average calculated from at least ten determinations.

### 3.3.3 SPECIFIC GRAVITY OF PARTICULATE FILLERS

The procedure, as described in ASTM D153 [87], consists in first, determining the specific gravity of the immersion liquid (kerosene) such that the specific gravity of the filler may thereafter be evaluated.

In order to ensure reproducible results, the specific gravity of the kerosene was determined under controlled conditions, in which a 50 ml pycnometric flask was first filled with freshly boiled distilled water at 24°C and was allowed to come to constant temperature at 25°C in a water bath. The procedure was repeated with the flask filled with kerosene. The specific gravity of the kerosene was determined by calculating the ratio of the weight of kerosene to that of water.

A pre-weighed oven-dried sample of filler (1-20g) was then placed in the flask and both flask and sample transferred to a vacuum desiccator fitted with a separatory funnel filled with kerosene. The desiccator was then evacuated to 3mm absolute pressure after which sufficient kerosene was added to cover the filler. After removal of the vacuum, the flask was completely filled with kerosene and weighed.

The specific gravity for each of the particulate fillers used in this study is reported as an average of at least six determinations and the results are given in Tables 3.5a and 3.5c.

### 3.4 CHARACTERIZATION OF UNFILLED & FILLED ELASTOMERS

#### 3.4.1 CHARACTERIZATION USING THE SWELLING METHOD

Swelling tests were used to determine the number average molecular weight between crosslinks ( $M_{c,s}$ ) of the elastomer formulations and to assess the degree of interaction between the various particulate fillers and the elastomeric matrix.

##### 3.4.1.1 Molecular Weight Between Crosslinks of PUR Elastomers

It is known that a three-dimensional network of polymer chains will swell in the presence of a non-reactive solvent, in which the long chain portions (soft segments) are extended in proportion to the amount of solvent present in the polymer [65,71,88]. An elastic retractive force opposes the swelling such that after a limited time immersed in the solvent (e.g. 5-10 days), the swelling reaches an equilibrium point (i.e. equilibrium between the attractive forces and those causing swelling is attained). The theory developed by Flory & Rehner [88] indicates that the molecular weight between crosslinks is inversely proportional to the elastic forces at equilibrium. This may be expressed in the form given in equation 3.6.

$$\frac{\delta}{M_{c,s}} = \frac{\phi_{p,s}^{1/3} \sigma}{RT (\alpha - \alpha^{-2})}$$

Equ. 3.6 [88]

- $\delta$  = density (g/cc);  
 $M_{c,s}$  = number average molecular weight between crosslinks g/mol);  
 $\phi_{p,s}$  = volume fraction of polymer in the swollen sample;  
 $\sigma$  = force per unit area (of unswollen sample) required to deform sample to the deformation ratio,  $\alpha$  (MPa);  
 $\alpha$  = deformation ratio =  $\delta L/L$ ;  
 $R$  = Universal gas constant (82057 cm<sup>3</sup>·g/K·mole);  
 $T$  = absolute temperature (K).

The method adopted by Damusis et al. [89], based on work undertaken by Cluff et al. [90] was used to determine the elastic properties of the swollen polymer. Cylindrical disks (height = 12.5 mm (0.5")); diameter = 32 mm (1.25")) were swollen in toluene until equilibrium was attained after which they were subjected to compression-deflection measurements while immersed in solvent. An Instron Universal Testing machine operating at a crosshead speed of 0.1 mm/min was used to obtain the load-deformation curve. The slope of the linear portion along the curve was used to evaluate the number of effective network chains per unit volume,  $\nu_e/V$ , based on the equation:

$$\frac{\nu_e}{V} = \frac{h_o S}{3 a_o RT} = \frac{\delta}{M_{c,s}}$$

Equ. 3.7 [89,90]

where:

- $\nu_e/V$  = number of effective network chains per unit volume, (cc);
- $h_o$  = height of the undeformed, unswollen disk, (cm);
- $S$  = slope of the compression-deflection curve, (g/cm);
- $a_o$  = cross-sectional area of disk, (cm<sup>2</sup>);
- $R$  = Universal gas constant, (82057 cm<sup>3</sup>-g/K<sup>2</sup>-mole);
- $T$  = absolute temperature, (K);
- $\delta$  = density of polymer, (g/cc);
- $M_{c,s}$  = number average molecular weight, (g/mole);

An average value of the slope obtained from three specimens was used to calculate the required data.

### 3.4.1.2 Swelling Phenomenon in Filled Elastomers

The swelling for a large number of elastomers containing reinforced fillers has been found to obey an equation of the form [91]:

$$\frac{\nu_{r_o}}{\nu_r} = 1 - \frac{\phi_f}{1 - \phi_f} [ 3C ( 1 - \nu_{r_o}^{1/3} ) + \nu_{r_o} - 1 ]$$

Equ. 3.8 [91]

- where :  $\nu_{r_o}$  =  $\nu_r$  of unfilled elastomer;
- $\phi_f$  = volume fraction of filler in the filled elastomer;
- $C$  = constant, which is characteristic of the filler (but independent of the polymer, solvent or degree of crosslinking).

The data suggest that the restrictions in swelling depend to a fair degree of approximation only on the filler and the extent to which an otherwise identical unfilled elastomer will swell. This further suggests that the restriction of swelling depends only on the fact that a firm bond between elastomer and filler is established, but also does not depend on the number and strength of the individual linkages.

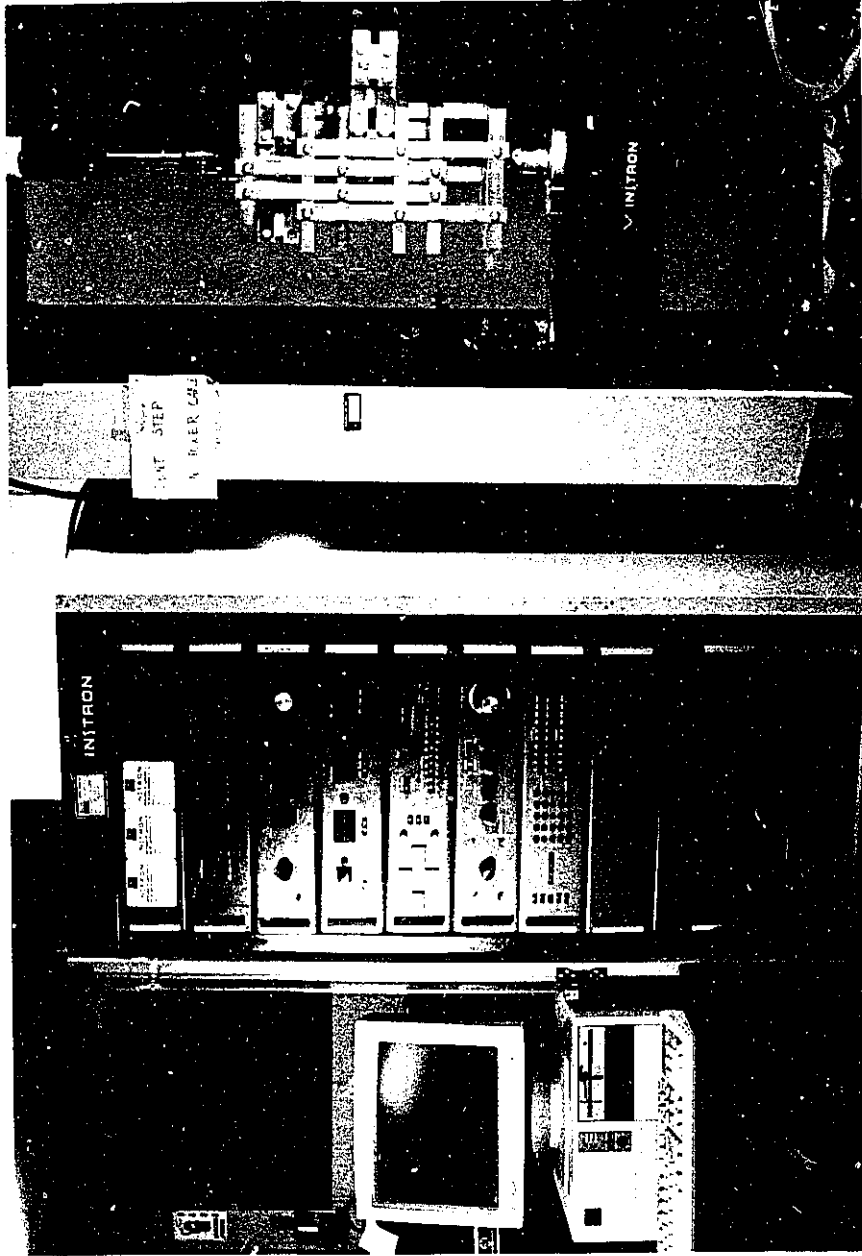
### 3.4.2 MECHANICAL PROPERTIES IN TENSION & COMPRESSION

The elastic constants (i.e. Young's modulus, E and the shear modulus, G) and the stress-strain characteristics of the various elastomer formulations were evaluated by the use of both tension and compression tests. The tests were performed using an Instron Universal Testing machine (model 1125) in conjunction with a 500 kg load cell, accurate to  $\pm 1\%$  of full scale load. The test set-up is shown in figure 3.7.

Data from the tests was retrieved and stored on disk using a LabMaster data acquisition system coupled to a XT based personal computer. A brief description of each test series is given below.

---

Figure 3.7 Test set-up for tension & compression testing. 1. Instron Universal Testing Machine; 2. Instron UTM control module; 3. XT based personal computer hosting data acquisition system.



#### 3.4.2.1 Tensile Tests

Two different tensile tests were used to assess the mechanical properties of the elastomers. In the first instance, tensile tests, referred to as "TA" type tests were conducted in accordance with the standard ASTM D412 [92]. Dumbbell specimens, cut from a 3.2 mm thick cast specimen slab with die "D", were marked with a standard gauge length of 25 mm. The cross sectional area of the specimens was determined with a micrometer dial gauge, accurate to 0.0254 mm (0.001"), by measuring the depth and width of the specimens at three equidistant points along the gauge length. Stress was calculated based on the original cross sectional area. Tests were conducted on at least nine but in most cases on twelve specimens at room temperature using a crosshead speed of 50 mm/min. The load/crosshead displacement data were simultaneously recorded on the testing machine's chart recorder as well as on digital disk. A video camera (Sony CCD-F40) recorded the change in gauge length in relation to an adjacent millimetric rule. The method is precise to at least 4% of the gauge length. A standard specimen and testing set up is shown in figure 3.8.

In a second type of tensile test, referred to as "TB" type tests, specimens were prepared according to CGSB CAN2-19.0-M77, method 14.1 [93] in which samples, adhered to an aluminum substrate, were used to assess the adhesive and cohesive strength of the various blends. The usefulness of this test is apparent from the specimen configuration, shown in figure 3.9, which more closely approximates the shape of a sealant bead commonly found to exist in practice.



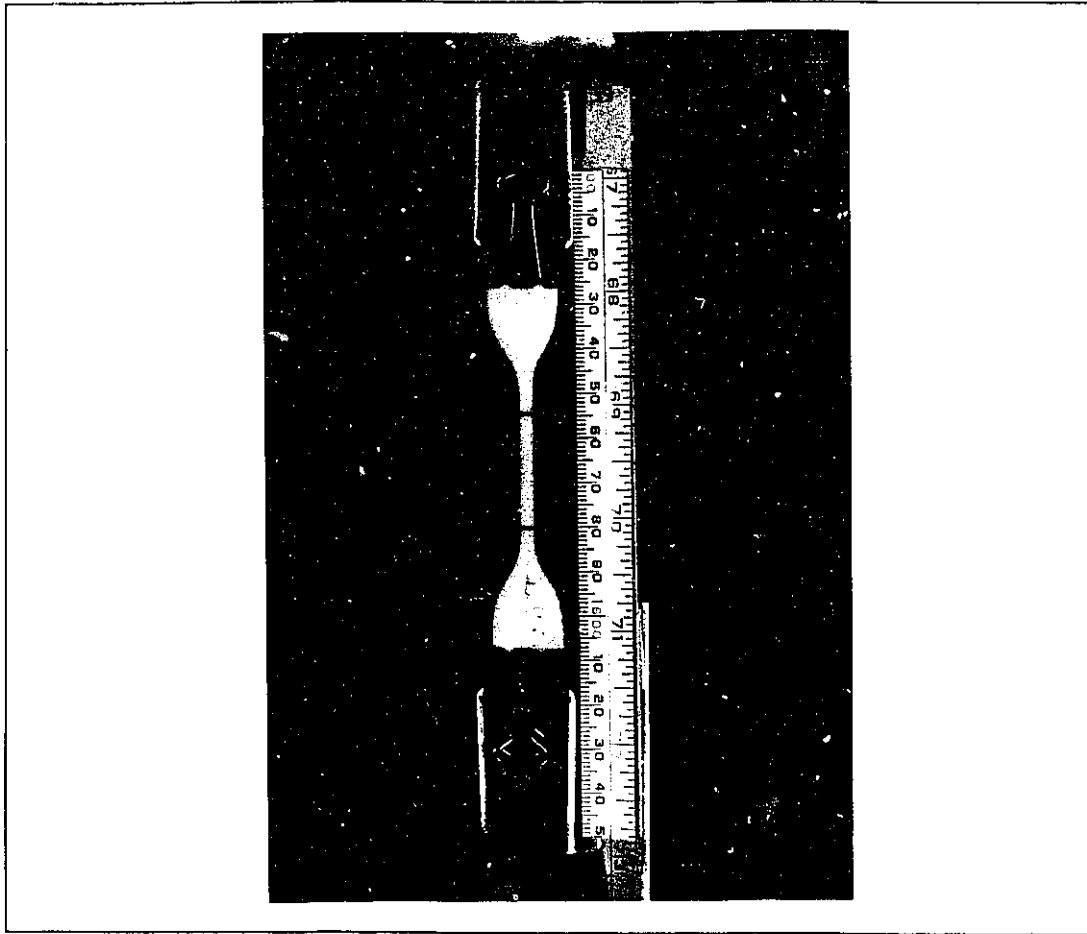


Figure 3.8 TA type tensile test specimen & test set-up.

An aluminum substrate was chosen as a basis to assess the adhesive tenacity of the unfilled formulations and a mortar substrate for filled specimens. Aluminum substrates have been shown to be more difficult to adhere to in comparison to other standard substrates such as wood and mortar [2].

In all cases, the surface of the substrate was primed, with the exception of those tests conducted to evaluate the adhesive /cohesive strength of commercial products. In this case, the manufacturer's instructions were followed with respect to substrate preparation.

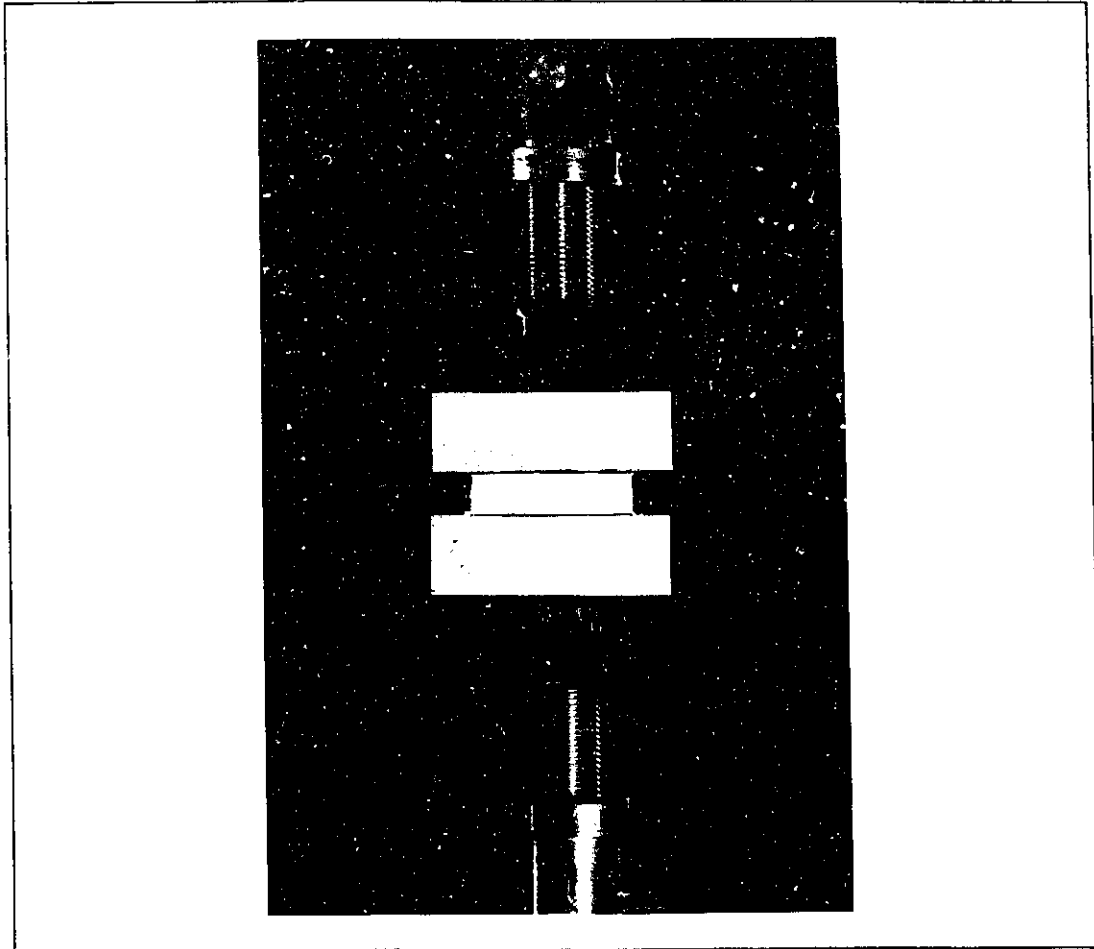


Figure 3.9 TB type tensile specimen and test set-up.

Aluminum substrates were prepared by first degreasing the bars with soap and water, then placing them in an etching solution of  $H_2SO_4$  and sodium dichromate at  $60^\circ C$  for 10 minutes. The bars were then rinsed, dried in a forced air oven at  $110^\circ C$  and allowed to cool to room temperature. A 5% amino silane primer was then applied to the substrate with a fine bristle brush.

For each casting series, six to nine pairs of bars were assembled on a casting bed, in which a silicone release paper had been placed. The gauge length (12.7 mm) between adjacent bars of a specimen was maintained using precision

machined metal blocks, whereas the width (50.8 mm) of the specimens was verified using micrometer callipers.

Tests were conducted at room temperature and at a crosshead speed of 2 mm/min. The load/displacement data was collected as before, whereas the strain was calculated simply on the basis of the displacement of the crosshead. Stress was calculated based on the original cross sectional area. In all cases tensile tests were conducted until rupture occurred such that the ultimate adhesive or cohesive properties of the blends could be determined.

#### 3.4.2.2 Compression Tests

Compression tests were made according to ASTM D575 [94] in which standard 32 mm (1.25") diameter cylindrical disks of 12.7 mm (0.5") height were subjected to a compressive load until a 50% deformation was attained. For each elastomer series, three specimens were tested at room temperature using a crosshead speed of 10 mm /min. The load/deformation data was recorded as described earlier.

#### 3.4.2.3 Compression Set

Compression set tests are intended to measure the ability of elastomeric compounds to retain elastic properties after prolonged action of compressive stresses [66]. This is especially significant in the case of elastomer based sealants because such type of loading conditions are evidently part of the in service conditions which exist for sealants in general.

The tests were conducted according to ASTM D395 [95] in which the residual deformation of a standard size cylindrical elastomeric disk is measured after having subjected the specimen to a prescribed deformation for a definite time under specified conditions.

Hence, 32 mm (1.25") diameter cylindrical disks of 12.7 mm (0.5") height were subjected to a 25% deformation for 22 hours at 70°C. The test was conducted on unfilled as well as filled elastomer specimens and results from these tests are reported in sections 4.3.2.3 and 4.4.2.3 respectively.

#### 3.4.2.4 Hardness Tests

Hardness tests are based upon the increase in the depth of penetration of a rigid indenter (spherical, conical or otherwise) into a flat pad of rubber (or similar elastomeric materials) when an applied load is increased by a standard amount. Gent [96] has reviewed the relationship between the various measures of rubber hardness and the modulus of elasticity. It has been shown that the penetration of a rigid spherical indenter follows the laws of classical elasticity for indentations as large as 10 percent of the diameter of the indenter, and at depths of penetration as great as 30 percent, the deviation is not great [96].

The Shore "A" durometer has a frustum cone impresser pin 1.2 mm (3/64") in diameter, having a flat tip of 0.8 mm (1/32") in diameter. The indicator hand departs from zero after a pre-load of 57 g (2 oz.), then proceeds to 822 g (29 oz.) at which point 100 is indicated on the scale. The total stroke of the pin is 2.54 mm

(0.1") so that each division on the dial represents 0.0254 mm (0.001") of travel [97].

The hardness test, using the Shore "A" durometer, is specified for the evaluation of sealants in both Canadian and U.S. standards (i.e. CGSB CAN2-19.0-M77, method 8; ASTM D2240 [98,99]). The Canadian standard specifies a Shore A of no less than 15 and no greater than 50 after a minimum 21 day curing period.

Hardness tests were used to monitor the cure of all formulations by taking hardness readings as a function of time. Hence the results of these tests are given in all phases in which physical tests are described. This includes preliminary investigations, given in section 4.2, and the characterization of unfilled and filled elastomers in sections 4.3.2.1 and 4.4.2 respectively.

### 3.4.3 THERMAL BEHAVIOUR - GLASS TRANSITION TEMPERATURE

The glass transition temperature ( $T_g$ ) may be determined by using either a differential scanning calorimeter (DSC) or a dynamic mechanical analyzer (DMA). In this study, the DSC was used to assess the thermal properties of unfilled elastomers and the DMA was found useful for elucidating both the thermal behavior and the interaction between filler and polymer matrix phases in filled elastomer specimens.

#### 3.4.3.1 Differential Scanning Calorimetry

The DSC method uses the differences in heat capacity of a reference and sample material analyzed over a predetermined time-temperature program [75]. Reference and sample specimens are placed in individual cells or pans which sit on a thermoelectric disk. Heat is transferred at a constant rate to the disk and into both reference and sample via the specimen pans. The differential temperature of the specimens is monitored by area thermocouples located on the underside of the disc beneath each specimen pan. Since the thermal resistance to the specimens is held constant, differential temperatures are directly proportional to differential heat flows. At  $T_g$ , the heat required to change the sample from a glassy to a rubbery matrix induces a difference in heat flow between sample and reference such that a negative heat flow is observed in this region.

A DuPont model 910 DSC was used to analyze various sealant blends according to ASTM D3418-81 [100]. Samples were placed in the DSC cells at

room temperature and cooled to well below the assumed  $T_g$  of the blend. The thermographs were determined between -100 and 200°C, at a heating rate of 20°C/min, while being maintained in a nitrogen atmosphere.

#### 3.4.3.2 Dynamic Mechanical Analysis

If a viscoelastic material, such as a filled elastomer, is deformed and then released, a portion of the stored deformation (strain) energy is released at a rate that is a fundamental property of the material [101]. That is, the material goes into damped oscillation after being deformed. For an ideal elastic material, the energy incorporated into oscillation is equal to that introduced by deformation, with the frequency of the resultant oscillation being a function of the modulus of the material. For viscoelastic materials however, a portion of the deformation energy is dissipated in other forms such as heat, resulting in a damping of the deformation-induced oscillation. Hence dynamic-mechanical techniques may facilitate the measurement of both elastic and viscous properties of viscoelastic materials [101].

Filled elastomers are viscoelastic composite materials having essentially two discrete phases. The rubbery matrix constitutes the continuous phase and the filler the discontinuous phase. In general, the addition of filler to the matrix increase the dynamic modulus, this effect being more pronounced below rather than above the  $T_g$  of the matrix [102]. In high concentrations, fillers can significantly broaden the glass transition region. Furthermore, fillers may also

decrease the damping as expressed by the loss-tangent  $\tan\delta$ , which represents the ratio of energy dissipated to the maximum energy stored during one oscillation [102]. In some cases the filler may shift the loss-tangent peak and  $T_g$  to higher temperatures. The shift in  $T_g$  is related to the surface area of the filler. The effect should increase with concentration and as the size of the particles decreases [102]. Hence a considerable amount of information related to the interaction between the filler and the polymer matrix may be obtained through the use of DMA.

The Dupont 982 DMA used in this study is a free oscillating resonant instrument in which a sample is mounted between two freely oscillating pair of parallel arms to form a compound resonant system. The natural resonant frequency of this system is primarily determined by the geometry and modulus of the sample and the damping is essentially resolved by the energy dissipation within the sample. The sample is set in motion and maintained at the natural resonant frequency of the compound system by means of a electromechanical transducer actuated by an LVDT feedback. The LVDT also serves to determine the number and amplitude of the oscillations from which the resonant frequency and damping can be experimentally obtained. The frequency can be converted to the modulus of the sample from the following relation [101]:



$$E = \frac{4\pi^2 f_o^2 J_o - P_c}{2w \left( \frac{l}{2} + l_c \right)^2} \cdot \left( \frac{l}{d} \right)^3$$

Equ. 3.9 [101]

where:

- E = modulus (Pa);
- $f_o$  = frequency (Hz);
- $J_o$  = moment of inertia of the arm ( $\text{kg}\cdot\text{m}^2$ );
- $P_c$  = spring constant of the pivot (N·m);
- $l_c$  = clamping distance (m);
- l = sample length (m);
- w = sample width (m);
- d = sample thickness (m).

Samples (14 mm x 10 mm x 3.6 mm) were placed in the DMA clamps at room temperature and cooled to well below the assumed  $T_g$  of the elastomer. The thermographs were determined between -100 and 0°C, at a heating rate of 20°C/min, while being maintained in a nitrogen atmosphere.

### 3.4.4 INFRARED & NUCLEAR MAGNETIC RESONANCE SPECTROSCOPY

#### 3.4.4.1 Infrared Spectroscopy

Infrared (IR) spectroscopy is an analytical tool used to identify the chemical structure of organic compounds. It uses the middle range of the infrared spectrum (wavelengths from 2.5 to 25 $\mu\text{m}$ ) to produce absorbance spectra of different compounds [103] thus providing a unique spectral pattern which is readily distinguishable from other absorption patterns of all other compounds.

Infrared analysis was used to identify the composition of prepolymers used in this study and as well, to assess the nature of interaction between lignin and the polyurethane matrix.

The IR spectra were obtained using a Beckman 4240 IR spectrophotometer, the scan being performed between 4000 and 200  $\text{cm}^{-1}$ . The samples were prepared using the KBr disk method with a mixing ratio of 1 mg of lignin to 100 mg KBr whereas in the case of elastomeric samples, a mixing ratio of 1.5 mg of PUR to 100 mg KBr was used. The PUR-KBr disks were prepared by first immersing the samples in liquid nitrogen and thereafter, grinding them while still in the frozen state. Results concerning the chemical interaction between blend components are given in section 4.4.5

#### 3.4.4.2 Nuclear Magnetic Resonance (NMR)

Nuclear magnetic resonance is a phenomenon caused by the resonance transitions between the magnetic energy levels of atomic nuclei in an external magnetic field [104]. It has been used in the determination of the composition of

copolymers and chemical functionality [71], and has proven to be a useful tool to investigate compatibility and miscibility in polymer blends [105].

If a magnetic field is applied to a polymeric material which has nuclear magnetic moments and is then removed, the magnetic polarization of nuclei will begin to decay because of thermal motions [103]. The phenomenon of spontaneous decay of magnetic polarization in the absence of an external magnetic field is referred to as the spin-lattice relaxation, and is caused by the thermal motion of atoms. The spin-lattice relaxation time is the time required for the decay to take place and is dependent on the structure and mobility of the polymeric material. Hence correlations can be made between relaxation times and, for example, the degree of crosslinking, of crystallinity, plasticizer content and the glass transition temperature in polymeric materials. It has also been used, as suggested by Stejskal et al. [106], for investigating the compatibility and miscibility in polymer blends.

This method consists of measuring the spin-lattice relaxation time in the rotating frame ( $T_{1\rho H}$ ) for both individual components of the blend and comparing the values found with the  $T_{1\rho H}$  of the blend. If the two components have  $T_{1\rho H}$  values that differ from one another, and an intermediate value is found for the blend, it can be assumed that there is molecular miscibility within the blend.

NMR spectra were recorded on a Bunker CXP-200 spectrometer at room temperature with the sample spinning in a Doty probe at rates of ca. 4 kHz [107].  $T_{1\rho H}$  values were measured using a pulse sequence with variable contact times.

### 3.4.5 SURFACE ANALYSIS TECHNIQUES

The mechanical and hence the performance properties of filled formulations such as sealants, is a function of the degree of interaction between the modifier and the polymer matrix. Theories which relate the increase in mechanical properties of the polymer to that of the modifier are based on the assumption that the filler is perfectly adhered to the matrix. It has been shown that significant deviations from the proposed mechanical behaviour occurs if the filler is not thoroughly bonded to the matrix or if debonding occurs as a result of stress concentrations at the interface between blend components [102,108]. It is evident that a method which is able to assess the interaction between blend components would be useful in determining the effectiveness of different modifiers.

Lee [61] has devised a relationship which describes and relates the characteristics of polymer-filler interaction. The relationship requires that the surface energy properties of both the polymer matrix and the modifier be determined. Measurements using the sessile drop method are used to evaluate the critical surface energy of the polymer matrix, from which the extent of interaction can be determined based on the following relationship:

$$\cos \theta = 1 + b \ln \left( \frac{\gamma_c}{\gamma_{LV}} \right)$$

Equ. 3.10 [61]

where:

- $\Theta$  = contact angle of a wetting liquid on the substrate;
- $b$  = extent of interaction;
- $\gamma_c$  = critical surface energy for wetting;
- $\gamma_{LV}$  = liquid /vapour surface energy of the wetting liquid;

The surface energy properties of the various modifiers used in the blends were determined using a filler-column method in conjunction with the technique perfected by Crowl and Wooldrige [109], which relates the rate of capillary rise of a given liquid through a column packed particles by the following relationship:

$$\frac{l^2}{t} = k \frac{\gamma}{2\eta} \cos \theta$$

Equ. 3.11 [62,109]

where:

- $l$  = distance of rise of a liquid through a column (cm);
- $t$  = time which liquid takes to rise a given distance (s);
- $\gamma$  = surface tension of wetting liquid (mPa·m);
- $\eta$  = viscosity of wetting liquid (Pa·s);
- $\Theta$  = contact angle of wetting liquid with the particles;
- $k$  = column packing constant, dependant on the nature of the filler and the degree of compaction.

The column packing constant,  $k$ , is first determined for a liquid which will completely wet the particles, i.e. one for which  $\cos \Theta = 1$ , such that  $k$  is given by the equation:

$$k = \frac{l^2}{t} \cdot \frac{2\eta}{\gamma}$$

Equ. 3.12

Hence the contact angle given for various liquids wetting the particles may readily be determined, and in using equation 3.9, the critical surface energy for wetting,  $\gamma_c$ , and the extent of interaction,  $b$ , for the various modifiers may also be evaluated.

Based on these relationships, the interaction parameter,  $b$ , and the polymer-matrix bonding coefficient,  $\Omega$ , can be calculated based on the following relationships [61-63]:

$$b = (b_p \cdot b_f)^{0.5}$$

Equ. 3.13 [63]

where the subscripts  $p$  and  $f$  refer to the polymer and filler respectively.

$$\Omega = \frac{1}{b} \cdot \exp\left(1 - \frac{1}{b}\right)^{0.5}$$

Equ. 3.14 [63]

The techniques used to assess the critical surface energy for wetting for both the polymer and modifiers are given below.

#### 3.4.5.1 Surface Analysis of Elastomer Matrix

A sessile drop method was used to obtain the critical energy of wetting of neat polymer blends. The apparatus used to record contact angles of various liquids on the surface of the polymer is shown in figure 3.10. It consists of essentially three parts: an environmental chamber, a microscope, and a recording device.

The chamber is comprised of an inner transparent glass box used to accommodate the specimen and a small quantity of test liquid, such that the test is conducted in an atmosphere saturated with the test liquid. The glass box is positioned at the centre of the larger enclosure and along the optical axis of the microscope. The outer enclosure serves to minimize thermal fluctuations, and as well, provide appropriate conditions for capturing video images or for taking photographs of the test.

An Olympus ZX stereo microscope with 4X magnification was used to view the specimens and the formation of sessile drops on the specimens. A backlight was used to achieve a picture having sufficient contrast from which data could be extracted. The microscope was fitted onto a two-axis sliding carriage and a double-acting pivoting head such that its horizontal and vertical position could be adjusted as well as the angle of inclination and rotation with respect to the longitudinal viewing axis. Two different types of recording devices were used to capture images of sessile drops being formed on the surface of the substrates. In the first instance, a 35 mm single lens reflex camera with special eyepiece and graticule was used to produce photographs from which the contact angle, height, and diameter of the drops could be measured.

In the second instance, a video camera (JVC C40) was used to record a continuous set of events from the moment the drop was deposited onto the substrate until the time equilibrium was reached. The use of such a device for measuring contact angles enables the subsequent digitization of specific images

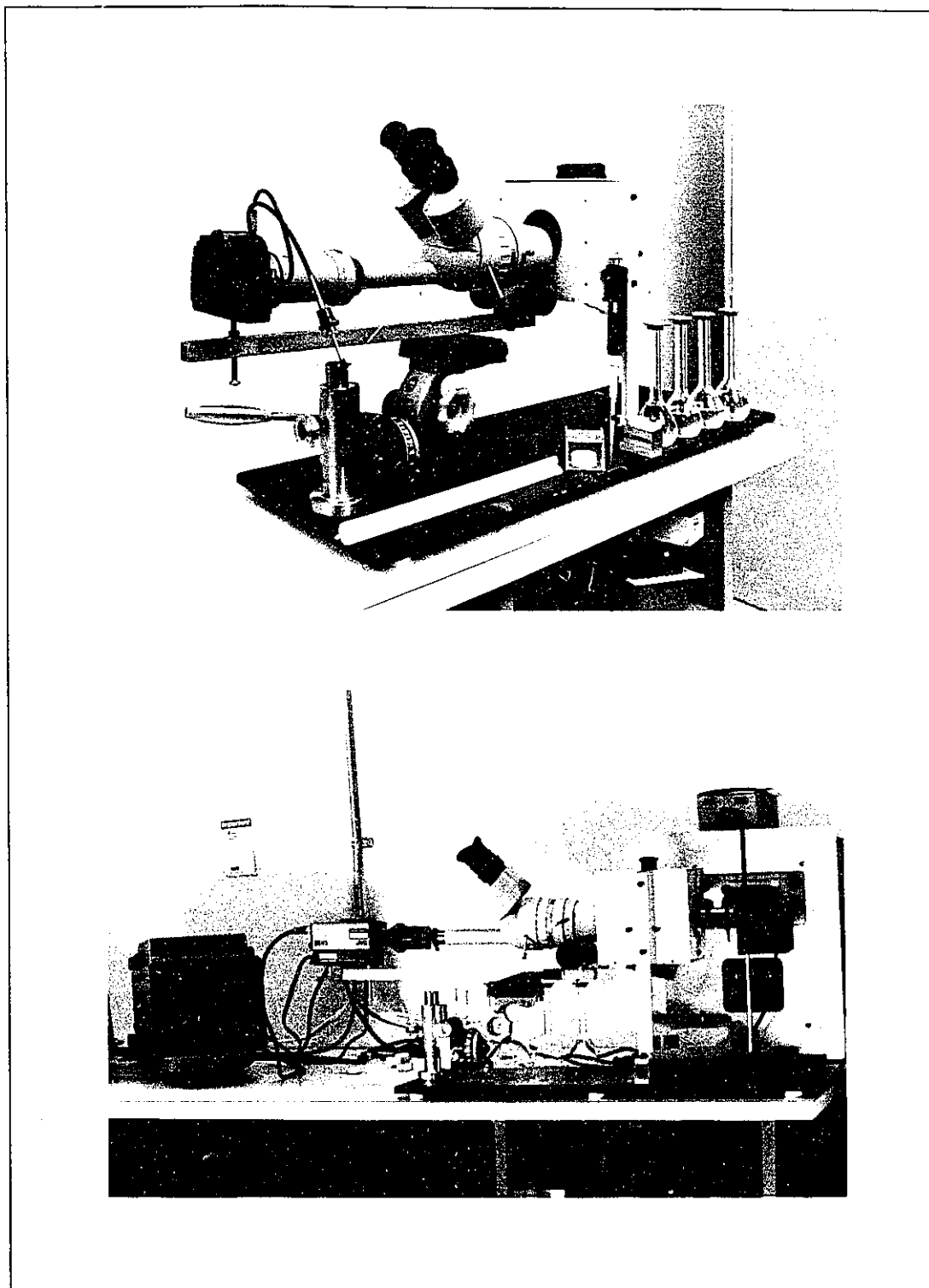


Figure 3.10 Surface analysis of elastomer matrix using the sessile drop technique: a) photographic set-up; b) video camera set-up.



using appropriate computer software.

In either case, the tests were conducted at room temperature (25°C) using a series of homologous liquids whose relevant characteristics are given in Table 3.7.

Table 3.7 CHARACTERISTICS OF WETTING LIQUIDS USED IN SURFACE ENERGY EVALUATIONS		
WETTING LIQUID	SURFACE ENERGY $\gamma_{lv}$ mPa·m	Viscosity $\eta$ Pa·s
Acetic acid:Water 0:100	72.8	1.002
5:95	62.3	1.11
10:90	56.3	1.22
20:80	49.3	1.51
30:70	44.9	1.69
70:30	38.4	2.65
Hexane	18.4	0.326

Cylindrical samples (12.7 mm height, 32 mm diameter) were first cleaned using tap water and detergent followed by repeated rinsing with singly distilled water. The specimens were then wicked dry with absorbent paper after which they were placed in an oven at 90°C for 10 min. The cleaned samples were stored in a desiccator prior to use.

A digital micro-pipettor was used to produce 5 $\mu$ l sessile drops on the substrate. Up to four drops could be placed on any given substrate and at least

twenty-four measurements were taken for each liquid.

The formation of the drop was recorded on video tape and an image was reproduced from the digitized data representing the form of the drop 10 seconds after it was deposited on the surface of the substrate.

#### 3.4.5.2 Surface Analysis of Particulate Fillers

The flow of specific wetting liquids was measured under capillary pressures generated by a packed particle bed contained within a vertical glass column. This technique is similar to that used by Lee [62], by Cheever and Ulicny [110] and was developed by Crowl and Wooldrige [109] based on the work of Washburn [111].

The apparatus used for measuring the capillary flow of liquids through a packed tube is shown in figure 3.11. It consists of a 10 mm (i.d.) x 120 mm glass tube filled with the particulate filler to be tested and stoppered at either end with filter paper and surgical cotton plugs. To facilitate the even flow of liquid through the tube, the glass columns were pre-rinsed in the appropriate wetting liquid, dried in a forced air oven and finally stored in a desiccator.

To insure reliable values for the column constant  $k$ , a number of packing methods were evaluated to determine the means by which uniformly packed columns could consistently be obtained. The method adopted consists in placing a known weight of particulate matter in the column and packing it using a consolidation device. When a column containing a sample is placed on the device, the repeated vertical movement of the sample causes the particles to consolidate

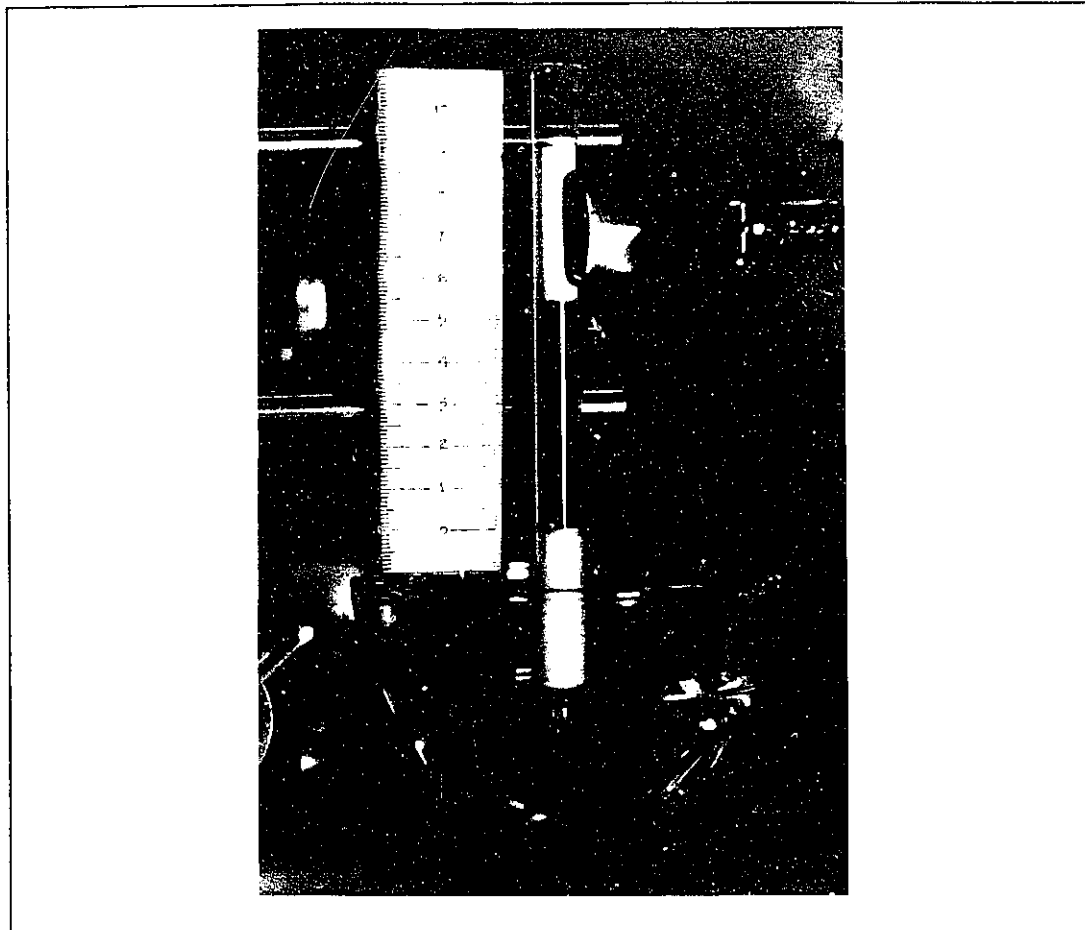


Figure 3.11 Apparatus for evaluating the capillary flow rates of various wetting liquids through a column of packed particulate matter.

themselves into a uniformly packed bed.

The tube was then placed in contact with a wetting liquid. A millimetric card, placed adjacent to the tube, was used to determine the rate of rise of the liquid front through the packed bed. The value of the system constant,  $k$ , was determined by using a liquid which completely wets the particles. Hexane was used to determine these values. Values for  $\cos \Theta$  for each liquid type and particulate combination were determined from flow rate measurements.

### 3.4.6 PERFORMANCE TESTING OF SEALANTS

#### 3.4.6.1 Performance Test Methods

Performance tests may proceed through direct or indirect methods. Direct methods simulate the service conditions by assessing the adhesive and cohesive properties of the sealant product when subjected to extension and compression with simultaneous or continuous exposure to specified factors causing degradation. A list of degrading factors used in laboratory test simulation of aging and the putative effect each has on the sealant is given in Table 3.8 [112]. Indirect methods are useful for characterizing the sealant products and consequently many of the indirect test methods such as hardness, tension, compression and compression set tests, have been described in the section related to blend characterization. These tests have not only been used to characterize the blends, but have also served to screen sealant blends for subsequent performance testing. Although indirect methods are useful in characterizing the sealant product, their effectiveness for predicting the service life of sealants is limited. Essentially direct test methods, which have been developed with a view to including all the relevant service factors in appropriate combinations and at levels appropriate to the intended service conditions, are the most suitable for predicting the probable effective life of a product (i.e. time before remedial maintenance or replacement is required) [112].

Table 3.8 [112]	
DEGRADING FACTORS USED IN LABORATORY TESTS SIMULATION OF AGING	
Factor	Putative Effect
a) Elevated temperature	Acceleration of rate of chemical change (oxidation) causing changes in salient properties
b) Low temperature	Increase in sealant modulus (stiffness) & consequent increase in stresses within sealant, and at the sealant substrate interface tending to increase the risk of failure
c) Water	<ul style="list-style-type: none"> <li>i) absorption of moisture by sealant causing softening &amp; reduction of modulus for some products;</li> <li>ii) increase in modulus when subjected to low temperature after absorption of water by sealant;</li> <li>iii) deleterious effects on adhesion for certain combinations of sealant &amp; substrate;</li> <li>iv) effect on cure rate for moisture-curing sealants;</li> <li>v) adsorption of moisture by porous substrates: possible damage when subsequently subject to low temperatures which may affect adhesion of sealant.</li> </ul>
d) Ultra-violet radiation	<ul style="list-style-type: none"> <li>i) effect on cure of product;</li> <li>ii) chemical reactions resulting in surface damage, or increase in hardness or stiffness leading to increased risk of adhesive or cohesive failure.</li> </ul>

A brief review of direct test methods developed by different research facilities is presented and a description of two testing devices which have been developed as a means of evaluating the performance of sealants is outlined.

#### 3.4.6.2 Review of Direct Test Methods

The Princes Risborough Laboratory (PRL), Building Research Establishment, UK, have devised a natural exposure movement simulation rig which uses black PVC driving bars to respond to temperature change and give rise to movement at a joint. The simulated sealant-filled joints exposed to weather on these rigs show daily and seasonal movement similar to those on buildings (figure 3.12a) [113].

Investigations on the possibility in predicting the performance of sealants from laboratory testing indicated that cycling tests provide the closest laboratory reproduction of outdoor behaviour [114]. At low joint movement rates occurring in practice, however, laboratory methods are impractical and a strain-cycling outdoor exposure rack was designed [115]. Standard sealant specimens exposed on this outdoor sealant weathering rack, underwent the natural aging process experienced by exterior surfaces of buildings (figure 3.12b). This includes the physicochemical changes induced by radiation, temperature changes, the effect of air and moisture, and by the movement to which joints are subjected to.

The movement is produced by using the differential movement between steel and aluminum. Two types of observations can be obtained from this rack:

1. one can evaluate relative fatigue performance of a large number of specimens;
2. one can observe the ultimate movement a sealant can safely tolerate, i.e., the movement capability of a sealant.

Results of tests on one-part chemically cured silicone sealants using this device indicates that strain-cycling movement is the predominant factor which causes failure during weathering of these sealants; outdoor weathering alone is negligible [116]. Failure is also influenced by the extent of movement, becoming more extensive at higher yearly strain-cycles. Tensile tests reveal a notable decrease in strength beyond about +22% movement.

In a similar study, a two-part polysulphide sealant formed cavities on the side sheltered from direct sunshine [117]. The same material, when weathered without cycling or stored in the laboratory, did not undergo permanent deformation. This underlines the importance of the effect of cyclic movement on the performance of two-part polysulphide sealants, revealing it as the most important factor in test methods intended to evaluate their performance.

It is possible to produce with hand-operated vices the same permanent deformation of sealant specimens that occurs on the strain-cycling outdoor exposure rack [118]. The vice (fig. 3.13) enables the sealant specimens to be subjected to cyclical movements [119] and these may be imposed on sealant specimens through manual adjustment at arbitrarily chosen intervals. The simplicity of the vice enables users to make accelerated testing where one of the aging factors is cyclical movement, and this can be accelerated by increasing the amplitude and frequency of the cycling.

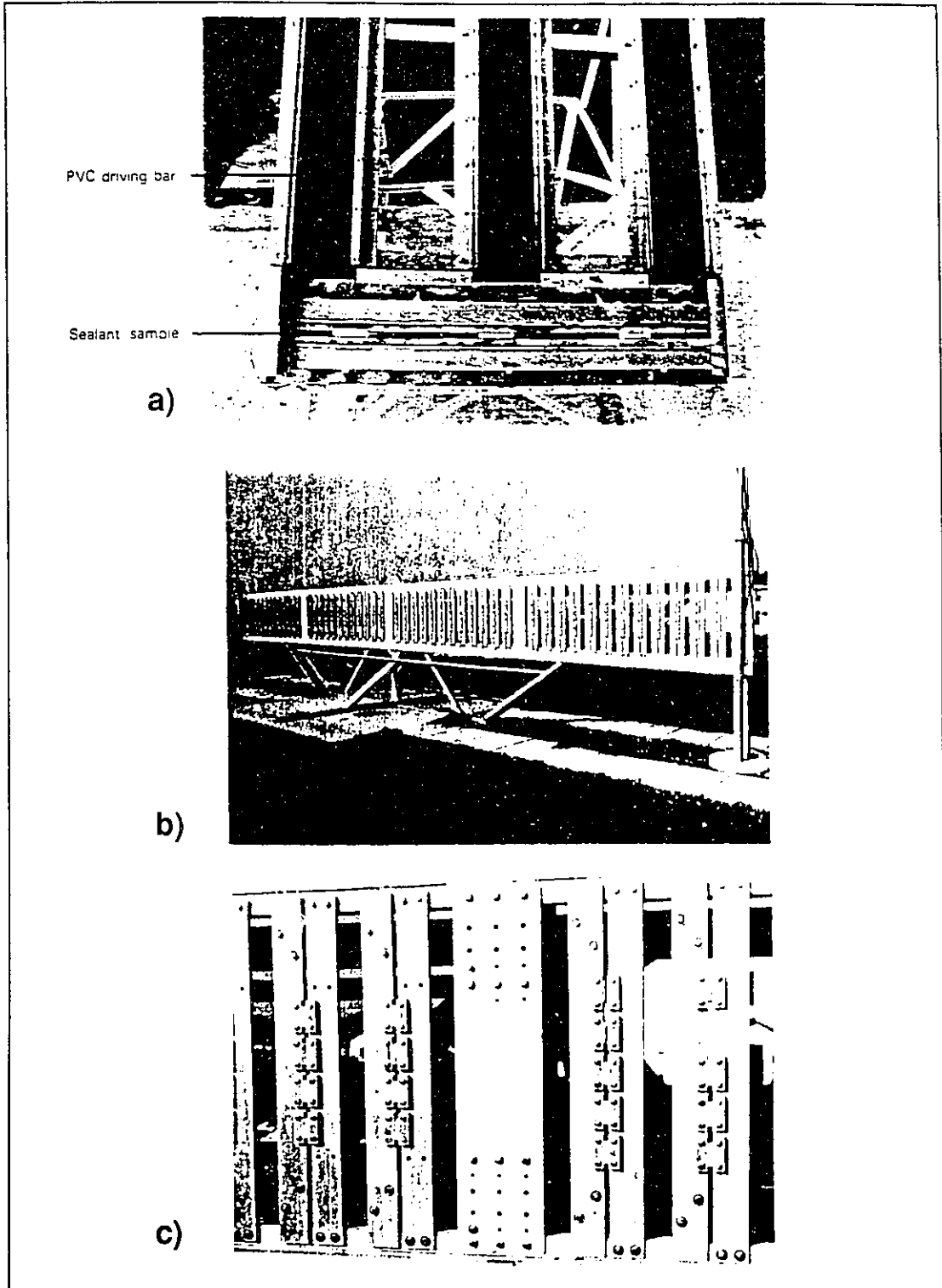


Figure 3.12 a) PRL natural exposure test rig; b) Sealant weathering test rack; c) Close-up of centre of test rack [113,115].



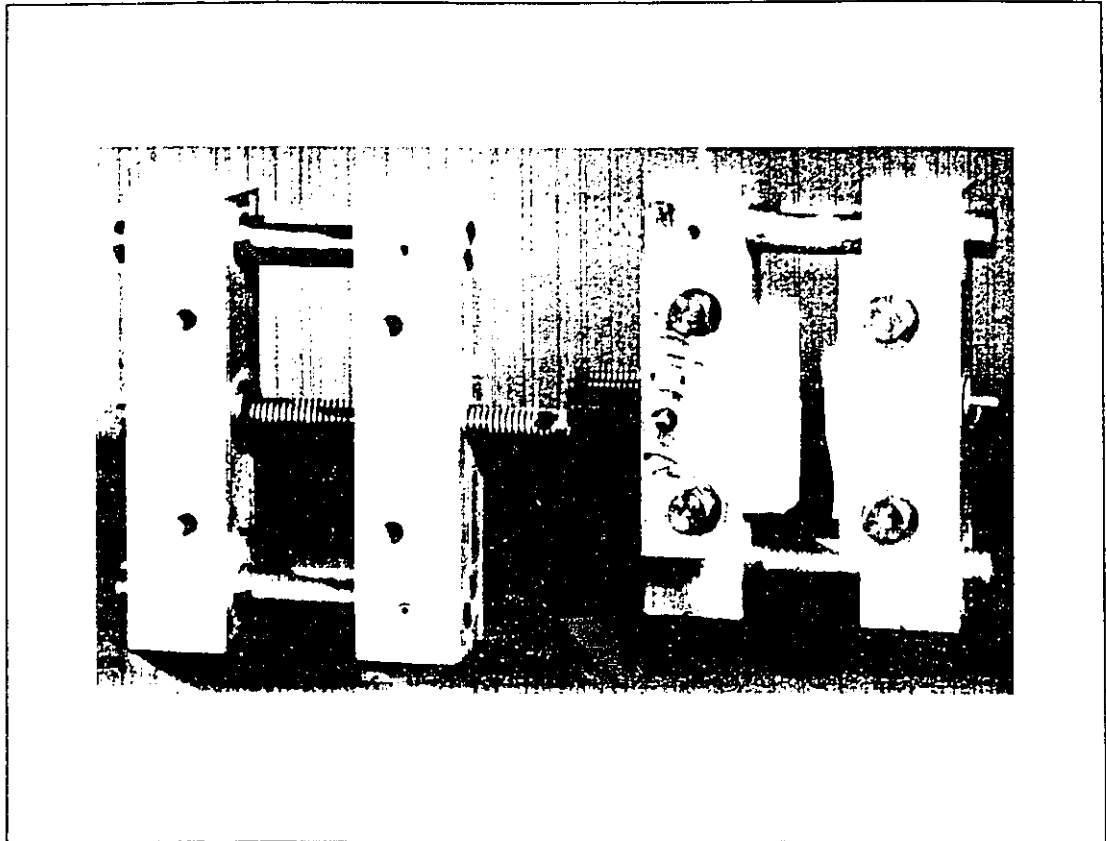


Figure 3.13 Hand operated sealant testing device [119].

This has been illustrated in the performance testing of a polysulphide sealant and the results show that the vices can replace the strain-cycling exposure rack that imitates the performance of sealants in building joints. Hence this work helps establish a link between outdoor performance and laboratory tests of sealants, since the vices can be used in the laboratory, with some changes in the conditions imposed. It establishes three stages of permanent deformation for one make of two-part polysulphide sealant and provides photographs as a guide to the process. This can form the basis of an evaluation of sealants of any chemical type provided that deterioration occurs by a similar process of permanent deformation.

### 3.4.6.3 Description of Sealant Testing Devices

#### i) Karpati sealant testing device & rig assembly

The Karpati sealant testing device is similar to the one developed at the Institute for Research in Construction, in that:

1. the joint spacing may be manually adjusted.
2. uses the same sealant specimen specifications.

The device designed for this project differs in the mechanism used to strain the sealant bead and the number of specimens it is capable of testing at any one time.

A series of six specimens (3 on either side) may be attached to the device shown in figure 3.14, by means of four bolts located on either side of the joint. The bolts fix the substrate, to which the sealant is adhered, onto the testing rig.

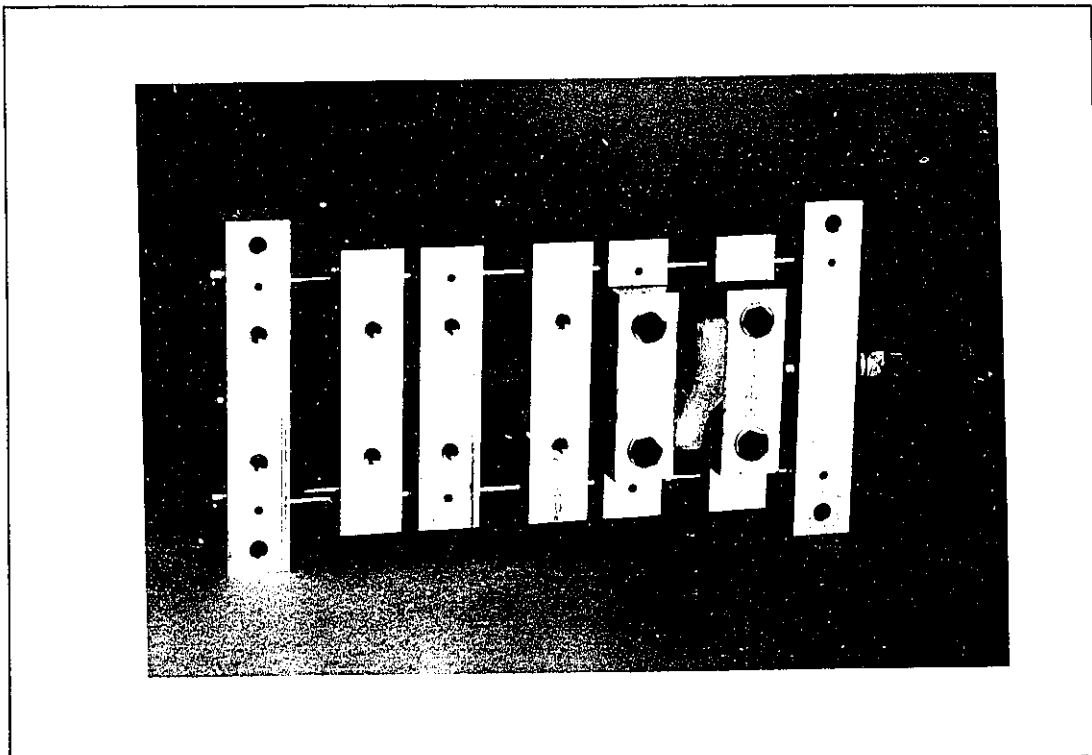


Figure 3.14 Sealant testing vise used in Karpati performance test.

Of the seven bars on the jig, three are capable of movement in a direction perpendicular to that of the sealant bead, as shown by the arrows in figure 3.14. The three moveable bars are interconnected by a single threaded rod which runs through the centre of the rig and is threaded through the main loading bar. A turn of the threaded rod causes a predetermined movement in the moveable bars, and consequently the distance between complementary bars may easily be adjusted.

Using this device, sealant specimens may be subjected to cyclic performance testing based on a predetermined cycling program. The program to be used in this study is based on one developed by Karpati [120], in which specimens are subjected to a number of extension ratios at predetermined cycling rates. The performance of each sealant is assessed by visually evaluating their capacity to withstand repeated cyclic movement without permanent deformation.

In the present study, thirty-six (36) testing devices were used to subject the various elastomers to a cyclic testing program. A set of 18 testing devices are shown mounted on a test frame in figure 3.15. Two such frames have been fabricated to accommodate the 36 devices.

Each series of three devices (18 specimens) was used to subject specimens to different strains such that twelve strain programs could be initiated at any one time. Each strain program included six different blends, comprised of three specimens. The number of cycles at which both permanent deformation is just observable and perforation occurs was recorded for each strain program. The long term performance was estimated based on these results using the methods

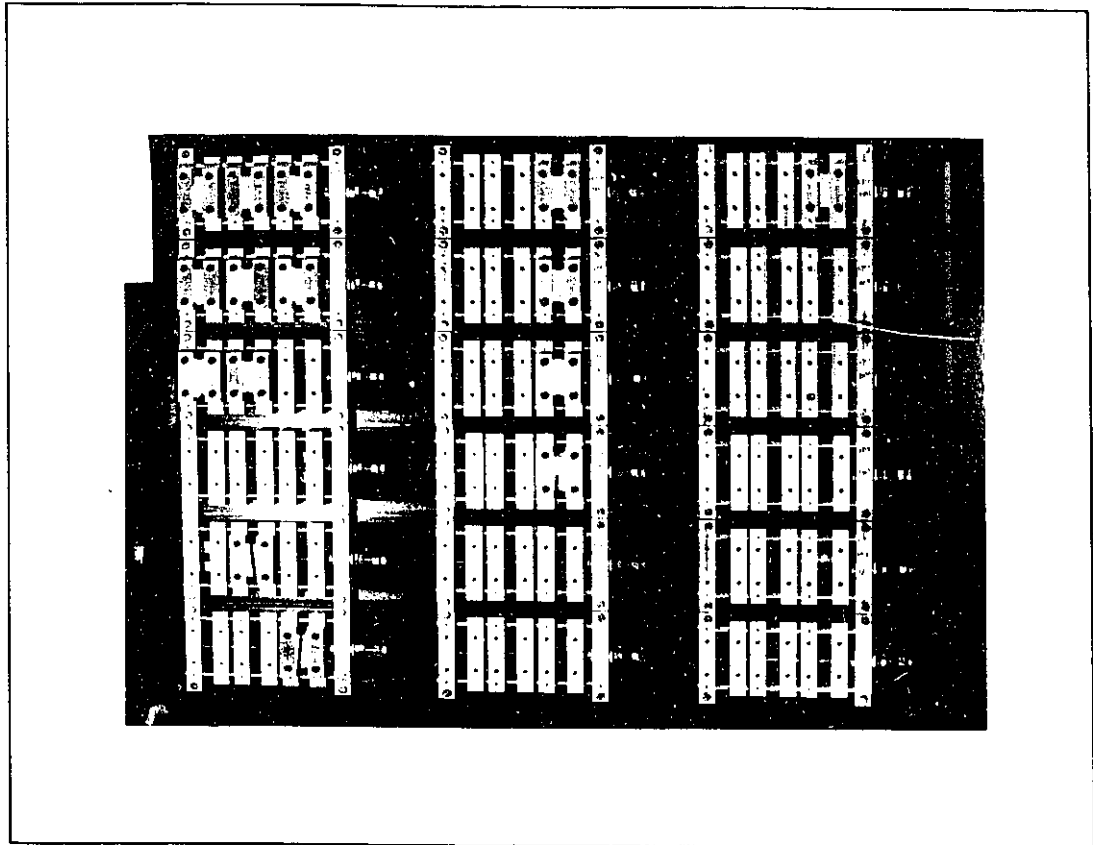


Figure 3.15 Sealant testing devices shown mounted on a test frame.

developed by Karpati [120].

ii) Automatic sealant cyclic testing system

The concept for the automatic sealant cyclic testing system, shown in figure 3.16, was devised by the author of this thesis, who also designed the rig and supervised the fabrication and assembly of the device.

This sealant testing system is made up of four major components:

1. Testing frame & hydraulic system;
2. Sealant testing rig;
3. Hydraulic power unit;
4. Central processing unit (CPU).

The *testing frame and hydraulic press* are part of an existing test platform which has been modified to accommodate the cyclic test system.

The *sealant test rig*, shown in greater detail in figure 3.17, accepts up to 36 standard sealant specimens on three separate sets of parallel plates. This is achieved by placing a series of two sub-assemblies on each set of plates, each assembly in turn able to accommodate a maximum of six (6) specimens. In order to load the rig, specimens are first mounted on the sub-assemblies, after which these are bolted to the rig. The specimens can be subjected to tensile and compressive loads while undergoing cyclic movement. The top of the rig is fixed to the test frame, whereas the opposite end is attached to the moveable platen on the press.

A *hydraulic unit* provides the necessary fluid power for movement of the main hydraulic cylinder. It consists of a 5HP (220V) electric motor which drives a manually adjusted variable displacement pump to produce a working pressure of up to 10.35 MPa (1500 psi). This fluid power is capable of imparting a 33.2 tonne compressive load or an 11.9 tonne tensile load to the rig.

The rate and direction of movement is controlled via an electro-mechanical servo valve which receives the appropriate electronic signals from the *central processing unit*. The two output ports on the servo valve lead to either the top or the bottom portion of the hydraulic cylinder. Fluid flowing to the top causes the piston to be lowered, the rig to lengthen, and the specimens to be extended; the opposite effect is achieved if fluid flows to the bottom of the cylinder. Alternately

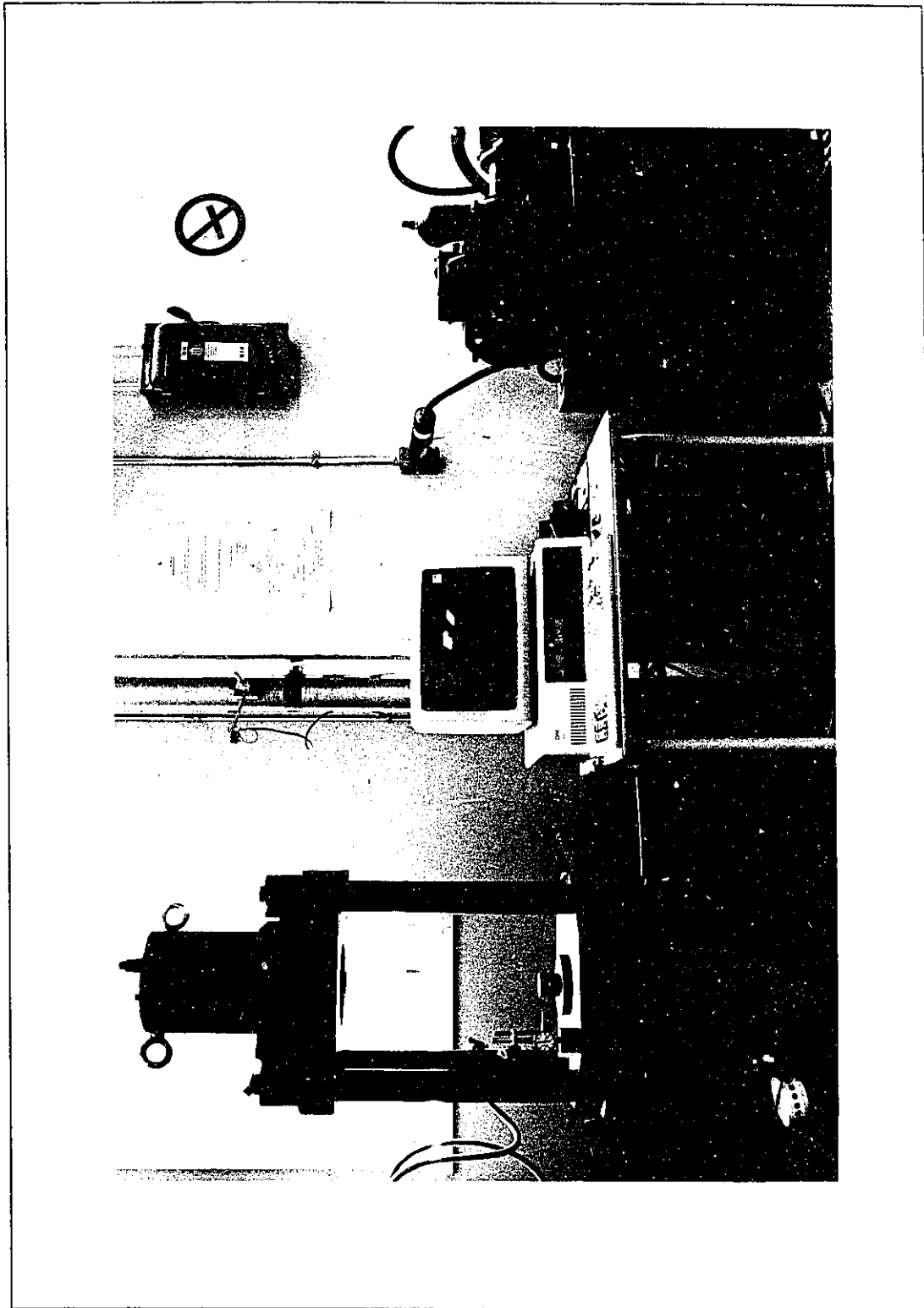


Figure 3.16 Automatic sealant testing set-up.

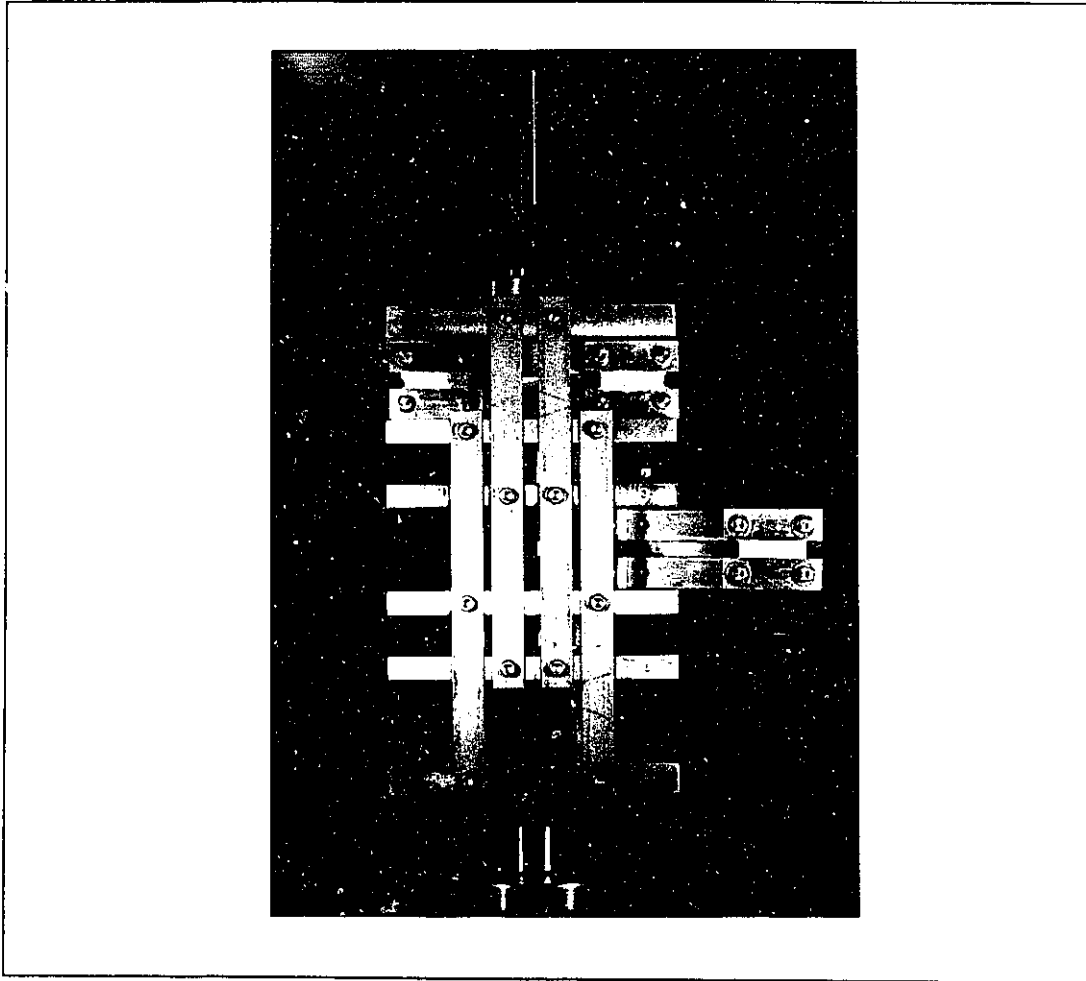


Figure 3.17 Detail of sealant testing rig.

having fluid move from the top to the bottom portion of the cylinder produces a cyclic movement.

A XT based IBM compatible personnel computer fitted with a data acquisition and control module serves as the CPU. It records the number of cycles, sets the amplitude according to the prescribed requirements and controls the rate of movement by a closed loop feedback control system. The CPU sends the appropriate signals to an electro-hydraulic controller card which in turn controls

the servo valve. A feedback signal is provided by a linear variable displacement transformer.

The system operation uses interactive software such that input parameters can be entered directly from answering questions on the CRT screen. The system was used to test various types of elastomer blends in an accelerated cyclic testing mode in contrast to the Karpati performance test where specimens are subjected to a much lower rate of deformation. It was of interest to know if similar types of deformation patterns occur in specimens subjected to this cyclic test in comparison to those in the previously described cyclic test.

At least three and in some cases up to six test specimens from ST and TO filled formulation series were subjected to a series of five different strain sets. Testing was conducted at a rate of 20 mm/min and at amplitudes ranging between  $\pm 25\%$  strain (based on original joint width of 12.7 mm) and  $\pm 60\%$  until failure occurred. Results from this performance test are given in section 4.6.3.



## CHAPTER 4

### RESULTS AND DISCUSSION

#### 4.1 INTRODUCTION

Experimental results are reported in five parts, the first part of which was used to establish a base formulation from which subsequent filled formulations were produced.

Within the initial part, the limits of hardness and extensibility of a series of PUR formulations was established based on the compounding of a variety of different prepolymer combinations. The results of this initial test series permitted establishing a base formulation suitable for use as a sealant.

The second phase of the experimental program was used to determine the effect of varying specific chemical parameters on the mechanical, thermal and chemical properties of the base formulation. This implies varying the stoichiometric ratio, the plasticizer content and the polyol ratio in the formulation, thus enabling a general physical characterization of the network structure based on prior knowledge of the chemical and physical characteristics of the components. From observations made in this portion of the study, a specific formulation was chosen from which subsequent filled formulations were blended.

The third phase of experimental work was used to characterize the nature of the filled network as well as establish the particular mechanical properties pertinent to the development of a sealant. Within this phase, an assessment of

the possible interaction between the lignin filler and the elastomeric matrix is made based on thermal, IR spectroscopy and NMR studies. A study on the swelling behaviour was also useful in outlining the nature of the interaction in such type of lignin binary mixtures.

To further enhance the study of the nature of the activity of lignin, an investigation of the surface properties of both the filler and the elastomeric matrix was made in the fourth phase of the experimental program. Results from this phase were used to substantiate the results obtained from studies on network structure and mechanical properties.

The final experimental work consisted of establishing the performance properties of selected formulations based on standard tensile tests and short term accelerated cyclic loading programs. The cyclic programs are meant to simulate in service conditions by subjecting the sealants to repeated cycles of tensile and compressive strain. The performance of these new sealants was compared to existing two-part PUR based sealants based on their capacity to withstand the prescribed cyclic loading program.

## 4.2 PRELIMINARY INVESTIGATIONS

### 4.2.1 THERMAL ANALYSIS OF SEALANT FORMULATION COMPONENTS

The results of DSC analysis to evaluate the glass transition temperatures of base formulation components given in Tables 3.1 to 3.3 are presented below in Table 4.1. The data are based on at least two determinations, and in some cases five specimens were tested to evaluate the  $T_g$  of the components. Plasticizers have, in general, a low  $T_g$ , however it is of interest to note that the value for the  $T_g$  of Desmophen 1920D (-63.9 °C) is essentially the same as that of the plasticizer (i.e. -63.5 °C) and consequently the effect of plasticizer on the  $T_g$  of the elastomer is expected to be small in the amounts used in this formulation.

Values for  $T_g$  of polyols vary according to chain length and degree of branching. That Desmophen 1920D has the highest molecular weight and lowest OH content necessarily implies that it has, in comparison to the other polyols, a chain structure which is longer and possibly less branched, and this is reflected in its lower  $T_g$ .

Castor oil is the polyol present in Baylith L paste (50% wt.) and the low value of its  $T_g$ , in comparison to that of the isocyanate component, is useful in that it will not tend to increase the overall  $T_g$  of the elastomer into which it is incorporated.

There is very little difference in the  $T_g$ 's of the Desmodur isocyanates however it will be seen that different properties may be obtained when combined with the same polyol.

Table 4.1

RESULTS OF THERMAL ANALYSIS OF FORMULATION COMPONENTS  
USING THE DSC TECHNIQUE

FORMULATION COMPONENT DESCRIPTION	GLASS TRANSITION TEMPERATURE °C
<p>A. ISOCYANATE BASED COMPOUNDS</p> <p>1. DESMODUR E14 2. DESMODUR VL 3. MONDUR XP 743</p>	<p>-49.6 -47.7 -52.7</p>
<p>B. POLYOL BASED COMPOUNDS</p> <p>1. DESMOPHEN 550U 2. DESMOPHEN 1140 3. DESMOPHEN 1150 4. DESMOPHEN 1920D 5. BAYLITH L PASTE</p>	<p>-46.3 -53.4 -47.6 -63.9 -57.8</p>
<p>C. PLASTICIZERS</p> <p>1. MESAMOLL 2. SANTICIZER 160</p>	<p>-63.4 -63.5</p>

#### 4.2.2 PARTICLE SIZE ANALYSIS OF FILLERS

The particle size distribution curves for fillers used in this study are given in figure 4.1. The curves for silica, Tomlinite, and Indulin AT were obtained using the sedimentation technique described in section 3.3.5. The particle size distribution for both the Titanox and Sillitin Z86 fillers were obtained from literature [121,122]. The curve describing the particle size distribution for the Titanox-Sillitin Z86 combination was calculated based on the particle size distribution curves of each component taking into consideration the weight ratio of components in the mixture (Titanox:Sillitin:: 7 g : 22.2 g).

Based on these particle size distribution curves the average equivalent spherical diameter for each filler series is equal to the particle diameter at the mid-point of the distribution (i.e at 50% finer than). See Table 4.2 for these values.

An estimate of the specific surface area can be made based on the particle size distribution curve according to the method developed by Gates [123] as described by Ferrigno [59]. The reciprocal of the equivalent spherical diameter is plotted as a function of the percent finer and the area beneath the curve represents the specific surface area.

Hence the specific surface area is given by:

$$SA = \frac{Q}{\delta_f} \left( \sum \frac{dW}{X_m} \right)$$

Equ. 4.1 [59]

where:

- SA = specific surface area , m<sup>2</sup>/g;
- Q = proportionality constant;
- dW = weight increment, g;
- $\delta_f$  = density of filler, g/cc;
- $X_m$  = average particle size in weight increment,  $\mu\text{m}$

The proportionality constant is applied because the computational values are based on the areas of equivalent spheres and hence a correction must be made to take into account other particle shapes. The assumed value of Q for each of the fillers, taken from the work of Gates [59], is provided in the table below.

Table 4.2			
PARTICLE SIZE OF FILLERS AS DETERMINED BY THE SEDIMENTATION TECHNIQUE			
Filler	Average Equivalent Spherical Diameter $\mu\text{m}$	Specific Surface Area  m <sup>2</sup> /g	Q
Titanox	0.3	10	6
Titanox/Sillitin	0.9	11.7	21
Sillitin	1.35	12	24
Silica	7.4	0.6	6
Indulin AT	8	1.5	9
Tomlinite	16.2	0.7	9

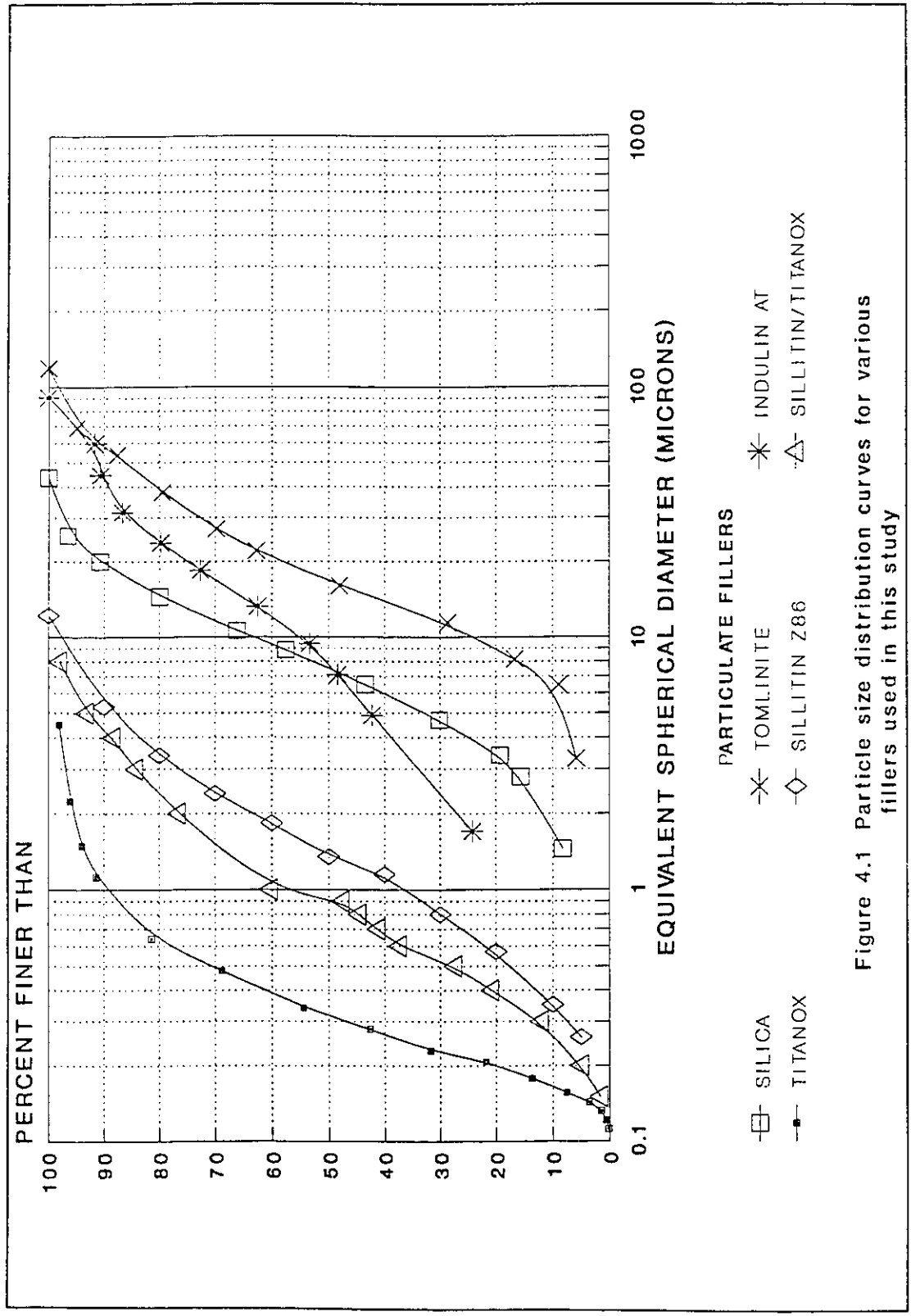


Figure 4.1 Particle size distribution curves for various fillers used in this study

In order to further illustrate the size and distribution characteristics of the various fillers, a series of photomicrographs at different magnifications (75X, 150X, 300X & 750X) were made of the filler particles using a light microscope. Microscope slides were made by placing a drop of solvent containing the dispersed filler onto the slide and allowing the solvent to evaporate thereby leaving a thin layer of particles. This procedure was more successful for the lignin derived fillers than for the kaolin filler.

Four sets of photomicrographs are shown in figure 4.2, each depicting different filler particles magnified either 150 (left photo) or 300 (right photo) times. The uppermost set of photomicrographs show Indulin AT, followed by sets of photos of Eucalin, Tomlinite and Sillitin Z86 particles. It is evident by viewing the photomicrographs of Sillitin particles that, as mentioned earlier, these were not as well dispersed in the solvent in comparison to the other fillers. The appearance of the remaining fillers at 150X magnification generally show an even distribution of particles over the slide.

The use of these photomicrographs permits an assessment of the shape and an estimate of the average size and size distribution of the various filler particles. These observations are summarized in Table 4.3:

---

Figure 4.2 Photomicrographs of filler particles: Set #1 (uppermost series of 2): Indulin AT @ 150X (left ) & 300X (right); Set #2 : Eucalin; Set #3: Tomlinite; Set #4: Sillitin Z86.



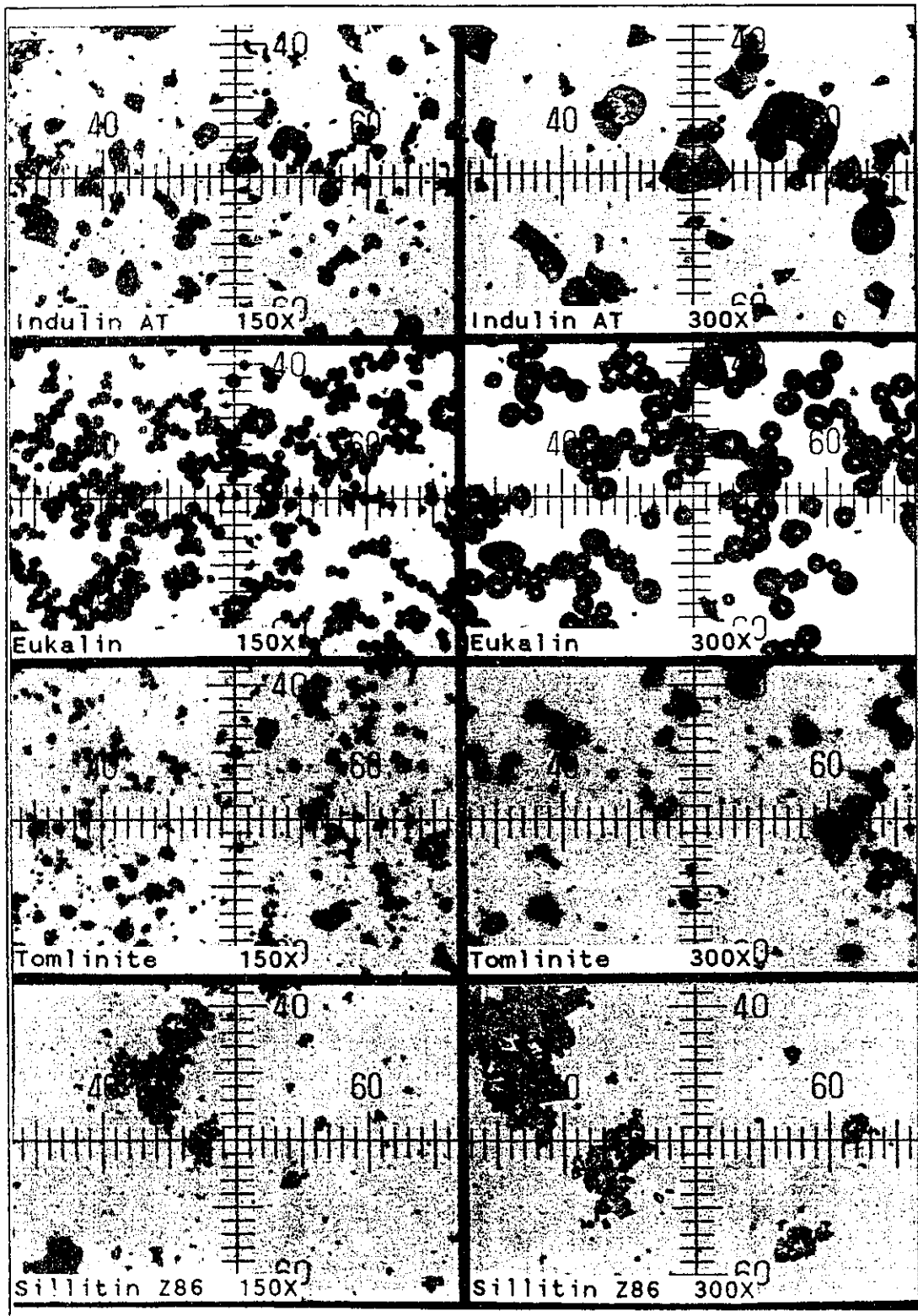


Table 4.3			
RESULTS FROM MICROSCOPIC OBSERVATION OF FILLER PARTICLES			
Filler Type	Particle Shape	Estimated Size Distribution μm	Estimated Average Size μm
Indulin AT	blocky, angular	2 - 40	10
Eucalin	spheroidal	6.5 - 15	10.5
Tomlinite	blocky, rounded	2 - 20	12
Sillitin Z86	flaky, angular	<1 - 5	2

The observations made from the photomicrographs generally confirm the results obtained from the sedimentation analysis. Furthermore, they permit an estimate to be made of the average particle size and size distribution of Eucalin particles, which were not available during the time the sedimentation analysis was being performed.

#### 4.2.3 MECHANICAL PROPERTIES OF PRELIMINARY ELASTOMER FORMULATIONS

Two criteria were used to define a suitable base sealant: hardness and extensibility. The hardness test was used to establish the upper and lower bounds of elastic modulus of the sealant. The lower bound defines the value below which the sealant is not considered to have sufficient strength to withstand in-service extension ratios and the upper bound, the value above which substrate failure in low strength substrates becomes problematical. The lower bound value is a function of curing rate and consequently, given that the daily joint movement may reach as much as one third the total yearly movement, the rate of cure must be such that the sealant achieves a minimum level of hardness within twenty-four hours of being cast.

The hardness requirements set out by the CGSB standard CAN-19.24-M80 specify a minimum Shore A hardness of 15 and a maximum of 50 after full curing is achieved (i.e. 21 days). However, no specifications are given for hardness values after twenty-four hours of cure. Hence, an arbitrary lower bound value after one day of curing has been set at a Shore A hardness of 5.

The minimum extensibility of a sealant is the same as that specified for similar two-component PUR based sealant products, currently available for commercial use. i.e. 25% of the original joint width. The extensibility of standard sealant specimens was assessed by a tension test described in section 3.4.2.1. Within this framework, the sealant blends must possess sufficient adhesive and cohesive strength to maintain the required extension without failure.

Based on these criteria, a series of ten elastomer formulations was developed as summarized in Tables 4.4 to 4.6. The list proceeds in numerical order indicating the trial series (T) and the associated formulations (F) (e.g. trial 1, formulation 1: T1F1). The first six trials were formulated without a catalyst such that the effect of additives on the activation energy (energy required to promote a chemical reaction) could be assessed. Although this series of trials provided inconclusive results with regards to their activation energy, they did enable the elaboration of formulation and testing methods in the development of subsequent elastomer formulations. The remaining three trial formulations (T7-T10) were based on a sealant formulation provided by the Bayer Corporation, the details of which were given in section 3.2.

Manual inspection of T1 to T3 indicated that these sealants were not suitable for further study due to their brittle behaviour. Trial formulation No. 4 used a standard hardness test to evaluate the resilience of different elastomer formulations at various polyol ratios.

Although this series displayed improved elasticity in comparison to the previous formulations, it was rejected since the Shore A hardness in all cases was greater than 50.

Both hardness and tensile tests were used to evaluate specimens obtained in TF-6. Unacceptably high values for hardness were obtained and as well, results of tensile tests revealed that specimens failed at much lower values of strain than the specified 25% minimum.

Table 4.4

## SUMMARY OF TRAIL FORMULATIONS Nº 1 TO Nº 3

T	F	NCO BASED COMPOUNDS		OH BASED COMPOUNDS						Filler	PLAS	BPR	NCO/OH
		ISOCYANATE PREPOLYMER		POLYOL PREPOLYMER				MS					
		XP g	VL g	550U g	1140 g	1150 g	1920D g		BP g				
1	1	14.3	-	-	-	-	30.3	6.1	24.7	24.6	0.592	1.0	
1	2	-	18.1	-	15.9	15.9	-	8.0	42.1	-	0.097	1.0	
1	3	-	8.8	-	-	11.0	24.0	9.0	34.0	13.2	0.298	1.0	
1	4	-	15.7	5.5	-	22.0	-	6.8	50.0	-	0.098	1.0	
2	1	-	8.7	-	-	11.0	24.0	8.8	34.3	13.3	0.292	1.0	
2	2	-	9.1	-	-	12.4	22.3	8.7	34.3	13.3	0.288	1.0	
2	3	-	10.4	-	-	20.0	14.3	8.6	34.3	13.3	0.192	1.0	
2	4	-	10.4	-	-	16.8	16.8	8.5	34.3	13.3	0.216	1.0	
2	5	-	11.5	-	-	20.5	12.3	8.2	34.3	13.3	0.181	1.0	
3	1	14.6	-	1.5	-	-	30.2	2.9	25.5	25.2	0.282	1.0	
3	2	17.4	-	2.7	-	-	26.7	2.7	25.5	25.2	0.297	1.0	
3	3	21.3	-	4.3	-	-	21.5	2.3	25.5	25.2	0.315	1.0	
3	4	25.8	-	6.2	-	-	15.2	2.0	25.5	25.2	0.387	1.0	
3	5	29.9	-	7.9	-	-	9.9	1.6	25.5	25.2	0.475	1.0	

MS: MOLECULAR SIEVE; BP: BAYLITH PASTE; PLAS: PLASTICIZER;  
 BPR: BAYLITH PASTE RATIO; NCO/OH: STOICHIOMETRIC RATIO.

Table 4.5

SUMMARY OF TRAIL FORMULATIONS Nº 4 & Nº 6

T	F	NCO BASED COMPOUNDS				OH BASED COMPOUNDS				PLAS g	Filler g	BPR	NCO/OH	TEST RESULTS		
		VL g	1150 g	1920D g	BP g	1150 g	1920D g	BP g	SHORE A					$\sigma_b$ kPa	$\epsilon_b$ %	
4	1	9.2	10.1	21.9	11.3	13.3	34.3	0.407	1.0	68	-	-				
4	2	9.7	11.1	19.9	11.8	13.3	34.3	0.407	1.0	69	-	-				
4	3	10.3	12.4	17.3	12.5	13.3	34.3	0.407	1.0	75	-	-				
4	4	11.1	14.0	14.0	13.4	13.3	34.3	0.407	1.0	76	-	-				
6	1	9.2	10.1	21.9	11.3	13.3	34.3	0.407	1.0	65	179	2.2				
6	2	10.1	7.9	26.2	8.2	13.3	34.3	0.407	1.0	64	155	3.2				
6	3	7.5	6.6	28.9	9.4	13.3	34.3	0.407	1.0	63	181	2.5				
6	4	6.3	3.9	34.3	8.0	13.3	34.3	0.407	1.0	-	-	-				
6	5	5.5	2.3	37.6	7.1	13.3	34.3	0.407	1.0	-	-	-				
6	6	4.4	-	42.2	5.9	13.3	34.3	0.407	1.0	39	142	2.9				

BP: BAYLITH PASTE; PLAS: PLASTICIZER; BPR: BAYLITH PASTE RATIO; NCO/OH STOICHIOMETRIC RATIO;  $\sigma_b$ : STRESS @ BREAK;  $\epsilon_b$ : STRAIN @ BREAK.

Table 4.6

SUMMARY OF TRAIL FORMULATIONS N° 7,9 & N° 10  
& PRELIMINARY TEST RESULTS

T	F	E14 g	1920D g	BP g	PLAS g	CAT + SOLV g	Filler g	BPR	NCO/OH	TEST RESULTS		
										SHORE A	$\sigma_b$ kPa	$\epsilon_b$ %
7		19.7	20.2	4.0	22.6	8.4	29.5	0.588	1.05	34	53	2.9
9		17.5	19.5	6.6	22.4	8.4	30.0	1.0	0.75	30	59	2.9
10	1	16.6	34.1	11.6	32.0	6.7	-	1.0	0.41	-	75	14.0
10	2	27.9	28.6	5.7	32.1	6.7	-	0.588	1.02	-	173	37.4
10	3	27.5	28.9	5.8	32.1	6.7	-	0.588	1.0	-	153	25.8
10	4	27.2	29.2	5.8	32.1	6.7	-	0.588	0.98	-	130	17.2
10	5	28.3	28.3	5.7	32.1	6.7	-	0.588	1.05	-	140	25.7
10	6	28.1	28.5	5.7	32.1	6.7	-	0.588	1.04	-	179	34.0
10	7	28.6	28.0	5.6	32.1	6.7	-	0.588	1.07	-	225	46.0

E14: TDI ISOCYANATE PREPOLYMER; 1920D: POLYETHER POLYOL PREPOLYMER DISPERSOID;  
BP : BAYLITH PASTE (MOLECULAR SIEVE IN 50% WT. CASTOR OIL); PLAS: PLASTICIZER;  
CAT: CATALYST; SOLV: SOLVENT; NCO/OH: STOICHIOMETRIC RATIO;  
BPR: BAYLITH PASTE RATIO; SHORE A: SHORE "A" HARDNESS;  $\sigma_b$ : STRESS AT BREAK;  
 $\epsilon_b$ : STRAIN AT BREAK

For specimens blended using the Bayer formulation, results from tests on the initial blends, T7 and T9, did not show improved strain at failure, however their hardness was within acceptable limits. This indicated that the formulation lacked sufficient adhesive strength to withstand even the lowest extensions and that the substrate required a primer such that the adhesive tenacity of the sealant could be augmented.

In order to accelerate the development of the base sealant, the sealant was formulated without a filler. Results of hardness tests on series T7 and T9, taken over an extended period of time (figure 4.3), show that these type of blends could be formulated with a sufficiently low modulus to meet the specified values.

An investigation of the tensile characteristics of the unfilled sealant provided a means to determine the maximum adhesive and cohesive strength of the blend within a range of extension ratios.

Results based on the primed substrate (T10F2 - T10F7) show that the adhesive strength at failure after twenty-four hours of cure, is proportional to the stoichiometric ratio, as shown in figure 4.4. Each point on the plot is an average of six tensile tests. The tests also revealed that in some cases the sealant may fail in cohesion as opposed to adhesion. In these instances, the sealant may fail at 320 kPa and 80% extension, in comparison for example to T10F7 which failed at 219 kPa and 44% extension. This indicates that further improvements in the adhesive strength may be obtained using a more suitable primer.



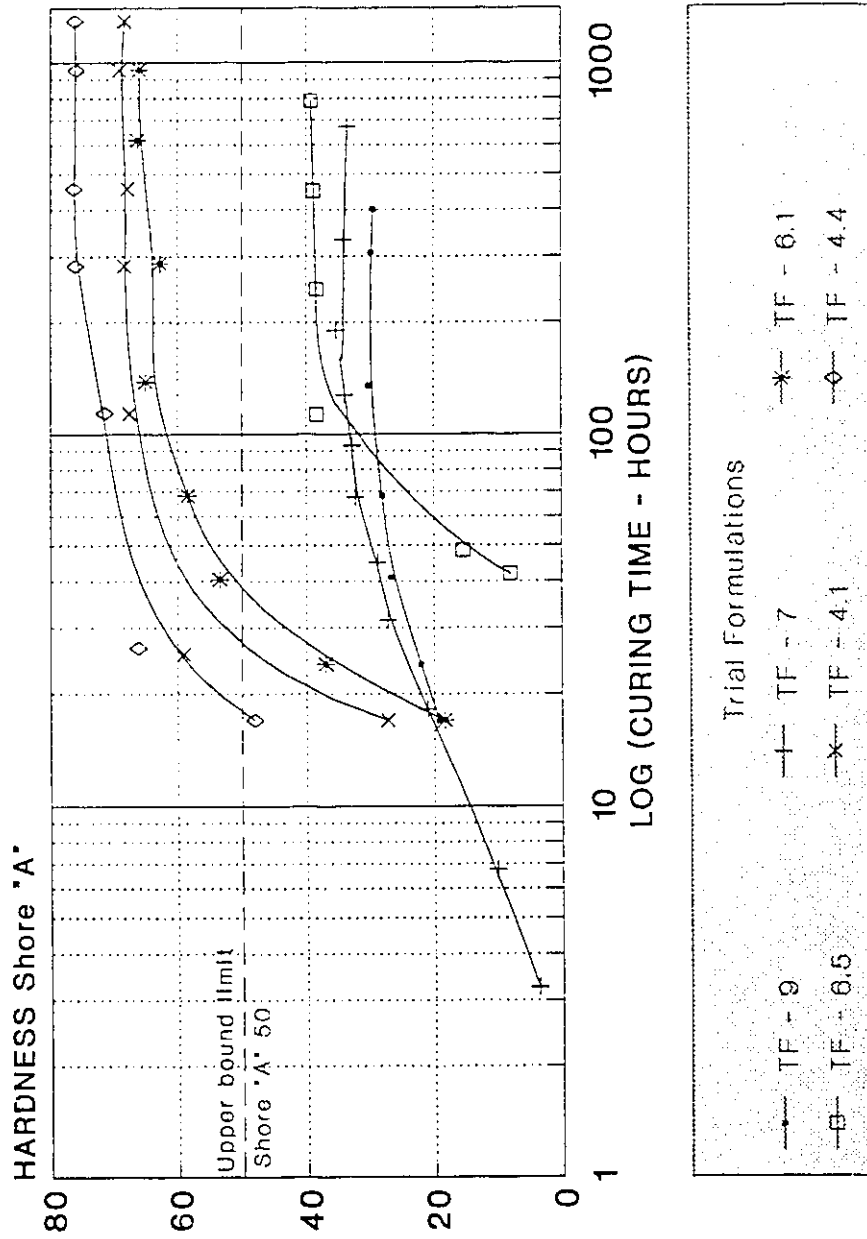


Figure 4.3 Shore "A": indentation hardness of preliminary PUR based sealant formulations in relation to curing time.

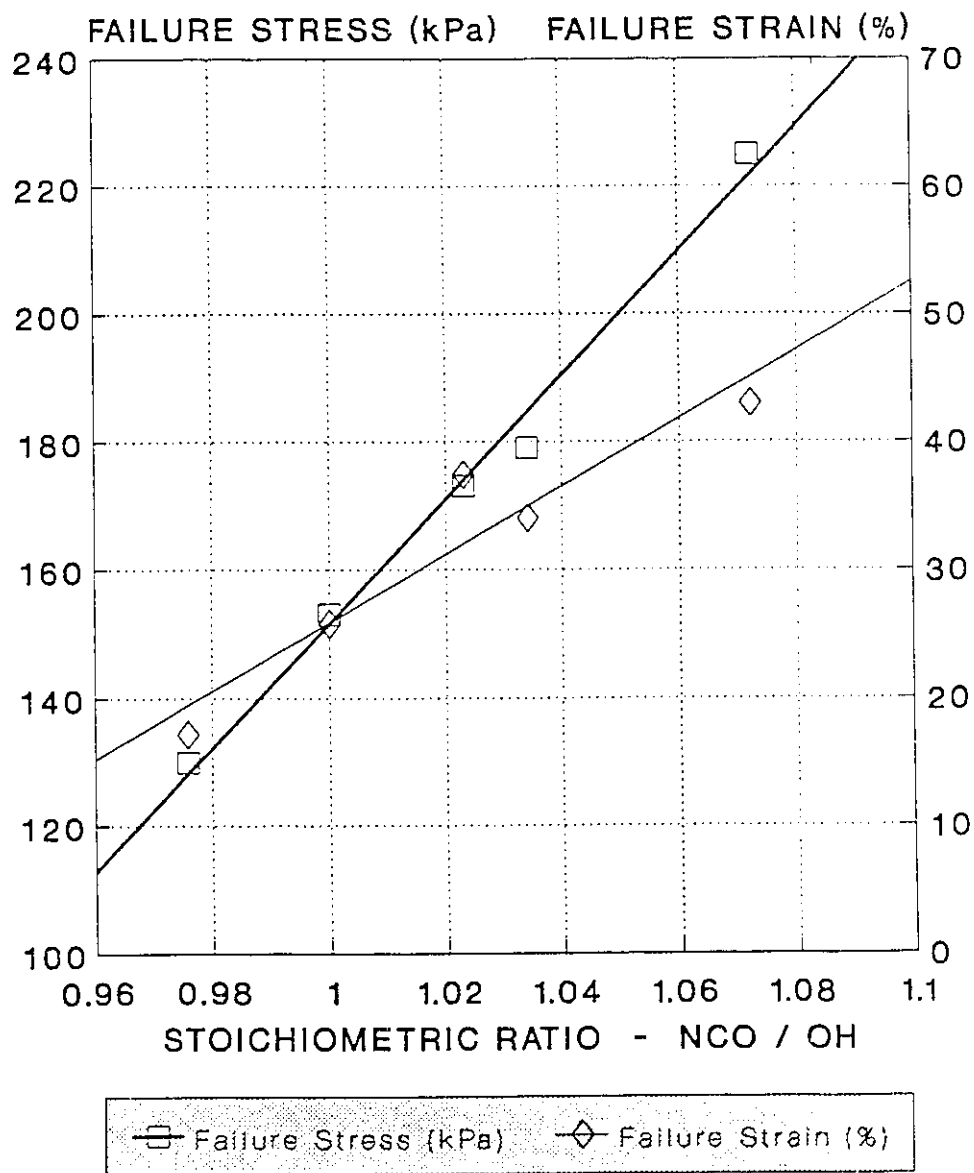


Figure 4.4 Adhesive strength of unfilled elastomer formulations in relation to stoichiometric ratio.

### 4.3 CHARACTERIZATION OF UNFILLED ELASTOMERS

#### 4.3.1 MOLECULAR WEIGHT OF PUR BY THE SWELLING METHOD

The number average molecular weight between network crosslinks ( $M_{c,s}$ ) for the various PUR elastomers formulated in this study, as determined using the swelling method described in section 3.4.1.1, are given in Table 4.7. The slope,  $S$ , of the load-deformation curve of compressed swollen samples is used to calculate the number of effective network chains per unit volume,  $\nu_e/V$ , according to equation 3.7. The factor labelled  $f$ , is used to take into account the presence of additives (e.g. plasticizer and curing agents) which make no contribution to the molecular weight. This factor is given by the following relation [89]:

$$f = \left( \frac{V_r}{V_r + V_a} \left( 1 - \frac{V_a}{V_r + V_a + V_s} \right) \right)^{-\frac{1}{3}}$$

Equ. 4.2 [89]

where  $V_r$ ,  $V_a$  and  $V_s$  are the volume of elastomer, additives and solvent in the sample respectively. Hence by combining equation 3.7 and 4.2,  $M_{c,s}$ , as determined by swelling, is given by:

$$\frac{\delta}{M_{c,s}} = \frac{\nu_e}{V} \cdot f$$

Equ. 4.3

Table 4.7  
CALCULATION OF  $M_{c,s}$  OF UNFILLED ELASTOMERS

Series	S kg/mm	$\nu_e/V$ $\times 10^{-4}$ mol/cc	f	$\delta$ g/cc	$M_{c,s}$ g/mol
15A	7.78	1.701	1.247	1.0987	5180
18A	8.06	1.762	1.246	1.0973	5010
20A	8.32	1.819	1.245	1.0997	4860
35A	7.53	1.647	1.248	1.1062	5380
38A	7.79	1.703	1.247	1.1043	5200
40A	7.91	1.730	1.246	1.1053	5130
25A	6.60	1.443	1.250	1.1065	6130
28A	6.94	1.518	1.249	1.1089	5850
30A	7.11	1.555	1.248	1.1046	5690
15B	5.67	1.240	1.280	1.1014	6940
18B	6.09	1.332	1.279	1.0997	6450
20B	6.36	1.391	1.278	1.1029	6200
38B	6.56	1.434	1.280	1.1057	6020
40B	6.91	1.511	1.279	1.1057	5720
25B	5.49	1.198	1.283	1.1092	7220
28B	5.49	1.200	1.282	1.1065	7190
30B	5.58	1.220	1.281	1.1091	7100
15C	5.01	1.095	1.322	1.1025	7620
18C	5.34	1.168	1.320	1.1034	7160
20C	5.50	1.203	1.319	1.0982	6920
35C	5.11	1.117	1.324	1.1161	7550
38C	5.21	1.139	1.323	1.1070	7350
40C	5.37	1.174	1.322	1.1044	7120
25C	4.73	1.034	1.324	1.1057	8080
28C	4.80	1.050	1.324	1.1035	7940
30C	4.88	1.067	1.323	1.1025	7810

The dependency of  $M_{c,s}$  of the formulations on the various chemical parameters is illustrated in figure 4.5. There are three blocks of data arranged in sets of nine data points, each set corresponding to the molecular weights derived for blends having a particular Baylith paste ratio (BPR). Hence the left, centre and right blocks have BPR's of 0.588, 0.740 and 1.0 respectively. Within each block the data is arranged in order of increasing stoichiometric ratio (SR) and plasticizer content (PC). The SR increases from left to right, starting with a value of 1.023 and proceeding to a final value of 1.1 whereas the PC for the various blends increases from front to back of the plot.

The general trends which can be observed from this figure are the following:

- i)  $M_{c,s}$  increases with the addition of both plasticizer and Baylith paste (castor oil);
- ii) There is a decrease in the  $M_{c,s}$  with corresponding increase in SR.

The addition of plasticizer is known to reduce the  $T_g$  of blends as a result of separating chains, decreased interaction between chains and increased chain mobility [64]. This same effect provides an explanation for the increase in molecular weight with the addition of castor oil.

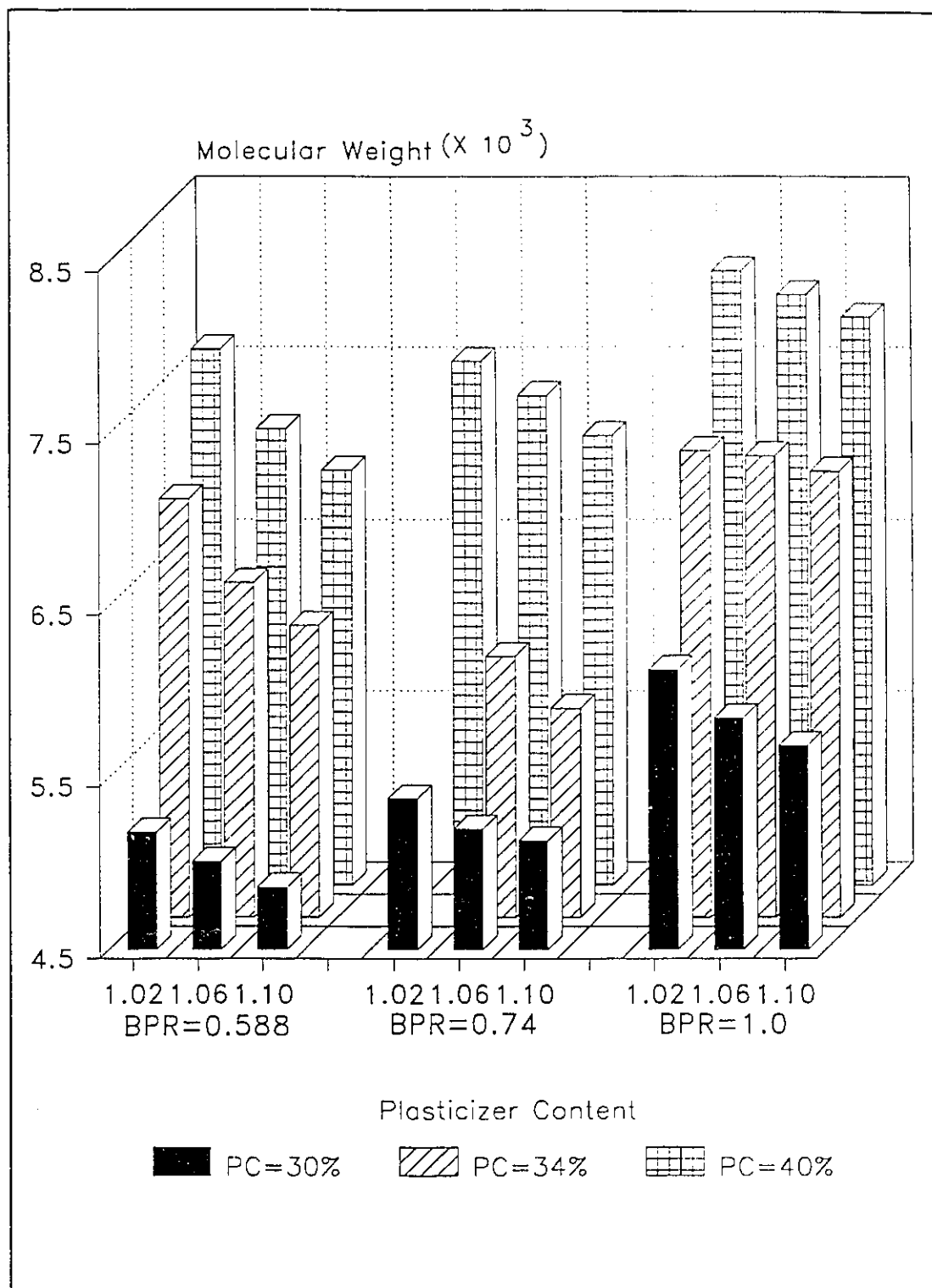


Figure 4.5 Number average molecular weight of PUR elastomer formulations as a function of SR, BPR, & PC.

If it is supposed that the castor oil takes part in the reaction to form a crosslinked network, then there should be a reduction in the molecular weight between crosslinks with the addition of castor oil by virtue of its lower molecular weight in comparison to that of the long chain polyol prepolymer. Since this is evidently not the case, it is supposed then that there is little or no reaction between castor oil and the isocyanate prepolymer, and that further, the castor oil acts as a diluent in the same manner as the plasticizer.

The decrease in  $M_{c,s}$  with a corresponding increase in SR is due to the formation of supplemental crosslinks with urea groups present in the elastomer. As has been noted elsewhere, [65] the higher the SR, the greater the amount of free isocyanate groups left for curing with other active groups for the formation of additional crosslinks which occurs, for instance, in the formation of biuret groups.

Molecular weights for the various elastomers can also be determined from a theoretical basis provided the molecular weights of the base components are known. The following equations relate the molecular weights of the base components to that of an idealized network based on the combination of two moles of polyol prepolymer to three moles of isocyanate prepolymer. Hence the ideal structure has three chains for every two crosslink points.

$$M_t = \frac{[M_\infty] + \frac{1}{BPR} [M_{1920D}]}{1 + \frac{1}{BPR}} + \frac{3}{2} [M_{E14}]$$

Equ. 4.4

Where:

$[M_t]$  = Theoretical molecular weight between crosslinks.

$[M_\infty]$  =  $M_n$  of castor oil ( 1020 g/mol);

$[M_{1920D}]$  =  $M_n$  of polyol prepolymer ( 4800 g/mol);

$[M_{E14}]$  =  $M_n$  of isocyanate prepolymer ( 2400 g/mol).

$[M_n]$  = Number average molecular weight of component.

If castor oil does not participate in the reaction, then the equation reduces to:

$$M_t = [M_{1920D}] + \frac{3}{2} [M_{E14}]$$

Equ 4.5

An adjustment to the molecular weight can be made for the increase in stoichiometric ratio by considering that one mole of excess isocyanate may react with urethane groups within the structure to form two additional crosslinks. In such a case the theoretical molecular weight is given by:

$$M_t ( SR ) = \frac{M_t ( SR=1 ) + M_t ( r ) \cdot ( SR-1 )}{SR}$$

Equ. 4.6

Where:  $M_t(SR)$  = Molecular weight at given SR.

$M_t(SR=1)$  = Molecular weight at SR = 1.

$M_t(r)$  = Molecular weight of polyol.

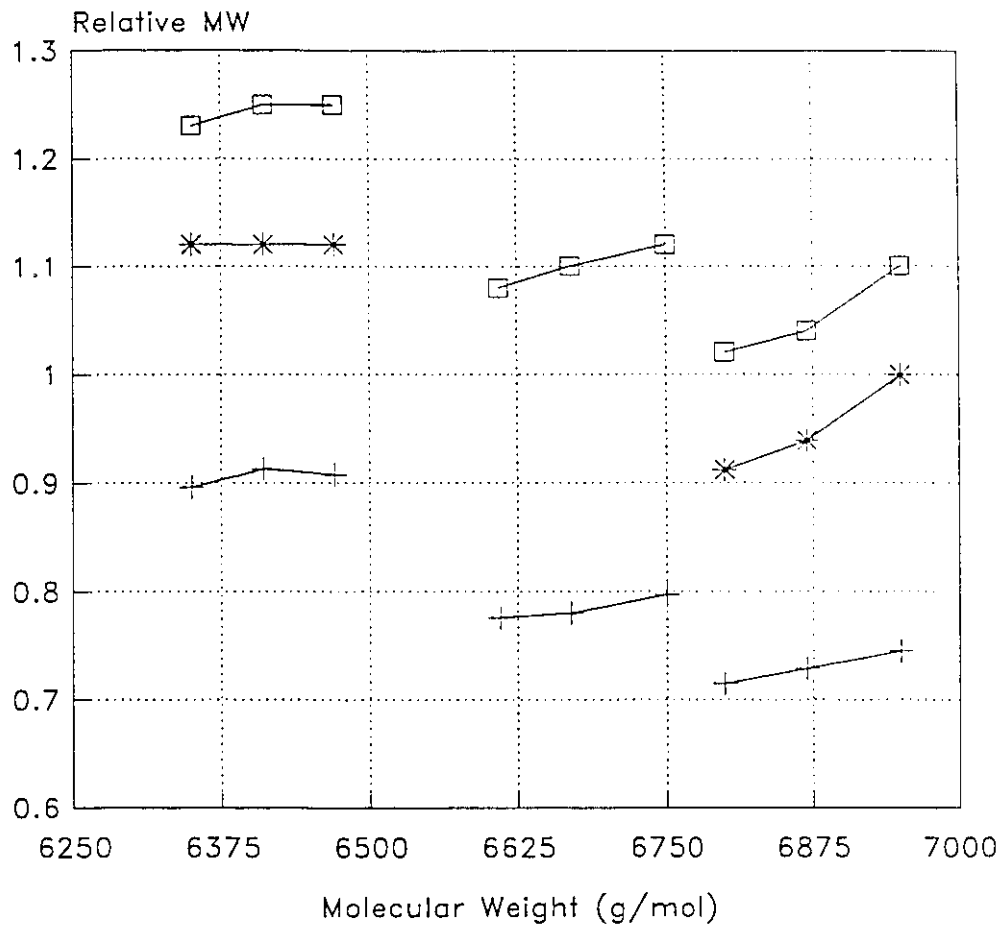
SR = Stoichiometric ratio.



Based on the above equations, the theoretical molecular weights for elastomers having different SR's and BPR's are given in Table 4.8.

Table 4.8				
THEORETICAL MOLECULAR WEIGHTS FOR PUR ELASTOMERS				
SR	BAYLITH PASTE RATIO			
	0	0.588	0.740	1.1
1.0	8400	7000	6790	6470
1.023	8320	6950	6750	6470
1.062	8190	6870	6670	6410
1.10	8070	6800	6610	6350

Figure 4.4 shows a plot of the ratio of theoretical to experimental molecular weights determined in this study. It is evident that for any given elastomer series, the ratio of experimental to theoretical molecular weight is increased with the addition of either plasticizer or castor oil to the blend. Furthermore it can be seen that the decrease in molecular weight with a corresponding increase in SR, as predicted in theory, occurs for all formulations but interestingly this effect is greater in blends having lower castor oil contents.



Series Ay: PC=30%; By: PC=34%; Cy:PC=40%  
 Series x1: BPR=1; x74: BPR=0.74;  
 x588: BPR=0.588.

Figure 4.6 Comparative analysis of theoretical to experimental number average molecular weights between crosslinks for unfilled PUR elastomers

## 4.3.2 MECHANICAL PROPERTIES OF UNFILLED ELASTOMERS

### 4.3.2.1 Curing Mode as Determined Using Hardness Tests

Hardness tests were useful because they permitted evaluation of the curing mode of the various elastomers by assessing their indentation hardness as a function of time. The degree of cure is important in the early stages of network formation because of the need for a sealant to possess a minimum hardness after 24 hours of cure, the hardness being indicative of a particular modulus. The modulus corresponds to a particular resistance to movement, or resilience of an elastomer and hence provides an assessment of the potential strength of the elastomer although this is evidently limited by the adhesive strength on the bond.

The hardness test was also useful in this instance because it permitted the evaluation of the relative modulus of the elastomers such that those elastomers considered most suitable for further testing could be selected for subsequent tensile tests to destruction. In this way the overall number of tensile tests conducted was kept to a minimum.

An assessment of the curing mode of three elastomer series having different plasticizer contents is shown in figure 4.7. The figures specifically represent the Shore "A" indentation hardness as a function of the common logarithm of the time, in hours, for elastomer formulations having varying SR at constant BPR. The two curves in each figure depict the extreme limits of the SR used in this study.

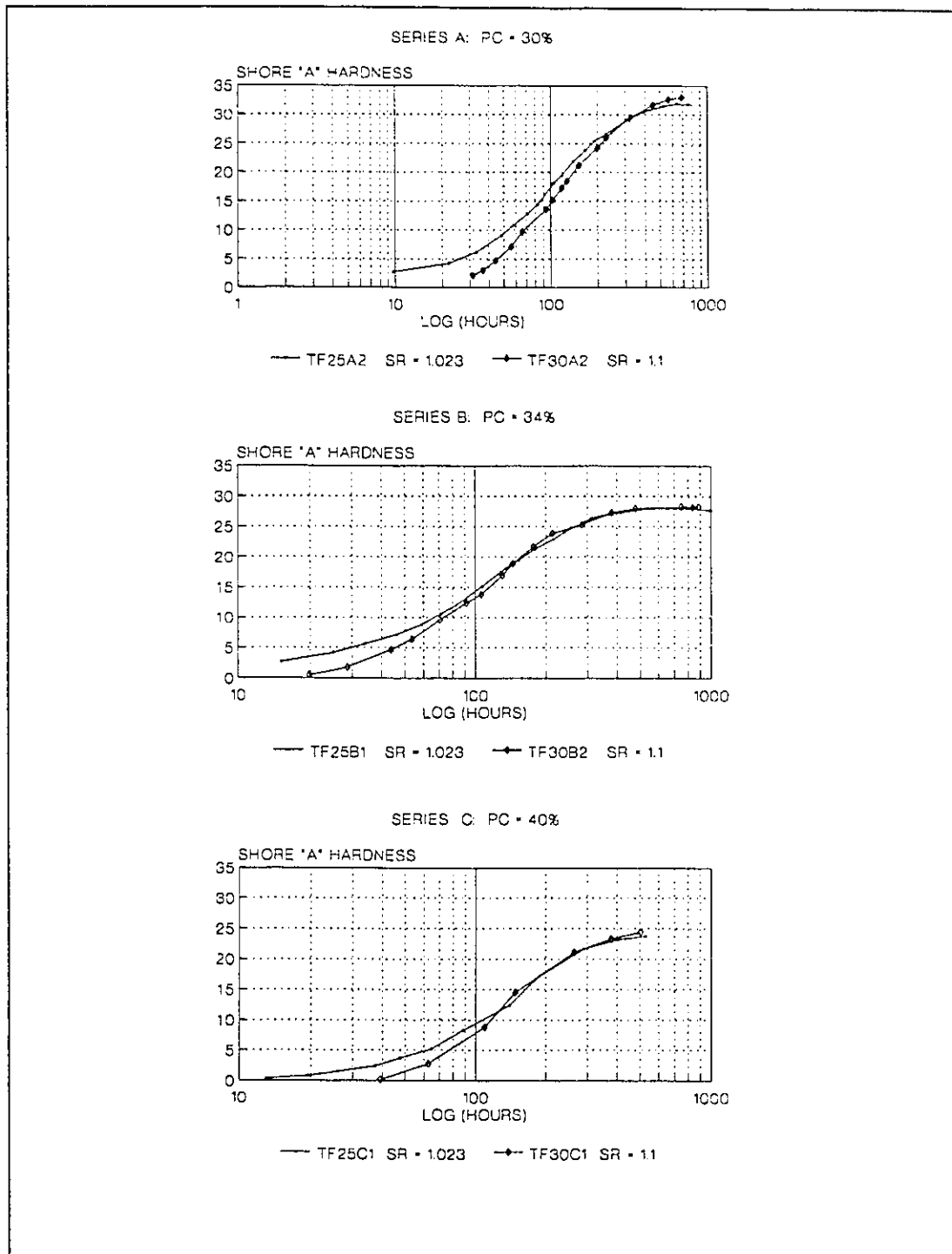


Figure 4.7 Indentation hardness (Shore "A") as a function of time for unfilled elastomers at constant BPR (BPR=1) having different plasticizer contents and stoichiometric ratios. Series A: PC = 30%; B: PC = 34%; C: PC = 40%.

The uppermost figure represents the curing mode for the initial elastomer series (series A) having a PC of 30%. When compared to the other series the curing mode is seen to proceed more rapidly in comparison to those elastomer formulations having a greater quantity of plasticizer. This may more clearly be understood if one compares the gel time of the various elastomer series, where the gel time is characterized as the amount of curing time required for the elastomer to attain a Shore "A" hardness of 5. In the case of those elastomers having a SR of 1.023, series A reaches gel time in 25 hours in comparison to series B and C which reach the gel time in 30 and 60 hours respectively. Hence the addition of plasticizer retards the gel time of the elastomer. Furthermore, it also limits the maximum hardness which can be attained for any given elastomer since the maximum hardness attained for the series having 40% plasticizer (Shore "A" 24) content is less than that of the series having 30% plasticizer content (Shore "A" 32) for elastomers having comparable cure times and stoichiometric ratios. The time required to reach the maximum is not seemingly affected.

The SR is shown to retard the gel time in the initial stages of the cure (i.e. < 100 hrs) and thereafter its effect is diminished until such time as to have no effect. This point occurs at 200-300 hours of cure.

Maximum hardness was attained at 600 hours (25 days) and these results, which are presented in figure 4.8, show the maximum hardness as a function of Baylith paste ratio and plasticizer content.

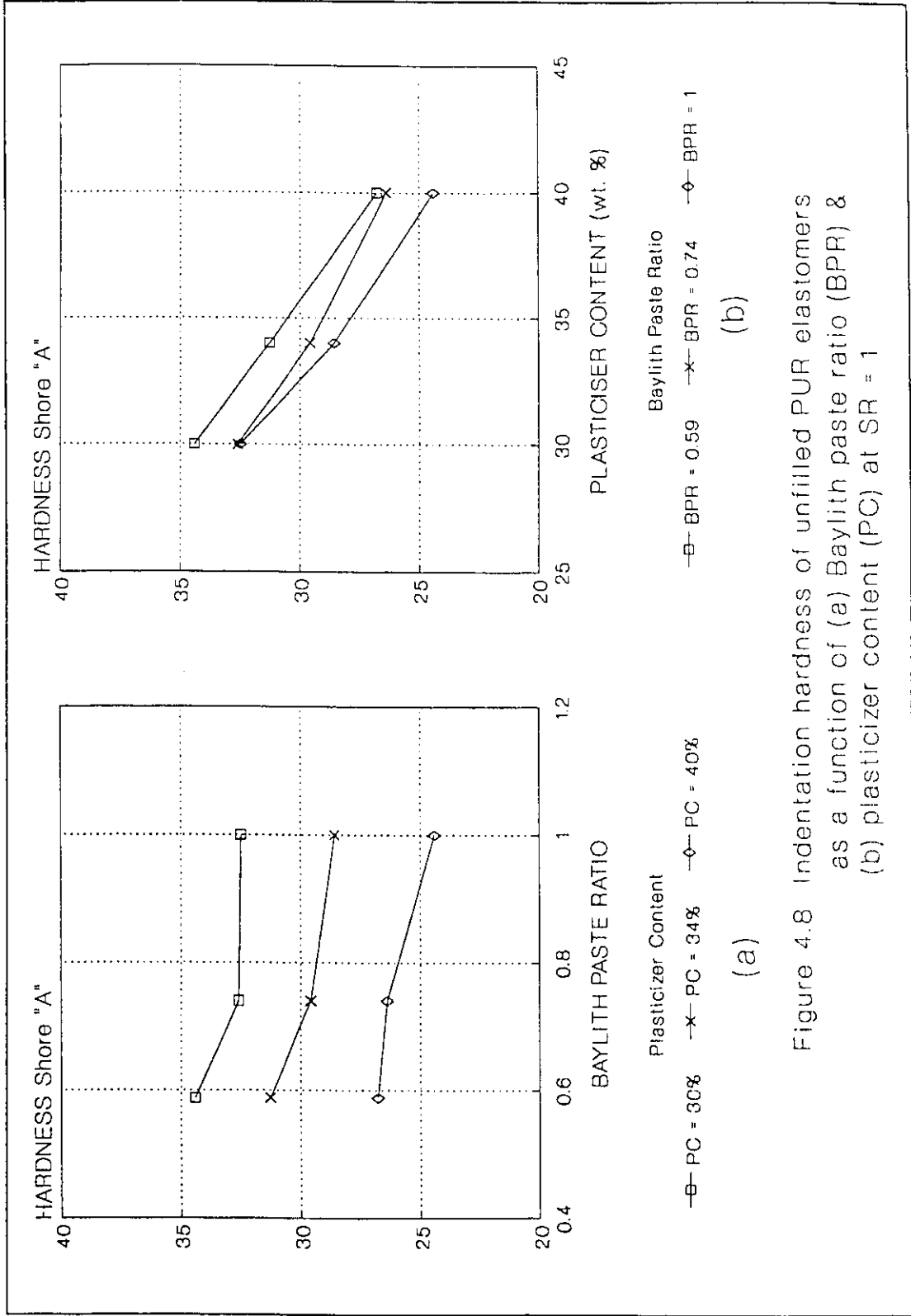


Figure 4.8 Indentation hardness of unfilled PUR elastomers as a function of (a) Baylith paste ratio (BPR) & (b) plasticizer content (PC) at SR = 1

It is clearly demonstrated that the hardness is reduced with a corresponding increase in plasticizer content. A similar but not as significant effect is noted for the addition of Baylith paste to the formulation. Hence, both the plasticizer and the Baylith paste act as diluents which cause a reduction in the modulus. This is in accordance with what was discussed in the section concerning the structure-property relationships as determined by swelling.

#### 4.3.2.2 Tensile Characteristics

##### a) Introduction

Values reported for tensile and compression tests have been computed with the aid of a computer program developed by the Centre for Building Studies specifically for analyzing tensile and compression data obtained from testing elastomer specimens using the Instron Universal testing machine. The program is provided with extension or compression data, in an appropriate digital format, for each specimen being analyzed and calculates the average strain energy density, and stress and strain to rupture. It also generates elastic constants based on the theory of rubber elasticity. The equations are fit to the data using a general linear least squares program provided by Press et al. [124]. The accompanying figures showing tensile or compression stress-strain curves have experimental data plotted in the form of data points and the theoretical curve is a continuous line running through the points.

The strain energy density, for any given specimen, is calculated by integrating the area beneath the load-deformation curve [125], shown in figure 4.9.

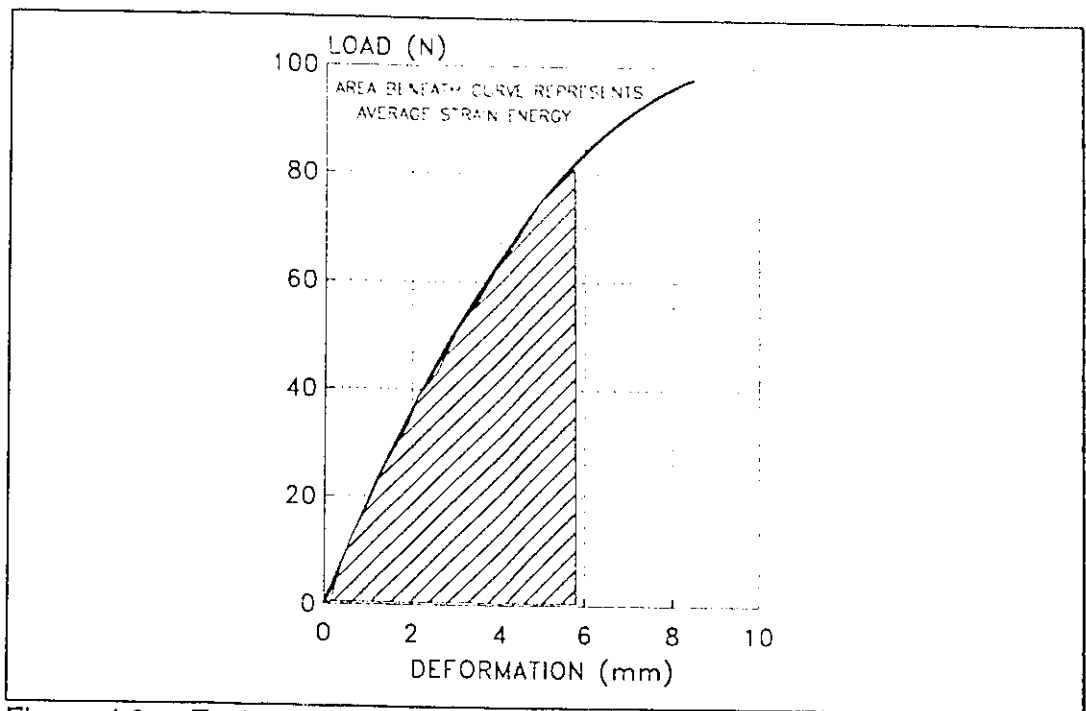


Figure 4.9 Evaluation of the strain energy density based on the load-deformation properties of the test specimen.

Hence the strain energy density ( $U_i$ ) is given by:

$$U_i = \int_0^{\epsilon_b} \sigma_i \delta \epsilon_i = \int_0^{\epsilon_b} \frac{p_i}{a_o} \cdot \frac{\delta l_i}{l_o} = \frac{1}{a_o l_o} \int_0^{\epsilon_b} p_i \delta l_i$$

Eqn. 4.7 [125]

where:

- $\sigma_i$  = stress during loading cycle (MPa);
- $\epsilon_i$  = strain
- $p_i$  = load during loading cycle (N);
- $\delta l_i$  = deformation (mm)
- $a_o$  = cross-sectional area (mm<sup>2</sup>);
- $l_o$  = gauge length (mm).



and

i refers to the  $i^{\text{th}}$  specimen;

o refers to the beginning of the cycle;

b refers to the break (rupture) point.

If n specimens are tested, then the average strain energy density for similar specimens is simply :

$$U_n = \sum_i^n \frac{U_i}{n}$$

Equ. 4.8

The average stress and strain to rupture may be evaluated from a knowledge of the average strain energy density and the average curve,  $\sigma_{av}(\epsilon)$ , the latter developed using an appropriate fitting program. The average stress and strain at rupture lie somewhere on the average curve, hence these points may be established by integrating the curve until the integral is equal to the average strain energy density. i.e.:

$$U_n = \int_0^{\epsilon_b} \sigma_{av}(\epsilon) \cdot \delta\epsilon$$

Equ. 4.9

The stress at rupture,  $\sigma_b$ , is calculated by evaluating the function  $\sigma_{av}(\epsilon)$  at  $\epsilon_b$ .

The program also calculates elastic constants based on the theory of rubber elasticity [71,126] which relates the stress to the strain in the following manner:

$$\sigma = G \left( \alpha - \frac{1}{\alpha^2} \right)$$

Equ 4.10 [71]

where:

- $\sigma$  = nominal stress (based on original cross section);
- $G$  = shear modulus =  $E/3$  for an incompressible material (i.e. having  $\mu = 0.5$ );
- $\alpha$  = extension ratio =  $1 + \epsilon$ ;
- $\epsilon$  =  $\delta l / l$  engineering strain.

b) Results from tensile tests on TA type specimens

Results from tensile tests on type TA specimens are reported in Tables 4.9 to 4.11 and supporting figures 4.10 to 4.12. The results are given in terms of the strain energy density, stress and strain at rupture and the elastic modulus. The data have been arranged such that an assessment can be made of the effect of the different chemical parameters (i.e. plasticizer content (PC), Baylith paste ratio (BPR), stoichiometric ratio (SR)) on the mechanical properties of the various elastomers. Hence Table 4.9 shows the variation in mechanical properties as a function of PC; Table 4.10, as a function BPR; Table 4.11 as a function of the SR. The modulus,  $E$ , is evaluated from the theoretically fitted curve, and the reduced modulus,  $E_p$ , is given by:

$$E_p = E \cdot v_2^{2/3}$$

Equ. 4.11

Table 4.9						
TENSILE PROPERTIES OF UNFILLED PUR ELASTOMER TYPE TA SPECIMENS AS A FUNCTION OF PLASTICIZER CONTENT						
Series	$U_n$ J/cc	$\sigma_b$ MPa	$\epsilon_b$	$\nu_2$	E MPa	$E_p$ MPa
28A	1.029	0.738	2.46	0.5853	0.648	0.542
28B	0.874	0.643	2.43	0.5493	0.563	0.461
28C	0.976	0.616	2.72	0.5076	0.498	0.397

Table 4.10						
TENSILE PROPERTIES OF UNFILLED PUR ELASTOMER TYPE TA SPECIMENS A FUNCTION OF BAYLITH PASTE RATIO						
Series	$U_n$ J/cc	$\sigma_b$ MPa	$\epsilon_b$	$\nu_2$	E MPa	$E_p$ MPa
18C	0.847	0.621	2.43	0.5125	0.546	0.437
38C	1.008	0.679	2.67	0.5105	0.553	0.442
28C	0.976	0.616	2.72	0.5076	0.498	0.397

Table 4.11						
TENSILE PROPERTIES OF UNFILLED PUR ELASTOMER TYPE TA SPECIMENS AS A FUNCTION OF STOICHIOMETRIC RATIO						
Series	$U_n$ J/cc	$\sigma_b$ MPa	$\epsilon_b$	$\nu_2$	E MPa	$E_p$ MPa
25C	0.974			0.5062	0.499	0.398
28C	0.976	0.616	2.72	0.5076	0.498	0.397
30C	0.783	0.522	2.66	0.5089	0.431	0.344

The strain energy density is dependent on both the stress and strain at rupture. There is very little difference in the values of  $U_n$  simply due to the reduced stress at rupture brought about by the addition of plasticizer. This is offset by the increase in strain at break in the case of TF28C. Hence the trend is evidently one of reducing the modulus and stress at rupture with a corresponding increase in PC. This phenomenon is clearly illustrated in figure 4.10.

It is worth noting however that the greatest strains at rupture are achieved in those elastomers having the highest degree of plasticization and this is a particularly useful trait in the preparation of filled elastomers since these elastomers will necessarily have lower rupture strains than the unfilled ones.

An analysis of Table 4.10 (figure 4.11) reveals that there are no specific correlations which can be made between any of the mechanical properties of the elastomers and their related BPR's. Essentially the results indicate that the addition of castor oil to the elastomer formulation increases the strain at break. This effect can be attributed to the same phenomenon as that which occurs in the case of plasticizer.

Results for elastomers evaluated on the basis of varying SR are given in Table 4.11 and figure 4.12. The data suggests that an increase in SR decrease both the stress and strain at break however, this trend is not reflected in the figures.

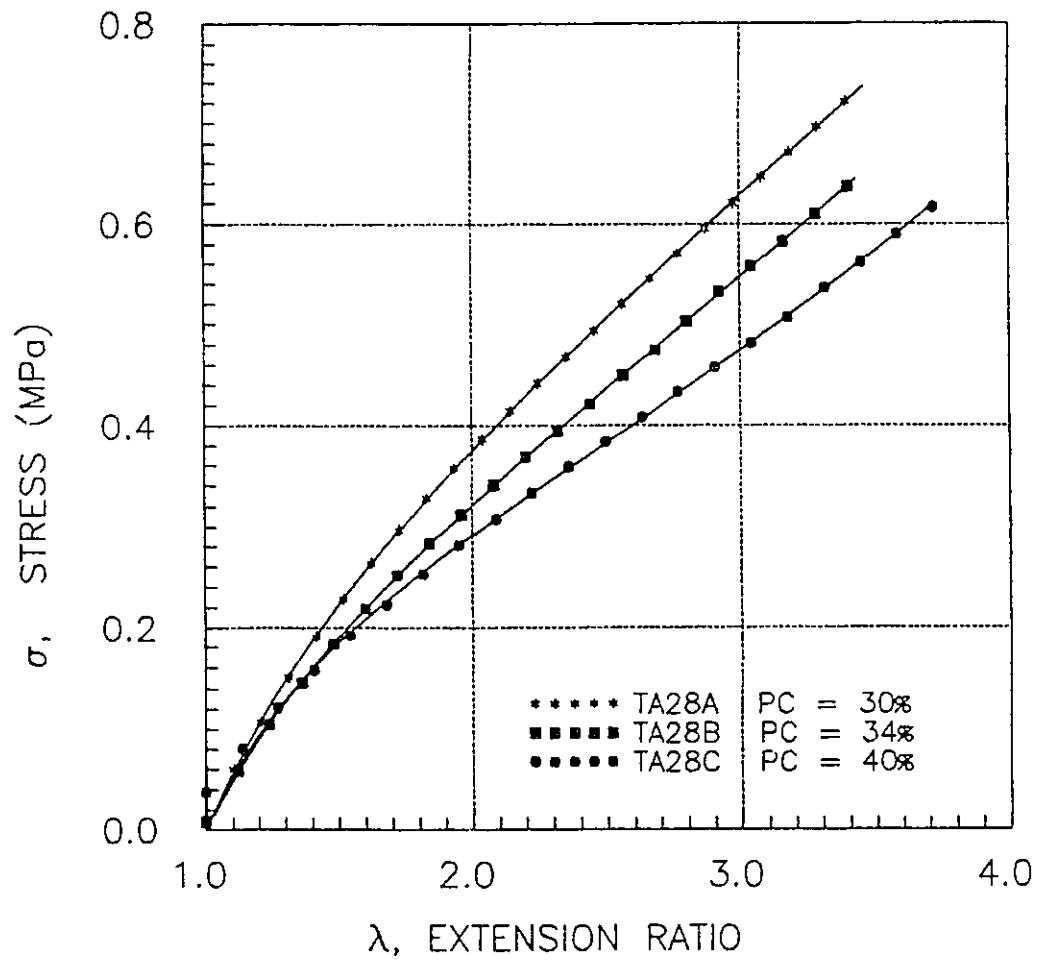


Figure 4.10 Tensile test on unfilled PUR elastomer type TA specimens for formulations having different plasticizer contents.

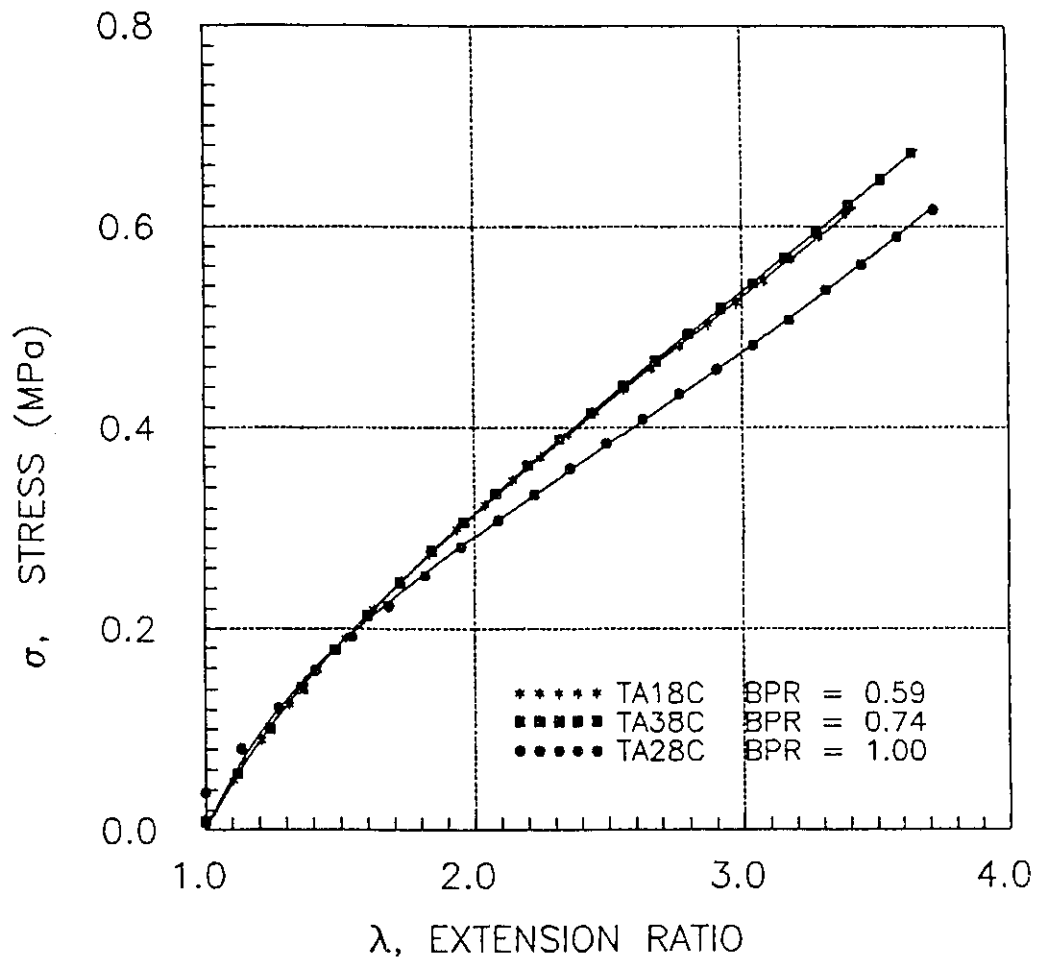


Figure 4.11 Tensile tests on unfilled PUR elastomer type TA specimens for formulations having different polyol ratios (Baylith OH/ Desmophen OH).

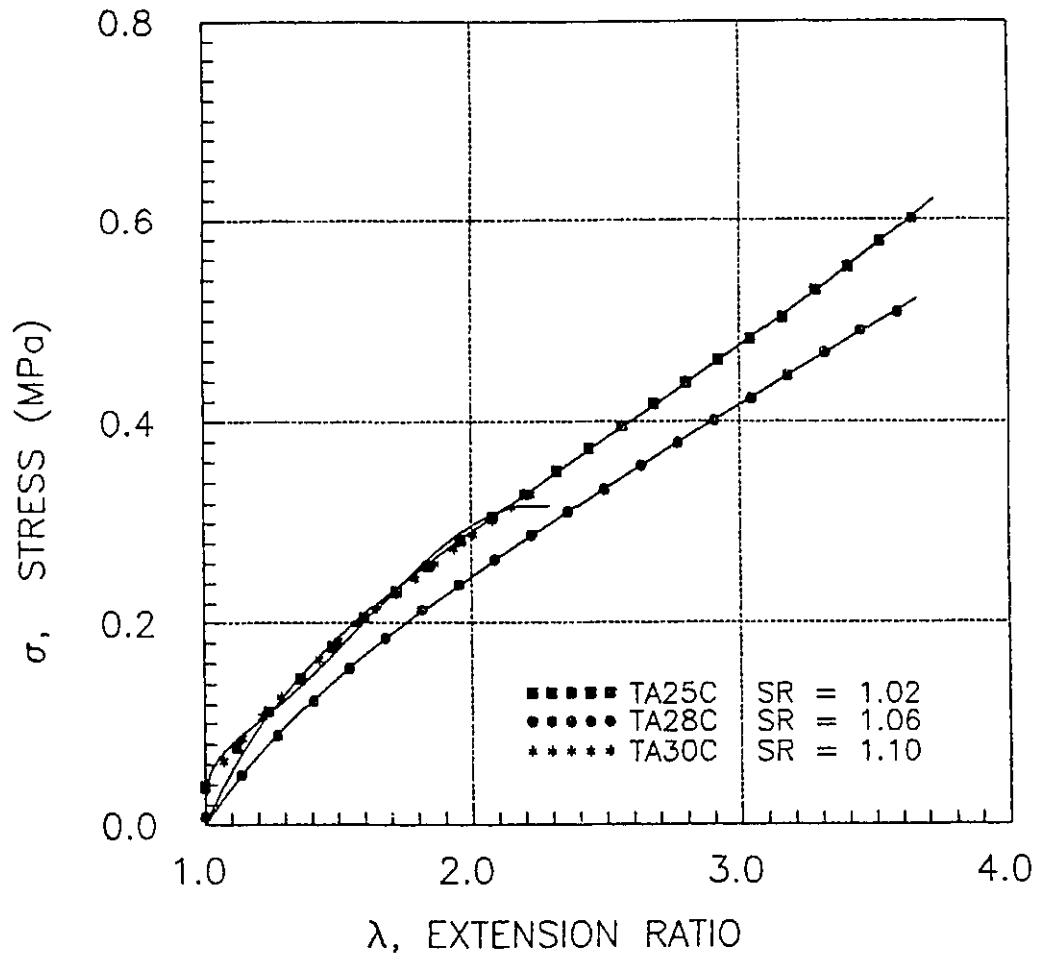


Figure 4.12 Tensile tests on PUR elastomer type TA specimens for formulations having different stoichiometric ratios (NCO/OH).

c) Results from tensile tests in TB type specimens

Tensile tests on TB type specimens were used primarily to assess the adhesive tenacity of neat PUR blends to a primed aluminum substrate. Results from these tests are presented in Table 4.12 and figures 4.13 to 4.15.

Table 4.12					
TENSILE PROPERTIES OF UNFILLED PUR ELASTOMER TYPE TB SPECIMENS					
Series	Varying Parameter	$U_n$ J/cc	$\sigma_b$ MPa	$\epsilon_b$	$E_p$ MPa
28A	PC = 30%	0.0989	0.453	0.376	1.36
28B	PC = 34%	0.0269	0.225	0.211	1.19
28C	PC = 40%	0.1128	0.377	0.507	0.858
18C	BPR=.588	0.0508	0.298	0.303	1.002
28C	BPR=1.00	0.1128	0.377	0.507	0.858
15C	SR=1.023	0.0642	0.327	0.345	0.992
18C	SR=1.062	0.0508	0.298	0.303	1.002
20C	SR=1.100	0.0414	0.276	0.271	1.017
25C	SR=1.023	0.0979	0.365	0.465	0.877
28C	SR=1.1	0.1128	0.377	0.507	0.858

\* values for  $\nu_2$  are the same as those given in the previous tables



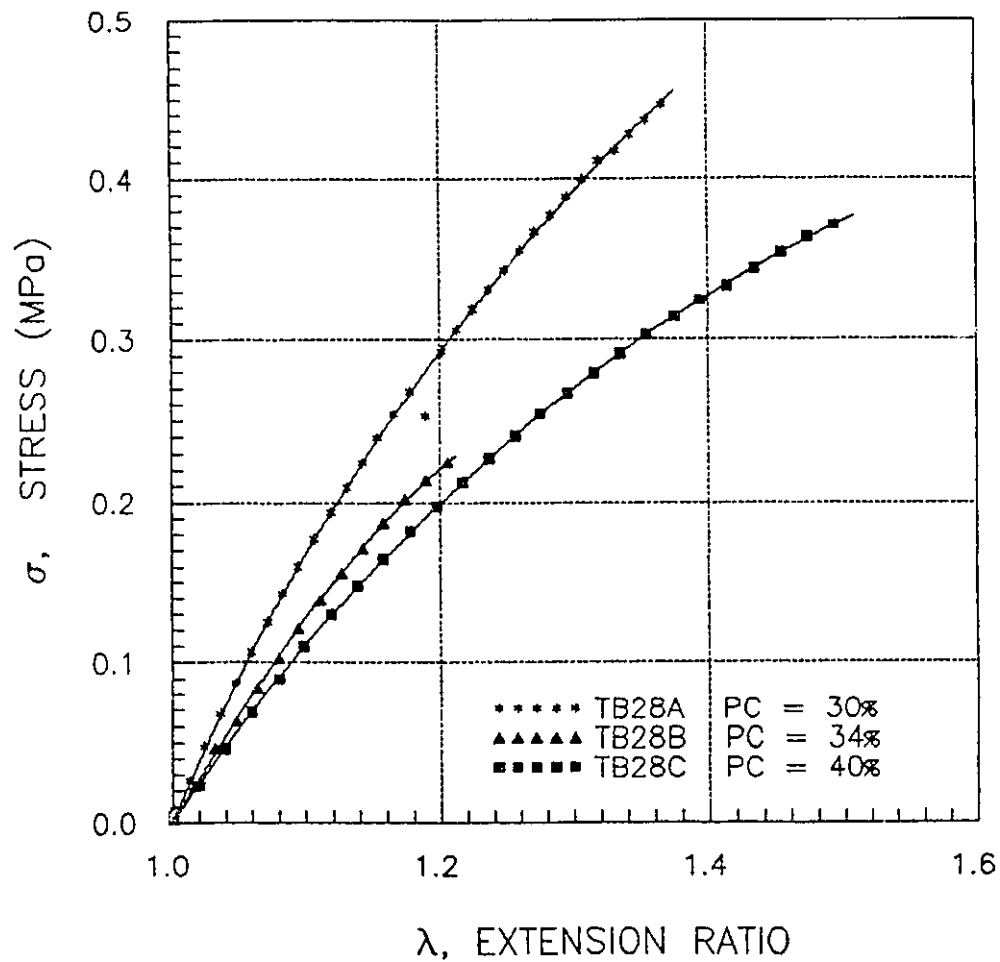


Figure 4.13 Tensile tests on unfilled PUR elastomer type TB specimens for fomulations having different plasticizer contents.

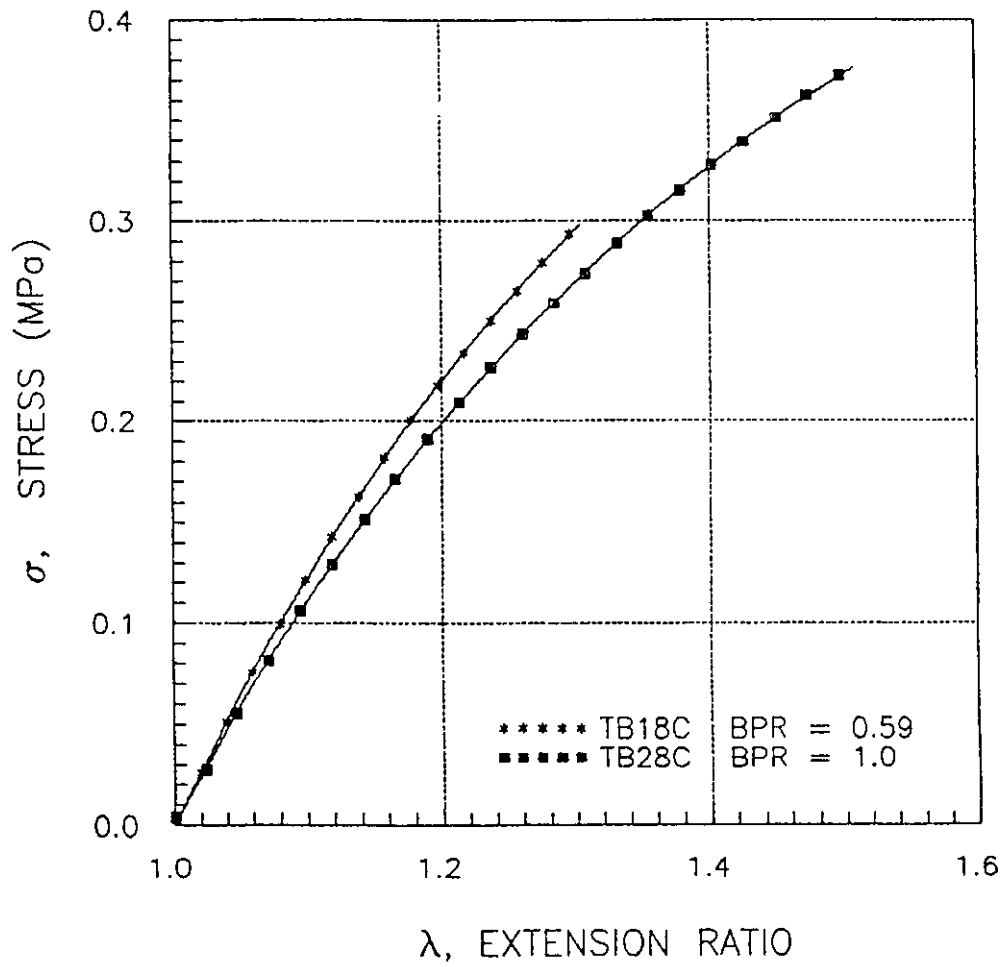


Figure 4.14 Tensile tests on unfilled PUR elastomer type TB specimens for formulations having different polyol ratios (Baylith OH/ Desmophen OH).

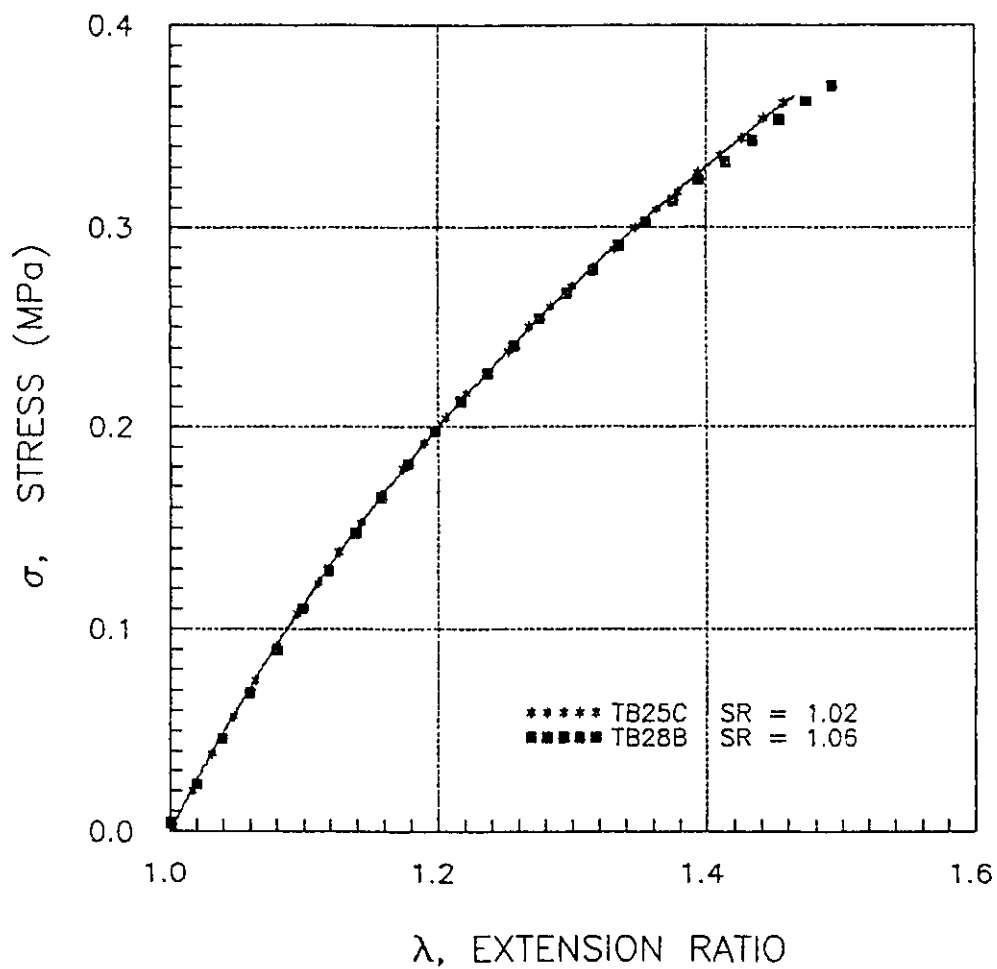


Figure 4.15 Tensile tests on unfilled PUR elastomer type TB specimens for formulations having different stoichiometric ratios (NCO/OH).

#### 4.3.2.3 Compression Characteristics

##### a) Stress-strain behaviour

Compression tests were performed as a means to easily assess the structure property relationships of the neat polymers in comparison to that obtained through swelling tests without the need to test until failure. Accordingly, the test was conducted up to an extension ratio of approximately 0.5. It must be emphasized that this test did not take into consideration whether an equilibrium modulus was attained since the test was conducted at only a single temperature at a set strain rate. Consequently, a comparison of values from different types of test is more qualitative than quantitative, and confirmation of relative changes in values is what is being investigated.

The theory of rubber elasticity relates the shear modulus,  $G$  to the following molecular parameters:

$$G = \frac{\delta RT}{M_{c,c}} \cdot \nu_2^{1/3}$$

Equ. 4.12 [71]

where

$\delta$	=	density of the polymer (g/cc)
$R$	=	gas constant ( $8.205 \times 10^{-10}$ g·cm <sup>3</sup> /mol·K)
$T$	=	absolute temperature (273 + 25 = 298K)
$\nu_2$	=	volume fraction of polymer in elastomer matrix
$M_{c,c}$	=	Molecular weight between crosslinks (g/mol)

Hence, given the shear modulus  $G$ , which can be evaluated from curve fitting to experimental data, the molecular weight between crosslinks can be

determined provided the density and the volume fraction of polymer in the blend are known. The relevant values are presented in Table 4.13.

Table 4.13  
CALCULATION OF  $M_{c,c}$  BASED ON COMPRESSION TESTS

Series	G/2 g/cm <sup>2</sup>	Density g/cc	$v_2^{1/3}$	$M_{c,c}$ g/mol
C15A	2278	1.0967	0.5894	4970
C18A	3207	1.0973	0.5904	3530
C20A	2535	1.0997	0.5920	4470
C35A	3037	1.1062	0.5871	3720
C38A	2744	1.1043	0.5885	4120
C40A	2365	1.1053	0.5899	4780
C25A	2488	1.1065	0.5837	4530
C28A	2317	1.1089	0.5853	4870
C30A	2237	1.1046	0.5867	5050
C15B	1018	1.1014	0.5532	5780
C18B	2025	1.0997	0.5544	5480
C20B	1987	1.1029	0.5556	5590
C38B	2144	1.1057	0.5523	5170
C40B	1834	1.1057	0.5536	6050
C25B	1577	1.1092	0.5477	7010
C28B	1466	1.1065	0.5493	7550
C30B	1922	1.1091	0.5506	5760
C15C	1083	1.1025	0.5113	9970
C18C	1363	1.1034	0.5125	7930
C20C	1646	1.0982	0.5137	6572
C35C	698	1.1162	0.5092	15460
C38C	1002	1.1070	0.5105	10770
C40C	1544	1.1044	0.5117	7000
C25C	909	1.1057	0.5062	11850
C30C	1343	1.1025	0.5089	8030

b) Compression set

Sealants exhibiting low percentages of compression set are less likely to remain permanently deformed after a compression cycle at elevated temperatures, such cycles as are encountered during the summer months when the sealant in a joint is in its most compressed state. Hence the compression set of sealant elastomers has a direct effect on the performance properties of the elastomer.

Results from tests used to determine the percentage of compression set of the various elastomers are shown in Table 4.14.

Table 4.14									
DEGREE (%) OF COMPRESSION SET OF UNFILLED PUR ELASTOMERS AS A FUNCTION OF BAYLITH PASTE RATIO, STOICHIOMETRIC RATIO & PLASTICIZER CONTENT									
PC %	BAYLITH PASTE RATIO								
	0.588			0.740			1.0		
	S R			S R			S R		
	1.0	1.06	1.1	1.0	1.06	1.1	1.0	1.06	1.1
30	3.4	2.7	3.6	1.8	0.8	0	0.9	0.4	1.5
34	1.9	3.2	3.3	2.7	3.4	3.3	3.9	2.5	3.0
40	2.6	2.5	3.5	3.6	2.9	2.0	3.5	2.7	5.4

SR: Stoichiometric ratio;  
PC: Plasticizer content.

Based on these results, certain observations with respect to the performance of these elastomers in relation to their specific formulation may be made:

- i) The degree of compression set for all unfilled elastomers is relatively moderate, on average 2.6%, and this is in accordance with what has been observed for similar elastomeric sealant formulations [127].
- ii) The degree of set is not sensitive to changes in stoichiometry in the range of values used in this study (i.e SR = 1.02 to 1.1).
- iii) The Baylith paste ratio, which is indicative of the proportion of castor oil in the formulation, has a more significant effect in limiting the compression set at low plasticizer contents than at high plasticizer contents, at a given stoichiometric ratio.
- iv) The addition of plasticizer increases the degree of set with the exception of those elastomers containing the least amount of castor oil (i.e having the smallest BPR).

The fact that the degree of set is insensitive to changes in the SR is to be expected due to the relatively small increase in intermolecular bonding sites with increased SR.

The strength of urethane elastomers is thought to be due to both primary (covalent) and secondary (intermolecular) bonding, the latter considered to contribute significantly to the overall strength of the polymer matrix [64]. The number of possible secondary bonding sites is dependent on the presence of



urethane groups, as shown below in figure 4.16, and this in turn is a function of the SR of the blend.

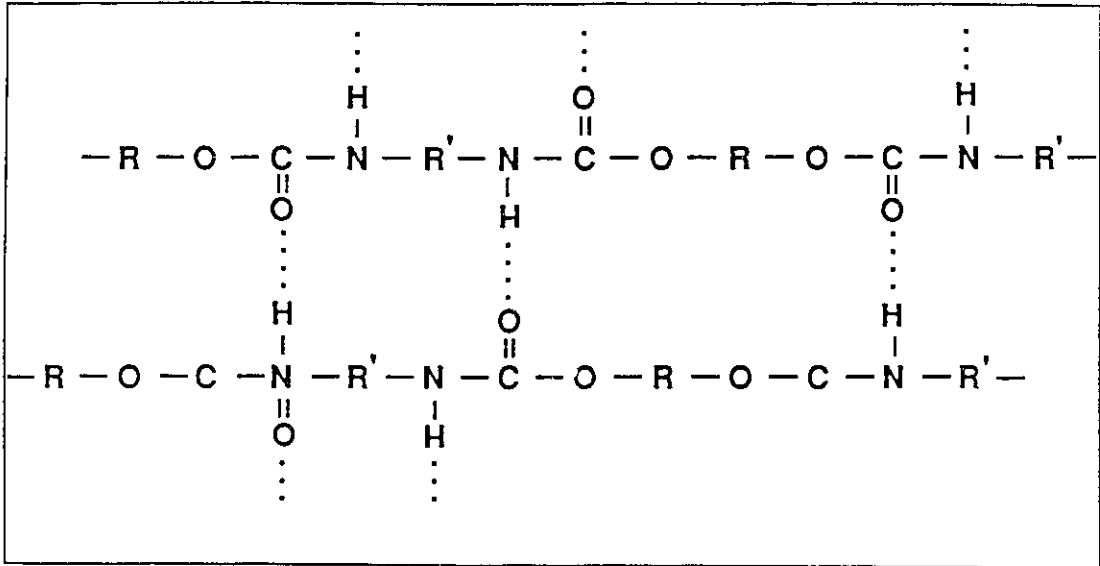


Figure 4.16 Supposed secondary (intermolecular, e.g. hydrogen) bond formation in urethane elastomers [64].

However, the relative increase in urethane groups in relation to the overall macromolecular structure remains small (e.g. 2.1% wt. urethane groups at an SR=1 vs. 2.3% wt. at SR=1) and consequently, this change is not considered significant enough to produce a corresponding change in the degree of set of these blends.

The precise role of castor oil in limiting the degree of set is difficult to ascertain. Due to steric hindrances, it is not considered that the castor oil plays a significant, if any, role in the formation of crosslinks in this system. However, the fact that castor oil possess polar groups does not preclude the possibility that secondary bonds may form provided conditions exists which are amenable to their formation. The formation of such bonds will affect the compression set by

reducing the degree of set. Hence, as shown in figure 4.17, at constant SR and PC, an increase in the BPR reduces the compression set by a factor of approximately two.

This effect is lost in those elastomer formulations which incorporate greater quantities of plasticizer. The degree of recovery from the compressed state may be assumed to be primarily influenced by a balance between a recovery force and of restraining forces [64]. The recovery force is a function of the number of primary bonds, i.e. crosslinks a particular system possess. The restraining force may be due to a number of factors including the formation of entanglements while in the compressed state. Entanglements may form provided the internal viscosity of the system is reduced and this may be achieved by the addition of a suitable plasticizer. Consequently there is a higher degree of set for more highly plasticized elastomers in comparison to those having a lower plasticizer content.

The effect of castor oil on the degree of set is opposite to that of the plasticizer, hence based on the above observations, it can be expected that the least amount of set is found in blends having the greatest amount of castor oil and the least amount of plasticizer.

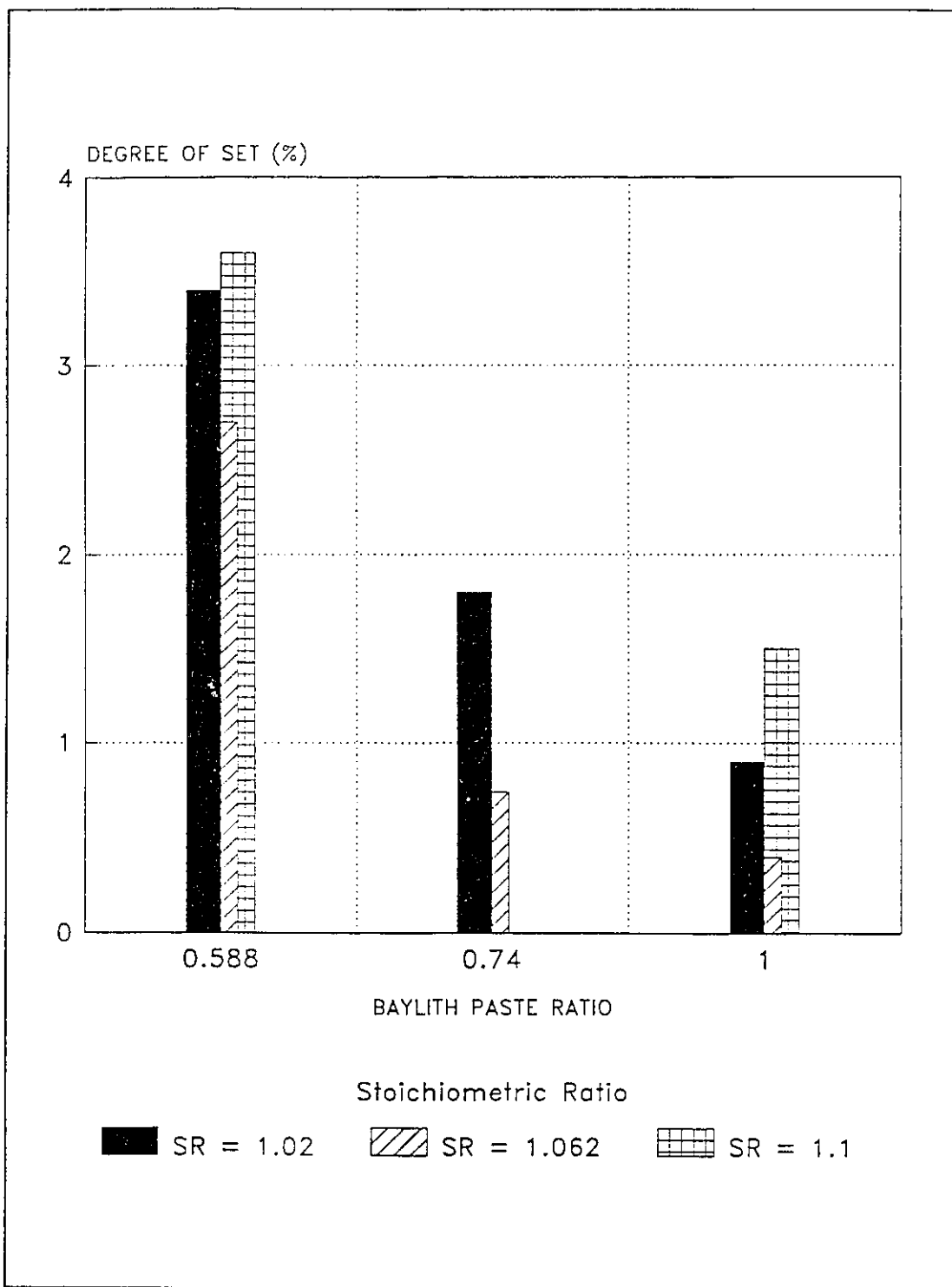


Figure 4.17 Degree (%) of compression set of unfilled PUR elastomers in relation to the Baylith paste & stoichiometric ratios of the formulation.

### 4.3.3 THERMAL ANALYSIS OF UNFILLED ELASTOMERS

Crosslinked PUR is generally considered a heterophase polymeric system [64,66], however as already mentioned in section 3.2, the quantity of hard urethane segments is comparatively small. A consequence of this is that the particular elastomer behaves essentially as an amorphous simple phase PUR whose properties are those of the primary molecular network, mainly dependent on the chemical structure, chain length and the degree of branching of the high molecular weight polyol [66]. Predictably then, the thermal behaviour of such a system would suggest a single major transition, any other distinguishable transitions being sufficiently small as to be of no particular consequence in explaining the thermal behaviour of the elastomer. Results from the DSC analysis on selected PUR elastomer formulations, given in Table 4.15, support this contention. Thermograms are given in Appendix V.

Series	BPR	SR	PC %	T <sub>g</sub> °C
18C	0.59	1.062	40	-52.7
25C	1.0	1.023	40	-52.7
28A	1.0	1.062	30	-52.1
28B	1.0	1.062	34	-52.5
28C	1.0	1.062	40	-53.0
30C	1.0	1.1	40	-52.7
38C	0.74	1.062	40	-52.7

A comparison of results from the DSC analysis is shown in figures 4.18a and 4.18b. The dependency of the  $T_g$  on the plasticizer content is demonstrated in figure 4.18a, where it is seen that there is a slight increase (1.6% in relation to the lowest  $T_g$ ) in  $T_g$  with the incorporation of increasing quantities of plasticizer to the elastomer formulation. The change in plasticizer content is significant in relation to the weight fraction of diluent (e.g. 21.4% difference in PC between series 28A & 28C), however the increase in  $T_g$  is small because the  $T_g$  of the diluent (-63.5°C) is in the same order of magnitude as that of the polymer formulation. This may more clearly be understood by considering the relation proposed by Jenkel and Hausch [128] which has been used to evaluate the  $T_g$  of a binary system comprised of polymer matrix and diluent. The relationship has the following form:

$$T_g = T_{gp} \cdot w_p + T_{gd} \cdot w_d - w_p \cdot w_d \cdot \frac{\Delta k_n}{\Delta \beta}$$

Equ. 4.13 [128]

where:

$T_{gp}$	=	$T_g$ of the polymer ;
$T_{gd}$	=	$T_g$ of the diluent;
$w_p$	=	Weight concentration of polymer;
$w_d$	=	Weight concentration of diluent;
$\Delta k_n / \Delta \beta$	=	$T_{gp} - T_{gd}$ .

The term  $\Delta k_n$ , is an expression incorporating the derivation from the addition of the indices of refraction of the pure material, and  $\Delta \beta$  is a similar expression for the temperature coefficient of the refractive index [129].

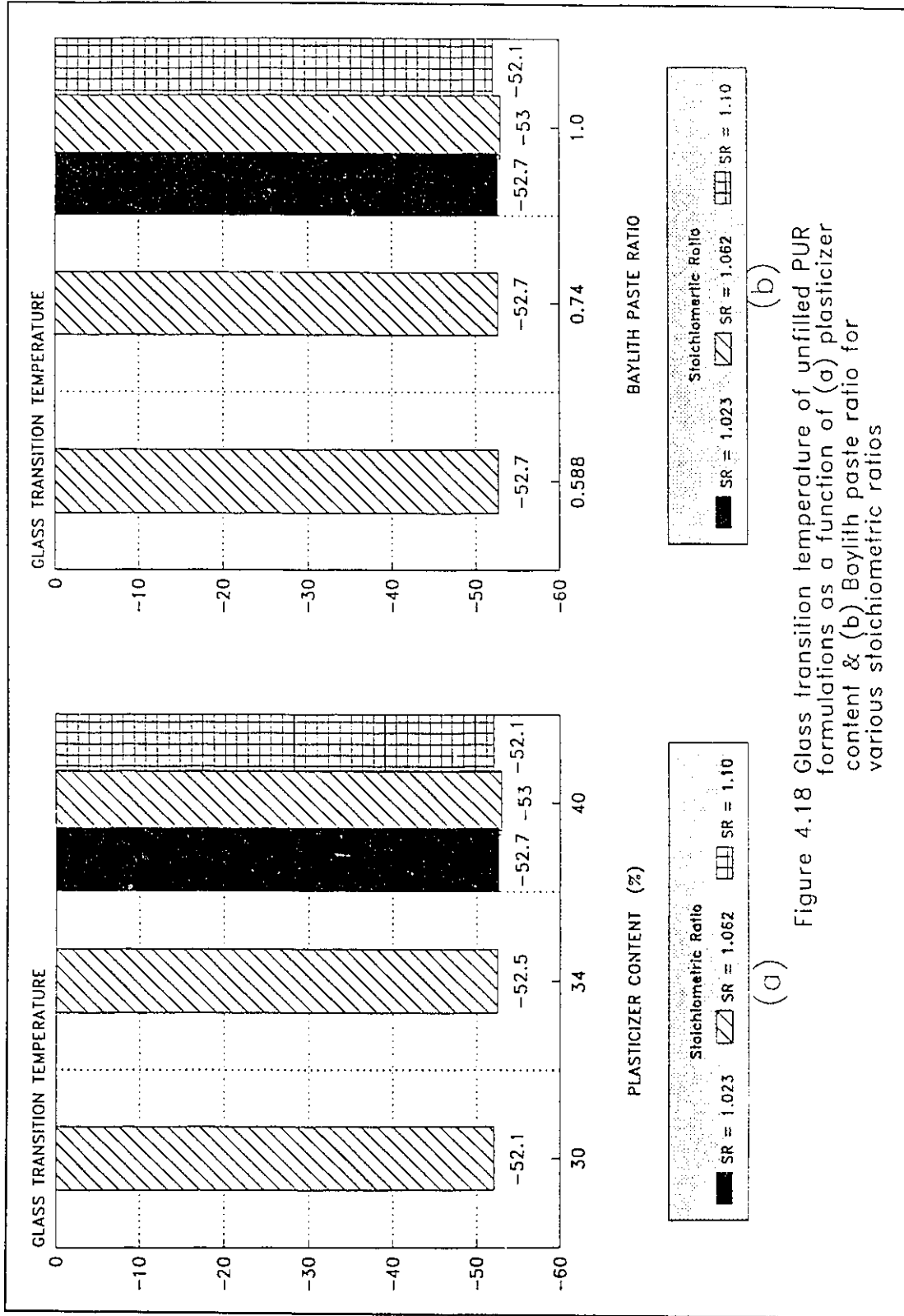


Figure 4.18 Glass transition temperature of unfilled PUR formulations as a function of (a) plasticizer content & (b) Baylith paste ratio for various stoichiometric ratios

It has been established by experimentation that  $\Delta k_p/\Delta\beta$  is equivalent to the difference between the  $T_g$ 's of the polymer and the diluent [129]. Assuming values of  $-50.4^\circ\text{C}$  and  $-62.6^\circ\text{C}$  for the  $T_g$ 's of the unplasticized polymer and the diluent respectively then the relation between  $T_g$  of the mixture and  $w_p$  may be evaluated as shown in figure 4.19. Estimates for values of  $T_g$  of formulations 28A and 28C are plotted on the figure.

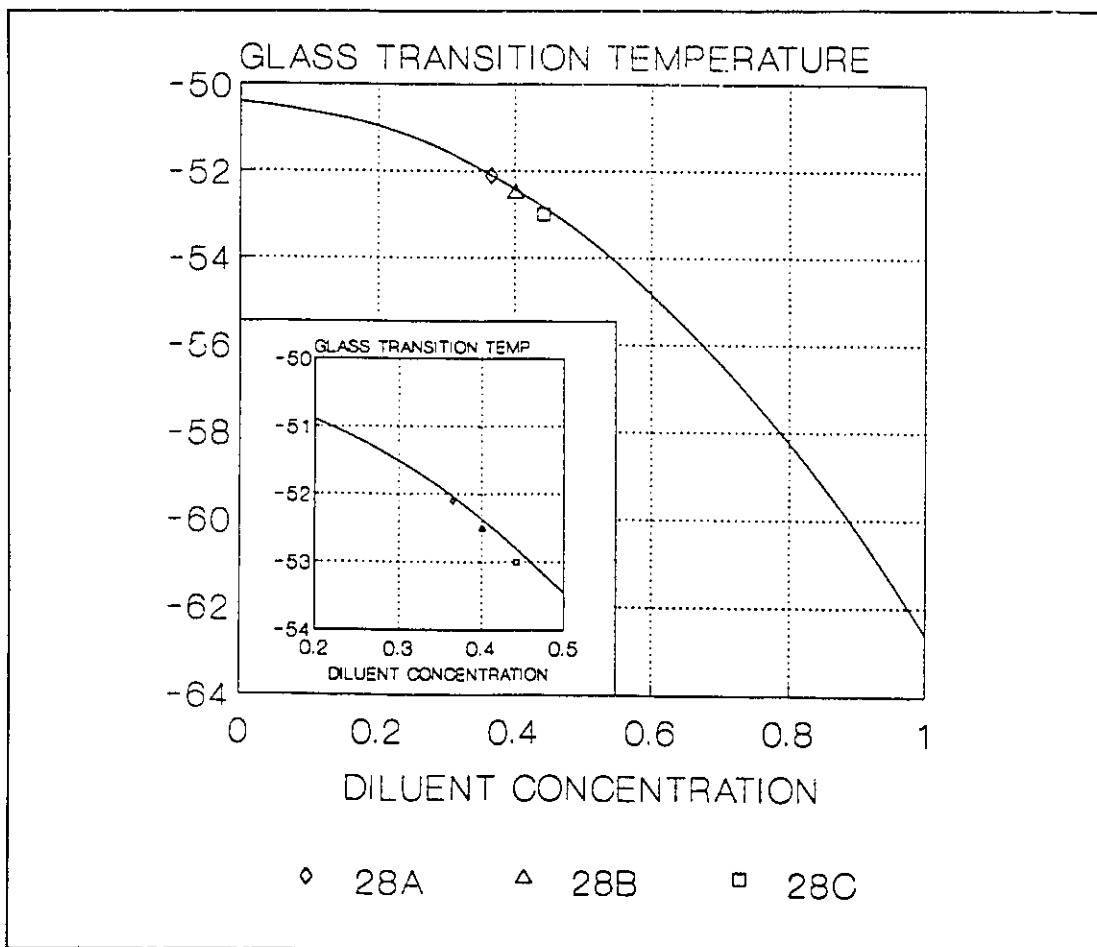


Figure 4.19 Glass transition temperature of polymeric mixture as a function of diluent concentration.

The values shown in the figure compare well with those obtained experimentally, assuming the values for  $T_{gp}$  and  $T_{gd}$  are correct. It seems reasonable to assume that the value of  $T_{gp}$ , based on a knowledge of the experimental values of the  $T_g$ 's of the constituent portions, will certainly be less than the  $T_g$  of the polyol (-63.9°C) and most probably in the vicinity of the  $T_g$  of the isocyanate (-48.6°C) by virtue of the presence of the urea dispersion in the polyol which acts to increase the  $T_g$  of the undiluted polymer.

Hence an estimate of the  $T_g$  of the undiluted polymer based on the weighted average of the polyol, urea dispersion and isocyanate prepolymer (1920D:Urea:E14::16:4:25.5) yields a  $T_g$  of -51°C, which compares favourably with the assumed value.

The value of  $T_{gd}$  can easily be obtained by considering the effective  $T_g$  of the diluent is a function of the  $T_g$ 's of both the plasticizer and the castor oil, the castor oil being assumed to act, at least partially, as a diluent. In this case the weighted average of the  $T_g$  is calculated from values of -63.5°C and -58°C for the plasticizer and castor oil respectively.

Figure 4.18b shows the range of values for  $T_g$  of formulations having different BPR's and SR's. Evidently, neither the addition of Baylith paste nor the increase in SR significantly affects the thermal behaviour of these elastomers.



#### 4.4 CHARACTERIZATION OF FILLED ELASTOMERS

##### 4.4.1 SWELLING BEHAVIOUR

Two possibilities may occur when a filled elastomer is swollen in an appropriate solvent. The interaction between the elastomer and particulate modifier is disturbed by the action of the solvent and the bonds at their interface break down; the elastomer remains fully or partially bound to the surface of the particulate matter even in the presence of the solvent [130].

If all bonds at the filler-elastomer interface rupture, then around each particle will form cavities which will fill with solvent. In this case, the particles do not influence (i.e. restrict) the swelling behaviour and consequently, there is an increase in the swelling of the rubber [130].

In the latter case, the swelling is restricted by the influence of the particles and the behaviour may be characterized by the relation derived by Kraus [91,130,131], previously given in section 3.4.1.2, and provided below in a modified form:

$$\frac{v_{r_0}}{v_r} = 1 - m \left( \frac{\phi_f}{1 - \phi_f} \right) \quad (a)$$

$$m = \{ 3C ( 1 - v_m^{1/3} ) + v_{r_0} - 1 \} \quad (b)$$

Equ. 4.14a,b [91]

where :  $v_{r0}$  =  $v_r$  of unfilled elastomer;  
 $\phi_f$  = volume fraction of filler;  
 $C$  = constant, which is characteristic of the filler (but independent of the polymer, solvent or degree of crosslinking).

The value of  $m$  is simply the slope of the line plotted according to equation 4.14a, provided  $v_{r0}/v_r$  is plotted as a function of  $\phi_f / (1 - \phi_f)$ . Results from swelling tension modified formulations are given in Table 4.16. The weight of the solvent absorbed by the specimen,  $W_{sol}$ , is simply the difference between the swollen weight,  $W_s$ , and the initial weight,  $W_o$ . The volume fraction of elastomer in the swollen specimen,  $v_r$  is given by the following relation:

$$v_r = \frac{1}{1 + \frac{W_{sol}}{W_o} \cdot \frac{\delta_e}{\delta_{sol}}}$$

Equ. 4.15

where  $\delta_e$  and  $\delta_{sol}$  are the densities of the elastomer and solvent respectively. The value of  $v_{r0}$  is calculated from the base formulation used for preparing all modified compounds. The reduced data is shown in figure 4.20 and is plotted according to equation 4.14a which relates the restriction in swelling to the quantity of particulate matter in the elastomer and the degree to which the elastomer can swell. Provided a firm bond is established between the elastomer matrix and the filler, the degree of swelling will be restrained. The slope of the straight line for each series of points establishes the extent of the restraint, and according to equation 4.14b, is related to the coefficient  $C$ .

Table 4.16

## SWELLING RESULTS FROM FILLED ELASTOMERS

SERIES	$W_o$ g	$W_s$ g	$W_{sol}$ g	$V_o/V_s$	$v_o/v_r$
50AT	10.8508	28.1203	17.2695	0.3305	0.927
75AT	11.2572	27.9772	16.7200	0.3459	0.885
100AT	10.9557	26.1566	15.2009	0.3615	0.847
125AT	11.1439	25.6617	14.5178	0.3762	0.814
150AT	11.0222	24.3839	13.3617	0.3932	0.779
50EU	11.0090	29.0187	18.0097	0.3240	0.944
75EU	10.9848	28.2706	17.2800	0.3330	0.920
100EU	11.2793	27.7853	16.5060	0.3493	0.377
125EU	11.0396	26.4696	15.4300	0.3600	0.851
150EU	11.0522	25.8206	14.7684	0.370	0.827
50ST	11.7268	29.4881	17.7613	0.3415	0.897
75ST	12.4172	29.4715	17.0543	0.3639	0.841
100ST	12.6594	28.5463	15.8869	0.3850	0.795
125ST	13.6776	29.2664	15.5888	0.4080	0.750
150ST	13.3376	26.7200	13.3824	0.4391	0.597
50TO	10.9704	28.1305	17.1601	0.3343	0.916
75TO	11.1425	27.3795	16.2370	0.3500	0.874
100TO	11.4434	27.1008	15.6574	0.3647	0.840
125TO	11.3570	25.5638	14.2068	0.3858	0.794
150TO	11.1351	24.3237	13.1886	0.3990	0.768
28C	10.7082	29.7648	19.0566	0.3062	1.0

Specimens were immersed in toluene and permitted to swell, at room temperature, until no significant change in weight was measured; values provided in the table are an average of three determinations; the value of  $v_o$  is derived from formulation 28C;  $\delta_o = 1.1035$  g/cc;  $\delta_{sol} = 0.8669$  g/cc.

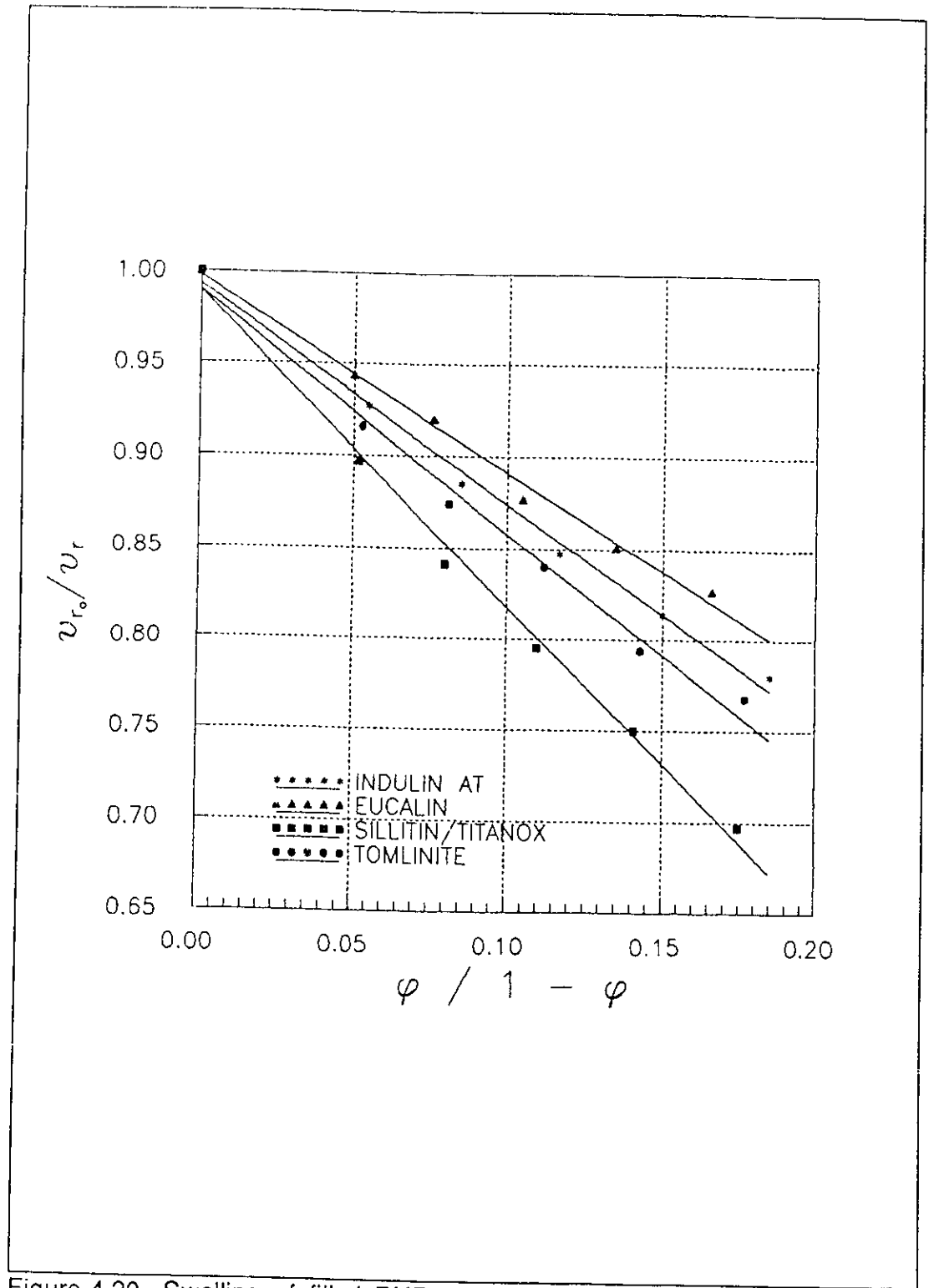


Figure 4.20 Swelling of filled PUR elastomer formulations. Dependence of elastomer on the volume loading of particulate fillers.

Lipatov [130] has suggested that this coefficient can be used as a qualitative characteristic of the adhesion of the elastomer to the particulate surface.

The slopes and corresponding "adhesion" coefficients for the four particulate modifier series are given in Table 4.17. The values indicate that the "ST" series, consisting of a mixture of siliceous clay (Sillitin Z-86) and titanium dioxide (Titanox), provides the greatest restraint to swelling. It is also evident that less restraint is provided by modifiers of series TO, AT and EU, given in order of their decreasing contribution.

Table 4.17		
CHARACTERISTIC PARTICULATE FILLER COEFFICIENTS BASED ON SWELLING BEHAVIOUR		
Particulate Filler Series	m	C
ST: Sillitin Z-86/Titanox	1.83	2.58
TO: Tomlinite	1.44	2.18
AT: Indulin AT	1.27	2.01
EU: Eucalin	1.09	1.82
Values were calculated using equation 4.14b and a value for $\nu_0 = 0.3062$ .		

These results will be referred to again in those sections dealing with the tensile and compressive strengths of modified formulations as well as in the section in which the surface properties of both the elastomer matrix and the particulate matter are evaluated.

#### 4.4.2 CURING KINETICS OF FILLED ELASTOMERS

The results from hardness tests on filled elastomer formulations are depicted in figures 4.21, 4.22 and 4.23, where the hardness, as determined using the method described in section 3.4.2.3, is given in relation to the logarithm of the curing time in hours.

The values shown in figures 4.21a and 4.21b are for results obtained on Tomlinite and Indulin AT filled PUR elastomer formulations respectively, and those shown in figures 4.22a and 4.22b for formulations filled with Eucalin and Kaolin.

The effect of the addition of filler to the elastomer formulation is clearly evident from these diagrams. The addition of filler increases the hardness at a given time in relation to the unfilled elastomer. Furthermore this effect is dependent on the quantity of filler in the formulation; the greater the filler loading, the greater the increase in hardness at a given time. Hence it may be argued that the filled specimens cure at a faster rate than the unfilled ones by virtue of the time required to achieve a given hardness reading. In fact the curing rate, as characterized by the slope of the hardness-time curve, is seemingly the same as that of the unfilled formulations, indicating that the curing mode is essentially the same in both types of formulations and that the curing process (i.e. the formation of a crosslinked structure) is unhindered by addition of filler.

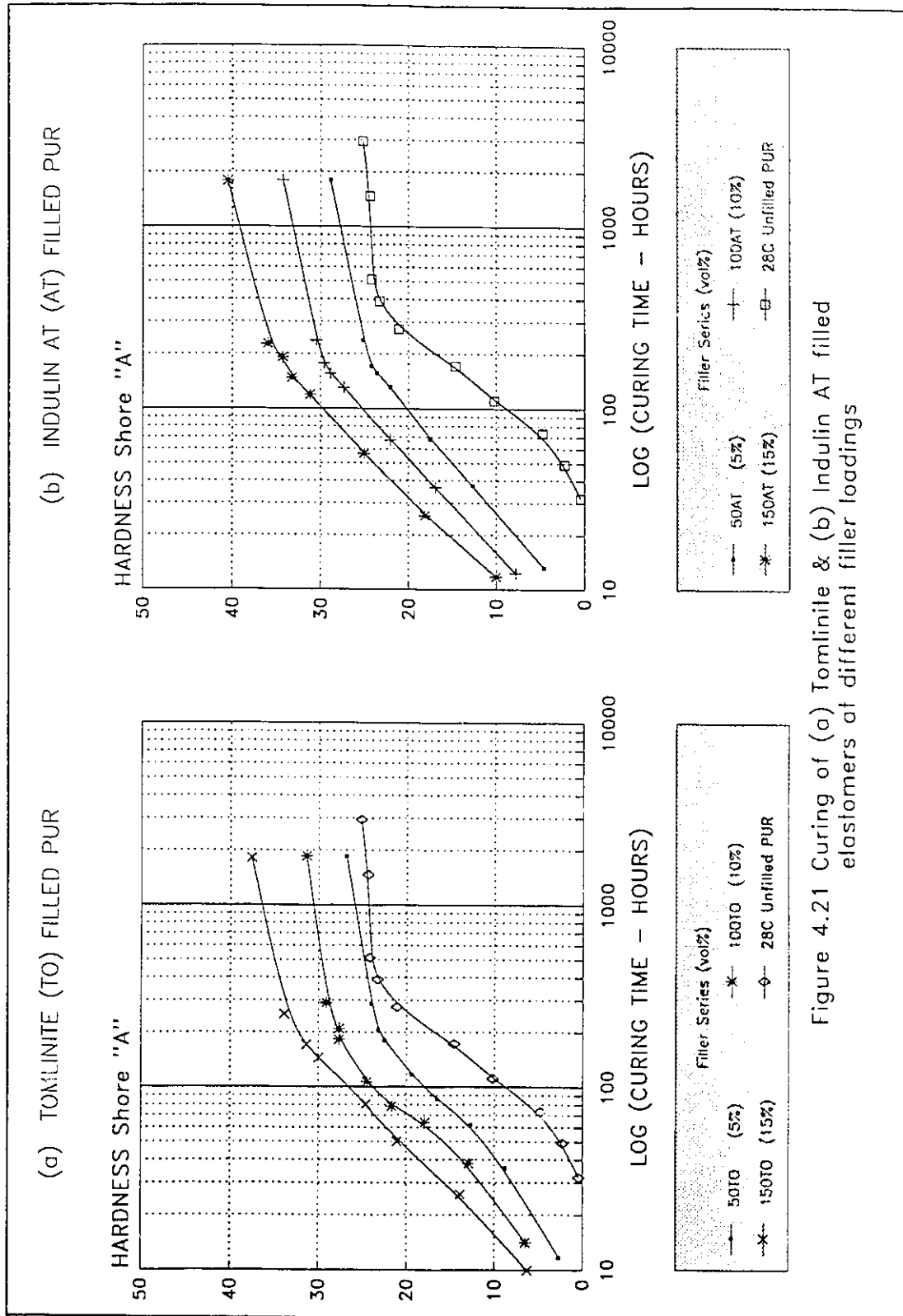


Figure 4.21 Curing of (a) Tomlinite & (b) Indulin AT filled elastomers at different filler loadings

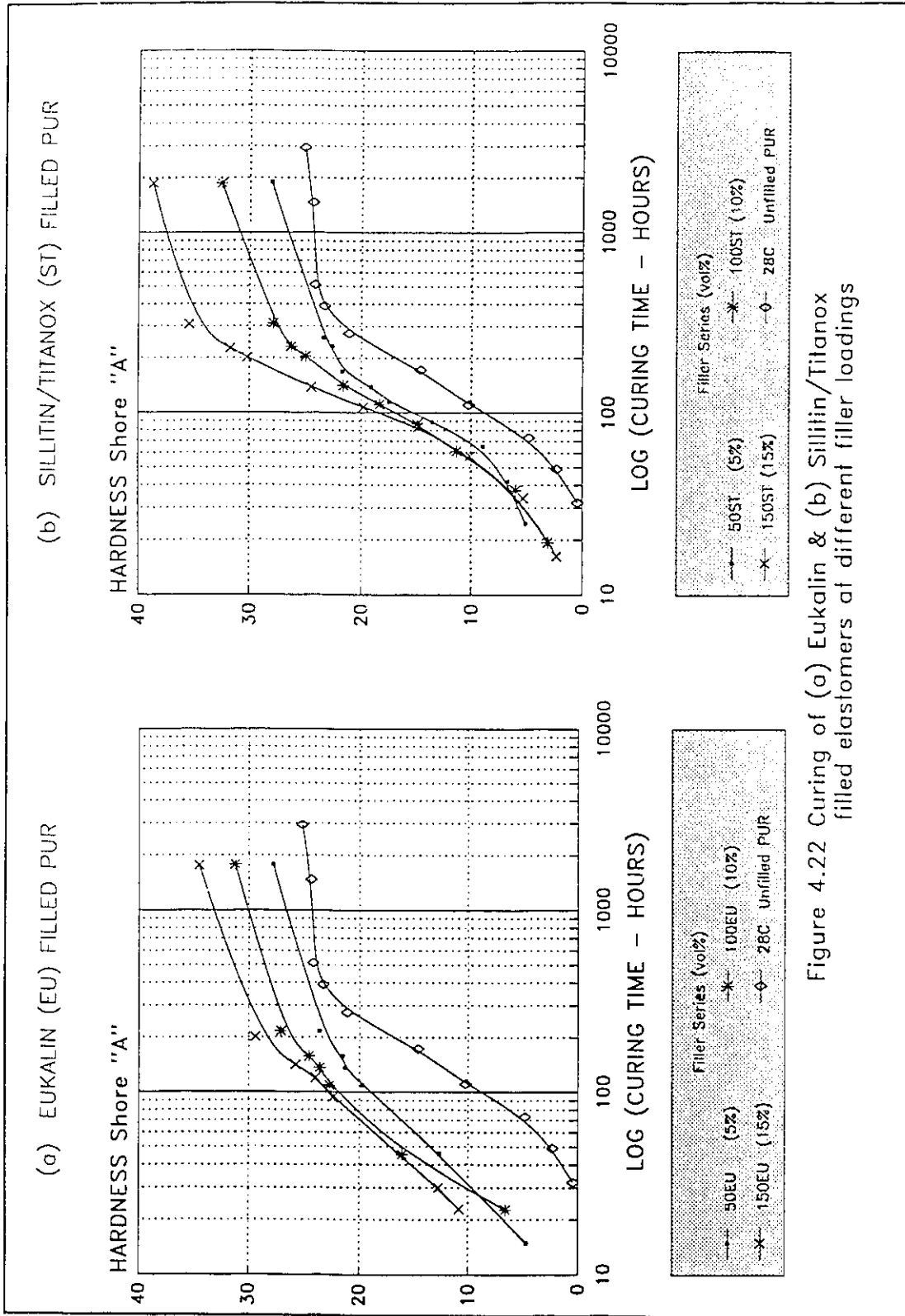


Figure 4.22 Curing of (a) Eukalin & (b) Sillitin/Titanox filled elastomers at different filler loadings



It may be shown however that the curing mode of elastomers formulated with the Sillitin/Titanox based filler behave slightly differently in relation to those formulated with the lignin based fillers. A comparative analysis is shown in figure 4.23 of the relation between the curing mode of the different types of filler in relation to the unfilled elastomer. The filled elastomers have a volume loading of 15%. Although the curing mode of the filled elastomers is essentially the same as that of the unfilled ones, the Sillitin/Titanox filled series has a prolonged rise in hardness in relation to the lignin based fillers. This is thought attributable to the physical characteristics of the Sillitin/Titanox filler.

Since the hardness of the specimens is related to their modulus, the increase in hardness can be attributed to the same effects which contribute to the increase in modulus in elastomers with the addition of filler.

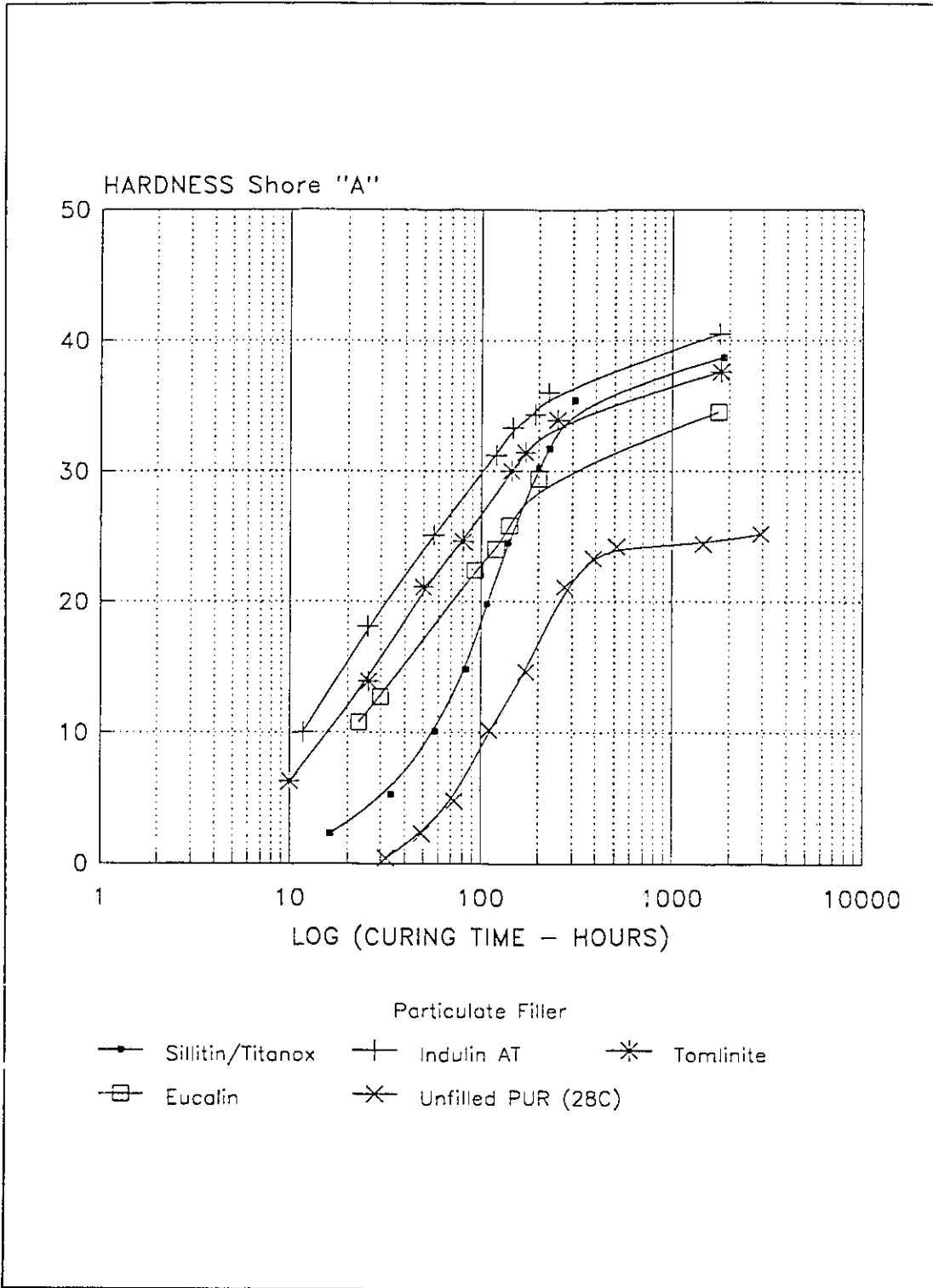


Figure 4.23 Curing kinetics of various filled formulations at 15% volume loading in relation to the base unfilled formulation (28C).

#### 4.4.3 MECHANICAL PROPERTIES IN TENSION

The results from tensile tests on type TA specimens are presented in Table 4.18 and the corresponding stress-strain characteristics for each filler series at given volumetric loadings are illustrated in figures 4.24 to 4.27.

The data in Table 4.18 are arranged to demonstrate the dependence of the strain energy to rupture ( $U_r$ ), stress ( $\sigma_b$ ) and strain ( $\epsilon_b$ ) at break, and the modulus ratio on the quantity and type of modifier used in the base elastomer formulation.

In general, the phenomenon of reinforcement of an elastomer by the addition of filler is manifested by the increase in the elastic modulus and stress at break, and a decrease in the strain at break. The energy required to rupture the specimens should increase up to some optimum point after which further addition of filler is detrimental to the performance of the blend.

The data given in Table 4.18 essentially reflect this premise, with the exception of those elastomers formulated with Sillitin/Titanox filler. In this instance, as shown more effectively in figure 4.28, the addition of filler increases both the stress and strain at break, thus contributing to the improved performance of this elastomer series in relation to the lignin based formulations. In this same elastomer series, there is a steady increase in energy to rupture up to a volumetric filler loading of 12.5%.

Table 4.18					
MECHANICAL PROPERTIES OF FILLED PUR ELASTOMERS					
Series	$U_n$ J/cc	$\sigma_b$ MPa	$\epsilon_b$	E MPa	E/E <sub>o</sub>
50AT	0.630	0.569	1.96	0.593	1.19
75AT	0.624	0.581	1.87	0.637	1.28
100AT	0.661	0.648	1.74	0.757	1.52
125AT	0.584	0.617	1.66	0.730	1.47
150AT	0.587	0.603	1.56	0.811	1.63
50EU	0.265	0.392	1.33	0.506	1.02
75EU	0.250	0.369	1.22	0.530	1.064
100EU	0.366	0.456	1.40	0.616	1.237
125EU	0.311	0.443	1.23	0.654	1.313
150EU	0.263	0.371	1.07	0.694	1.394
50TO	0.365	0.426	1.45	0.556	1.12
75TO	0.514	0.539	1.66	0.641	1.29
100TO	0.442	0.537	1.44	0.709	1.42
125TO	0.498	0.599	1.43	0.807	1.62
150TO	0.620	0.692	1.56	0.865	1.74
50ST	1.055	0.697	2.75	0.549	1.102
75ST	1.381	0.785	3.13	0.574	1.153
100ST	1.543	0.887	3.05	0.671	1.347
125ST	1.990	1.001	3.43	0.699	1.408
150ST	1.460	0.947	2.61	0.831	1.669
28C	0.976	0.616	2.72	0.498	1.00

Tests conducted at RT (25°C) & a strain rate of 2 mm/mm-m (x-head @ 50 mm/m; gauge 25 mm) using a standard ASTM D412 die "D" specimen.

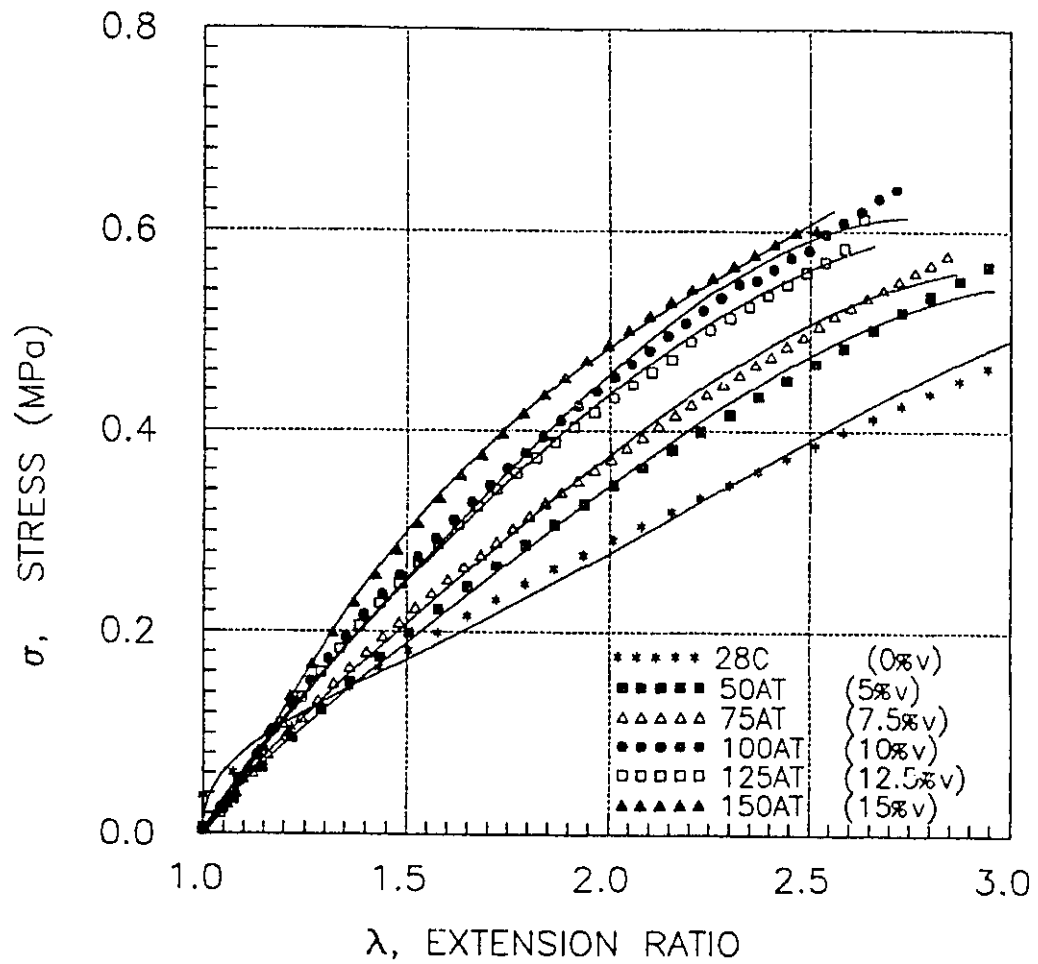


Figure 4.24 Tensile characteristics of TA type PUR based elastomer specimens filled with Indulin AT at different volumetric loadings.

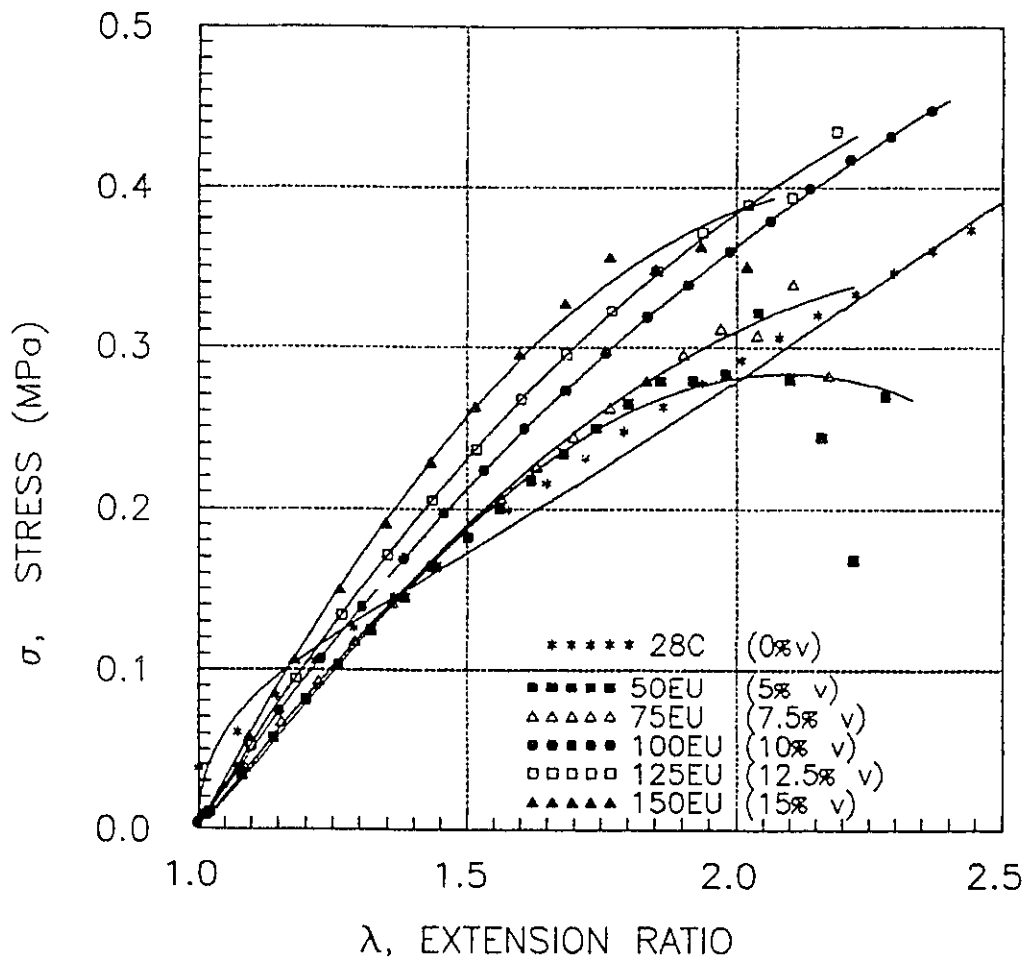


Figure 4.25 Tensile characteristics of TA type PUR based elastomer specimens filled with Eucalin at different volumetric loadings.

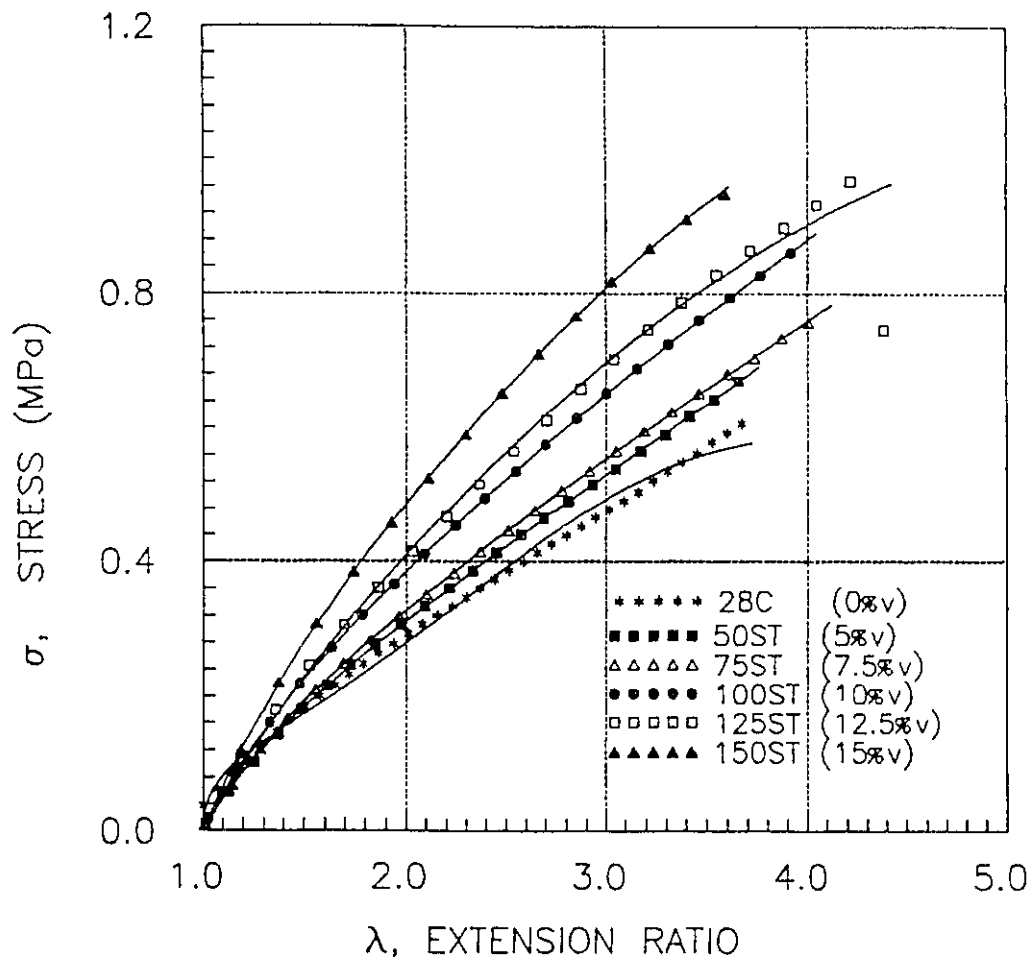


Figure 4.26 Tensile characteristics of TA type PUR based elastomer specimens filled with Sillitin/Titanox at different volumetric loadings.

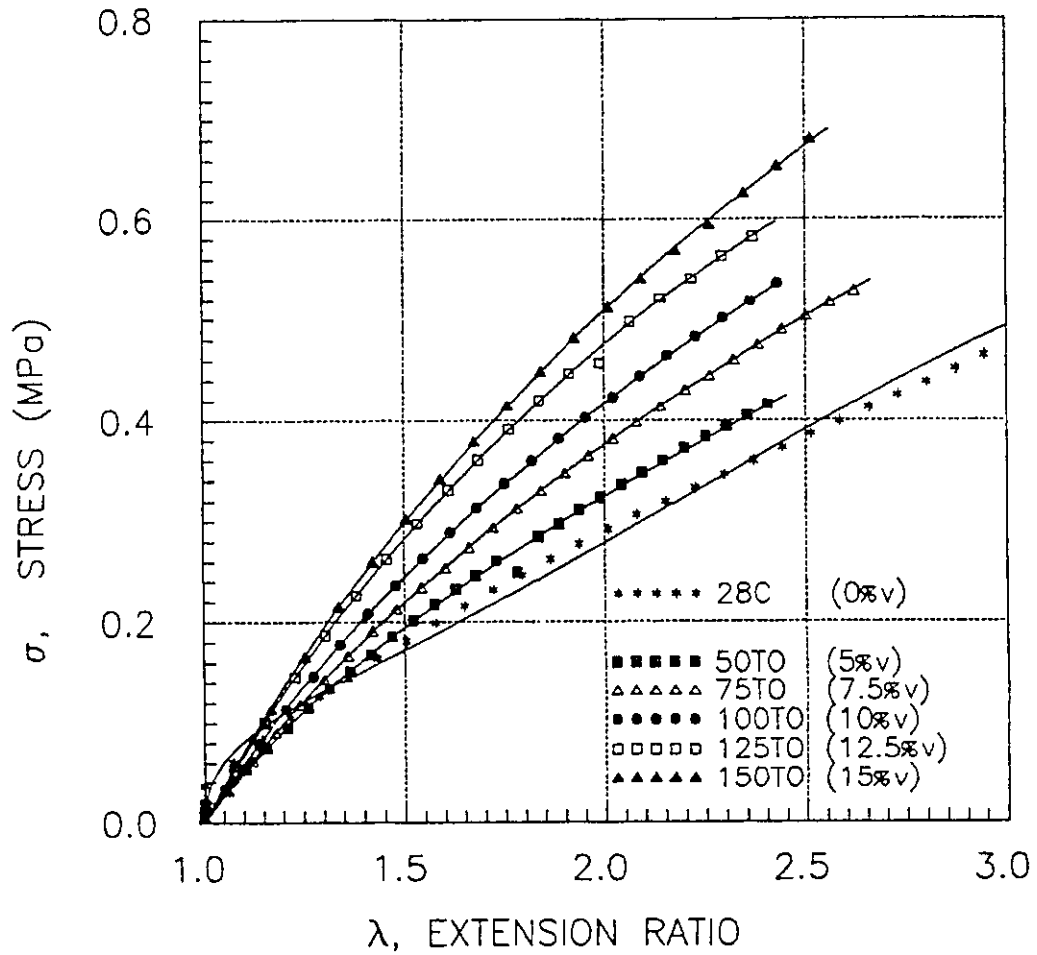


Figure 4.27 Tensile characteristics of TA type PUR based elastomer specimens filled with Tomlinite at different volumetric loadings.



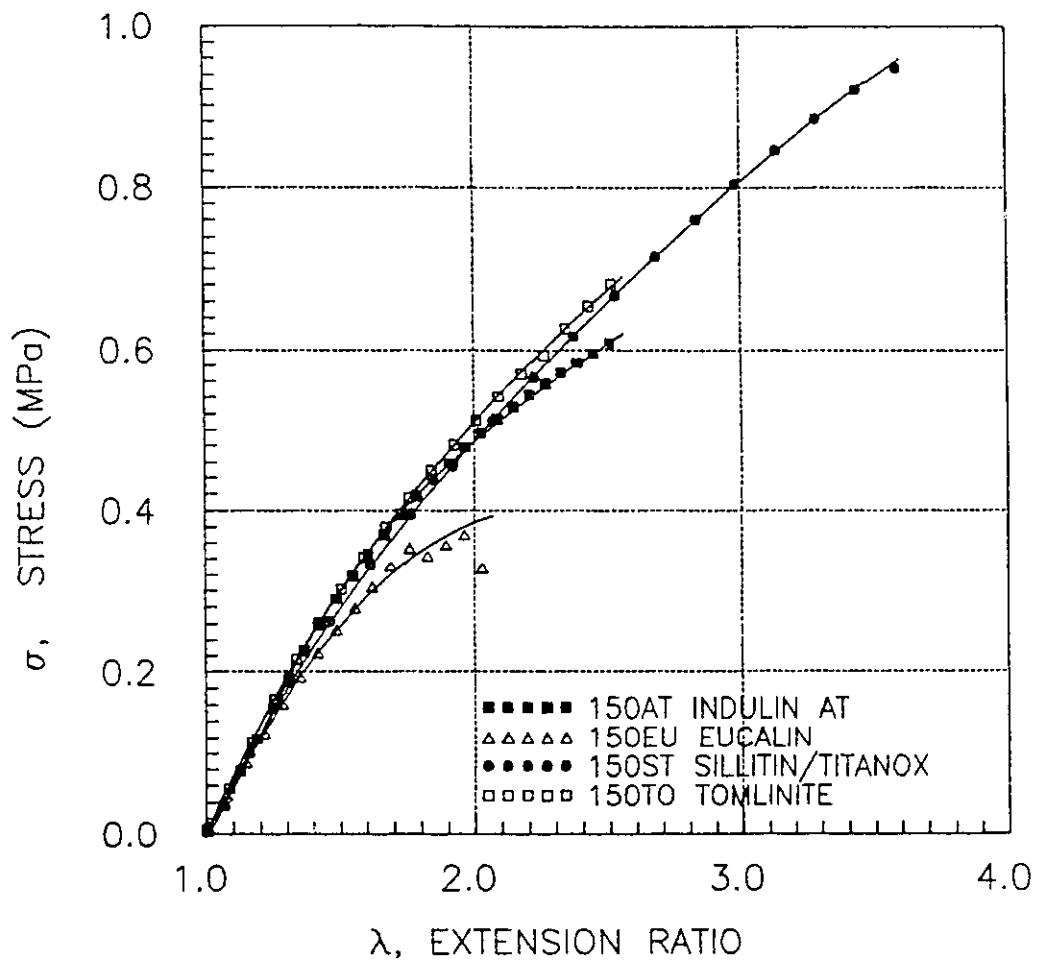


Figure 4.28 Tensile characteristics of TA type PUR based elastomer specimens having different filler types at 15% volumetric loading.

The modulus ratio, which is simply the ratio of the modulus of the modified to the unmodified elastomer ( $E/E_0$ ), is presented in figure 4.29 as a function of the % volumetric filler loading ( $\phi_f$ ). The theory regarding reinforcement, as developed by Smallwood [132] and extended by Guth [133], suggests that the modulus ratio is dependent on the filler loading according to the following relation:

$$\frac{E}{E_0} = 1 + 2.5 \cdot \phi_f + 14.1 \cdot \phi_f^2$$

Equ. 4.16 [133]

It has been shown that the tensile properties of filled elastomers are dependent, not only on the quantity of filler incorporated to the elastomer, but also on the packing characteristics of the the particles and on the interfacial bond between formulation components [133]. The relationship given in section 3.3.2, (Lewis & Neilsen [81-84]), takes into account these more subtle effects.

$$\frac{E}{E_0} = \frac{1 + \kappa \Gamma \phi_f}{1 - \Gamma \psi \phi_f}$$

$$\kappa = k_e - 1 = 2.5 - 1 = 1.5$$

$$\Gamma = \frac{(E_f / E_0) - 1}{(E_f / E_0) + \kappa} \quad \frac{E_f}{E_0} = \frac{6.6 \text{ GPa}}{0.6 \text{ MPa}} = 11000$$

$$\psi = 1 + \left( \frac{1 - \phi_m}{\phi_m^2} \right) \phi_f$$

Equ. 3.4 [84]

The value for the maximum packing fraction,  $\phi_m$  for each filler type is taken from Table 3.5.

Both these equations are plotted in figure 4.29 where it is seen that the experimental results compare favourably with the theoretical values.

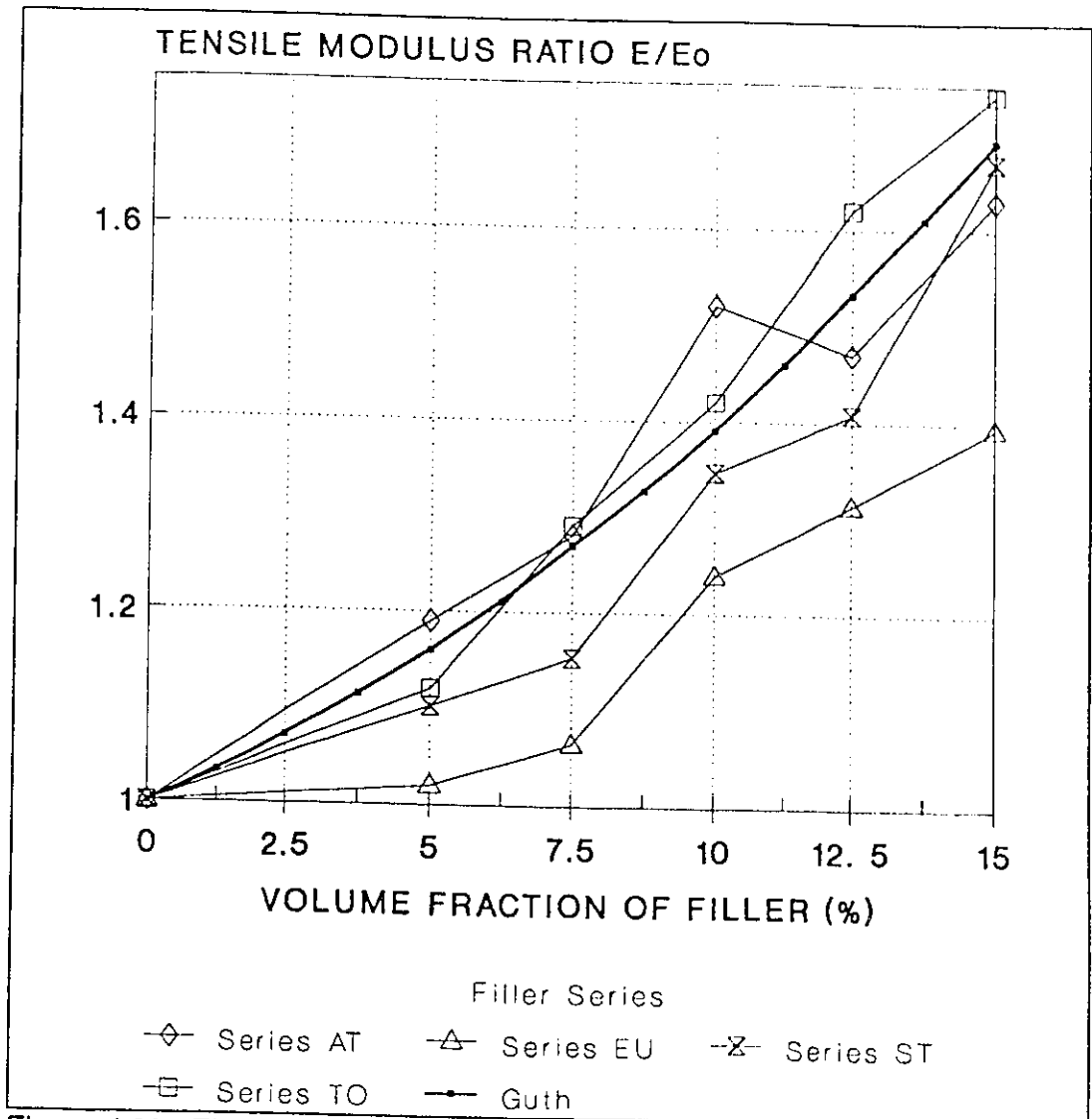


Figure 4.29 Elastic modulus ratio ( $E/E_0$ ) of filled PUR based elastomers as a function of volumetric loading (%) for different filler types in comparison to theory of Guth [133] & Nielsen [84].

#### 4.4.4 MECHANICAL PROPERTIES IN COMPRESSION

##### 4.4.4.1 Stress-strain Behaviour

The mechanical properties in compression were obtained by subjecting a filled elastomeric specimen, in the shape of a cylindrical pellet, to a deformation of 50% its original height. Since this test is not one which was conducted to failure, the results given in Table 4.19 include the strain energy to the specified deformation, and as well, the value of  $E$  and of  $E/E_0$  for the various formulations.

The stress-strain characteristics of the elastomer series at specified filler loadings are shown in figures 4.30 to 4.33. The increase in strain energy as well as in the modulus with increased filler loading is evident from the strength curves of all filler types.

The relative increase in modulus of the filled elastomer formulations as a function of filler loading is given in figure 4.34. The data are plotted in relation to a theoretical curve developed by Guth [133] that was presented in the preceding section.

The reduced modulus ratio of the Eucalin filler series at a given filler loading indicates that this type of filler does not reinforce to the same degree as Sillitin/Titanox, Tomlinite or the Indulin AT series.

Based on the relationship developed by Nielsen [84], as presented in the previous section, the average particle size and particle size distribution determines the packing characteristics of the filler and hence the extent to which reinforcement can be achieved at specified filler loadings.

TABLE 4.19  
MECHANICAL PROPERTIES OF FILLED PUR ELASTOMERS IN  
COMPRESSION

Series	$U_n$ kg/mm <sup>2</sup>	E MPa	E/E <sub>0</sub>
50AT	0.03425	2.01	1.14
75AT	0.03701	2.19	1.24
100AT	0.04416	2.60	1.47
125AT	0.04735	2.80	1.59
150AT	0.05246	3.06	1.73
50EU	0.02885	1.93	1.09
75EU	0.03143	2.02	1.14
100EU	0.03670	2.18	1.23
125EU	0.04086	2.37	1.34
150EU	0.04532	2.62	1.48
50ST	0.02411	1.63	1.20
75ST	0.02768	1.73	1.28
100ST	0.03283	2.01	1.49
125ST	0.03655	2.15	1.59
150ST	0.04156	2.46	1.82
50TO	0.02784	1.57	1.16
75TO	0.02882	1.64	1.21
100TO	0.03126	1.78	1.32
125TO	0.03841	2.20	1.63
150TO	0.04575	2.73	2.02

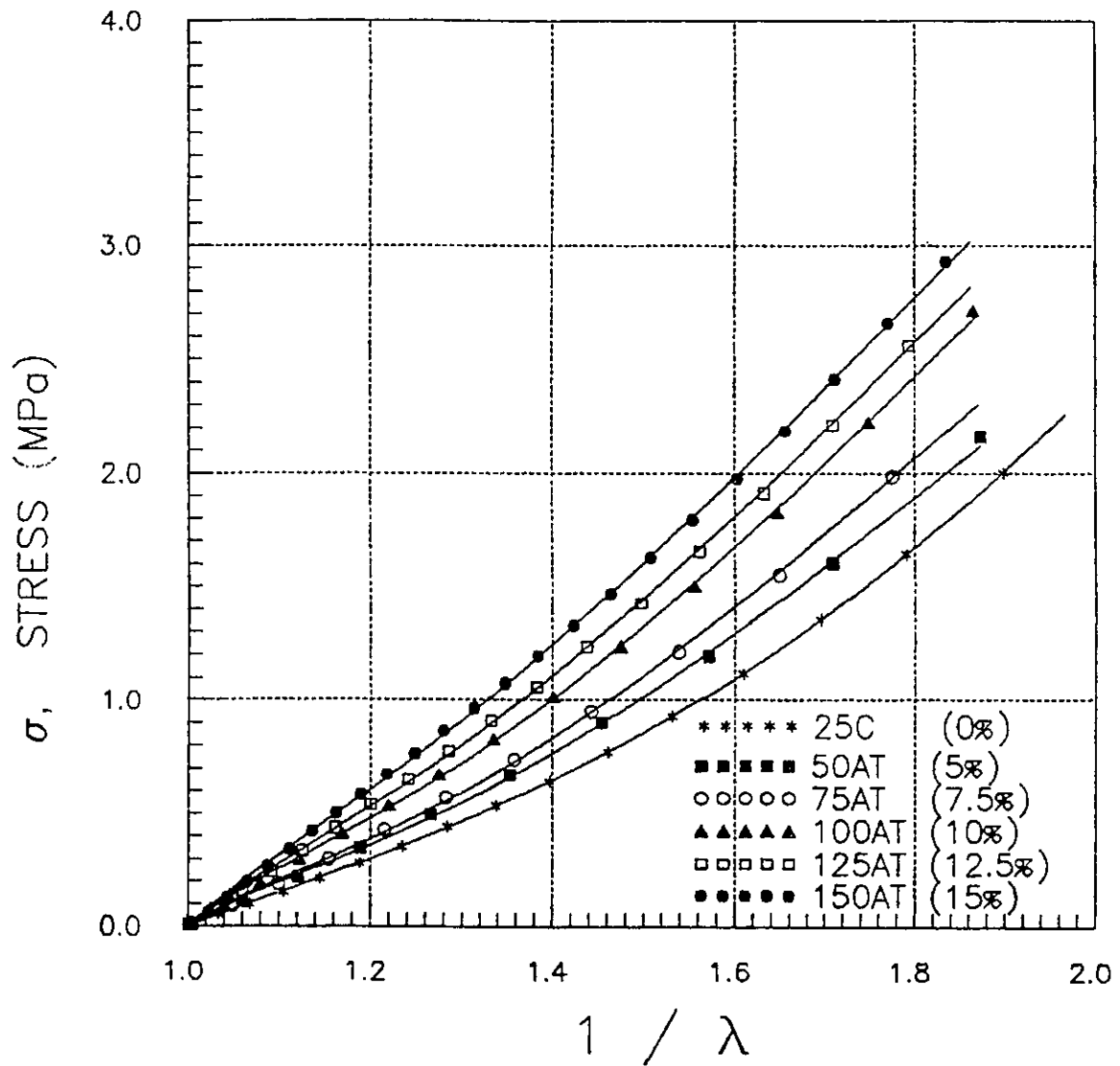


Figure 4.30 Compression tests on type C PUR based elastomer specimens filled with Indulin AT at different volumetric loadings.

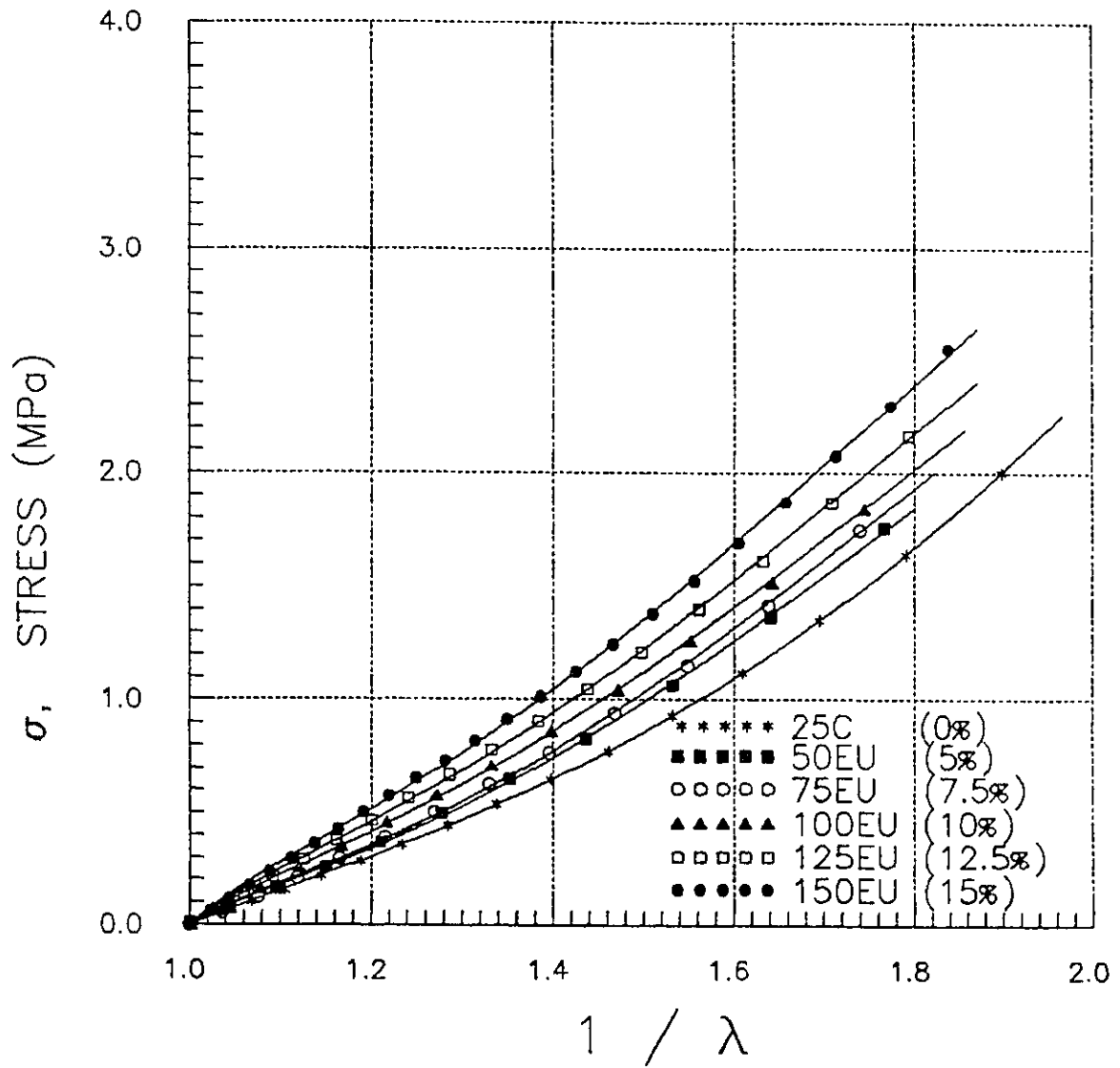


Figure 4.31 Compression tests on type C PUR based elastomer specimens filled with Eucalin at different volumetric loadings.

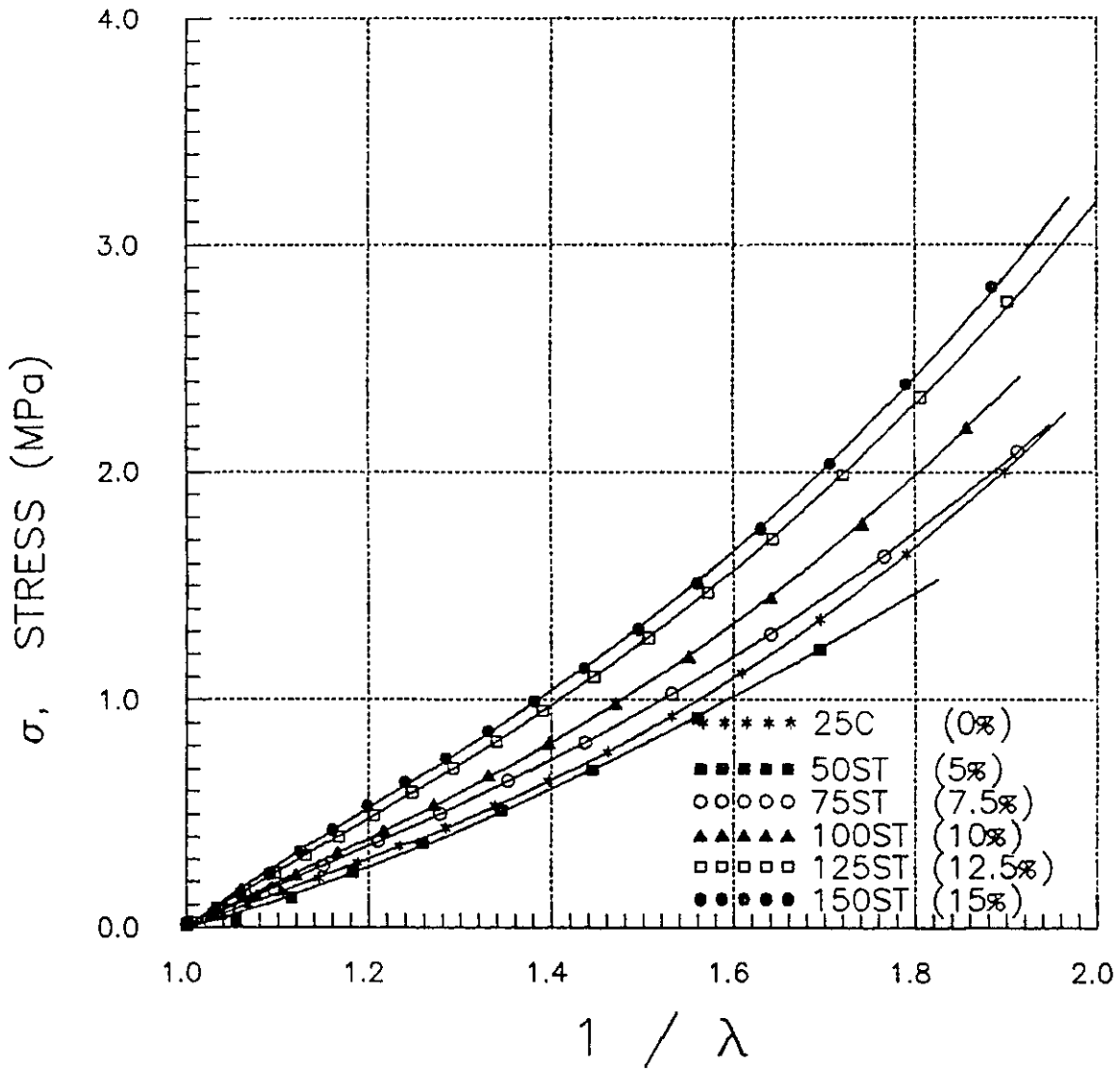


Figure 4.32 Compression tests on type C PUR based elastomer specimens filled with Sillitin/Titanox at different volumetric loadings.



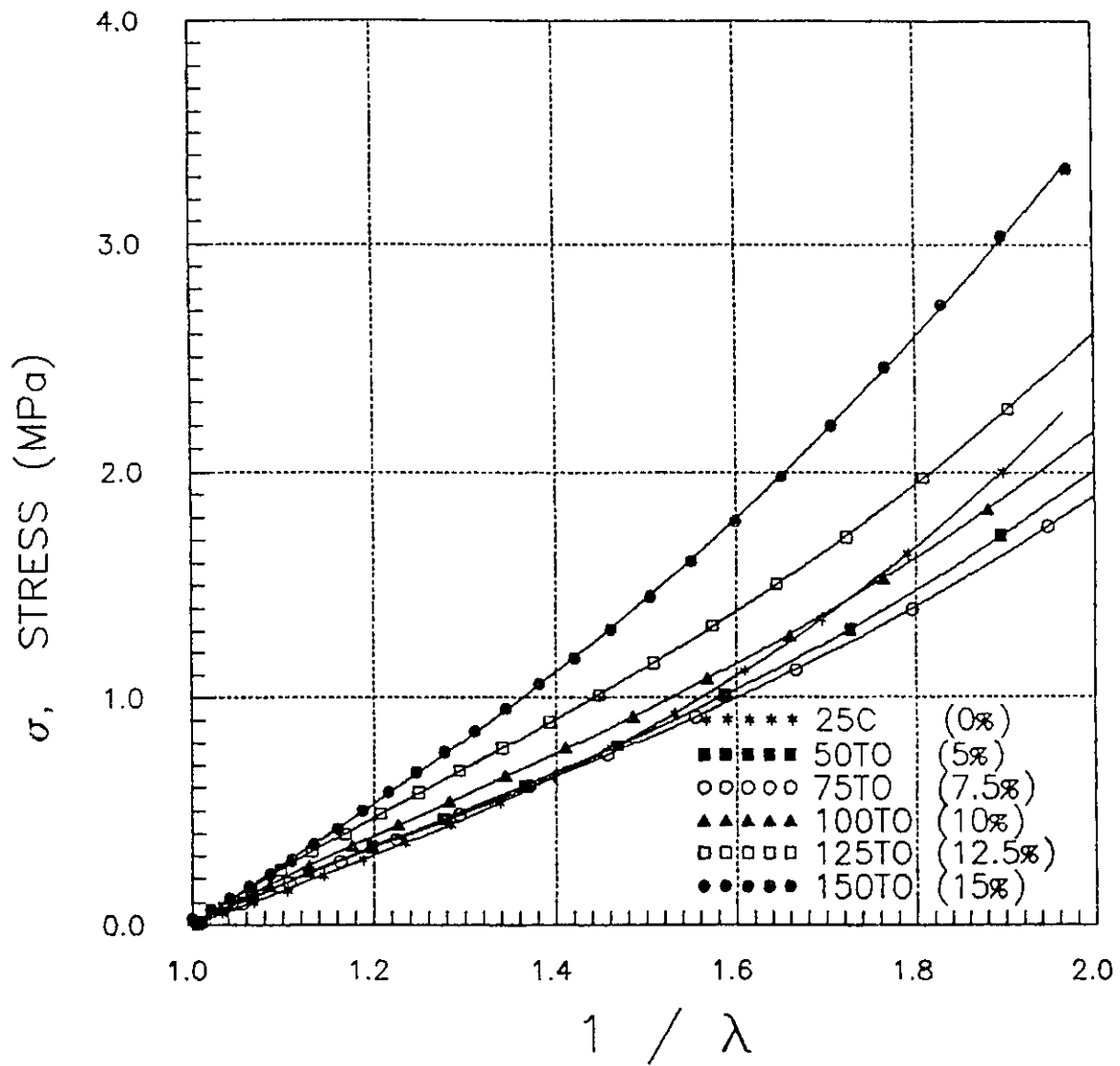
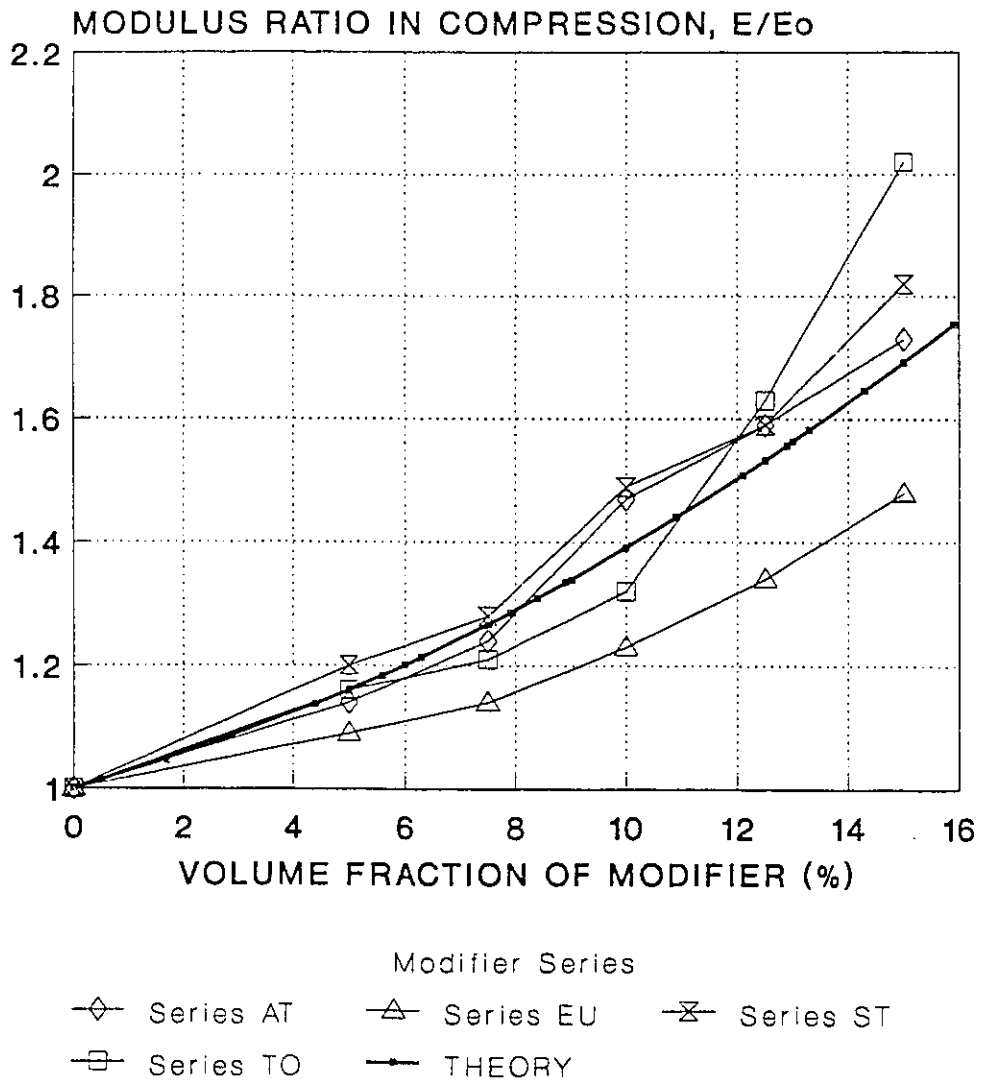


Figure 4.33 Compression tests on type C PUR based elastomer specimens filled with Tomlinite at different volumetric loadings.



Theoretical curve derived from the work of Guth [133]

Figure 4.34 Elastic modulus ratio in compression for filled PUR based elastomers as a function of volumetric loading for different filler types.

#### 4.4.4.2 Compression set

Results from tests to evaluate the compression set of filled elastomers are (Tab. 4.20) indicate that no relation exists between the degree of set and the amount of loading. However, as a general rule, filled polymers have a greater degree of set than unfilled polymers [102]. For example, results obtained for filled elastomers have on average 2.5 times greater set than unfilled elastomer (e.g. 7% set vs 2.7% set for unfilled elastomers). Eukalin filled elastomers are observed to have a lower average degree of compression set in comparison with the other elastomers (e.g. 3.7% set EU vs. 7.8%, 8.0% & 8.6% for AT, TO & ST) and it was also seen to interact the least with the polymer matrix, (least value of the swelling coefficient, C, Table 4.17). Hence this filler least affects the compression set of the filled elastomer in comparison to the other fillers.

Table 4.20			
COMPRESSION SET OF FILLED PUR ELASTOMERS			
Series	% Set	Series	% Set
50AT	8.6	50ST	0.5
75AT	9.9	75ST	13.3
100AT	7.7	100ST	7
125AT	6.4	125ST	9.5
150AT	6.2	150ST	12.7
50EU	8.2	50TO	7.8
75EU	2.8	75TO	8.3
100EU	2.3	100TO	9.2
125EU	2.3	125TO	8.2
150EU	3.0	150TO	6.6

#### 4.4.5 SPECTROSCOPIC ANALYSIS

##### 4.4.5.1 Infrared (IR) Spectroscopy

The results from the IR analysis of mixtures of PUR and Tomlinite lignin presented below, are taken from a parallel study whose results are presented elsewhere [134]. The following description presents the most salient aspects of this work with respect to the IR analysis of PUR-L mixtures.

Figure 4.35 shows the spectra for lignin (Tomlinite), unfilled PUR samples and PUR containing 10% (wt.) of lignin. The IR spectra were quite diffuse due to the inherent complexity of the PUR elastomers being studied, however it is evident that the unfilled PUR elastomer spectra is one which depicts a PUR [135,136].

In the case of filled PUR elastomer specimens, the spectra are more difficult to interpret due to the fact that many groups from either PUR or lignin absorb in the same regions and others disappear because of the interferences which occur in the spectrum. Consequently, it was not possible to distinguish differences in spectra of filled PUR samples having different lignin contents.

A comparison made between PUR and a lignin filled PUR elastomer with a 10% lignin content suggests that chemical interaction between components does not occur.

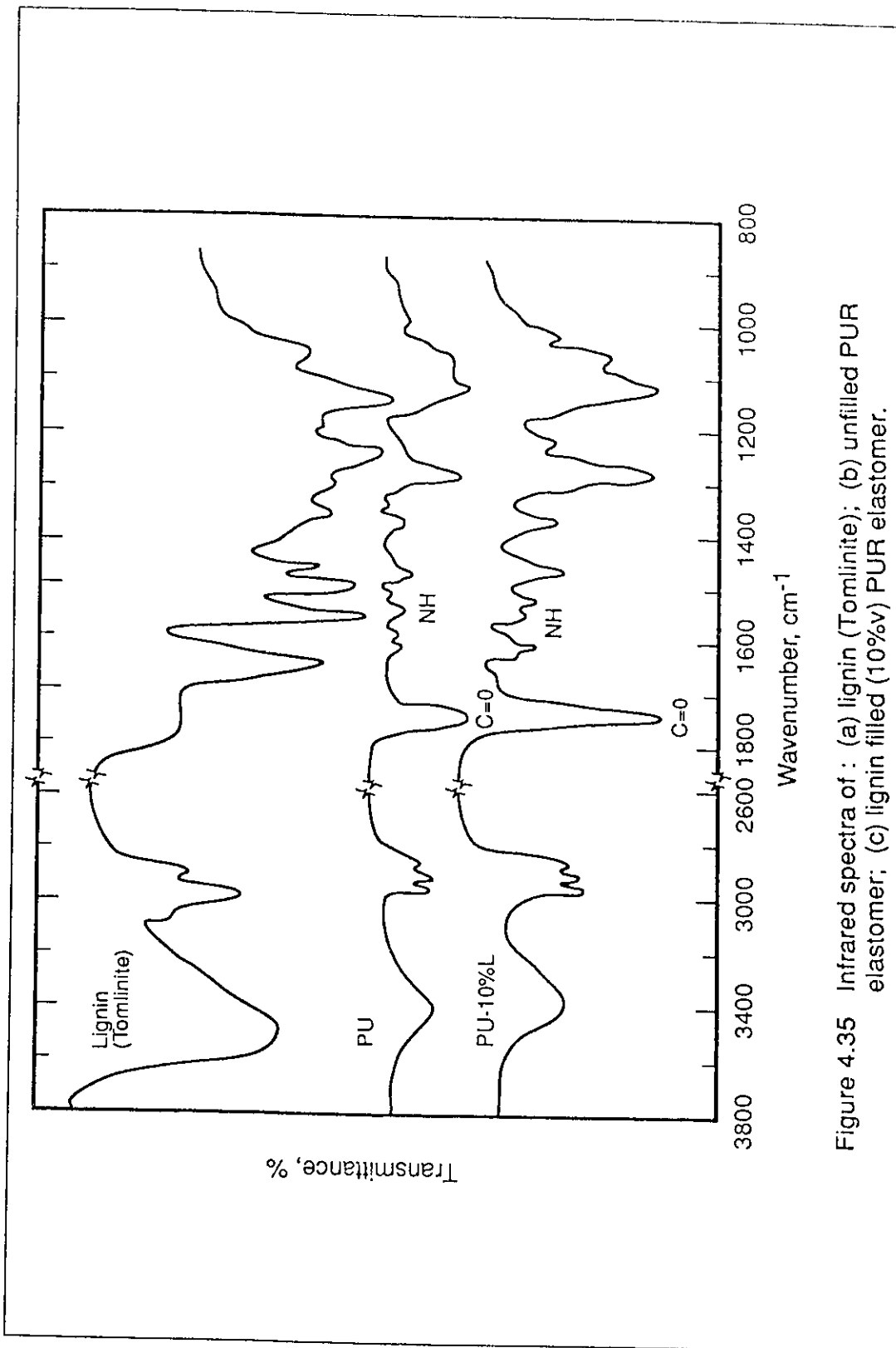


Figure 4.35 Infrared spectra of : (a) lignin (Tomlinite); (b) unfilled PUR elastomer; (c) lignin filled (10%) PUR elastomer.

#### 4.4.5.2 CP-MAS NMR

Results from CP-MAS NMR spectra of (a) Tomlinite lignin, (b) filled PUR elastomer (30% wt.) and (c) unfilled PUR elastomer specimens, presented in figure 4.36, have been previously reported elsewhere [107]. The more significant results of this study are briefly described below.

The spectrum of lignin is assignable according to the literature [137], the most important signals being those of the aromatic methoxy carbons (56 ppm) and those of carbons 3 and 4 of the aromatic ring, where the methoxy groups are bonded (149 ppm).

For the same contact time (2ms), the PUR does not exhibit any carbon spectrum. However, by increasing the contact time, a spectrum is obtained as in figure 4.36 (c), consisting of two main groups of signals. The quasi triplet around 75 ppm is assignable to carbons directly bonded to oxygen atoms, and in the soft segment they will be the methylene and methine carbons. At 18 ppm, the signal can be assigned to the carbon-carbon methyl group of the polyether. This spectrum has been obtained with a contact time of 20 ms.

The best spectrum for lignin was obtained at 2 ms contact time and at contact times longer than 25 ms, the signals tend to disappear. In the case of the PUR sample, a maximum signal is obtained at 20 ms contact time with a gradual decay in the signal beyond this point. Hence the spectra of a mixture of both the elastomer and lignin components would only be possible in a range between 2 and 25 ms since above 2 ms lignin signals start decaying whereas the PUR signals

start appearing. At 10 ms contact time both signals appear as shown in figure 4.36 (b).

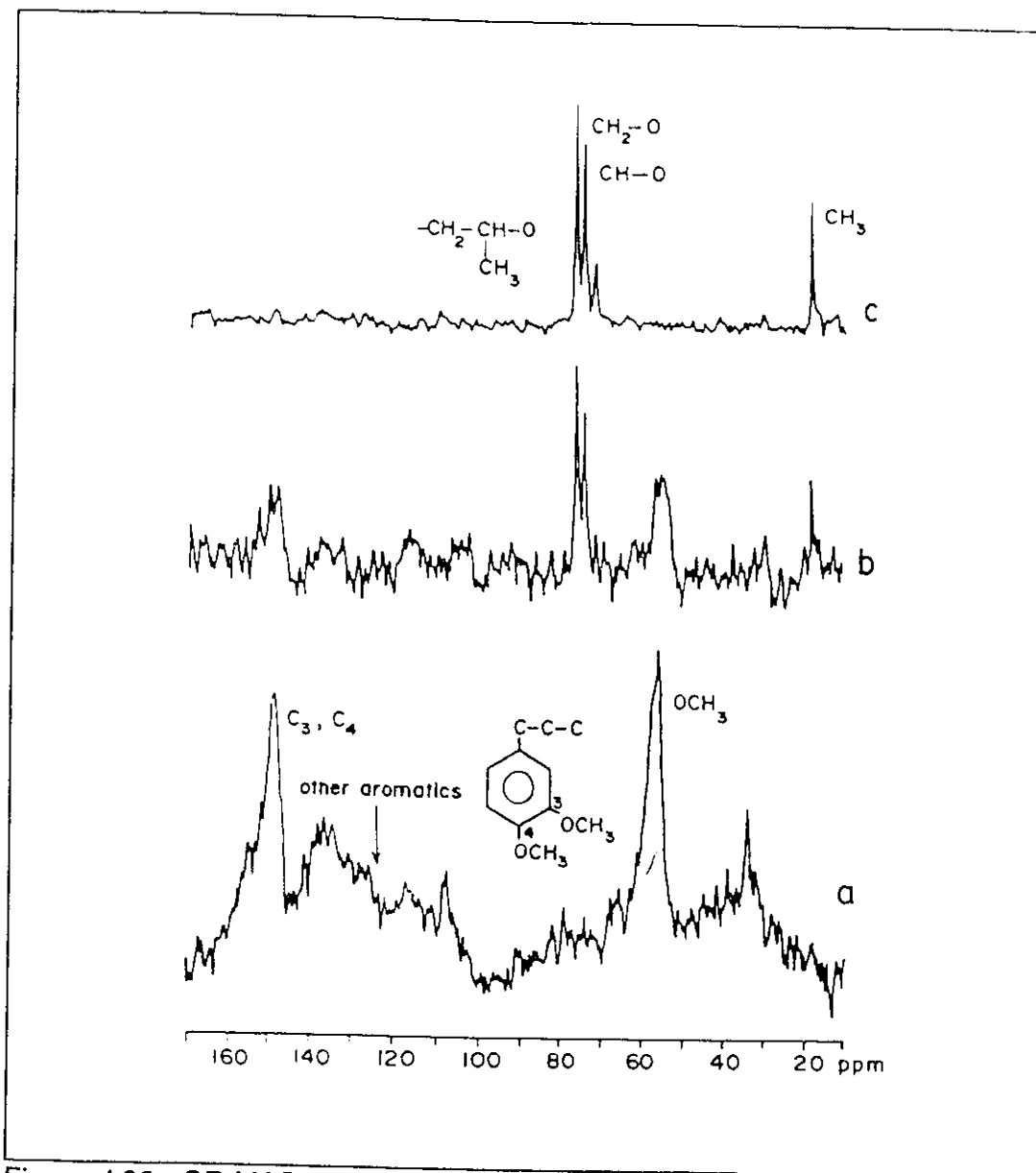


Figure 4.36 CP-MAS NMR spectra of: (a) lignin (TOMLINITE), 100scans, 2ms contact time; (b) polyurethane lignin formulation (30% lignin by weight), 200 scans, 10 ms contact time; (c) polyurethane, 1500 scans, 20 ms contact time.

Figure 4.37 shows the evolution of magnetization for the PUR signals as a function of contact time. From the slope of this curve at longer contact times [138] one can reasonably conclude that  $T_{1\rho H}$  remains constant at 70 ms for both PUR and the mixture which indicates that there is definitely a phase separation which exists between PUR and lignin.

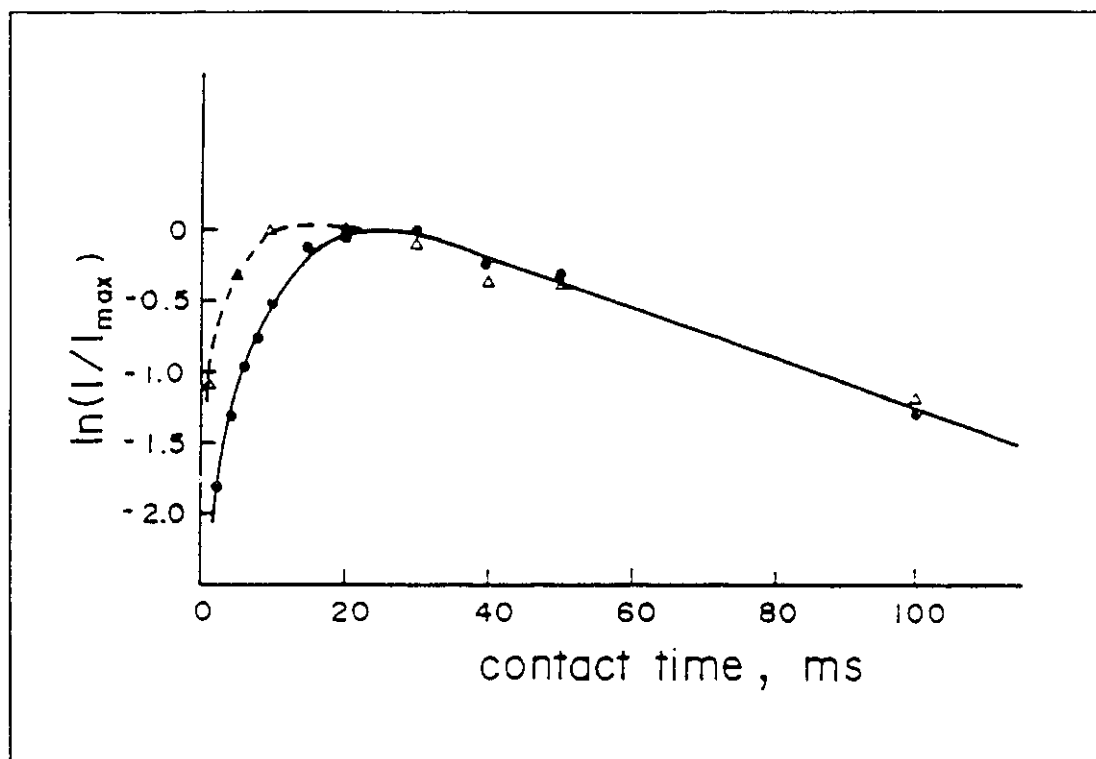


Figure 4.37 Signal intensity at 76 ppm for the polyurethane as such [ $\Delta$ ] and blended with kraft lignin (TOMLINITE) [ $\bullet$ ] against contact time.



#### 4.4.6 THERMAL ANALYSIS OF FILLED ELASTOMERS

Results from dynamic mechanical analysis (DMA) of unfilled and filled elastomers are shown in figure 4.38 in which  $\tan \delta$  for various PUR lignin filled elastomer combinations is given in relation to the temperature. The different curves represent the value of the damping coefficient ( $\tan \delta$ ) as the experiment proceeds through the glass transition temperature of the given elastomer. The value of  $\tan \delta$  reaches a maximum at the  $T_g$  of the specimen.

It is worthwhile to note that the  $T_g$  obtained from results of DMA on the unfilled specimen is higher than that determined using the DSC method. This is to be expected [139] since the frequency at which the DMA functions is higher than that of the DSC (e.g. 0.1 - 80 Hz vs  $\ll 1$  Hz), a consequence of which causes the glass transition temperature to move to higher temperatures.

Fillers are known to often decrease the damping coefficient in proportion to the amount of filler in the elastomer [102]. In this instance, the addition of filler is shown to either decrease or increase the coefficient depending on the type of filler incorporated in the elastomer. For example, there is a slight decrease ( $<1\%$ ) in  $\tan \delta$  for elastomers filled with increasing amounts of Eucalin lignin, whereas an increase can be observed for the value of  $\tan \delta$  of Sillitin/Titanox filled specimens. The relative change in  $\tan \delta$  for specimens having the same volumetric loading is also relatively small (i.e. 2.2% for EU series; 12.4% for ST series ), however the comparative increase in  $\tan \delta$  for ST specimens is significantly larger.

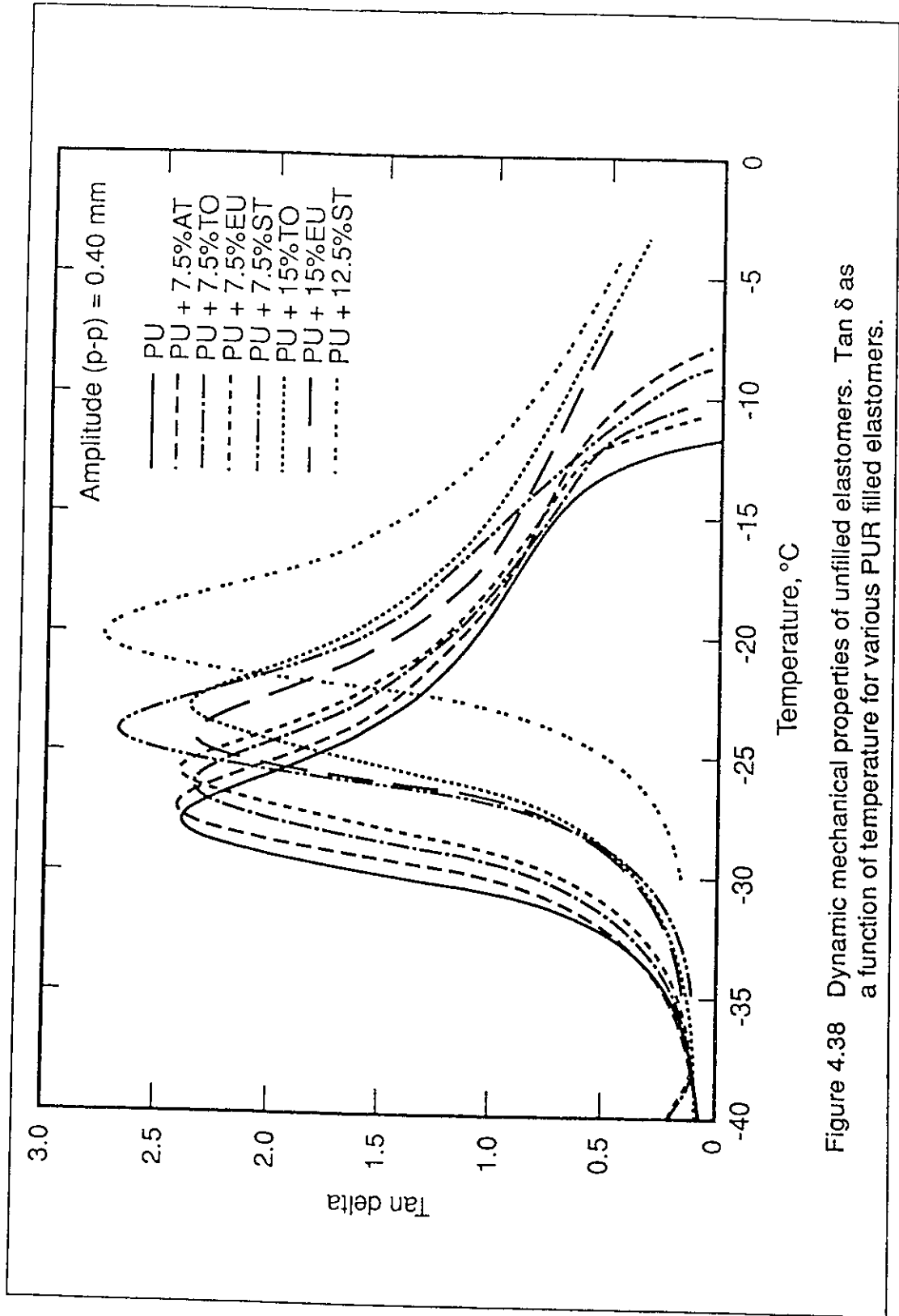


Figure 4.38 Dynamic mechanical properties of unfilled elastomers.  $\tan \delta$  as a function of temperature for various PUR filled elastomers.

This suggests that there exists a greater degree of polymer-filler interaction for ST filled specimens in comparison to the lignin filled specimens.

This may more clearly be illustrated by considering the effect of fillers on the  $T_g$  of the elastomer. Figure 4.39 is a plot of the shift in  $T_g$ , measured in degrees centigrade, as a function of the volumetric loading for different filler types. It shows that the incorporation of fillers shifts the  $T_g$  to higher temperatures in direct proportion to the amount of filler in the elastomer. Furthermore, this phenomenon is a function of the type of filler, and the degree of shift for any filler type may be characterized by the slope of the line of the shift-volume fraction function. This relationship is suggestive of a similar phenomenon observed for swollen filled elastomers discussed in section 4.4.1 in which the restriction in swelling is related to the quantity of filler in the elastomer and the degree to which the elastomer can swell. The extent of restraint is related to the coefficient  $C$ , which Lipatov [129] suggests could be used to characterize the adhesion of the elastomer to the particulate surface.

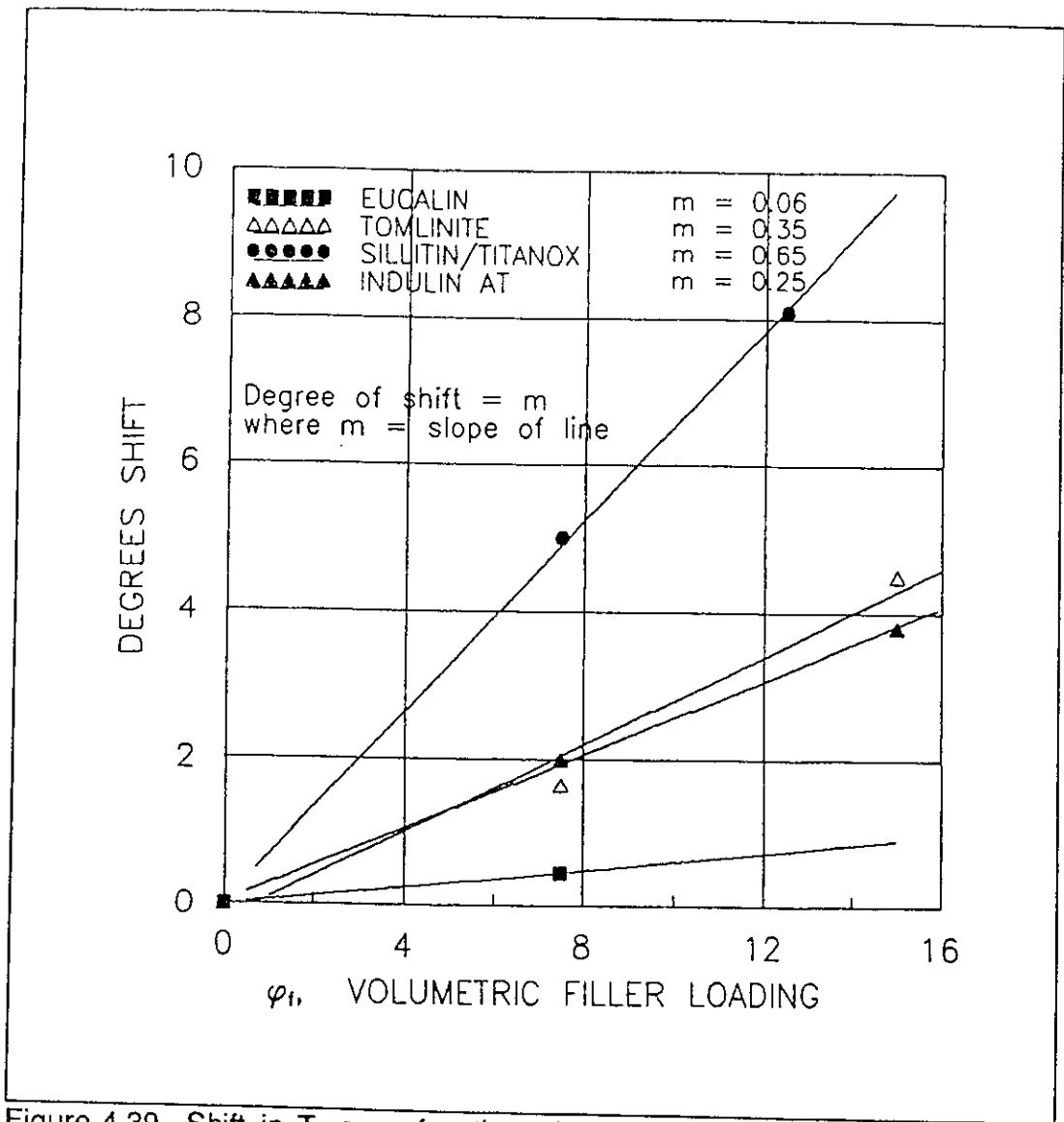


Figure 4.39 Shift in  $T_g$  as a function of volumetric filler loading for various fillers.

If values of the coefficient  $C$  are plotted as a function of the degree of shift, as shown in figure 4.40 below, there is seen to be a general correlation between values of these two variables. Hence for filled elastomers, the same phenomenon which restricts swelling also causes a shift in the  $T_g$ .

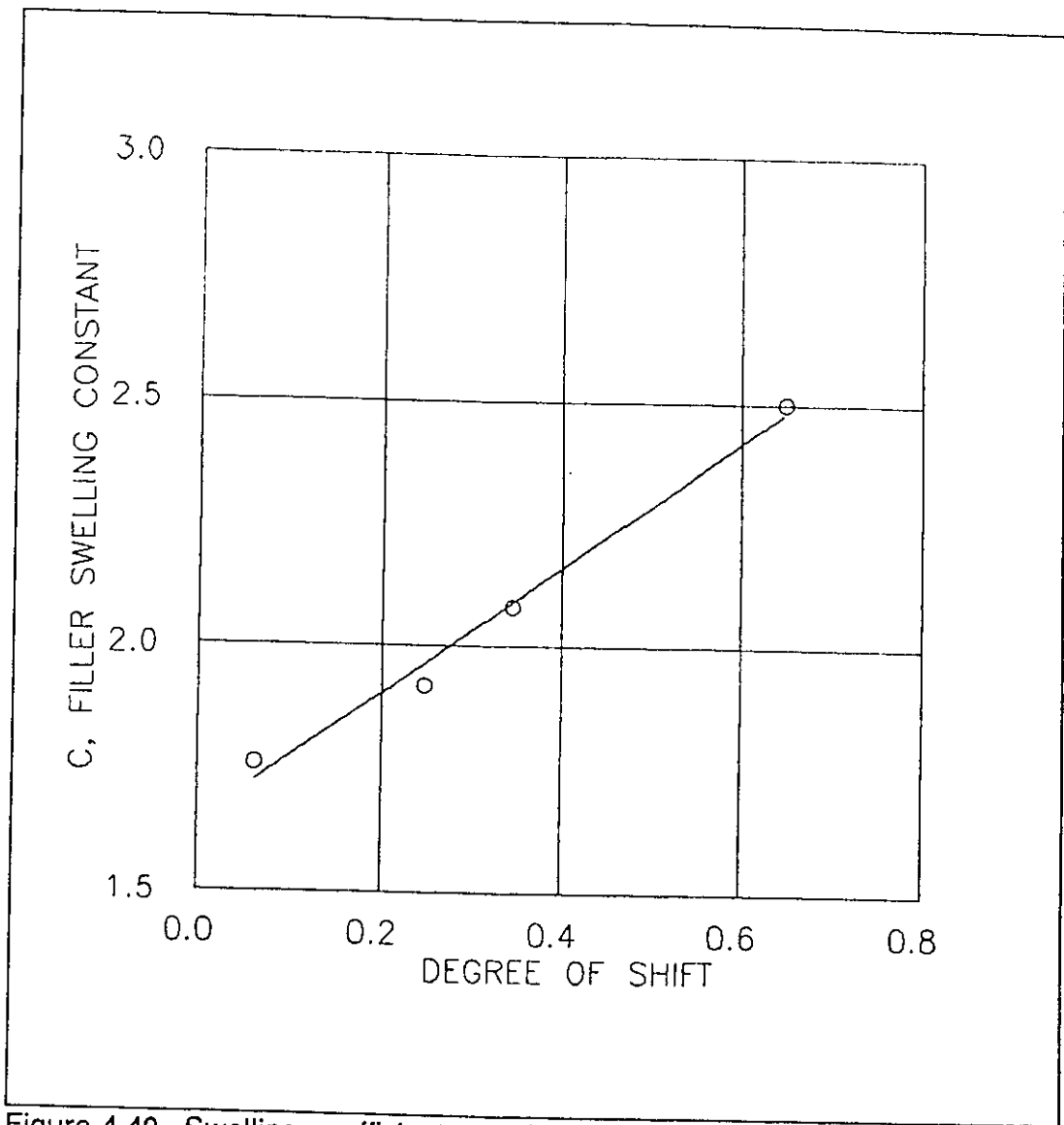


Figure 4.40 Swelling coefficient as a function of degree of shift.

Nielsen has suggested that the shift is largely due to the differences in specific surface area or particle size [102]. A plot of C as a function of the maximum packing fraction is shown (figure 4.41) to produce a useful trend.

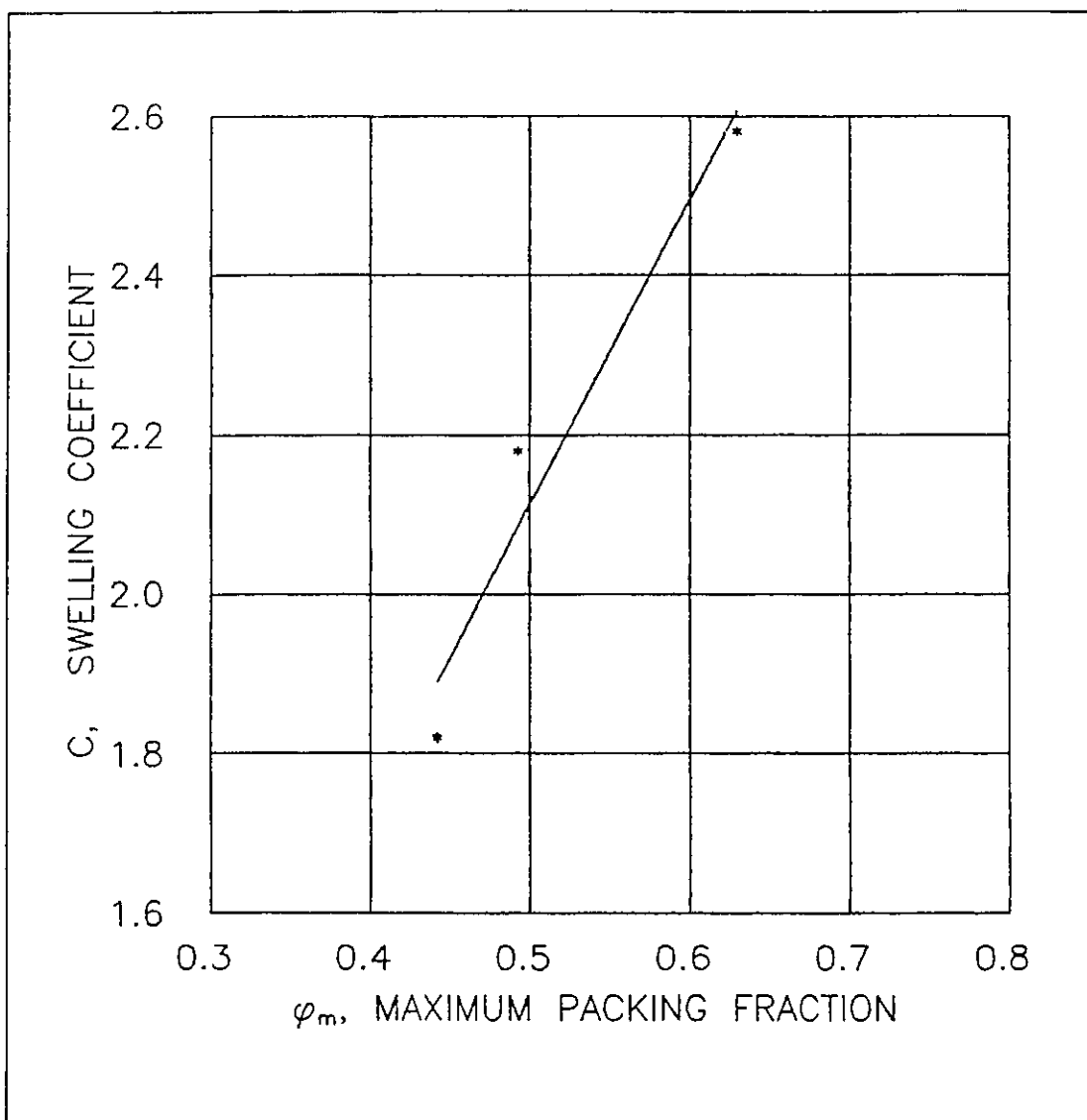


Figure 4.41 Filler characterization: swelling coefficient as a function of maximum packing fraction.

## 4.5 ANALYSIS OF THE SURFACE PROPERTIES OF PUR ELASTOMERS & PARTICULATE FILLERS

### 4.5.1 SURFACE PROPERTIES OF THE ELASTOMER MATRIX

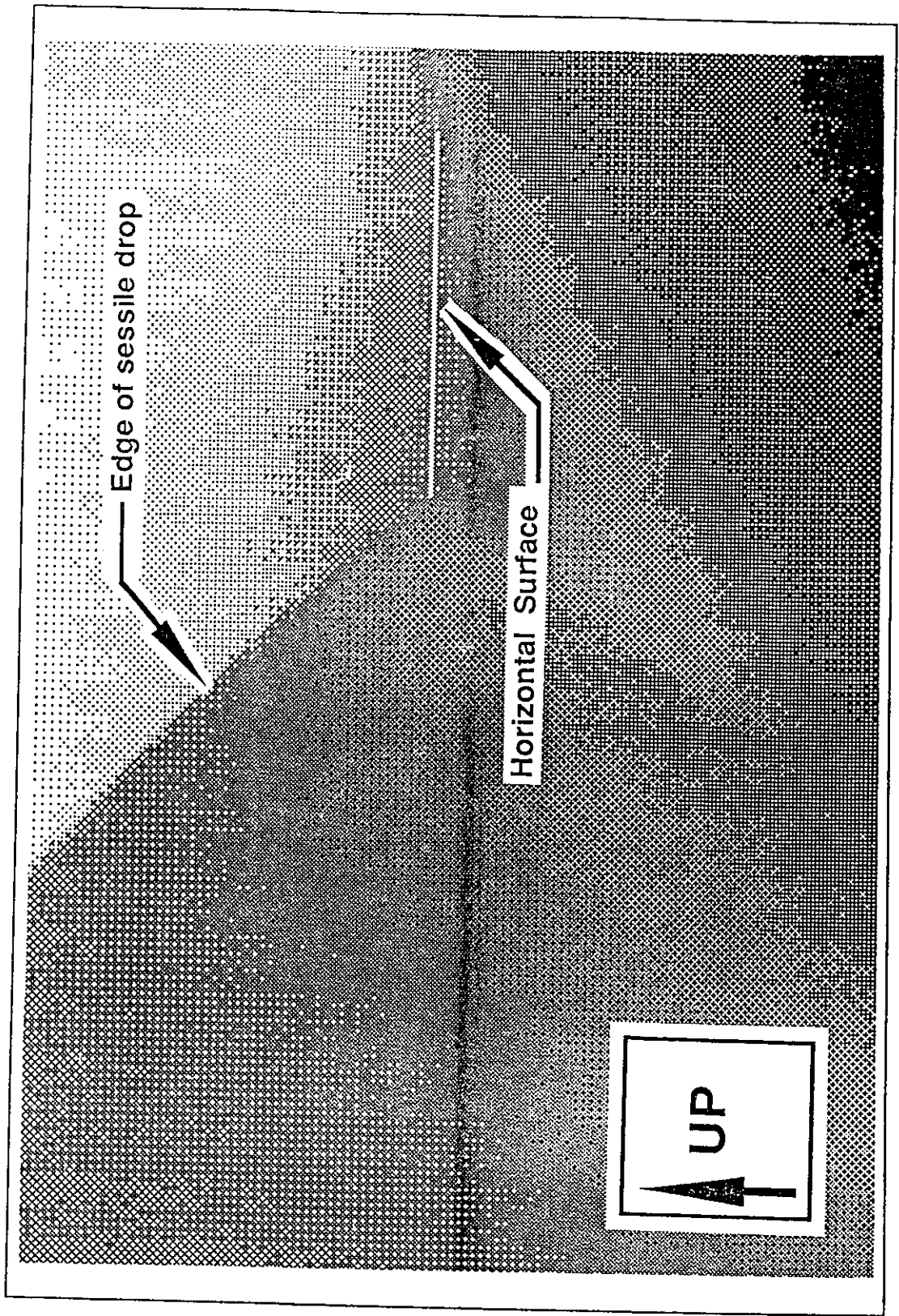
The surface energy properties of selected elastomer formulations were determined using contact angle measurements obtained by the technique described in section 3.4.6.1. The contact angle of a drop of wetting liquid on the surface of the unfilled PUR elastomer was measured from the digitized video image. An example of such an image is shown in figure 4.42 which depicts the profile of a drop of water magnified 100 times, 10 seconds after being deposited on the surface of the elastomeric matrix.

The straight line which runs parallel to the edge of the image represents the interface between the sessile drop and the surface of the elastomer matrix. The contact angle is the angle between a line perpendicular to the profile of the drop at the liquid matrix interface and the line representing the interface.

A continuous recording of the event was found to be quite useful from the point of view of being able to extract information of a given event at prescribed times or time intervals. The events can also be recorded using photographic techniques, however the task is logistically more complicated by virtue of the number of operations required at the beginning of a test sequence. It was also found that consistent results were more easily obtained using the video camera technique.

---

Figure 4.42 Digitized image (100X) of a sessile drop of water on the surface of a PUR elastomer 10 seconds after contact with the surface.





Results from tests on two similar PUR elastomer formulations (15B & 28C) are given in Table 4.21. The data, reduced from readings extracted off of profiles of at least 24 drops, are plotted according to equation 3.4 on figure 4.43. The figure shows the cosine of the contact angle as a function of the logarithm of the liquid-vapour surface energy of the wetting liquid for the two formulations.

Table 4.21			
RESULTS FROM CONTACT ANGLE MEASUREMENTS ON PUR ELASTOMERS USING THE SESSILE DROP TECHNIQUE			
Wetting Liquid	Surface Energy of Liquid $\gamma_{sv}$ mPa·m	Average Contact Angle	
		TF 28C	TF 15B
Acetic acid: water			
0:100	72.8	86.2	80.3
5:95	62.3	79.3	76.1
10:90	56.3	73.1	68.9
20:80	49.3	64.8	59.7
30:70	44.9	56.4	51.9
70:30	38.4	43.5	28.3

The values for the critical surface energy of the polymer,  $\gamma_{c(p)}$  and the interaction parameter,  $b$ , were determined graphically from the plot in figure 4.43. The value of  $\gamma_{c(p)}$  was evaluated by determining the intercept of the x-axis at  $\cos \theta$  equal to 1. The interaction parameter is simply the slope of the straight line drawn through the data points.

The solid-vapour surface energy,  $\gamma_{SV(p)}$ , is determined from the following equation:

$$\gamma_{SV(p)} = \left( b_p \cdot \exp\left[\frac{1}{b_p} - 1\right] \right) \gamma_{c(p)}$$

Equ. 4.17 [63]

where:

- $\gamma_{SV(p)}$  = Solid/Vapour surface energy of elastomer (mPa.m);
- $b_p$  = extent of interaction between wetting liquid and elastomer;
- $\gamma_{c(p)}$  = critical surface energy for wetting elastomer (mPa.m).

Values obtained for  $\gamma_{SV(p)}$ ,  $b_p$ , and  $\gamma_{c(p)}$  for formulation 28C are given in Table 4.22 below.

Table 4.22 RESULTS FROM ANALYSIS OF CONTACT ANGLE DATA FROM PUR ELASTOMERS		
Critical Surface Energy for Wetting, $\gamma_{c(p)}$ mPa·m	Extent of Interaction $b_p$	Solid/Vapour Surface Energy, $\gamma_{SV(p)}$ mPa·m
29.1	1.048	29.1

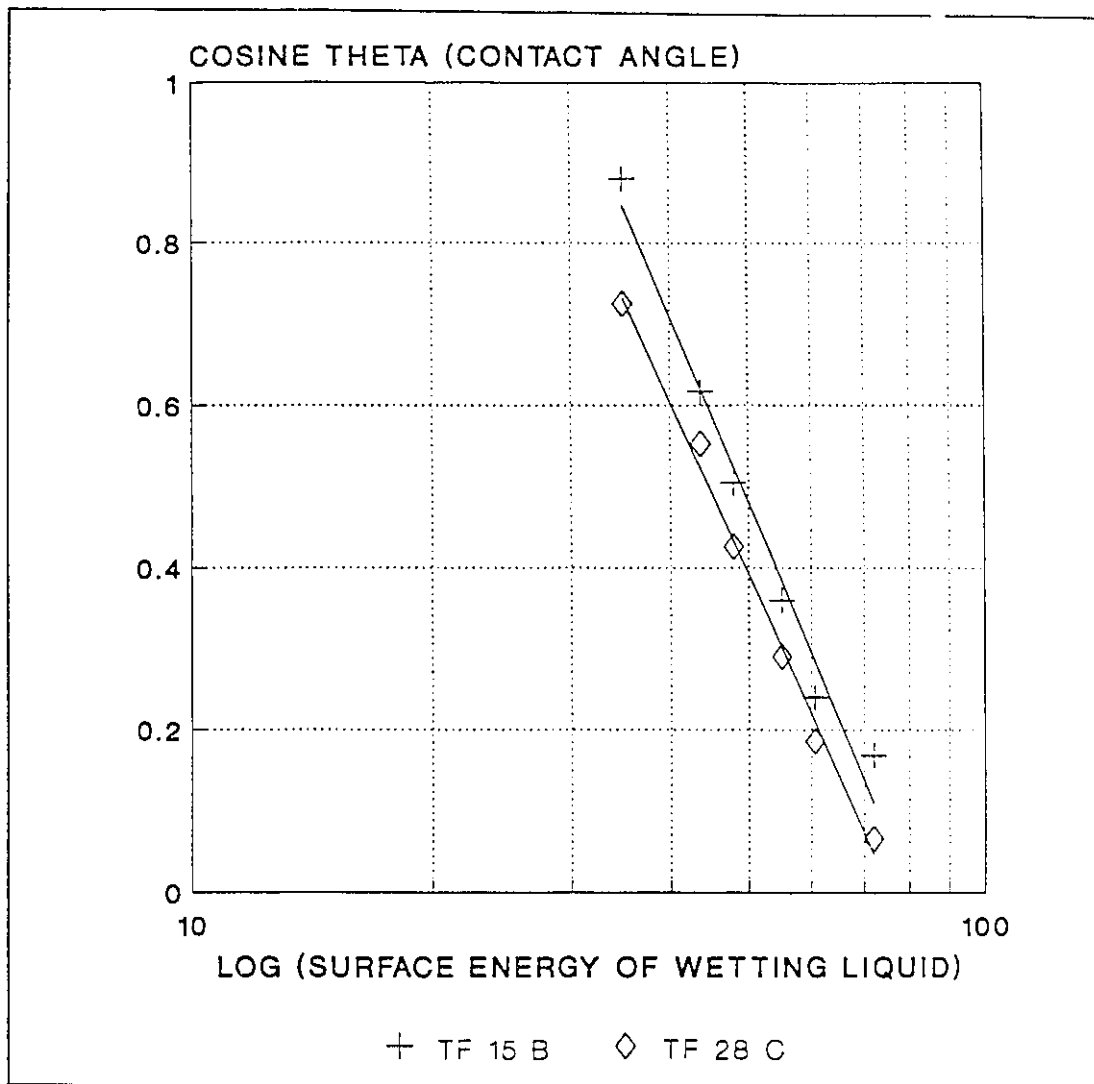


Figure 4.43 Contact angle of a wetting on the surface of a PUR based elastomer substrate as a function of the surface tension of the wetting liquid.

#### 4.5.2 SURFACE PROPERTIES OF PARTICULATE FILLERS

The Crowl Wooldrige method [109] for measuring the contact angle of pigments and fillers was used to assess the surface properties of the various particulate fillers being investigated. Use of this method enables the rate of rise of a known liquid through a bed of packed particles to be determined such that the contact angle can be evaluated based on the Washburn equation [111].

A plot of the reduced data is shown in figure 4.44 in which the cosine of the contact angle, calculated using equation 3.5, is given in relation to the logarithm of the surface energy of the wetting liquid. At least 12 trials were used for each determination. In the case of the Sillitin/Titanox filler, it was not possible to accurately assess the surface properties of this filler in the laboratory due to the inability to reproduce evenly packed particle columns. Values for this filler were taken from work by Cheever and Ulciny [110] whose work is shown in figure 4.45. The data represents contact angle data obtained using the same technique described above for pigments of clay and various grades of titanium dioxide. Both figures were analyzed graphically to extract the values of  $\gamma_{c(f)}$  and the interaction parameter,  $b_i$ , and the results are given in Table 4.23.

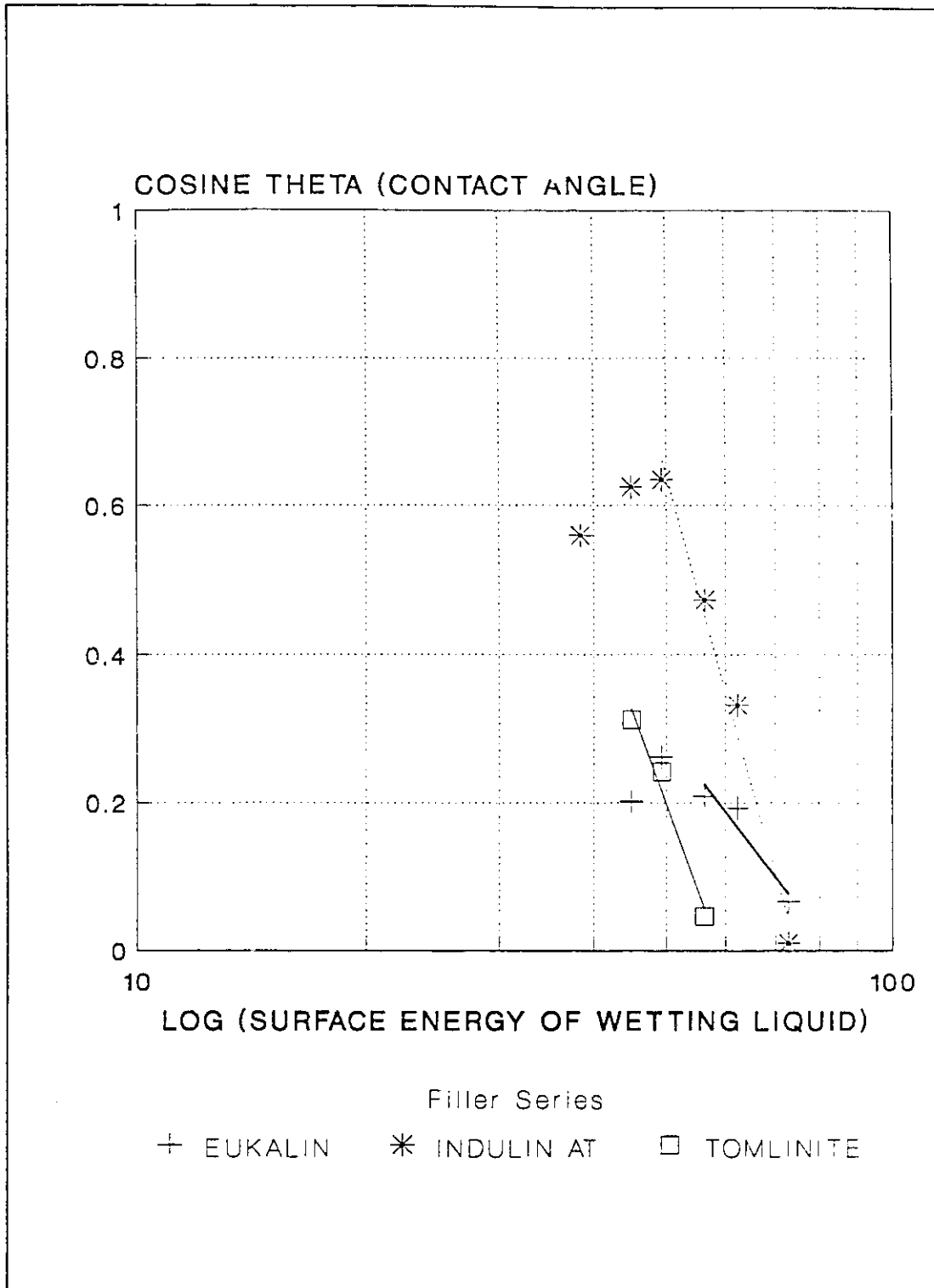


Figure 4.44 Contact angle analysis of lignin fillers. Cosine of the contact angle as a function of the surface energy of the wetting liquid.

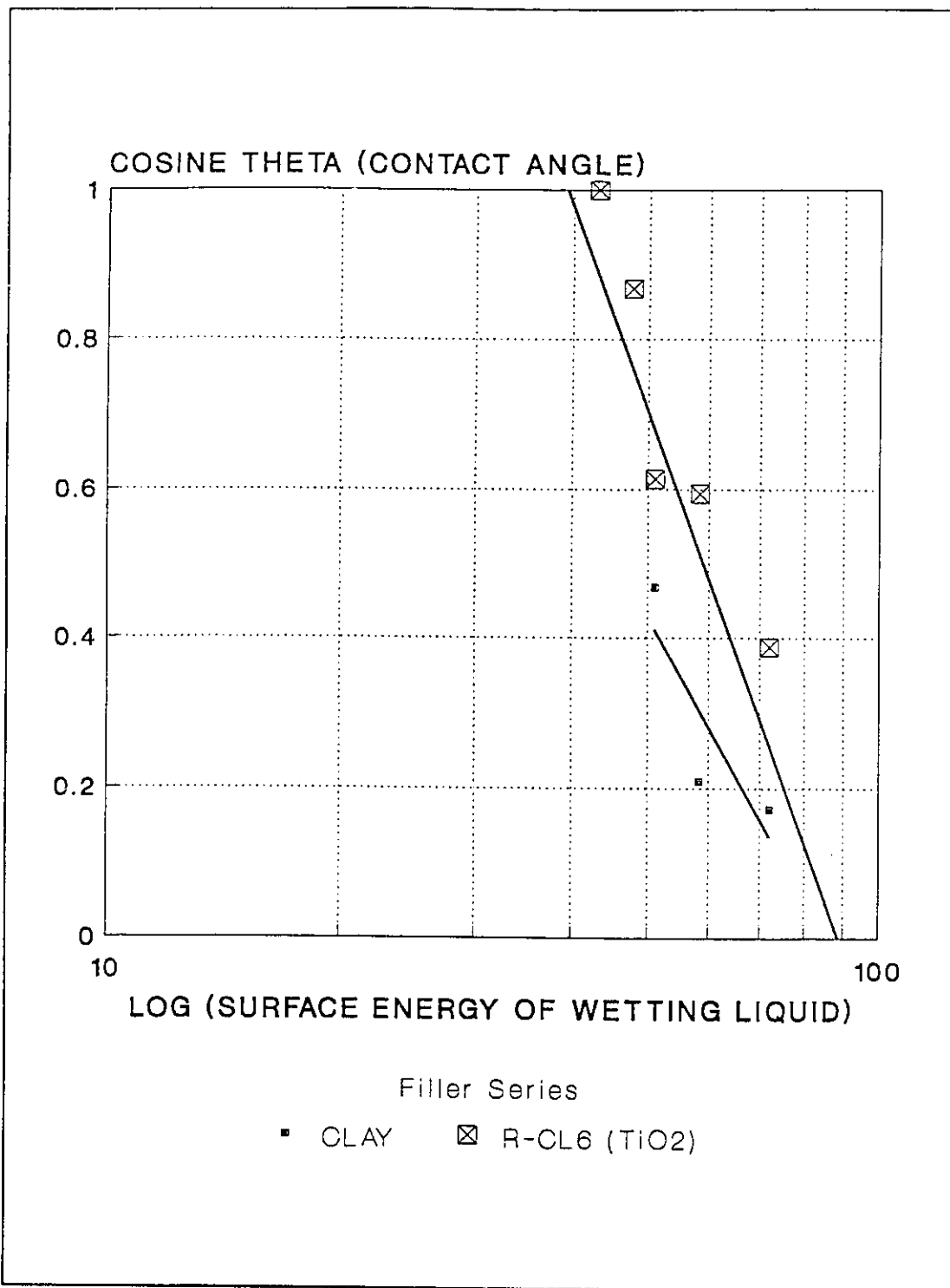


Figure 4.45 Contact angle analysis of selected pigments. Cosine of the contact angle as a function of the surface energy of the wetting liquid [110].

Table 4.23 RESULTS FROM ANALYSIS OF CONTACT ANGLE OF PARTICULATE FILLERS			
Filler	Interaction parameter $b_f$	Critical surface energy $\gamma_{c(f)}$	Solid-vapour surface energy $\gamma_{sv(f)}$
Eucalin	0.844	14.1	17.5
Indulin AT	1.70	40	25.9
Sillitin/Titanox	1.56	40	44.2
Tomlinite	1.53	25.2	39.4

Based on this data, an analysis was performed to determine the work of adhesion,  $W_a$ , and the work of cohesion,  $W_c$ , using the following equations:

$$\begin{aligned}
 b &= \sqrt{b_p \cdot b_f} & (i) \\
 &\vdots \\
 \Omega &= \sqrt{\frac{1}{b} \cdot \exp\left(1 - \frac{1}{b}\right)} & (ii) \\
 &\vdots \\
 W_A &= 2 \cdot \Omega \sqrt{\gamma_{sv(f)} \cdot \gamma_{sv(p)}} & (iii) \\
 &\vdots \\
 W_C &= 2 \cdot \gamma_{sv(p)} & (iv)
 \end{aligned}$$

Equ. 4.18 [61]

The results of this analysis are given in Table 4.24.

Table 4.24								
DEGREE OF INTERACTION BETWEEN FILLER & POLYMERIC MATRIX USING SURFACE ANALYSIS TECHNIQUES								
F	$b_i$	$b_p$	b	$\Omega$	$\gamma_{sv(f)}$	$\gamma_{sv(p)}$	$W_A$	$W_C$
EU	0.844	1.048	0.940	0.999	14.3	29.1	40.8	58.2
TO	1.53	1.048	1.270	0.987	45	29.1	71.4	58.2
AT	1.70	1.048	1.335	0.981	33.2	29.1	61.0	58.2
ST	1.56	1.048	1.279	0.986	43.4	29.1	70.1	58.2
F: Filler type; EU: EUCALIN ; TO: TOMLINITE; AT: INDULIN AT; ST= SILLITIN/TITANOX								

The degree of interaction between filler and polymer may be assessed from the relative values of the work of adhesion and the corresponding values of the work of cohesion for the various filler polymer combinations. Fillers which have a value for the work of adhesion,  $W_A$ , which is smaller than the corresponding work of cohesion,  $W_C$ , are not considered to interact strongly with the polymer and consequently, are more likely to undergo interfacial failure when being stressed. Furthermore, these filler types do not contribute as significantly to the reinforcement of the matrix as fillers having values of  $W_A$  equal to or exceeding that of  $W_C$ .

In an effort to demonstrate the relationship between the degree of interaction and the mechanical properties of the filled elastomers, the results are analysed in terms of the tensile modulus  $E$ , and the equilibrium work of adhesion  $W_A$ , according to the method adopted by Lee [62]. Both these terms represent an amount of stored energy: mechanical energy stored per unit volume in the case of the tensile modulus and interfacial energy per unit area between the filler and



polymer in the case of the work of adhesion. Lee assumes that there exists a power-law relationship between both terms such that a logarithmic plot of the data should yield a straight line. Figure 4.46 shows a series of log-log plots of the modulus  $E$ , as a function of the work of adhesion at different volumetric loadings. The results indicate that values of modulus are proportional to the work of adhesion.

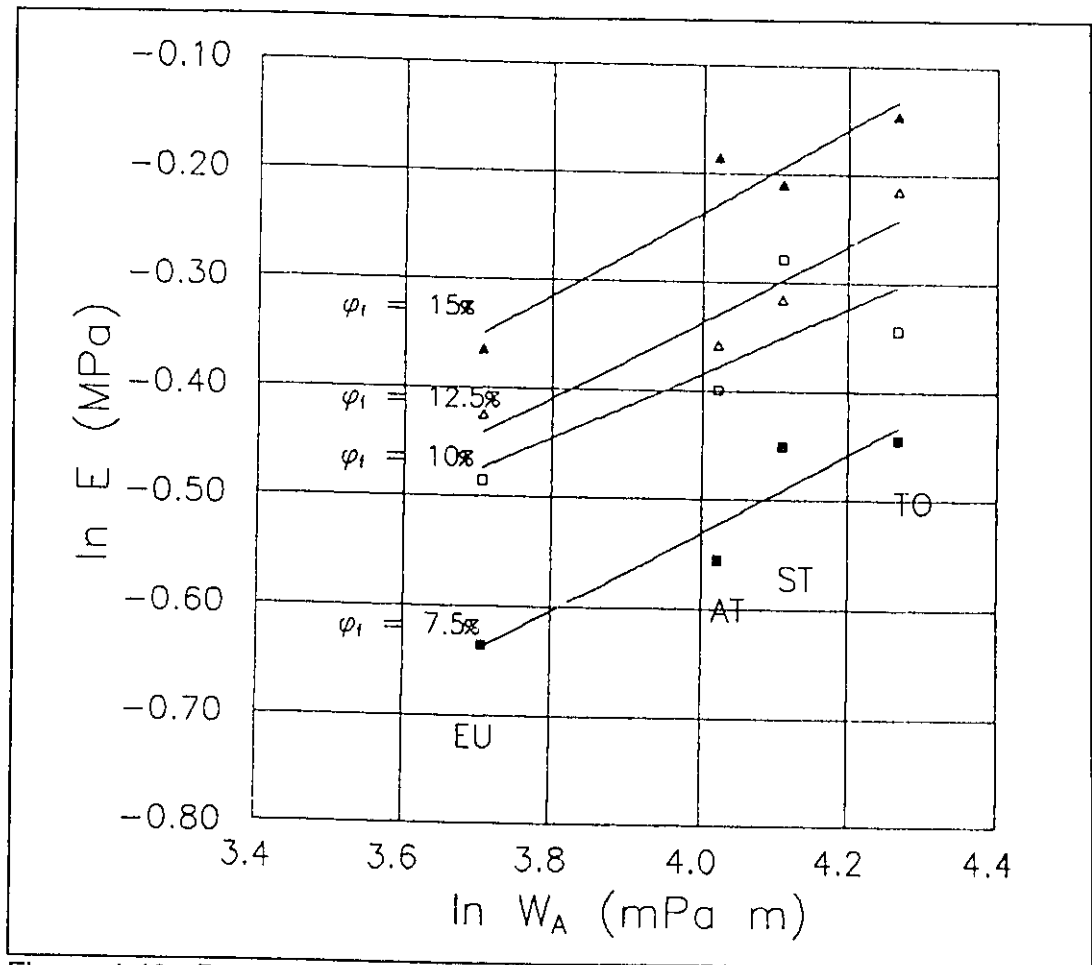


Figure 4.46 Dependency of the work of adhesion  $W_A$ , on the tensile modulus at different volumetric filler loadings.

#### 4.6 PERFORMANCE PROPERTIES

##### 4.6.1 TENSILE PROPERTIES

The tensile properties of the various types of sealants are summarized in Table 4.25 below. These properties were based on TB type tensile tests which were conducted on three different commercially produced two-part self leveling PUR based sealants (A1, A2, A3) as well as the ST and TO filled sealants. At least eight but in some cases up to twenty-one specimens were tested in each test series. The stress-strain characteristics of these sealants are shown in figure 4.47.

Table 4.25 TENSILE PERFORMANCE OF PUR SEALANTS		
Sealant Type	Extension at Failure (% gauge)	Engineering Stress at Failure (kPa)
A1	20	414
A2	145	909
A3	90	548
ST	80	753
TO	54	486

The inset figure more clearly illustrates the tensile properties of both ST and TO based sealants, which have essentially the same modulus as that of the A2 and A3 commercial sealants and a lower modulus than the A3 sealant. Higher modulus sealants often fail in adhesion due to excessive surface stresses at the sealant-substrate interface. This is the case for the A1 sealant which failed in

adhesion at a 20% extension. The other sealants failed in cohesion at much higher extensions and above the lower limit of 25% established earlier for such type of sealants.

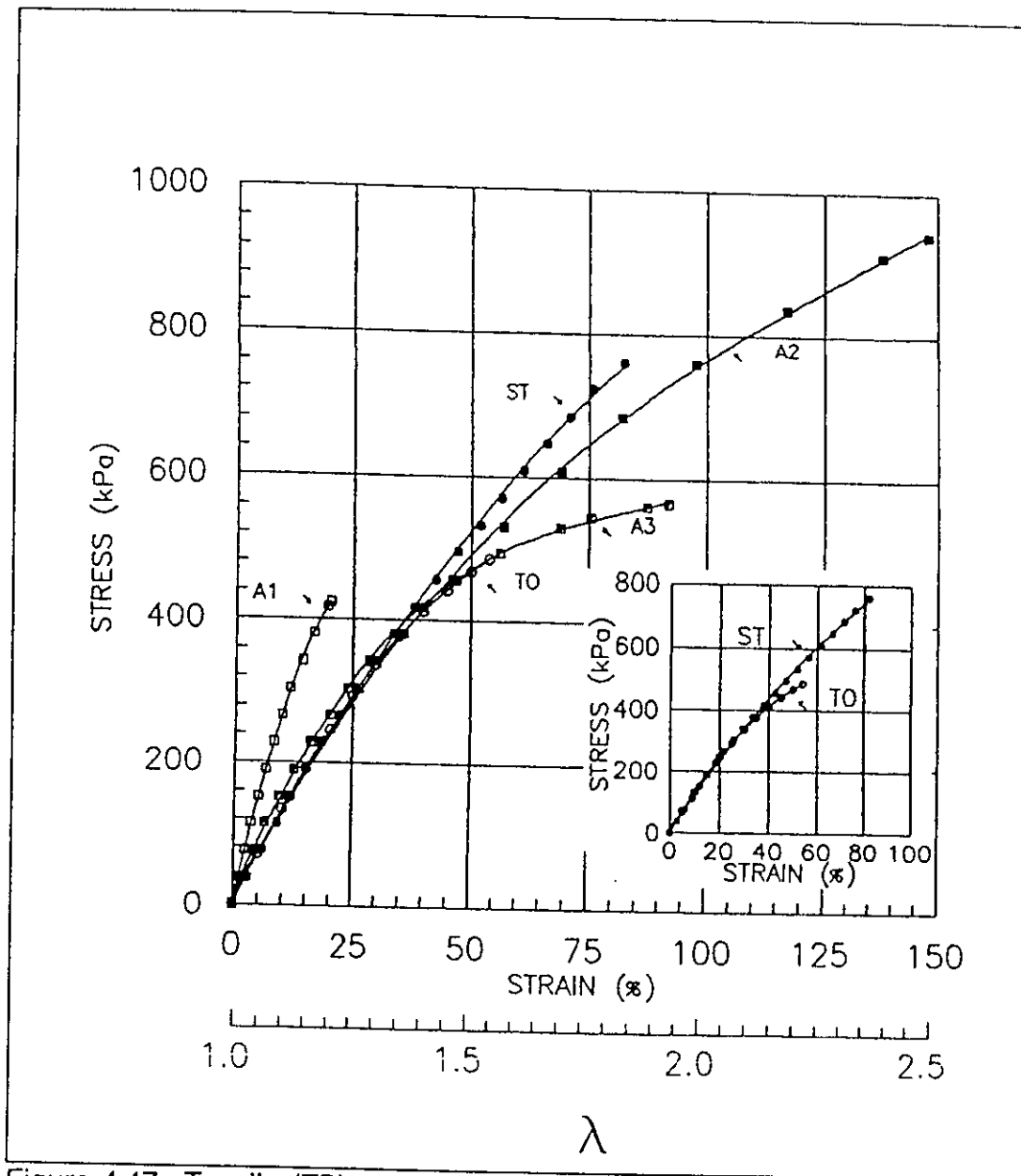


Figure 4.47 Tensile (TB) stress-strain characteristics of commercially based (A1,A2,A3) and filled (ST, TO) PUR based sealants.

#### 4.6.2 KARPATI PERFORMANCE TEST

The Karpati performance test was used to assess the long-term performance of the commercially based sealants (A1,A2,A3). The cured specimens were placed on hand-operated vices that imposed various extensions and compressions. The total movement ranged from  $\pm 25\%$  (+ % extension; - % compression) to  $\pm 80\%$  of the joint width (12.7 mm) in steps of 5 %. Triplicate specimens were used at each amplitude.

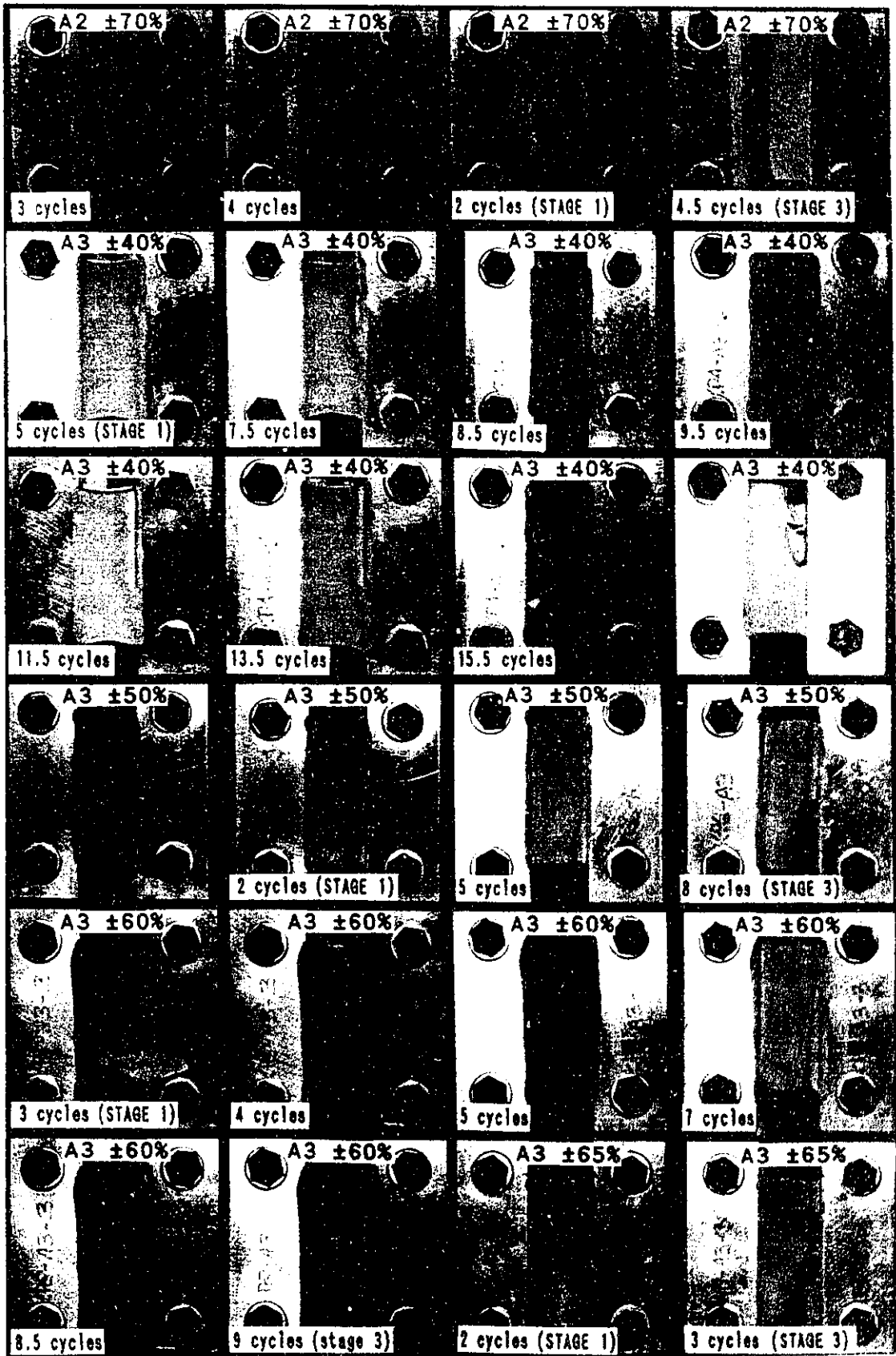
Karpati has shown that for two-part polysulphide based sealants subjected to a test program as described above, permanent deformation can be separated into three stages [118]:

- i) the smallest movement at which it is just observable;
- ii) formation of length-wise bulges with part of the sealant bead folded under;
- iii) the smallest amount of movement at and above which holes develop, i.e., perforation occurs.

The results from tests on commercially based two-part PUR based sealants indicates that only the first (STAGE 1) and last stages (STAGE 3) can be detected. Photographs of specimens at these stages of deterioration are shown in figure 4.48 below.

---

Fig. 4.48      Commercially produced PUR sealants (A2, A3) undergoing cyclic movement. Series of photographs proceeds from top to bottom and from left to right. Ser.1: A2 sealants @  $\pm 70\%$  width change (#1-#4); Ser.2: A3 sealants @  $\pm 40\%$  width change (#5-#8); Ser.3: A3 sealants @  $\pm 50\%$  width change (#9-#12); Ser.4: A3 sealants @  $\pm 60\%$  width change (#13-#18); Ser.5: A3 sealants @  $\pm 65\%$  width change (#19,#20).



The initial sequence of photographs, shown at the top of the colour plate, depict A2 type sealants subjected to  $\pm 70\%$  width change at 2,3,4,and 4.5 cycles respectively. The progressive deterioration of the sealant bead is clearly noticeable from this series of photographs. A more gradual degeneration is observed at smaller strain amplitudes as shown from the subsequent sequence of photographs depicting A3 type sealants undergoing strain amplitudes of  $\pm 40$ , 50, and 60% respectively. However for A3 type sealants at  $\pm 65\%$  width change, stage 3 occurs quite rapidly, after only 3 cycles.

It is evident from the photographs that permanent deformations occur over a range of amplitudes. This has been depicted graphically in figure 4.49, in which the line at the bottom of either figure represents the limit at which permanent deformation is just observable and the upper line shows the limit at which stage 3 occurs. Both lines are based on the average value obtained for three specimens.

It may also be observed that A2 sealants are not as resistant to cyclic movement as A3 specimens since these sealants are seen to reach stage 3 deformation at a lower number of cycles at a given strain amplitude. This is illustrated in figure 4.50 in which straight lines are obtained on a plot of log strain (width change) versus log time for stage 3 observations. The time is obtained by multiplying the number of minutes to complete a cycle by the number of cycles.

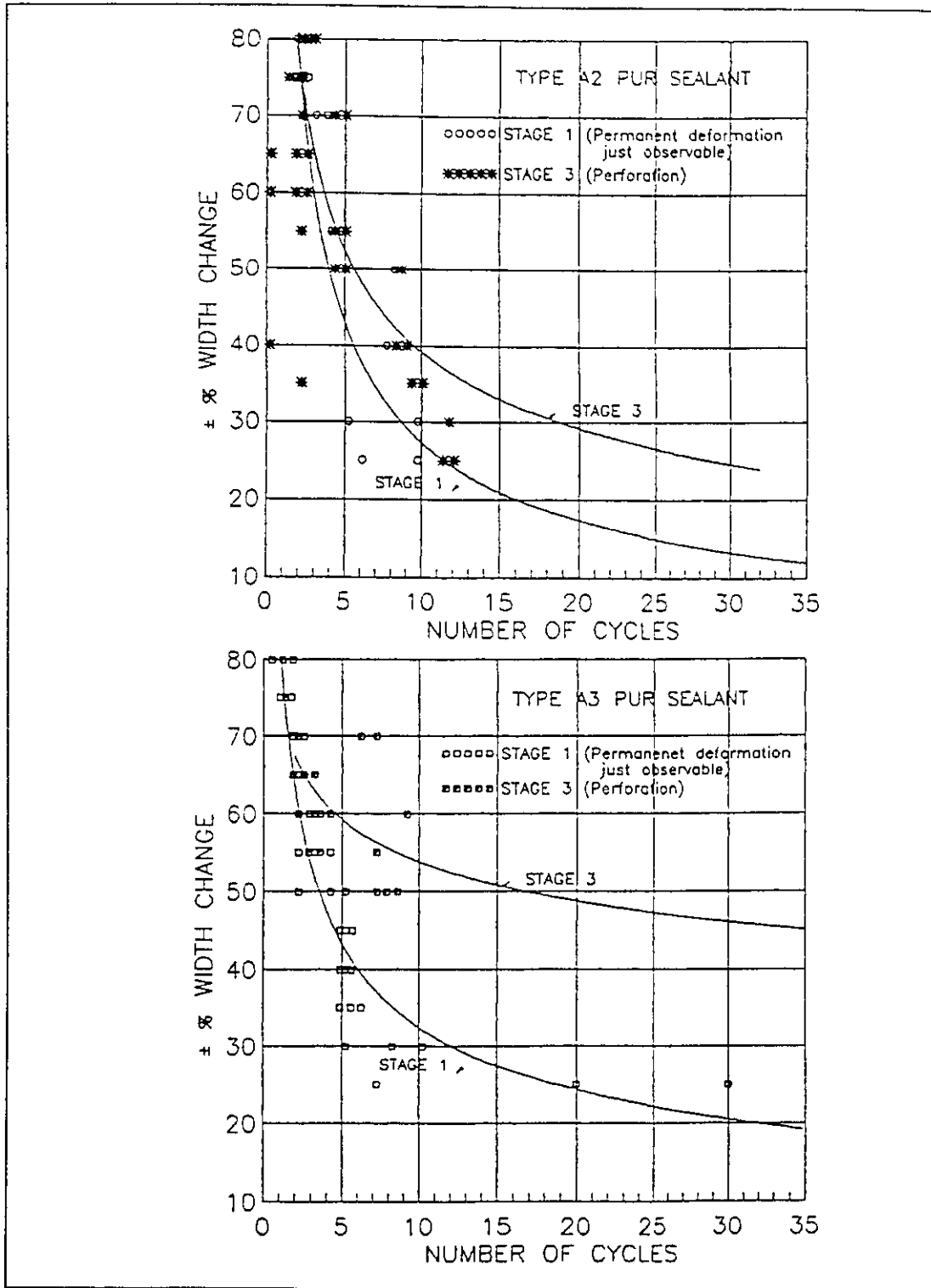


Figure 4.49 Stages of deformation:  $\pm$  width change as a function of the number of cycles to failure.

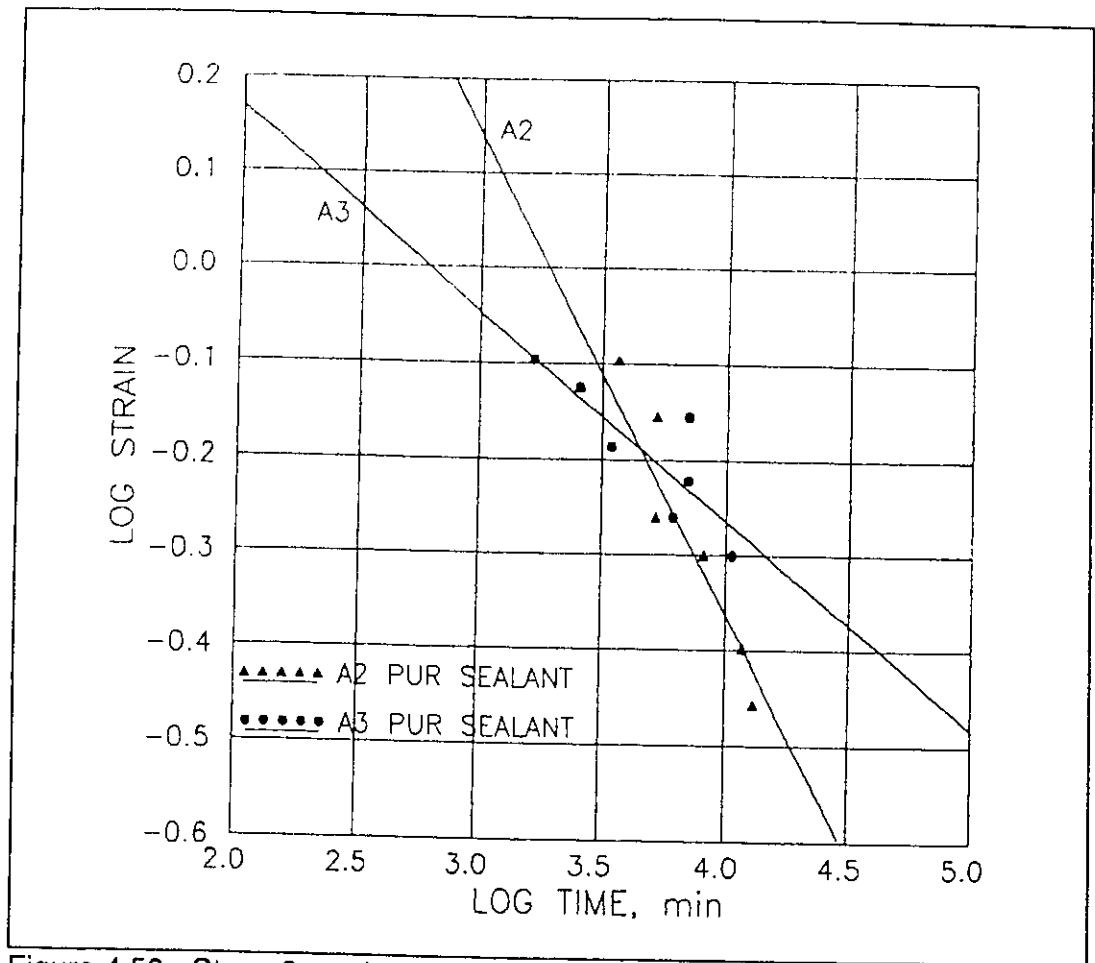


Figure 4.50 Stage 3 results for A2 and A3 type PUR sealants: log strain (width change) versus log time.

At  $\pm 20\%$  strain, sealant A2 is expected to reach stage 3 deformation within a year whereas A3 sealant can maintain performance up to 6 years. A twenty year life expectancy to stage 3 is only achieved for the A3 sealant if subjected to no greater a strain program than  $\pm 15\%$ .



#### 4.6.3 CYCLIC PERFORMANCE TESTS

It has been shown that for rubber or elastomer products subjected to cyclic deformations at constant strain amplitude the following relation between the number of cycles before failure,  $N$ , and the maximum deformation,  $e$ , is given by:

$$N e^m = C$$

Equ. 4.19 [140]

where:

- $e$  = pre-set maximum deformation;
- $m, C$  = constants which do not depend on  $N$ , and  $m$  depends neither on temperature nor the method of testing.

Hence a log-log plot of  $e$  versus  $N$  should yield a straight line and the slope of the line, given by  $m$ , serves to characterize the type of material being tested. Since both ST and TO filled sealants are based on the same PUR matrix it is expected that the parameter  $m$ , which characterizes the material, should also be the same for both sealants. i.e. the slope of the lines plotted showing the cycles to failure for either sealant should essentially be the same.

The usefulness of this type of function is apparent from observation of the results in figure 4.51. in which ST and TO filled PUR sealants were subjected to cyclic deformations of serrated form ranging from  $\pm 25\%$  to  $\pm 60\%$  (+ % extension, - % compression). The cycling rate was 1.57 cycles / min based on a rate of deformation of 20mm/min. The slope of both lines are seen to be essentially the same thus confirming the use of the fatigue relation described above. The results further indicate that the ST filled PUR sealants are capable of sustaining a greater

number of cycles to failure than the TO specimens at any given stain amplitude. This is not unexpected since the static strength of ST filled PUR sealants is also greater than that of the TO specimens.

It must also be stated that despite the lower resistance of TO filled PUR sealants to cyclic deformation, these specimens were still capable of sustaining a considerable number of cycles before failure. Although no definite claims can be made with respect to the longevity of their service life, it is apparent that they can maintain as adequate a seal as other commercial sealants (cf A1,A2) currently available on the market provided the necessary precautions are taken to insure an adequate adhesion between sealant and substrate.

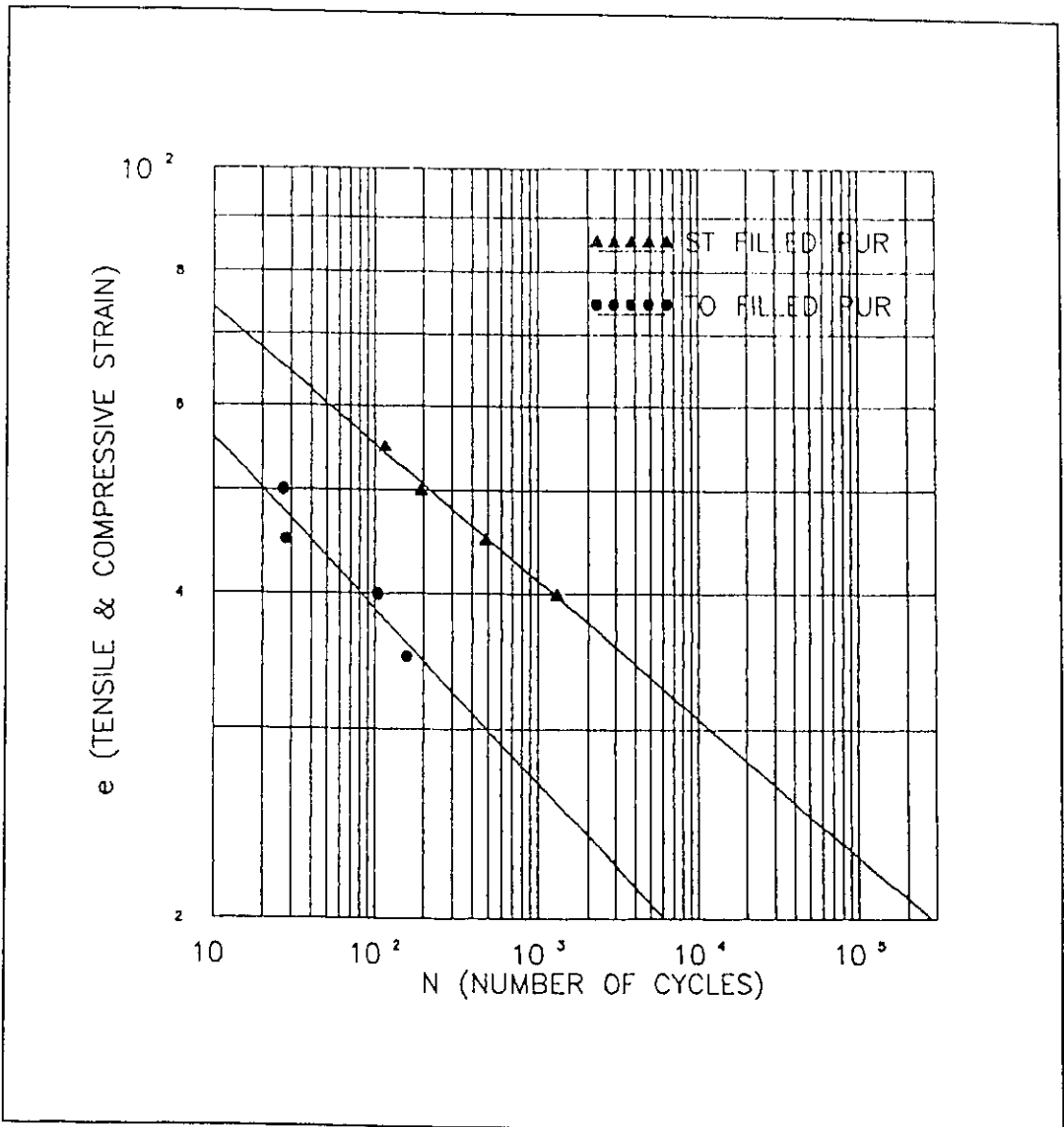


Figure 4.51 Strain amplitude as a function of the number of cycles to failure for ST & TO filled PUR based sealants.

An extrapolation from the above relations suggests that at  $\pm 20\%$  extension, TO filled specimens may sustain up to 8000 cycles to failure. If it is assumed that a sealant undergoes at least a cycle per day, then this reflects a performance without failure estimated at 22 years. This estimate may vary considerably since other degradative processes, which are known to occur over the lifetime the sealant, may in certain instances significantly reduce its service life.

## CHAPTER 5

### CONCLUSIONS & RECOMMENDATIONS

#### 5.1 CONCLUSIONS

Novel polyurethane based sealant formulations, incorporating various types of kraft processed lignins including softwood, hardwood, and eucalyptus wood lignin, were developed and their physico-chemical as well as their performance properties established in an extensive research program which sought to help develop more durable cost effective sealants as well as cultivate a market for lignin, a highly underutilized by-product of the pulp and paper industry.

Based on the results obtained in this study the following conclusions may be made:

- i) Polyurethane elastomers, for use in sealants, can be made with a wide variety of mechanical properties depending on the macromolecular characteristics of the polyol and isocyanate components of the formulation. Based on the results obtained through experimentation it has been demonstrated that sealants require a lightly crosslinked long chain structure such that a resilient thermoset can be produced which is capable of withstanding repeated cycles of extension and compression. Provided long chain low functionality components are used, an elastomer suitable for sealants can readily be formulated. Furthermore, the adhesion of PUR

elastomers to aluminum substrates has been found to be dependent on the stoichiometric ratio, with increased adhesive performance attained with formulations having excess isocyanate groups.

- ii) Based on knowledge of both the proportion of the formulation constituents and the magnitude of their respective glass transition temperatures, it has been demonstrated that the various elastomers formulated in this study are essentially single phase polyurethane structures. Moreover, their thermal behaviour was not greatly affected by changes in plasticizer content or stoichiometry within the formulation parameters used in this study. Hence their physico-mechanical properties are essentially dependent on the chemical structure, chain length and degree of branching of the high molecular weight polyol of the primary network.
  
- iii) In filled samples, it has been shown that once the curing process is initiated, the rate of curing, as measured using the Shore "A" apparatus to monitor the indentation hardness as a function of time, is not affected by the addition of lignin fillers. However, the initial setting time is affected by the type of filler incorporated in the formulation and is specifically dependent on the packing characteristics of the particular filler. In general, the larger the maximum packing fraction for a given filler (i.e. the more closely particles can be packed together), the smaller the effect on the initial setting time.

- iv) The addition of filler increases the modulus in proportion to that predicted by Neilson. Hence the mechanical properties in tension and compression are dependent on the packing characteristics of the various fillers. The enhancement of mechanical properties is particularly evident for Sillitin/Titanox filled elastomers which demonstrated an increase in both stress and strain at failure with the addition of filler. This particular phenomena is attributed to its reduced particle size.
  
- v) The use of both IR and NMR spectroscopy have established that chemical interaction does not occur between the filler and polymer matrix phases. Hence this is a binary phase system whose properties are primarily contingent on physical rather than chemical aspects of either of the phases.
  
- vi) The degree of physical interaction between phases was assessed using various techniques, including swelling in toluene, DMA and surface analysis. Interaction between polymer and filler as determined by swelling, is dependent on the type of filler, and can be characterized by the degree of restriction to swelling which a filler imparts to the polymer matrix. Lignins are found to restrict the degree of swelling less than that of the siliceous clay, titanium dioxide combination. Hence using this method, it is seen that lignins do not interact with the elastomer matrix to as great an extent as the Sillitin/Titanox filler combination.

- vii) The results obtained for the DMA analysis permitted a rationalization of the swelling phenomena in that the extent of interaction, as measured by the degree of restriction to swelling, was related to the degree of damping characterized by the shift in the glass transition temperature by various fillers. This suggests that the mechanisms which restrict swelling or induce damping are largely dependent on the maximum packing fraction of the filler.
  
- viii) The surface analysis was most useful for assessing the relative contributions to the work of adhesion of the various fillers. Hence for lignin fillers having essentially the same average particle size, the relative performance is dependent on the respective surface properties. At a given particle size, fillers having values of the work of adhesion equal to or exceeding the value of the work of cohesion are more likely to contribute to the reinforcing effect in filled elastomer. Thus the order of decreasing interaction potential was found to be: Tomlinite > Sillitin > Indulin AT > Eucalin filler. In the case of Sillitin however, particle size plays a more significant role in determining the final mechanical properties.
  
- ix) Performance properties were determined by both indirect and direct means. Indirect methods, including tensile tests on specimens adhered to mortar substrate, indicate that suitable formulations can readily be prepared and

these sealants perform adequately in relation to the Sillitin filled elastomer or other commercial products.

- x) Cyclic performance tests showed that at lower strain deformations, lignin filled elastomers can sustain significant cycles to failure in comparison to that of the Sillitin/Titanox filled elastomer.
  
- xi) The cost of lignin based fillers in the formulation of elastomeric compounds continues to make it an attractive alternative to fillers currently used in production. Table 5.1 below lists the bulk costs per kilogram and cubic centimetre for selected lignin fillers as well as for an air floated clay, titanium dioxide, and filler combination consisting of clay and titanium dioxide. An analysis of these unit costs indicates that lignin fillers are 6 to 10 times less costly than the clay/TiO<sub>2</sub> filler combination.



TABLE 5.1			
BULK COST OF FILLERS			
Type	Name-Producer	\$ / kg <sup>*</sup>	\$ / cc x 10 <sup>-3</sup>
Softwood kraft lignin	Indulin AT - Westvaco	1.25-1.50	1.86
Eucalyptus kraft lignin	Eucalin - Litchem	0.55-0.77	1.06
Clay (hydrated aluminum silicate)	PAF (Pioneer air floated) - Georgia Kaolin	3.18-4.27	11.10
Titanium dioxide	Titanox - Kronos	2.67	10.68
Clay/Titanium dioxide	(combination)	3.88	11.02
<p>* Unit costs are factory on board in bulk quantities (i.e. &gt; 1000 tonne) as of March 4/1991. Volumetric unit costs are based on the respective densities of the various fillers, given in Table 3.5. Combined costs for the clay/TiO<sub>2</sub> are derived from the same weight ratio used in the base formulation (i.e. 22g:7g:).</p>			

## 5.2 RECOMMENDATIONS

Recommendations may be made on a number of levels:

- i) with respect to continued studies concerned with the use of lignins in elastomers, such as sealants;
- ii) with respect to studies which incorporate lignin in other polymeric based building materials;
- iii) with respect to initiating studies using new and different types of technical lignins;
- iv) with respect to the use of specific techniques for characterizing the physical aspects of lignins relevant to the incorporation of these fillers in polymeric systems.
- v) with respect to the use of cyclic tests to assess the long term performance of sealants.

A brief review of each of these particular areas is given below.

### 5.2.1 Lignin Filled Elastomeric Sealants

Based on the results obtained in this study, it has been shown that particle size and size distribution plays a significant role in determining the mechanical performance of filled elastomers used as sealants. The lignins used in this study have larger average particle sizes than that of the reference filler and this is thought to restrict their capacity to perform as well as the base sealant. Consequently, studies related to the development of lignin with adequate particle size are of importance. For example, studies may be undertaken to determine the

factors which affect particle size formation at the stage at which lignin is precipitated from the black liquor. The extraction of the smaller particle size fraction using sedimentation or filtration technology may also be considered.

### 5.2.2 Use of Lignin in Other Polymeric Materials

The use of kraft lignin fillers in other polymeric based materials has been reviewed in chapter 2, however many of these studies considered the fundamental factors which affect the mechanical properties of standard specimens. Although much applied research has been undertaken to develop useful products such as wood adhesives and binders, efforts must be made to extend the potential use of lignin into other building products. Emphasis should be placed on higher priced products which would normally incorporate higher filler loadings thus taking advantage of the price differential which exists between lignin and conventional fillers. Hence development studies in the following building products areas may be of interest:

- i) epoxy based adhesives, mortars, grouts and overlays;
- ii) poly (vinyl chloride) based siding, eave troughs, window and door frames;
- iii) ABS and other polymeric based sewer and drainage pipes;
- iv) polyurethane based foam insulation.

### 5.2.3 Studies Using New Types of Lignin

This study considered the use of three different types of kraft lignin incorporated into an elastomer matrix of which only one is currently being marketed (Indulin AT). There exists other lignins which are processed as a by-product of the pulp and paper industry which have the potential to be used as either a filler, reinforcing agent or active ingredient in the production of polymeric based building materials. These include: steam explosion, organosolve, allcell, or wood hydrolysis (hydrolytic) lignins.

### 5.2.4 Lignin Particle Characterization

The characterization of particulate matter for the purposes of assessing their contribution to the physical properties of mixtures in which they are blended is relevant in two distinct areas:

- i) maximum packing fraction; and
- ii) surface energy.

The spatula rub-out method is used for determining the maximum packing fraction of a filler and the packing fraction is calculated using an empirical formula which is based on the density of the filler and the quantity of oil it is capable of absorbing. The difficulty with this method is that the medium in which the particles are being packed is not the same as that in which the filler will ultimately be placed. The degree to which a liquid matrix interacts with a filler is dependent on the physical and chemical nature of both the filler and the matrix a consequence

of which the packing characteristics of a given filler may be different when the filler is placed in a different matrix.

The use of a viscometer has proven to be useful in assessing the packing characteristics of fillers. The viscosity of a binary mixture of filler and suitable matrix is determined at different volumetric loadings and the maximum packing fraction can be calculated from a knowledge of the viscosity ratio of filled to unfilled mixture. Because of the thixotropic nature of the mixtures, values for viscosities based on shear rates may more easily be calculated using a cone-plate viscometer. The added advantage of using this apparatus is that the sample size is small thus reducing preparation and processing time.

The surface energy of the various fillers was determined using a column rise method based on the Washburn equation which relates the rate of rise of a liquid through a porous medium to the surface energy and density of the liquid as well as the contact angle the liquid makes with the medium. This method has proven to be reproducible provided considerable care is taken in packing the particulate matter. Another method for assessing the surface energy of the filler should be found which eliminates or reduces the effect of packing technique in determining useful results. One of these methods may be the use of a constant head permeability test, as used in soil mechanics to assess the permeability of particulate matter.

### 5.2.5 Cyclic Tests to Assess Long-term Performance

The Karpati performance test assesses the long-term performance of a sealant bead in terms of three stages of deterioration, each of which is defined physically by visual means and hence is documented using a series of photographs. In the development of this test, it was demonstrated through experimentation that the same stages of deformation were achieved regardless of the rate which sealant specimens underwent cyclical movement. This suggests that cyclic tests may be conducted at even higher rates of joint movement provided these can be correlated to long-term performance tests, as was undertaken in the development of the Karpati test. This could potentially reduce the amount of testing time required to assess the performance of sealants.

There are other reasons why the Karpati test needs refinement. Firstly, to carry out the test program, a battery of manually adjusted vices are required to accommodate the test specimens. The vices must be repositioned daily thus requiring a considerable expenditure in time. Secondly, because the stages of deformation are at times difficult to establish, a continuous set of photographs is made as the test progresses such that for each test sample the total number of photographs may become relatively large. Hence, in an extensive testing program, the documentation and analysis of events is necessarily time consuming. This greatly reduces the practicality of the test.

The cyclic fatigue test does not require that stages to deformation be recorded but only that the number of cycles at which failure in any one specimen

be noted. Furthermore, the failure event need not necessarily be visually recorded; only the cycle at which the event takes place must be determined. It is supposed that this can be achieved by some electronic or electro-mechanical means.

## REFERENCES

1. L.M. Beznaczk, Improving the Durability of Silicone Sealants Through Polyblending, M.Eng. Thesis, Concordia University, Montreal, 1985, pp. 105-109.
2. M. Lacasse, Sealant Polyblends with Lignin, M. Eng. Thesis, Concordia University, Montreal, 1986.
3. D. Feldman, M. Lacasse, *J. Appl. Polym. Sci.*, 35: 247- 257 (1988).
4. D. Feldman, M. Lacasse, D. Banu, *J. Polym. Mat.* 5: 53-61 (1988).
5. D.Feldman, M. Lacasse, *Morphology of Lignin-Polyurethane Blends*, *Mat. Res. Soc. Symp. Proc. Vol. 154*, Materials Research Society, Washington, 1989, pp. 265-270.
6. K. Karpati, *ACS Symp. Series No. 113*, 1979, pp. 157-179.
7. T. Pletzke, *Adhesives Age*, May 1986, pp. 22-24.
8. M. Reisch, *Chemical & Engineering News*, February 1988, p.16.
9. I.S. Goldstein, *Appl. Polym. Symp.*, No. 28, 1975, pp. 259-267.
10. J.J. Lindberg, V.A. Era & T.P. Jauhiainen, *Appl. Polym. Symp.*, No. 28, 1975, pp. 269-275.
11. T. Enkyist, *Appl. Polym. Symp.*, No. 28, 1975, pp. 285-295.
12. G.M. Irvine, *TAPPI* 67 (5): 118-121 (1984).
13. C.H. Hoyt and D.W. Goheen, in: Lignins: Occurence, Formation, Structure and Reactions (K.V. Sarkanen & C.H. Ludwig Eds.) Wiley-Interscience, N.Y. & London, 1971.
14. K. Kringstad, in: Future Sources of Organic Raw Materials, *CHEMRAWN I* (St. Pierre & Brown Eds.), Pergamon Press, N.Y., 1980, pp. 627-636.
15. D. Fengel, G. Wegener, Wood: Chemistry, Ultrastructure, Reactions, Walter de Gruyter, Berlin-N.Y., 1984, pp. 132-181.
16. I.A. Pearl, *TAPPI* 65 (5): 68-73 (1982).



17. I. Chodak, R. Brezny, L. Rychla, Chem. Papers, 40(4): 461-470 (1986).
18. C. Klason, J. Kubat, Plastics & Rubber Processing & Applications, 6(1): 17-20 (1986).
19. D. Feldman, Celuloza Hirt. 12 (8-9): 274-280 (1963).
20. E.I. Barg, *Technologia Materialelor Plastice Sintetice*, Editura Technica, Bucuresti, 1957, pp. 384-387.
21. K. Kratzl, K. Buchtela, J. Gratzl, J. Zauner & O. Ettinghausen, TAPPI 45 (2): 113-119 (1962).
22. H.H. Moorer, W.K. Dougherty & F.T. Ball, U.S. Pat. 3,419,581 (1970).
23. D.T. Christian, S. Leandro, M. Look, A. Nobell & T.S. Armstrong, U.S. Pat. 3,546,199 (1970).
24. O. H.-H. Hsu & W.G. Glasser, Appl. Polym. Symp., No. 28, 1975. pp. 297-307.
25. W.G. Glasser & O.H.-H. Hsu, U.S. Pat. 4,017,474 (1977).
26. W.G. Glasser, O.H.-H. Hsu, D.L. Reed, R.C. Forte & L.C.-F. Wu, Urethane Chemistry & Applications (K.N. Edwards Ed.) ACS Symp. Ser. No. 172, 1982, pp. 311-338.
27. W.G. Glasser, L.C.-F. Wu & J.-F. Selin, ACS Conf. on Food & Agricultural Residues on Uses for Feed, Fuels & Chemicals, Kansas City, 1982, Academic Press, N.Y., 1983. pp. 149-166.
28. L.C.-F. Wu, W.G. Glasser, J. Appl. Polym. Sci. 29: 1111-1123 (1984).
29. W.G. Glasser, C.A. Barnett, T.G. Rials & V.P. Saraf, J. Appl. Polym. Sci. 29: 1815-1830 (1984).
30. V.P. Saraf, W.G. Glasser, J. Appl. Polym. Sci. 29: 1831-1841 (1984).
31. T.G. Rials, W.G. Glasser, Holzforschung 38 (4): 191- 199 (1984).
32. T.G. Rials, W.G. Glasser, Holzforschung 38 (5): 269- 279 (1984).
33. V.P. Saraf, W.G. Glasser, G.L. Wikes & J.E. McGrath, J. Appl. Polym. Sci. 30: 2207-2224 (1985).

34. V.P. Saraf, W.G. Glasser, G.L. Wikes, *J. Appl. Polym. Sci.* 30: 3809-3823 (1985).
35. H. Yoshida, R. Morck, K.P. Kringstad, *J. of Appl. Polym. Sci.* 34: 1187-1198 (1987).
36. J.J. Meister & D.R. Patil, *Polym. Mater. Sci. Eng.* 52: 230-234 (1985).
37. J.J. Meister & D.R. Patil, *Polym. Mater. Sci. Eng.* 52: 235-239 (1985).
38. J.J. Meister & D.R. Patil, *Ind. Eng. Chem. Prod. Res. Dev.* 24: 306-313 (1985); 235-239 (1985).
39. D. Feldman, M. Lacasse, L. Beznaczk, *Lignin-Polymer Systems and Some Applications*, *Prog. Polym. Sci.* 12: 271-299 (1986).
40. J.-F. Matte, J. Doucet, *Recent Developments in Lignin Utilization and Wood Adhesives : A Review*, *Cellulose Chem. and Technol.* 22: 71-78 (1988).
41. H.H. Nimz, Lignin based wood adhesives. *Wood Adhesives* (A. Pizzi Ed.) Marcel Dekker Inc., N.Y. (1983).
42. E. Archibald, *Adhesives Age*, July 1982, pp. 27-29.
43. T. Sellers Jr., *Adhesives Age*, July 1981, pp. 19-22.
44. J.T. White, *Adhesives Age*, July 1981, pp. 19-22.
45. E.G. Lyubeshkina, *Lignins as Components of Polymeric Composite Materials*, *Russian Chem. Reviews* 52(7): 675-692 (1983).
46. O.M. Burke Jr., in : Reinforcement of Elastomers (G. Kraus Ed.), John Wiley & Sons, 1965, pp. 491-509.
47. Y. Lin, in : Progress in Biomass Conversion (D.A. Tilman & E.C. Jahn Eds.) Vol. 4, Academic Press, 1983, pp. 31-78.
48. J.J. Keilen, & A. Pollak, *Ind. Eng. Chem.* 39, 480 (1947); *Rub. Chem. Technol.* 20, 1099 (1947).
49. J.J. Keilen, W.K. Dougherty & W.R. Cook, *India Rubber World* 124, 178 (1951).

50. J.J. Keilen, W.K. Dougherty & W.R. Cook, *Ind. Eng. Chem.* 44, 163 (1952).
51. R.A.V. Raff & G.H. Thomlinson, *Can. J. Res.* F27: 399-418 (1949).
52. G.E. Mills, U.S. Pat. 2,845,397 (1958).
53. H.E. Haxo Jr. & G.E. Mills, U.S. Pat. 2,890,183 (1959).
54. J.B. Doughty, U.S. Pat. 2,911,383 (1959).
55. G.E. Mills & H.E. Haxo Jr., U.S. Pat. 2,906,718 (1959).
56. T.R. Griffith & D.W. MacGregor, U.S. Pat. 2,857,345 (1958).
57. G.E. Mills & H.E. Haxo Jr., Can. Pat. 580,894 (1959)
58. H.E. Haxo Jr. & G.E. Mills, Can. Pat. 591,081 (1960)
59. T.H. Ferrigno, *Principles of Filler Selection and Use*, in: Handbook of Fillers and Reinforcements for Plastics (H.S. Katz, J.V. Milewski Eds.), Van Nostrand Reinhold Co., N.Y., 1978, pp. 11-58.
60. O. Olabisi, L.M. Robeson, M.T. Shaw, Polymer-Polymer Miscibility, Academic Press, N.Y., (1979).
61. M.C.H. Lee, *Analytical Method for Determining the Surface Energy of Solid Polymers*, in : Adhesive Chemistry - Developments and Trends, L.H. Lee (Ed.), Plenum Press, N.Y., 1984, p. 93.
62. M.C.H. Lee, *J. Appl. Polym. Sci.* 33: 2479-2492 (1987).
63. M.C.H. Lee, S. Tensa, *J. Adhesion Sci. Technol.* 3(4): 291-303 (1989).
64. J.H. Saunder, K.C. Frisch, Polyurethanes, pt.1, Chemistry, Interscience Publ., N.Y., 1963, pp. 326-335.
65. A. Damusis (Ed.), Sealants, Reinhold Publ., N.Y., 1967, pp.120-121.
66. D. Dieterich et al., *Chemical & Physical Principles of Polyurethane Chemistry*, in: Polyurethane Handbook, (G. Oertel Ed.), Hanser Verlag, Munich, 1985, pp. 7-41.
67. B.A. Phillips, R.A. Taylor, *Polyurea Dispersions for RIM Applications*, *Rubb. Chem. Technol.* 52: 864-870 (1979).

68. Bayer Technical Publication No. LS 44399e (4.83 ed.), Bayer AG, LS Group, Leverkusen, Germany, 1983.
69. Bayer AG, German Pat. 2 513 815 (1975).
70. M. Dahn, K. Uhlig, *Raw Materials Additives & Auxiliary Materials*, in: Polyurethane Handbook (G. Oertel Ed.), Hanser Verlag, Munich, 1985, p. 90.
71. L.H. Spherling, Introduction to Physical Polymer Science, John Wiley & Sons, N.Y., 1986.
72. loc. cit. M. Dahn, K. Uhlig 1985, p.103.
73. P.H.T. Vollenberg, D. Henkens, Composite Interfaces, Proc. First Intl. Conf. Comp. Interf. (ICCI-I), May 1986 (H. Ishida, J.L. Koenig Eds.), Elsevier Science, N.Y., 1986, pp. 171-176.
74. A.N. Gent, J. Mat. Sci., 15: 2884-2888 (1980).
75. F.W. Billmeyer Jr., Textbook of Polymer Science, 2<sup>nd</sup> ed., Wiley Interscience, N.Y., 1971, pp. 123-126.
76. F.A. Collins, J. Bares, F.W. Billmeyer Jr., Experiments in Polymer Science, Wiley Interscience, N.Y., 1973.
77. ASTM D3360, Test for the Particle Size Distribution of the Common White Extender Pigment, vol. 28. Amer. Soc. for Testing & Materials, Book of Standards (1977).
78. ASTM D422, Particle Size Analysis of Soils, vol. 19. Amer. Soc. for Testing & Materials, Book of Standards (1977).
79. ASTM E100, Specifications for ASTM Hydrometers, vol. 28. Amer. Soc. for Testing & Materials, Book of Standards (1977).
80. E.H. Kerner, Proc. Phys. Soc., B69, 808 (1956).
81. L.E. Nielsen, *Dynamic Mechanical Properties of Filled Polymers*, Appl. Polym Symp. 12: 249-265 (1969).
82. T.B. Lewis, L.E. Nielsen, J. Appl. Polym. Sci., 14, 1449 (1970).
83. L.E. Nielsen, J. Appl. Phys., 41, 4626 (1970).

84. L.E. Nielsen, Predicting the Properties of Mixtures, Marcel Dekker Inc., N.Y., 1980, pp. 21-48.
85. T.C. Patton, Paint Flow and Pigment Dispersion, Interscience, N.Y., 1964, p.152.
86. ASTM D281, Test for Oil Absorption of Pigments by the Spatula Rub-out Method, vol. 28. Amer. Soc. for Testing & Materials, Book of Standards (1977).
87. ASTM D153, Tests for Specific Gravity of Pigments, vol. 28. Amer. Soc. for Testing & Materials, Book of Standards (1977).
88. P.J. Flory, J. Rehner Jr., J. Chem. Phys. 11(11): 521-526 (1943).
89. A. Damusis, W. Ashe, K.C. Frisch, J. Appl. Polym. Sci. 9: 2965-2983 (1965).
90. E.F. Cluff, E.K. Gladding, R. Pariser, *A New Method for Measuring the Degree of Crosslinking in Elastomers*, J. Polym. Sci. 45: 341-345 (1960).
91. G. Kraus (Ed.), *Interaction between Elastomers and Reinforcing Fillers*, in Reinforcement in Elastomers, Interscience Publ., John Wiley & Sons, N.Y., 1965, p.147.
92. ASTM D412, Tests for Rubber Properties in Tension, vol. 37. Amer. Soc. for Testing & Materials, Book of Standards (1977).
93. CAN2-19.0-M77, Methods for Testing Putty, Caulking and Sealing Compounds, Method 14.1, Tensile Tests, Canadian Government Standards Board.
94. ASTM D575, Tests for Rubber Properties in Compression, vol. 37. Amer. Soc. for Testing & Materials, Book of Standards (1977).
95. ASTM D395, Tests for Rubber Property-Compression Set, vol. 37. Amer. Soc. for Testing & Materials, Book of Standards (1977).
96. A.N. Gent, *On the Relationship Between Indentation Hardness & Young's Modulus*, Trans. inst. Rubber Industry, 34: 46-57 (1958).
97. L. Larrick, *The Standardization of Durometers*, Rubber Age (N.Y.), September: 387-392 (1940).

98. CAN2-19.0-M77, Methods for Testing Putty, Caulking and Sealing Compounds, Method 8.1, Shore "A" Hardness, Canadian Government Standard Board.
99. ASTM D2240, Test for Rubber Property-Durometer Hardness, vol. 37. Amer. Soc. for Testing & Materials, Book of Standards (1977).
100. ASTM D3418, Tests for Transition Temperatures of Polymers by Thermal Analysis, vol. 35. Amer. Soc. for Testing & Materials, Book of Standards (1977).
101. R.L. Blaine, P.S. Gill, R.L. Hassel, L. Woo, *A New Dynamic-Mechanical Analysis System for Characterization of Physical Properties*, J. Appl. Polym. Sci.: Appl. Polym. Symp. 34, 1978, pp. 157-171.
102. L.E. Nielsen, Mechanical Properties of Polymers & Composites, Vol.2, Marcel Dekker Inc., N.Y., 1974, pp. 379-452.
103. D.A. Skoog, D.M. West, Principles of Instrumental Analysis, 2<sup>nd</sup>ed., Saunders College, Philadelphia, 1980.
104. I.I. Perepechko, An Introduction to Polymer Physics, Mir Publishers, Moscow, 1981, pp. 173-194.
105. U.J. McBrierty, in: Comprehensive Polymer Science, Vol. 1, Pergamon, N.Y., 1988.
106. E.O. Stejskal, J. Schafer, M.D. Sefcik, R.A. McKay, *Macromolecules* 14, 275 (1981).
107. A. Natansohn, M. Lacasse, D.Banu, D.Feldman, *CP-MAS NMR Spectra of Polyurethane Lignin Blends*, J. Appl. Polym. Sci. 40: 899-904 (1990).
108. L.E. Nielsen, Mechanical Properties of Polymers, Reinhold Publ. Co., N.Y., 1962.
109. V.T. Crowl and W.P.S. Wooldrige, *A Method for the Measurement of Adhesion Tension of Liquids in Contact with Powders*, in: Wetting, SCI Monograph N.25, Soc. Chem. Industry, London, UK, 1967, pp. 200-214.
110. G.D. Cheever, J.C. Ulicny, *J. Coatings Technol.* 55 (697): 53-63 (1983).

111. E.W. Washburn, *The Dynamics of Capillary Flow*, Phys. Rev. 17(3): 273-283 (1921).
112. J.C. Beech, Bldg. Res. & Prac. 8(3): 158-169 (1980).
113. J.C. Beech, C.H.C. Turner, Bldg. Res. & Prac. 11(5): 287-291 (1983).
114. K.K. Karpati, 12th FATIPEC Cong., Garmisch-Partenkirchen (May 1974): 455-459 (1974).
115. K.K. Karpati, K.R. Solvason, P.J. Sereda, J. Coatings Technol. 49(626): 44-47 (1977).
116. K.K. Karpati, Adhesives Age 23(11): 41-47 (1980).
117. K.K. Karpati, J. Coatings Technol. 56(719): 57-60 (1984).
118. K.K. Karpati, Adhesives Age 28(5): 18-22 (1985).
119. K.K. Karpati, J. Coatings Technol. 50(641): 27-30 (1978).
120. K.K. Karpati, Durability of Building Materials, 5: 35-51 (1987).
121. Titanox technical literature
122. Sillitin technical literature
123. Press et al. Numerical Methods, Cambridge University Press, UK, 1986, p. 509.
124. M.A. Mandelsohn, F.W. Navish, Jr., D. Kim, *Effects & Chemical Composition on Viscoelastic-Mechanical Properties of Cast Elastomer Polyurethanes*, in: Advances in Urethane Science & Technology, Vol. 10, K.C. Frisch, D. Klempner, Eds., Technomic Publ., Lancaster, PA, 1987, pp. 16-36.
125. L.R.G. Treloar, The Physics of Rubber Elasticity, 3<sup>rd</sup>ed., Clarendon Press, Oxford, 1975.
126. H.R. Bylsma, I & EC Prod. Res. Devel. 3(3): 204-209 (1964).
127. E. Jenkel and R. Hausch, Kolloid-Z 130, 89 (1953).
128. M.C. Shen, A. Eisenberg, Rubber Chem. Technol. 43(19): 95-155 (1967).

129. Yu. S. Lipatov, Physical Chemistry of Filled Polymers, International Polymer Science & Technology, Monograph No. 2, RAPRA, UK, 1979, p.17.
130. G. Kraus, J. Appl. Polym. Sci. 7, 861 (1963).
131. J. Smallwood, J. Phys. 40(2): 253-258 (1944).
132. D.Feldman, C. Luchian, D. Banu, M. Lacasse, *Polyurethane-Maleic Anhydride Grafted Lignin Polyblends*, in press, (1990).
133. J. Haslam, H.A. Willis & D.C.M. Squirrell, Identification and Analysis of Plastics, Hyden, London, 1981, p.25.
134. J. Urbanski, M Czerwinski, K. Janicka, F. Majewska, & H. Zowall, Handbook of Synthetic Polymer & Plastics, Ellis Harwood Ltd., New York, 1977. pp. 321-322.
135. W. Kolodziejski, J.C. Frye, & G.E. Maciel, Anal. Chem., 54, 1419 (1982).
136. D.E. Axelson & K.E. Russel, Prog. Polym. Sci. 11, 221 (1985).
137. Work & Whitby, Encyclopedia of Chemical Technology, 12: 477-478 (1954), p.126.
138. C. Hepburn, *Progress in Rubber & Plastics Technology*, 3(3): 33-52 (1987).



## **APPENDIX I**

## DERIVATION OF ELASTOMER FORMULATIONS BASED ON CHEMICAL PARAMETERS

### NOTATIONS

BPR	=	Baylith paste ratio; weight ratio of short to long chain polyol OH content.
PC	=	Plasticizer content, in relation to the quantity of elastomer, including the weight of plasticizer
SR	=	Stoichiometric ratio
[E14]	=	weight of isocyanate (DESMODUR E14)
[1920D]	=	weight of long chain polyol (DESMOPHEN 1920D)
[BP]	=	weight of short chain polyol (Baylith L paste: zeolite in 50% wt. castor oil)
[W <sub>E</sub> ]	=	weight of elastomer
[P]	=	weight of plasticizer
[S]	=	weight of solvent
[K]	=	weight of catalyst; where [K <sub>c</sub> ] = wt. of Ca Octoate & [K <sub>p</sub> ] = wt. of Pb Octoate
<OH>	=	OH content, wt. %: 0.85% for [1920D] & 2.5% for [BP]
<NCO>	=	NCO content, wt. %: 3.5% for [E14]

### DERIVATION

The relationship between the essential components required to produce a polyurethane based elastomer is given by:

$$1. \quad SR = \left( \frac{\langle NCO \rangle [E14]}{42.017} \right) / \left( \frac{\langle OH \rangle [BP] + \langle OH \rangle [1920D]}{17.007} \right)$$

or

$$SR = \frac{17.007}{42.017} \times \frac{0.035 [E14]}{0.025 [BP] + 0.0085 [1920D]}$$

$$2. \quad BPR = \frac{0.025 [BP]}{0.0085 [1920D]} = 0.5882; 0.7407; 1.0$$

from which can be obtained:

$$[BP] = BPR \times 0.34 [1920D]$$

Substitution of 2. into 1. permits the determination of [E14] in terms of the SR and BPR:

$$3. \quad [E14] = SR \times 0.6 [1920D] \times (BPR + 1)$$

The total weight of the elastomer portion of the formulation,  $[W_E]$ , may now be evaluated in terms of the SR, BPR and [1920D].

Hence given that:

$$4. \quad [W_E] = [E14] + [BP] + [1920D], \text{ then by the substitution of 2 \& 3 into 4 one obtains:}$$

$$5. \quad [W_E] = [1920D] \{ (0.6 \times SR \times (BPR + 1)) + (0.34 \times BPR) + 1 \}$$

Given BPR & SR, and assuming an initial value for [1920D] (e.g. 20g), the value of  $[W_E]$  can be calculated as well as the values of [BP] & [E14].

The remaining component weights may then be evaluated based on the following parameters:

$$6. \quad PC = \frac{[P]}{[P] + [W_E]} = 0.3, 0.34, 0.4 \quad (0.2956; 0.3399; 0.39069)$$

$$7. \quad \text{Solvent \& Catalyst ratio} = \frac{[S] + [K]}{[P] + W_E} = 0.0607, \text{ where}$$

$$8. \quad \frac{[S]}{[K]} = 3, \quad \text{and}$$

$$9. \quad [K] = [K_d] + [K_p]; [K_d]/[K_p] = 9$$

Component weights for each formulation series are given in the table on the following page. Included, in the table are the respective volumes of each component determined using density data provided by the manufacturer. The volume fraction of elastomer,  $v_e$ , has also been given, based on the volume of additive & elastomer components which together form the total volume of formulation.

F	FORMULATION COMPONENT WEIGHTS (g)					FORMULATION COMPONENT VOLUMES (cc) & VOLUME FRACTION (%) OF "ELASTOMER" MATRIX - ADDITIVES IDENTIFIED AS "A" COMPONENTS					TOTAL VOLUME	V <sub>h</sub>	
	DESMOPHEN 1920D	BAYLITH PASTE	DESMODUR E14	SANTICIZER	NUODOX & SOLVLESSO	15:85,A:E DESMOPHEN 1920D	60:50,A:E BAYLITH PASTE	0:100,A:E DESMODUR E14	100:0,A:E SANTICIZER	100:0,A:E			
										NUODOX & SOLVLESSO			VOLUME ELASTOMER
15A	20.00	4.00	19.49	18.25	3.74	18.55	3.20	18.56	16.29	4.21	35.85	60.93	.58
16A	20.00	4.00	20.24	18.59	3.81	18.55	3.20	19.27	16.57	4.28	36.56	61.09	.59
20A	20.00	4.00	20.96	18.66	3.87	18.55	3.20	19.96	16.84	4.35	37.25	62.92	.59
35A	20.00	5.00	21.36	19.47	3.99	18.55	4.02	20.35	17.36	4.49	38.15	64.61	.58
38A	20.00	5.00	22.18	19.61	4.06	18.55	4.02	21.13	17.68	4.57	38.83	65.98	.58
40A	20.00	5.00	22.97	20.14	4.13	18.55	4.02	21.88	17.98	4.65	39.58	67.10	.58
25A	20.00	6.80	24.55	21.54	4.42	18.55	5.44	23.38	19.23	4.97	41.78	71.59	.58
28A	20.00	6.80	25.49	21.94	4.50	18.55	5.44	24.27	19.59	5.06	42.68	72.93	.58
30A	20.00	6.80	26.39	22.32	4.58	18.55	5.44	25.14	19.93	5.15	43.54	74.22	.58
15B	20.00	4.00	19.49	22.39	3.69	18.55	3.20	18.56	16.99	4.49	35.85	62.81	.55
16B	20.00	4.00	20.24	22.78	4.06	18.55	3.20	19.27	20.34	4.57	36.56	66.95	.55
20B	20.00	4.00	20.96	23.15	4.13	18.55	3.20	19.96	20.67	4.65	37.25	67.04	.55
35B	20.00	5.00	21.36	23.89	4.26	18.55	4.02	20.35	21.33	4.80	38.05	69.06	.55
38B	20.00	5.00	22.18	24.31	4.34	18.55	4.02	21.13	21.71	4.88	38.83	70.31	.55
40B	20.00	5.00	22.97	24.72	4.41	18.55	4.02	21.88	22.07	4.96	39.58	71.50	.55
25B	20.00	6.80	24.55	26.44	4.72	18.55	5.44	23.38	23.60	5.31	41.78	76.28	.55
28B	20.00	6.80	25.49	26.92	4.80	18.55	5.41	24.27	24.02	5.40	42.68	77.70	.54
30B	20.00	6.80	26.39	27.39	4.89	18.55	5.44	25.14	24.45	5.50	43.54	79.09	.54
15C	20.00	4.00	19.49	27.91	4.33	18.55	3.20	18.56	24.92	4.87	35.85	70.12	.51
16C	20.00	4.00	20.24	28.39	4.40	18.55	3.20	19.27	25.35	4.95	36.56	71.34	.51
20C	20.00	4.00	20.96	28.85	4.48	18.55	3.20	19.96	25.76	5.04	37.25	72.52	.51
35C	20.00	5.00	21.36	29.78	4.82	18.55	4.02	20.35	26.54	5.20	38.05	74.72	.50
38C	20.00	5.00	22.18	30.30	4.70	18.55	4.02	21.13	27.05	5.29	38.83	76.06	.51
40C	20.00	5.00	22.97	30.81	4.78	18.55	4.02	21.88	27.51	5.38	39.58	77.35	.51
25C	20.00	6.80	24.55	32.95	5.11	18.55	5.44	23.38	29.42	5.75	41.78	82.55	.50
28C	20.00	6.80	25.49	33.55	5.21	18.55	5.44	24.27	29.96	5.86	42.68	84.09	.50
30C	20.00	6.80	26.39	34.17	5.30	18.55	5.44	25.19	30.48	5.96	43.54	85.58	.50

## **APPENDIX II**

## FILLED ELASTOMER FORMULATIONS

Filled elastomers have been compounded from the base formulation No. TF28C, which has the following chemical parameters:

$$\begin{aligned} \text{SR} &= 1.0622 \\ \text{BPR} &= 1.0 \\ \text{PR} &= 40\% \end{aligned}$$

Hence the filled elastomers formulations used in this study are based on the following proportions:

COMPOUND	TYPE	WEIGHT (g)	DENSITY (g/cc)	VOLUME (cc)
POLYOL	DESMOPHEN 1920D	20.00	1.078	18.55
MOLECULAR SIEVE	BAYLITH PASTE	6.80	1.25	5.44
ISOCYANATE	DESMODUR E14	25.49	1.05	24.28
ANTIOXIDANT	VULKANOX BKF	0.60	1.04	0.58
PLASTICIZER	SANTICIZER 160	33.56	1.12	29.96
CATALYST & SOLVENT	NUODOX & SOLVESSO	5.21	0.889	5.86
FILLER	AT, EU, ST, TO	$W_F$	$\delta_F$	$V_F$

Where:

$$\begin{aligned} W_F &= \text{weight of filler portion of formulation, (g);} \\ V_F &= \text{volume of filler, (cc);} \\ \delta_F &= \text{density of filler, (g/cc).} \end{aligned}$$

The volume of the non-filler portion,  $V_{NF} = 84.67$  cc. This is based on volumes calculated using the density data obtained from manufacturer's literature.

Formulations have been compounded at different volumetric loadings, hence the weight of filler incorporated in the formulation can be calculated from the relationship between the volume fraction of filler and the volume of non-filler in the elastomer; i.e.:

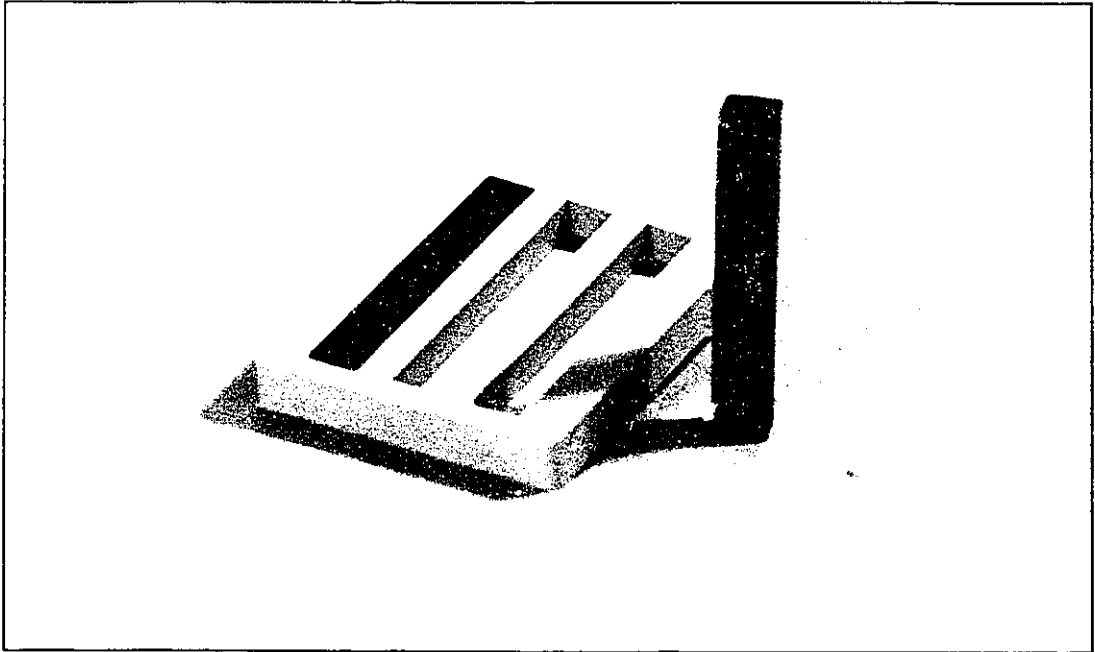
$$W_F = V_F \cdot \delta_F = \frac{\phi_f}{1 - \phi_f} \cdot V_{NF} \cdot \delta_F$$

Given the value of  $\phi_f$  and  $\delta_f$  for a particular filled elastomer formulation, the values of  $W_F$  can easily be determined, after which the weights of individual formulation components can be ascertained from a knowledge of the quantity of elastomer required to produce a series of specimens, and the properties of the respective components as given from the previous table. Component weights for filled elastomer formulations are tabulated below. Those formulations incorporating Indulin AT, Eukalin or Tomlinite fillers are based on a filler density of 1.3 g/cc whereas those incorporating the Sillitin/Titanox filler are assumed to have a composite density of 2.838 g/cc. The total weight of filled elastomer produced in all formulations is 200 g.

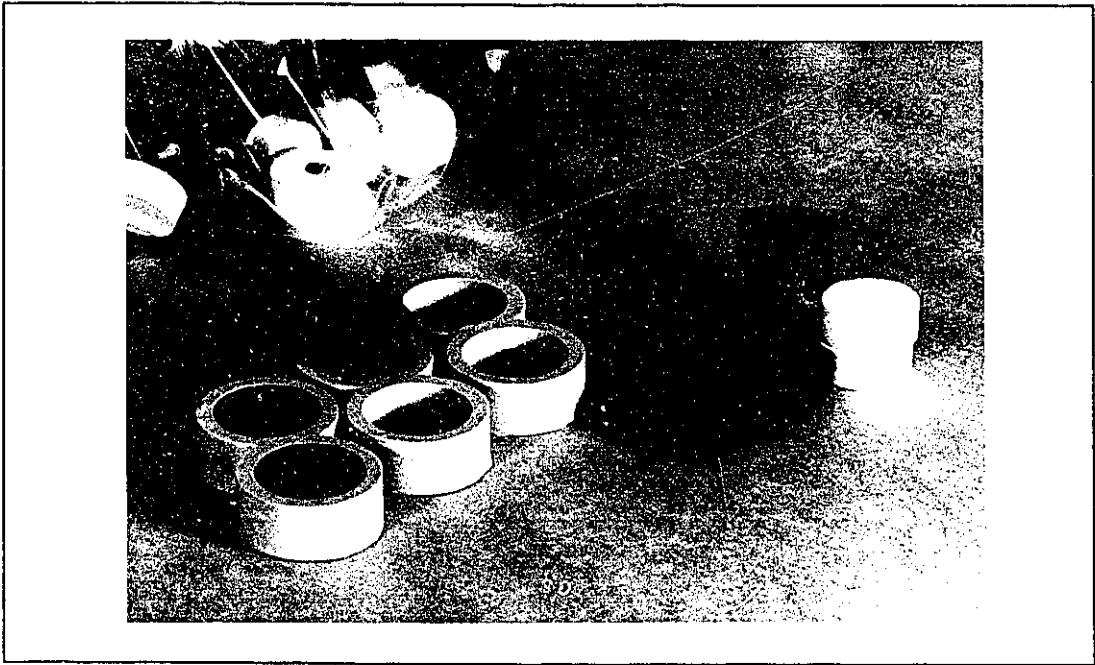
FILLED ELASTOMER FORMULATIONS COMPONENT WEIGHTS (g) FOR INDULIN AT (AT), EUCALIN (EU) & TOMLINITE (TO) FILLED ELASTOMERS					
FORMULATION	AT 50 EU TO	AT 75 EU TO	AT 100 EU TO	AT 125 EU TO	AT 150 EU TO
$\phi_f$ (% vol)	5	7.5	10	12.5	15
FILLER & SANTICIZER	80.77	84.46	88.15	91.79	95.39
BAYLITH L PASTE	13.95	13.52	13.09	12.66	12.24
DESMOPHEN 1920D	91.04	39.77	38.50	37.25	36.01
VULKANOX BKF	1.23	1.20	1.16	1.12	1.08
DESMODUR E14	52.32	50.69	44.07	47.48	45.90
NUODOX & SOLVESSO	10.69	10.36	10.03	9.70	9.38
FILLED ELASTOMER FORMULATION COMPONENT WEIGHT (g) FOR SILLITIN/TITANOX (ST) FILLED ELASTOMERS					
FORMULATION NO.	50 ST	75 ST	100 ST	125 ST	150 ST
$\phi_f$ (% vol)	5	7.5	10	12.5	15
FILLER & SANTICISER	97.45	109.76	122.18	134.71	150.15
BAYLITH L PASTE	14.34	14.08	13.79	13.49	13.44
DESMOPHEN 1920D	42.19	41.39	40.55	39.69	39.54
VULKANOX BKF	1.27	1.24	1.22	1.19	1.19
DESMODUR E14	53.77	52.75	51.68	50.59	50.39
NUODOX & SOLVESSO	10.99	10.79	10.57	10.34	10.30



## **APPENDIX III**



**Figure 1.** DMA and specific gravity specimens. 10 x 15 x 65 mm.



**Figure 2.** Substrate for contact angle analysis and specimens for hardness, swelling, compression and compression set tests. 32 mm diameter x 13 mm high.

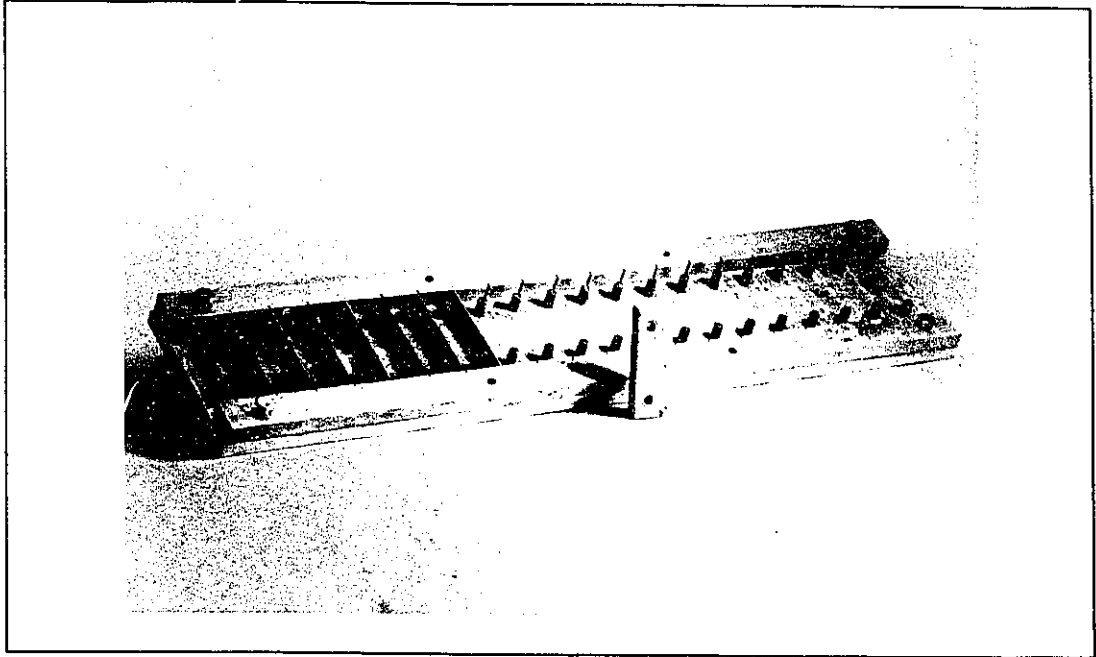


Figure 3. Mortar substrate casting plate.

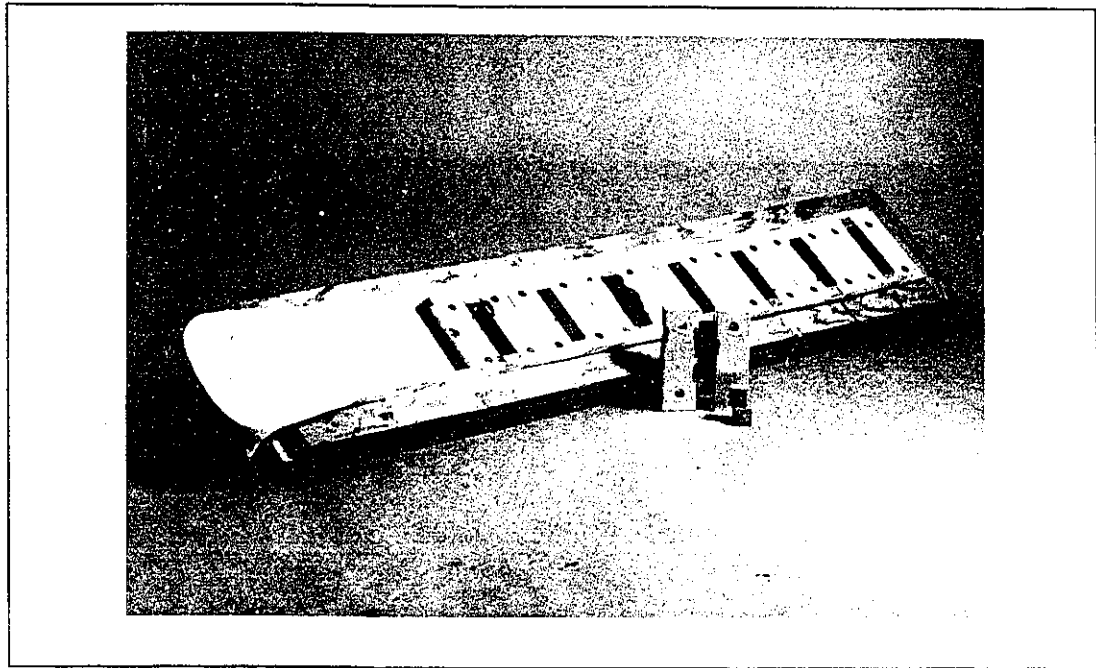
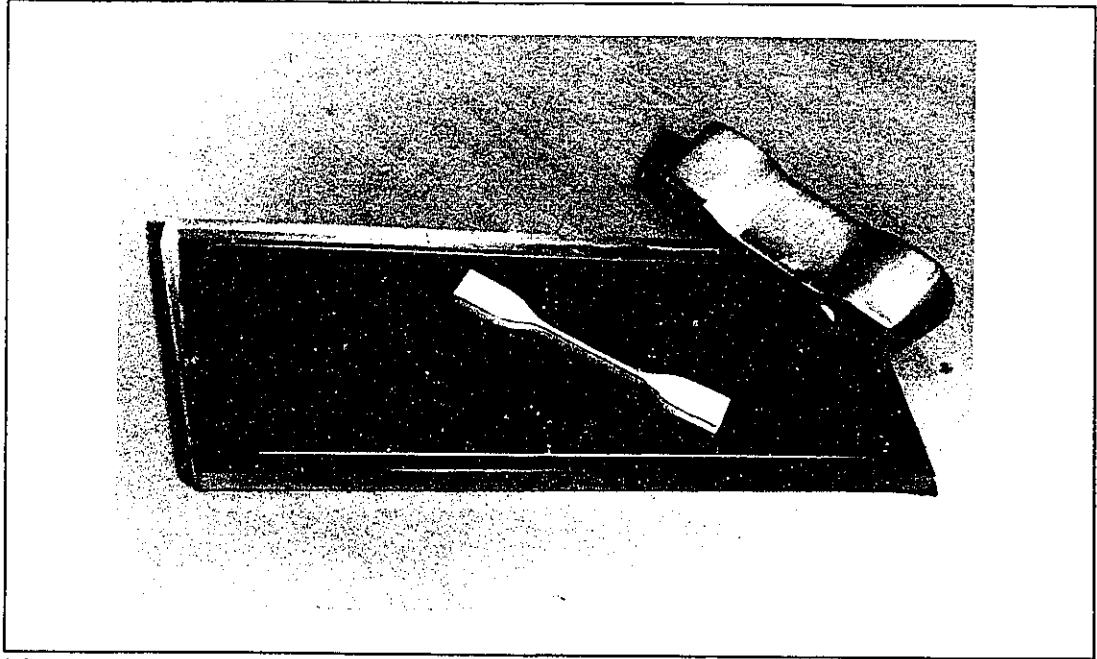


Figure 4. Tensile type TA sealant specimen casting plate, showing typical ASTM D412 die "D" specimen and cutting die.



**Figure 5.** Tensile type TB sealant specimen casting plate. Base of plate is lined with silicone release paper.

## **APPENDIX IV**

## PRIMER & COATING FORMULATIONS

### 1. Metal Primer Formulation (Union Carbide Corp.)

<u>Ingredient</u>	<u>Parts by Weight</u>
Organofunctional Silane*	5
SDA - Alcohol	40
Distilled Water	5
Toluene	40
n - Butanol	5
Butyl CELLOSOLVE®	5

The solution should be adjusted to pH 4-5 with acetic acid. The pH adjustment is not necessary for amino functional silanes.

Primer should be applied to a clean, grease-free substrate. Using either wiping, spraying or brushing techniques; primer should dry in approximately 30 min. at ambient temperature. (23°C, 50% RH).

---

\* Organofunctional silane types known to be effective for enhanced bonding to PUR:

- A-110; gamma - Aminopropyltri/methoxysilane
- A-187; gamma - Glycidoxypropyltri/methoxysilane
- A-189; gamma - Mercaptopropyl/trimethoxysilane

2. Porous Substrate Primer Formulation (Bayer Corp. #RR 2880)

<u>Ingredient</u>	<u>Parts by Weight</u>
DESMODUR 293705	59.0
XYLENE	16.2
DIBUTYL TIN DILAURATE (AIR PRODUCTS INC)	0.6
LEKUTHERM HARDENER M	0.4
ORGANO SILANE A-187 (UNION CARBIDE CORP)	0.3
HARDENER OZ	23.5

The primer should be applied to a dust free surface to saturate the substrate and to form a continuous film; primer should dry in approximately 30 min. at ambient temperature (23°C 50% RH).

3. PUR Coating Formulation

<u>Ingredient</u>	<u>Parts by Weight</u>
DESMOPHEN 1920D	20.00
MONDUR XP 743	5.78
ORGANOSILANE A-187 (UNION CARBIDE CORP)	0.17
CATALYST & SOLVESSO	0.10

The coating should be applied to a primed surface.

## **APPENDIX V**



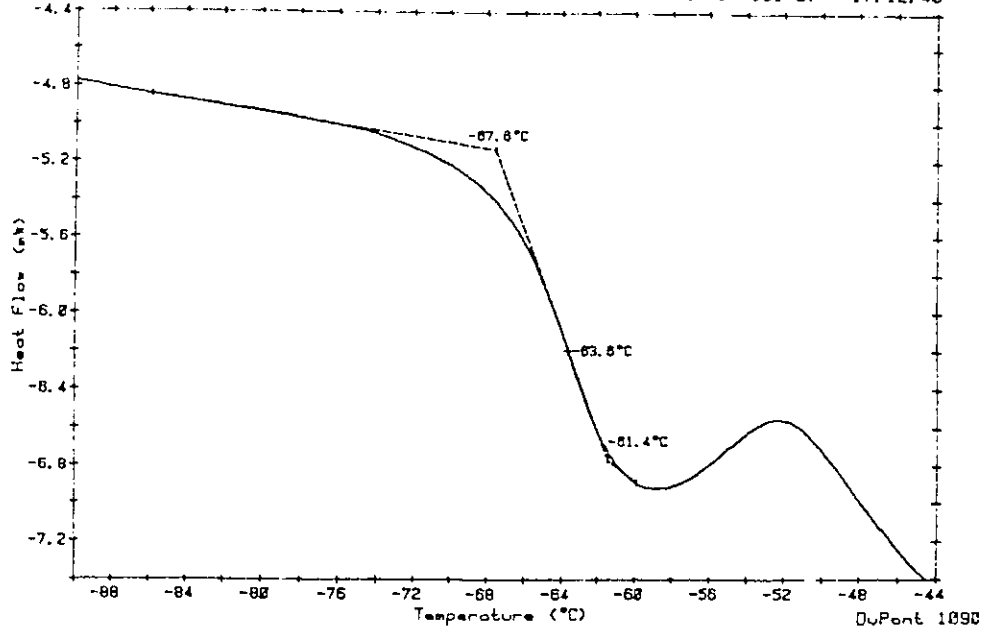
### Results of DSC Analysis on PUR Elastomers

Sample Identification	Weight mg	Glass Transition °C
28C - 2 # 4	16.561	-52.6
28C - 2 # 5	15.574	-53.0
28C N.S # 1	14.373	-52.8
28C N.S # 1	10.739	-53.2
28C N.S # 1	12.168	-53.4
Average (s.d.)		-53.0 (0.6%)
28B - 2 # 3	15.998	-52.7
28B - 2 # 4	15.573	-52.3
Average (s.d.)		-52.5 (0.5%)
28A - 2 # 4	14.657	-52.1
25C - 2 # 4	13.977	-52.2
25C - 2 # 3	16.845	-53.2
Average (s.d.)		-52.7 (1.3%)
30C - 2 # 3	17.146	-52.7
18C - 2 # 3	15.754	-52.6
18C - 2 # 4	18.521	-52.8
Average (s.d.)		-52.7 (0.3%)
38C - 2 # 3	14.731	-52.8
38C - 2 # 4	15.050	-53.0
38C - 2 # 5	17.350	-52.4
Average (s.d.)		-52.7 (0.6%)
18C: BPR=0.59; SR=1.062; PC=40%		
25C: BPR=1.0; SR=1.023; PC=40%		
28A: BPR=1.0; SR=1.062; PC=30%		
28B: BPR=0.59; SR=1.062; PC=34%		
28C: BPR=0.59; SR=1.062; PC=40%		
30C: BPR=0.59; SR=1.1; PC=40%		
38B: BPR=0.74; SR=1.062; PC=40%		

Sample: MESAMOLL I  
Size: 8.889  
Rate: 20C/MIN  
Program: Interactive DSC V2.0

DSC

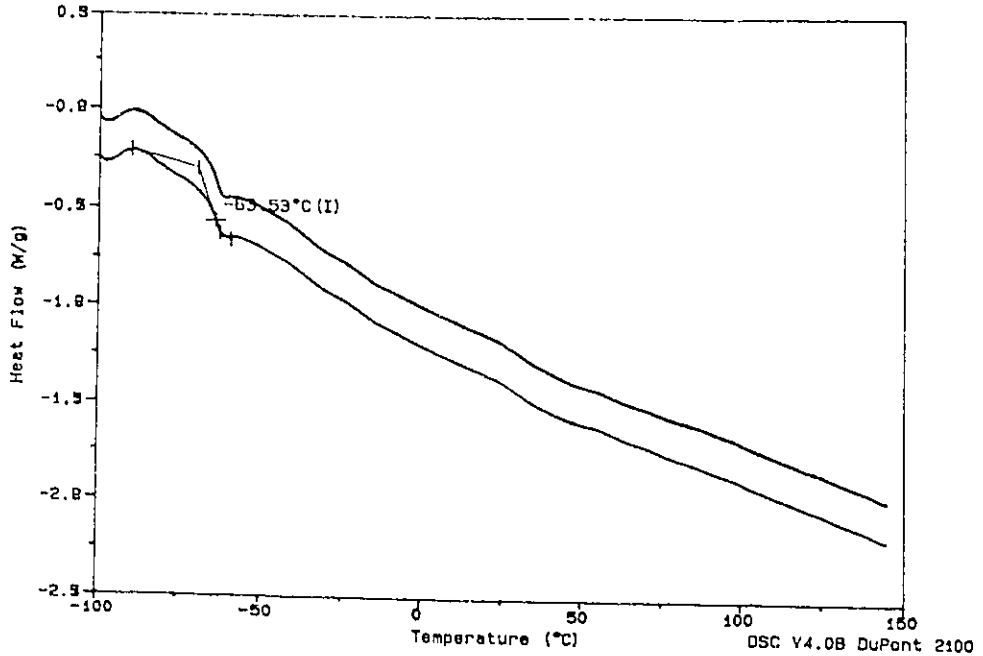
Date: 14-Jul-87 Time: 16:44:58  
File: MIKE.32 DISC DC1  
Operator: ML  
Plotted: 14-Jul-87 17:12:40



Sample: SANCITIZER 160#1 A  
Size: 3.4340 mg  
Method: P.U. 20°C/MIN.  
Comment: HEATING RATE 20°C/MIN.

DSC

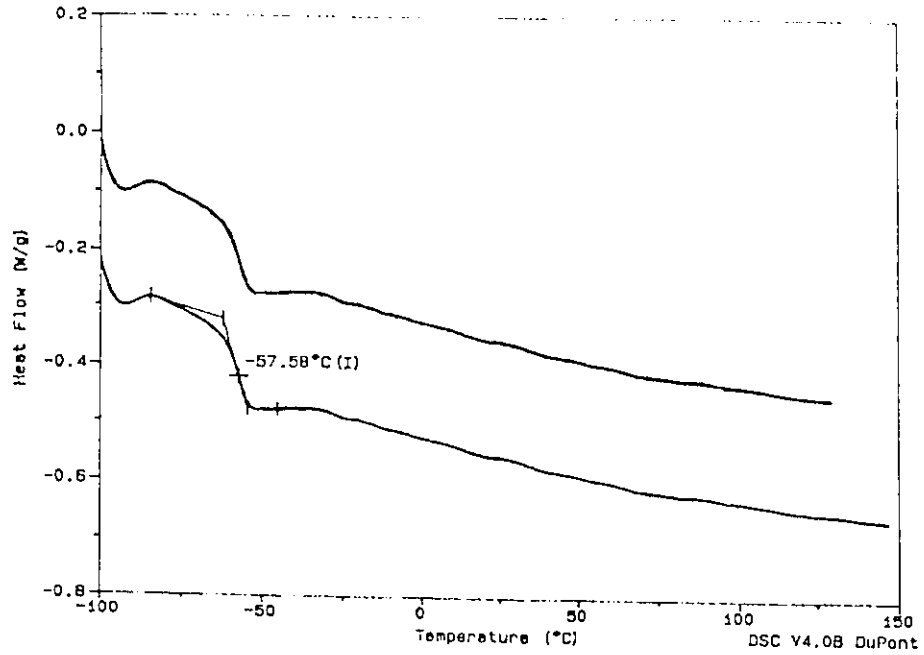
File: C:DORINA.75  
Operator: D.B.  
Run Date: 5-Sep-90 14:33



Sample: BAYLITH PASTE #1 A  
Size: 18.5780 mg  
Method: P.U. 20°C/MIN.  
Comment: HEATING RATE 20°C/MIN.

DSC

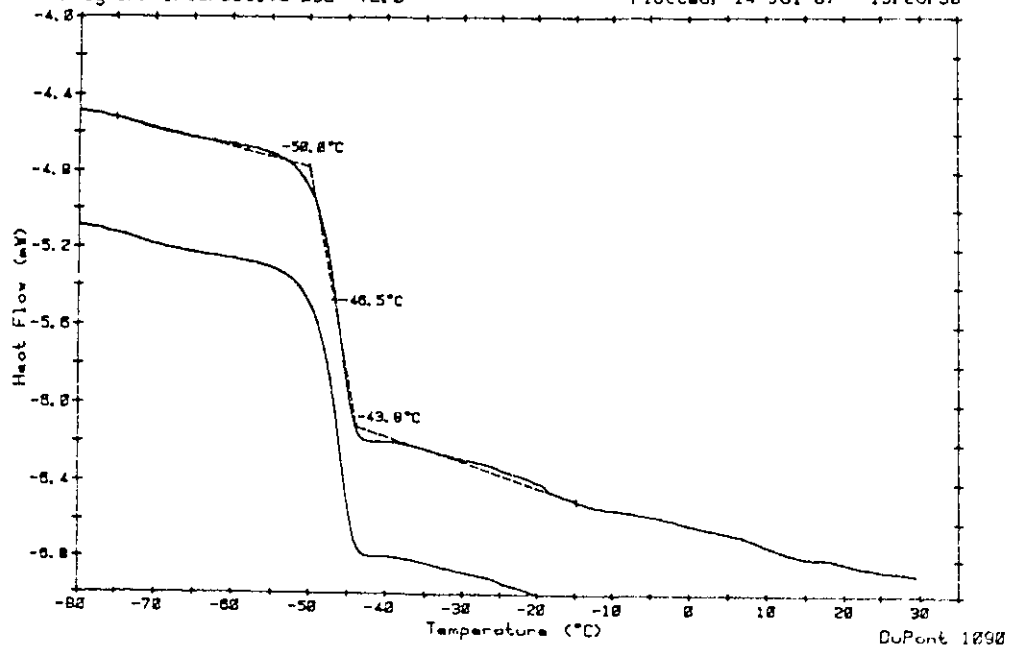
File: C:DORINA.77  
Operator: D.B.  
Run Date: 5-Sep-90 15:25



Sample: DESMOPHEN 550U 1  
Size: 5.839  
Rate: 20C/MIN  
Program: Interactive DSC V2.0

DSC

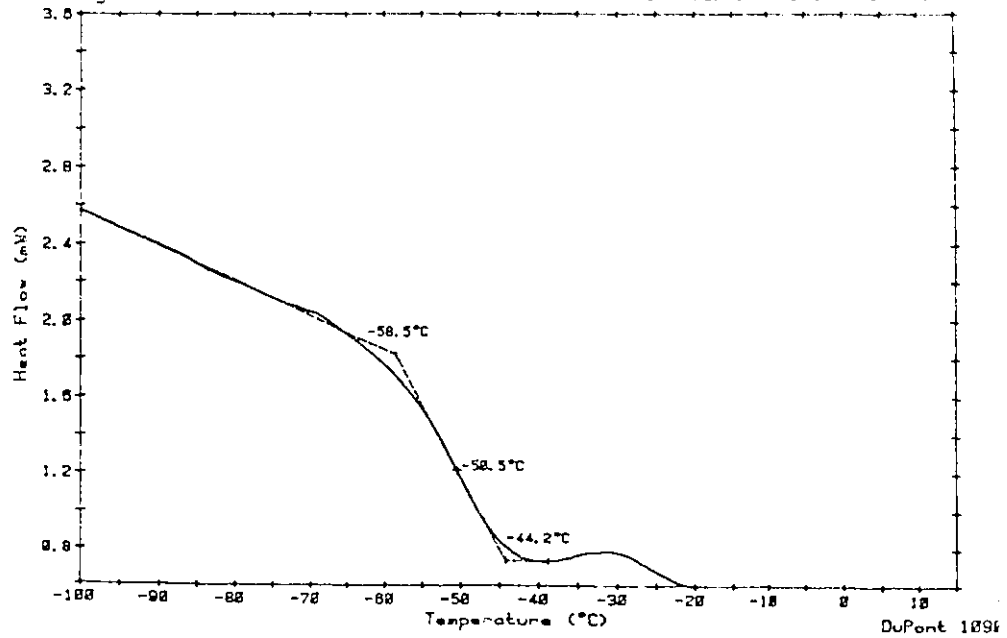
Date: 14-Jul-87 Time: 15:05:48  
File: MIKE.30 DISC OC1  
Operator: ML  
Plotted: 14-Jul-87 15:26:30



Sample: DESMOPHEN 1140 II/2  
Size: 9.976  
Rate: 20C/MIN  
Program: Interactive DSC V2.0

DSC

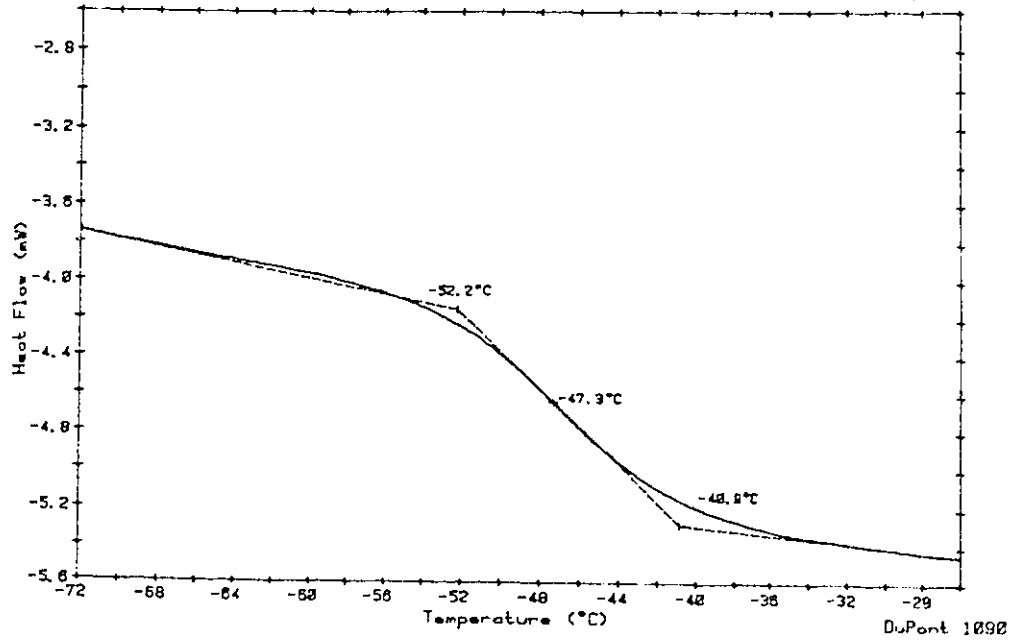
Date: 18-Jul-87 Time: 11:41:04  
File: MIKE.21 DISC DC1  
Operator: ML  
Plotted: 18-Jul-87 12:24:00



Sample: DESMOPHEN 1150 II  
Size: 6.520MG  
Rate: 20C/MIN  
Program: Interactive DSC V2.0

DSC

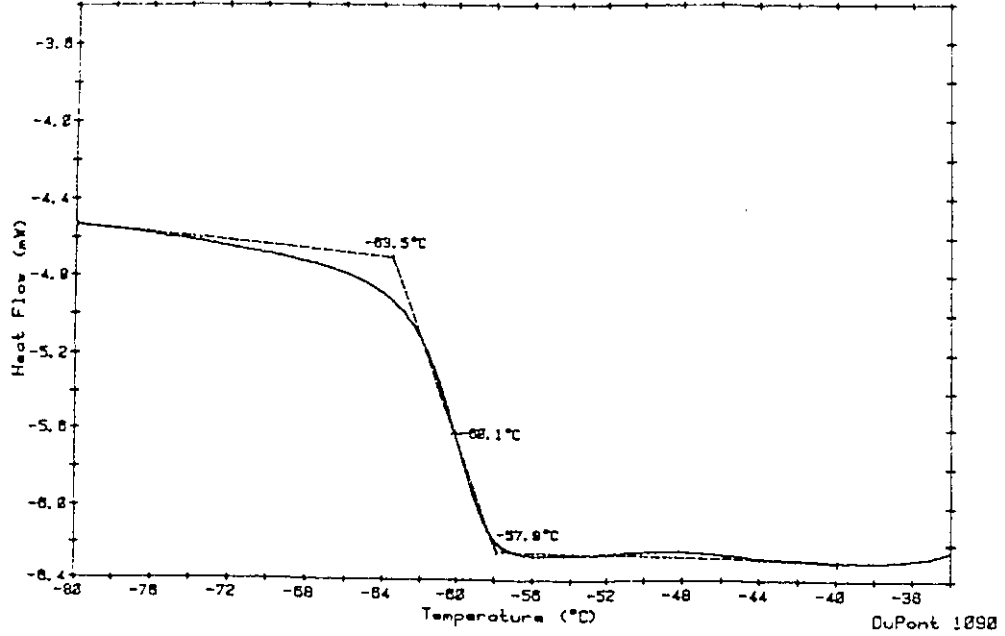
Date: 8-Jul-87 Time: 14:57:51  
File: MIKE.20 DISC DC1  
Operator: ML  
Plotted: 18-Jul-87 12:32:56



Sample: DESMOPHEN 1920D I  
Size: 8.814MG  
Rate: 20C/MIN  
Program: Interactive DSC V2.0

DSC

Date: 13-Jul-87 Time: 12:08:11  
File: MIKE.24 D1SC DC1  
Operator: ML  
Plotted: 13-Jul-87 12:25:24

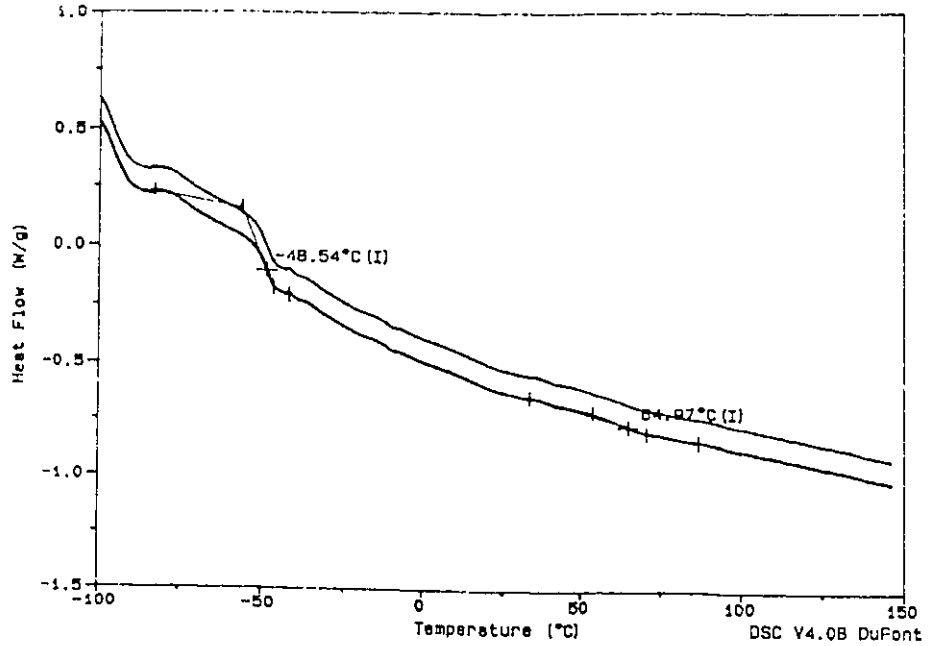


E-14

Sample: DESMODUR 19200#1 A  
Size: 4.3130 mg  
Method: P.U. 20°C/MIN.  
Comment: HEATING RATE 20°C/MIN.

DSC

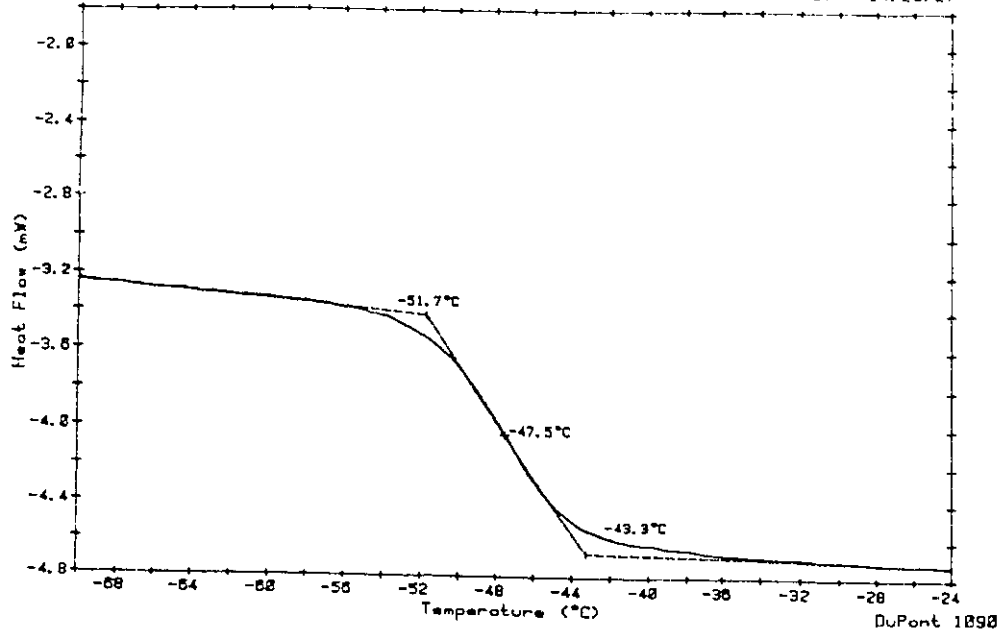
File: C:DORINA.71  
Operator: D.B.  
Run Date: 5-Sep-90 12:07



Sample: DESMOOR VL 3  
Size: 0.620MG  
Rate: 20C/MIN  
Program: Interactive DSC V2.0

DSC

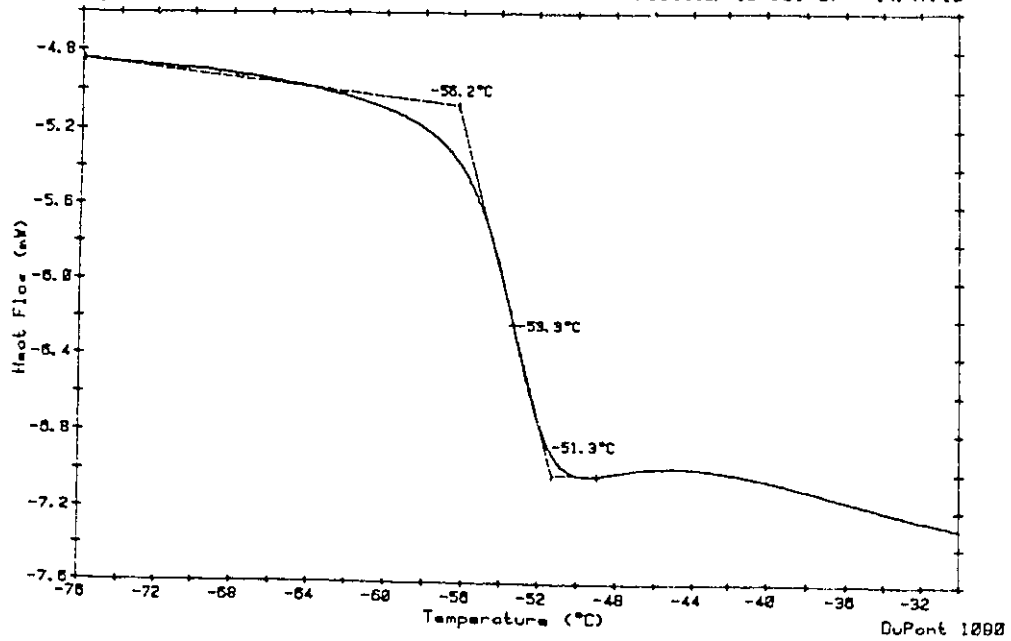
Date: 6-Jul-87 Time: 17:24:43  
File: MIKE.06 D1SC DC1  
Operator:  
Plotted: 10-Jul-87 14:26:27



Sample: MONODUR XP 743  
Size: 0.010MG  
Rate: 20C/MIN  
Program: Interactive DSC V2.0

DSC

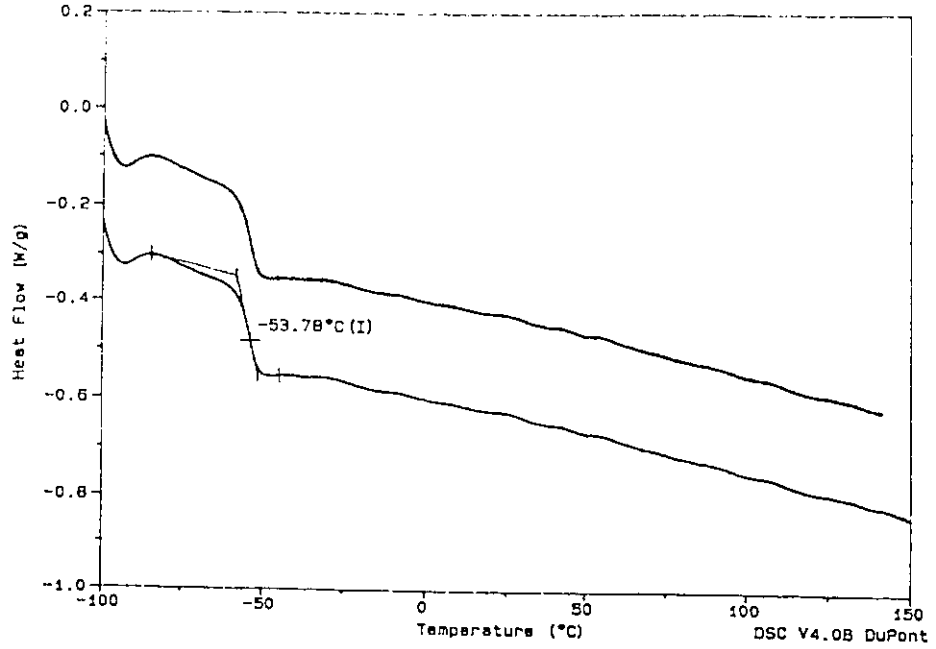
Date: 7-Jul-87 Time: 17:26:05  
File: MIKE.12 D1SC DC1  
Operator: ML  
Plotted: 10-Jul-87 14:47:13



Sample: P.U./M.L./DMA #1 A  
Size: 20.2100 mg  
Method: P.U. 20°C/MIN.  
Comment: HEATING RATE 20°C/MIN.

DSC

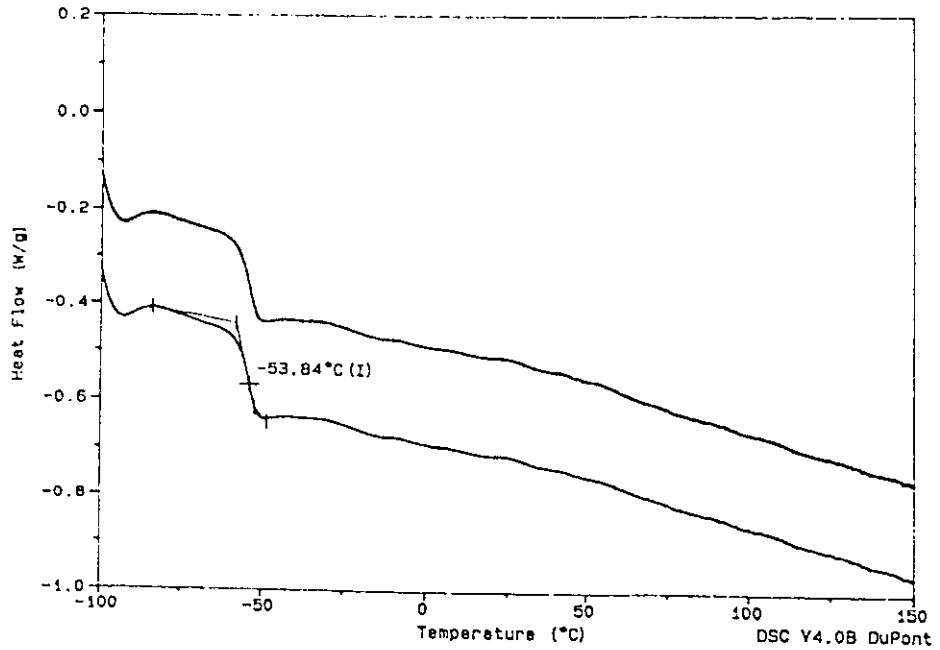
File: C:DORINA.69  
Operator: D.B.  
Run Date: 4-Sep-90 09:10



Sample: P.U./M.L./DMA #2 B  
Size: 21.0450 mg  
Method: P.U. 20°C/MIN.  
Comment: HEATING RATE 20°C/MIN.

DSC

File: C:DORINA.70  
Operator: D.B.  
Run Date: 4-Sep-90 09:10



## APPENDIX VI



## REGRESSION ANALYSIS ON LINEAR PLOTS

Fig. No.	Page No.	Item	Linear regression of the line { $y = mx + b$ }		
			Slope (m)	Intercept (c)	Regression coefficient (r)
4.4	124	Stress	980	-829	0.9888
		Strain	294	-269	0.9689
4.20	166	Filler-AT	-1.18	0.993	0.7998
		Filler-EU	-1.03	0.996	0.8143
		Filler-ST	-1.75	0.992	0.7844
		Filler-TO	-1.34	0.990	0.7954
4.39	198	Filler-AT	0.247	0.0459	0.9995
		Filler-EU	0.0602	0.0148	0.9991
		Filler-ST	0.649	-0.290	0.9967
		Filler-TO	0.345	-0.352	0.9908
4.40	199	Degree of Shift	1.29	1.65	0.9939
4.41	200	Packing fraction	3.97	0.129	0.9993
4.43	205	TF15B	-2.38	4.52	0.8579
		TF28C	-2.18	4.09	0.8286
4.44	207	Filler-AT	-3.75	7.02	0.8259
		Filler-EU	-1.45	2.77	0.9170
		Filler-ST	-2.79	4.94	0.8611
4.45	208	Filler-Clay	-2.50	4.72	0.8936
		Filler-RCL6	-2.96	5.81	0.9410
4.46	211	Filler vol % - 7.5	0.414	-2.19	-0.9803
		Filler vol % - 10	0.454	-2.21	-0.9697
		Filler vol % - 12.5	0.409	-1.98	-0.9586
		Filler vol % - 15	0.439	-1.99	-0.9168
4.50	218	Sealant - A2	-0.564	1.88	-0.9215
		Sealant - A3	-0.292	0.876	-0.9643
4.51	221	Filler - ST	-0.128	2.00	0.9824
		Filler - TO	-0.179	1.94	0.9751